The Dissertation Committee for Omar Alan Vicencio Certifies that this is the approved version of the following dissertation:

NITROGEN INJECTION INTO NATURALLY FRACTURED RESERVOIRS

Committee:

Kamy Sepehrnoori, Supervisor

Steven L. Bryant

Mojdeh Delshad

Todd J. Arbogast

Larry W. Lake

NITROGEN INJECTION INTO NATURALLY FRACTURED RESERVOIRS

by

Omar Alan Vicencio, B.S., M.S.

Dissertation

Presented to the Faculty of the Graduate School of

The University of Texas at Austin

in Partial Fulfillment

of the Requirements

for the Degree of

Doctor of Philosophy

The University of Texas at Austin

May 2007

This work is dedicated to my family,

my parents, Raul and Carolina, my sister, Evelyn, my brothers Nelson and Eliseo and my nephew Alan David for their love.

Acknowledgements

I would like to thank Dr. Kamy Sepehrnoori, my supervising professor, for providing me the opportunity to learn from him. I am very grateful for his patient guidance, and encouragement. I am also grateful to Dr. Larry Lake for the many useful discussions and suggestions throughout the analytical model. Also, I want to express my gratitude to Dr. Mark Miller for sharing his knowledge in the field application of simplified reservoir models. Thanks also to: Dr. Bryant, Dr. Delshad and Dr. Arbogast for their time and for serving as members of my dissertation committee.

I am grateful to the staff of the Petroleum Engineering Department for their help and support. Also very special thanks goes to my friends Baosheng Liang, Nemesio Miguel, Reza Naimi-Tajdar, F. Marcondes , Choongyong Han, Barish Guler and Davood Ghorbani, it has been a pleasure to work and share unforgettable moments with them.

Financial support from PEMEX and The Center of Petroleum and Geosystems Engineering at The University of Texas at Austin is gratefully acknowledged. My gratitude is also extended to Dr. Jose Luis Sanchez Bujanos and Dr. Nestor Martinez Romero for being interested in my work at The Field Center of Studies in the South Region of PEMEX.

Last but not least, my parents, Raul and Carolina, my sister, Evelyn, my brothers Nelson and Eliseo, and my nephew Alan David, who have made possible this work. This work is a tribute to their sacrifice.

NITROGEN INJECTION INTO NATURALLY FRACTURED RESERVOIRS

Publication No._____

Omar Alan Vicencio, Ph.D.

The University of Texas at Austin, 2007

Supervisor: Kamy Sepehrnoori

Naturally fractured reservoirs are complex and constitute a large amount of the world's oil reserves. Their complexity usually is represented by numerical models based on conceptual abstractions. When most recoverable oil is present in low-permeability rocks, the dual porosity model appears to be the most efficient approach for simulating naturally fractured reservoirs.

The rhythms of exploitation in a fractured reservoir can cause field pressure to decline drastically and be reflected in the reduction of oil production rates and the formation of a secondary gas cap. Therefore, field pressure maintenance using gas injection can be an attractive method from technical and economical points of view. A similar approach has been implemented in Cantarell field, the largest oil field in Mexico, characterized as a dual porosity system with a black oil fluid.

The simulation of the largest nitrogen injection project in the world for a giant naturally fractured reservoir was carried out to perform a detailed study of the nitrogen injection by using a conceptual model.

The objectives of this research are 1) Study the impact of nitrogen injection on oil recovery and nitrogen distribution by injecting nitrogen through different scenarios, and using simplified models with homogeneous and heterogeneous properties; 2) Study the injection of different gases at the same reservoir conditions; 3) Determine the variations of temperature that mainly occur in the gas cap and oil zone using a thermal compositional case study; 4) Study the impact of nitrogen distribution by injection at surface and elevated temperatures; 5) Study the nitrogen injection based on uncertain properties that impact the nitrogen distribution and the oil recovery under the gravity drainage mechanism; 6) Investigate the effects of matrix subgridding in vertical and horizontal directions on total oil production by using a stacked conceptual model; and 7) Develop an analytical model that describes the advancement of the nitrogen front through a fracture system for a gas-oil phase equilibrium system under reservoir pressure maintenance.

Since the data used for this research is based on black oil fluid characterization and the fractures are responsible for fluid transport, our starting point was the construction of a single porosity case study using a black oil formulation considering only the fracture pore volume. Subsequently, we increased complexity of the modeling to determine the variations of temperature in the reservoir and to investigate the impact of nitrogen distribution by injecting nitrogen at standard and elevated temperatures.

Finally, we developed a simple analytical model that describes the movement of nitrogen injected front by using basic equations for fluid-flow in permeable media such as the Buckley Leveret theory. The development of the analytical model will help reservoir engineers to better understand the problem of gravity drainage in fractured carbonate reservoirs and also to grasp the dynamics of fluid-flow in naturally fractured reservoirs.

Table of Contents

List of Tables

List of Figures

CHAPTER 1

INTRODUCTION

1.1 General background

A considerable percentage of the Mexican oil reserves exists in naturally fractured reservoirs. Approximately 48% of the total oil production in Mexico comes from the Cantarell field, the largest oil field in Mexico, characterized as a dual porosity system with a black oil fluid. Also, a considerable percentage of the world's oil reserves exists in naturally fractured reservoirs, and almost two-thirds of the world's oil reserves are in the Middle East, where 25% to 30% of the oil in place is in naturally fractured reservoirs (Saidi, 1987).

The rhythms of exploitation in a fractured reservoir can cause field pressure to decline drastically and be reflected in the reduction of oil production rates and the formation of a secondary gas cap. Therefore, field pressure maintenance using gas injection can be an attractive method from technical and economical points of view. The success of pressure maintenance comprises many variables, but the rock-fluid properties and distribution of the fractured system require special attention.

The simulation of the largest nitrogen injection project in the world for a giant naturally fractured reservoir (the Cantarell field) using a conceptual model to perform a detailed study of the nitrogen injection was carried out in this study. The simplified reservoir model of the Cantarell field was useful in order to compare the results with a developed analytical model, and also to perform a simple process evaluation using average reservoir properties (i.e. matrix porosity, matrix permeability, fracture porosity and fracture permeability). In addition, the simplified model helped us to study the main

mechanism (gravity force and gravity drainage) occurring by injecting nitrogen into naturally fractured reservoirs and this provided qualitative results for nitrogen injection in the Cantarell field.

The main oil recovery mechanisms in all the cases studied are: 1) the gravity force mechanism, which occurs in the gas cap zone and is mainly due to the difference in densities of injected gas and reservoir gas, and 2) the gravity drainage mechanism, which occurs mainly in the oil zone when the fractures are fully or partially saturated with gas. All simulation case studies considered nitrogen injection for pressure maintenance in a dual porosity system, and were conducted using a conceptual reservoir model of the Cantarell field.

Usually, the complexity of naturally fractured reservoirs is represented in numerical models based on conceptual abstractions. When most recoverable oil is present in low-permeability rocks, the dual porosity model appears to be the most efficient approach for modeling such reservoirs. The dual porosity model, a subclass of the continuum model, is a favorable approach to study flow in naturally fractured reservoirs. The model consists of a network of interconnected fractures surrounding porous matrix blocks. High conductivity but low storativity typically characterizes the fracture system, whereas the matrix is usually characterized as low conductivity but high storativity. The matrix generally acts as a source that transfers its mass to the surrounding fractures; then fluid is transported to production wells.

In the next section of this chapter, the research objectives of this work are presented. An overview of the other chapters in this dissertation is given in the third section.

1.2 Research objective

The objectives of this research are 1) The simulation of the world's largest nitrogen injection project in a giant naturally fractured reservoir; 2) Study the impact of nitrogen injection on the oil recovery and nitrogen distribution, by injecting nitrogen within different scenarios, and using simplified models with homogeneous and heterogeneous properties; 3) Study the injection of different gases at the same reservoir conditions; 4) Determine the variations of temperature that mainly occur in the gas cap and oil zone using a thermal compositional case study; 5) Study the impact of nitrogen distribution by injection at surface conditions and elevated temperatures; 6) Study the nitrogen injection into naturally fractured reservoirs based on uncertain properties that impact the nitrogen distribution and the oil recovery under the gravity drainage mechanism; 7) Investigate the effects of matrix subgridding in vertical and horizontal directions on total oil production by using a stacked conceptual model of two matrix blocks surrounded by fractures; and 8) Develop an analytical model that describes the advancement of the nitrogen front through fractures for a gas-oil phase equilibrium system under reservoir pressure maintenance, where nitrogen is injected at a constant rate and oil is produced at a constant bottomhole pressure.

Our simulation case studies considered the nitrogen injection for pressure maintenance of the largest oil field in Mexico (Cantarell), which is characterized as a dual porosity system with a black oil fluid, and where the injection of nitrogen has been selected as the best economic option.

Numerical simulation is a routine tool used by reservoir and production engineers, as well as by earth scientists. Simulation studies for a field can be performed at a small fraction of the cost of actual development and production. Since in practice, nitrogen is injected under low temperature conditions, there is some concern about nitrogen injection

early breakthrough. This idea originated because the higher density values of nitrogen under lower temperatures could accelerate the movement of nitrogen in a reservoir and, therefore, it will result in an early breakthrough of the nitrogen in production wells. The tool selected to study this problem was a thermal simulator. We constructed a thermal compositional case study for a dual porosity system injecting nitrogen at surface temperature conditions to access the impact of temperature on the oil recovery and the nitrogen distribution.

In addition, we constructed several case studies by using the commercial simulator ECLIPSE 100 (a black oil simulator) and ECLIPSE 300 (a compositional simulator) to cover a range of complexity, and each one added a value to the follow modeling in representation. We started with a black oil model in a fracture system, subsequently we increased the complexity of our modeling by considering a dual porosity system. Afterwards, we used an isothermal compositional model in a dual porosity system and finally, we constructed a thermal compositional model for a dual porosity system for our simulation studies.

Also, we performed the gas injection simulation under isothermal conditions and at the same reservoir conditions with three different gases: methane, whose density is less than the reservoir gas; reservoir gas (a mixture), whose density is the same as the gas at reservoir conditions; and nitrogen, whose density is higher than the reservoir gas. Then, we identified the flow pattern for each case study.

In order to perform an accurate and efficient simulation of the matrix-fracture fluids transfer, we considered a proper matrix grid resolution, which sub-divides each matrix block into a series of sub-cells, allowing the simulator to predict the transient behavior. We studied the impact of matrix subgridding in both vertical and horizontal

directions based on production forecasting and nitrogen distribution during nitrogen injection under a strong gravity drainage mechanism.

Finally, we developed an analytical model that describes the advancement of the nitrogen front through a fracture system, which can help reservoir engineers to grasp the problem of gravity drainage in fractured carbonate reservoirs and also to understand the dynamics of fluid-flow in naturally fractured reservoirs.

This research was conducted with field information using a simplified reservoir model. The model uses average properties, either measured or estimated, to achieve an idealized representation of the reservoir. The main utility of a simplified model lies in simple process evaluations. This helps to compare the results with published analytical models in literature, which become more effective as the system decreases in complexity. The qualitative results of these simulation case studies are often all that is needed to make an intelligent reservoir management decision, especially if critical performance data is lacking.

1.3 Review of Chapters

Several simulation case studies were constructed to study the process of injecting nitrogen into a naturally fractured reservoir. Each case study adequately represented the production conditions of the field studied before nitrogen injection and the reservoir pressure monitoring field data.

In Chapter 2, a review of the nature of a naturally fractured reservoir and nitrogen injection projects into naturally fractured reservoir is presented.

The reservoir modeling and simulation data used through out this study is described in Chapter 3. This information corresponds to a highly fractured carbonate reservoir of an offshore complex located in Southern Mexico. All simulation case studies using homogeneous properties are described in detail in Chapter 4, in which we describe

the construction of several case studies by using the commercial simulator ECLIPSE 100 (a black oil simulator) and ECLIPSE 300 (a compositional simulator).

Chapter 5 addresses the simulation of nitrogen injection of the field under study through different scenarios, considering heterogeneities in order to study its impact on nitrogen distribution and oil recovery. The nitrogen distribution and oil recovery results were compared and analyzed with case studies considering average properties.

In Chapter 6, we study the matrix subgridding in both vertical and horizontal directions based on production forecasting and nitrogen distribution, in order to perform an accurate and efficient simulation of matrix-fracture fluids transfer and consider the transient nature of flow. Chapter 7 describes the advancement of the nitrogen front through a fracture system of a gas-oil phase equilibrium system under reservoir pressure maintenance, where nitrogen is injected at a constant rate and oil is produced at a constant bottomhole pressure. A simple analytical model described in Chapter 7, was developed to help reservoir engineers understand the problem of gravity drainage in fractured carbonate reservoirs and also to comprehend the dynamics of fluid-flow in naturally fractured reservoirs. The analytical model describes the movement of the nitrogen injected front through fractured system by using basic equations for fluid-flow in permeable media using the Buckley Leveret theory. Chapter 8 presents the conclusions and recommendations for future research.

CHAPTER 2

LITERATURE REVIEW

The literature review presented in this chapter is divided into two sections. The first part is a review of basic aspects of naturally fractured reservoirs. The second part presents a brief description of nitrogen injection projects around the world.

2.1 Nature of naturally fractured reservoirs

In naturally fractured reservoirs, fluids exist in two interconnected systems: the rock matrix, which usually provides the bulk of the reservoir volume, and the highly permeable rock fractures.

If the matrix blocks are linked only through the fracture system, this is conventionally described as a dual-porosity single-permeability system, since fluid-flow through the reservoir takes place only in the fracture network with the matrix blocks acting as sources. If there is possibility of fluid-flow between neighboring matrix blocks, this is conventionally considered to be a dual-porosity dual-permeability system.

Some of the largest hydrocarbon reservoirs in the world such as those in the Middle East, Mexico and Kazakhstan, are naturally fractured carbonate reservoirs. The fracture detection, characterization, and modeling are challenges to accurately calculate recoverable reserves and predict production over time for such reservoirs.

The investigation of natural fractures during the exploration stage with relevant surface outcrops can form the basis of a lithological, structural, and stratigraphic foundation from which geologists build conceptual models (Bratton *et al.*, 2006). The nature and characteristics of fracture patterns have been studied in the laboratory and in outcrops by many authors (Wolff, 1987; Nelson, 2001; Sharp *et al.*, 2006). Nelson (2001)

classified natural fractures into four types: open fractures, deformed fractures, mineral-filled fractures, and vuggy fractures.

Wolff (1987) presented a fractured system model based upon observations of sedimentary rock outcrops. According to his model, fracture systems are usually composed of one main set of largely spaced and roughly parallel fractures and a secondary set of more irregular fractures, usually perpendicular to the main set, giving place to regular blocks of rock.

Several techniques are used to represent the nature of the fractures. But the most significant distinguishing factor of fracture modeling is the degree of uncertainty. The modelers will need to take an experimental approach to the reservoir, trying out various scenarios until an understanding of the main parameters governing uncertainty evolves.

The essential approach of the fracture characterization does not differ dramatically from modeling other types of heterogeneity, such as the one associated with deposition. Typically, one must:

1) Identify the location of the fractures through some form of trend.
2) Produce a representative model of the fractures themselves.
3) Attribute properties such as porosity and permeability to the fractures.
4) Scale up properties to a flow simulation model, preserving as much geological integrity as possible.

An experimental study (Lisle, 1994) reproduced the fracture trend from simple methods such as distance to fracture tip and curvature. A more recent study (Daly *et al.*, 2004) has indicated that the fractures observed in the reservoir follow some structural rules governing their spatial distribution, and it is necessary to capture the essence of these rules.

In situations where the fluid transfer from matrix to fracture occurs at a rate that is significantly slower than flow within the fractures, it is necessary to use a dual porosity approach to the flow simulation. In this case, the flow simulator needs to be supplied with permeability models for both the matrix and the fractures. One common approach to calculate fracture permeability is to try a direct calculation of permeability by building a grid using the Discrete Fracture Network (DFN), assigning parameters to individual fractures based on inferred fracture parameters (such as aperture) and calculating equivalent permeability from a flow model (Bratton *et al.*, 2006). This method will be accurate if the fracture spatial distribution and its parameters are accurate and the associated boundary conditions are fully appropriate. Unfortunately, we cannot always obtain the level of detail needed without considerable uncertainty in some, or all, of the assumptions (Daly *et al.*, 2004). The generation of DFNs still has limitations (Bratton *et al.*, 2006). DFNs are computationally intensive, so it is not possible to model all of the fractures within a reservoir in this way, and commercially available DFNs can handle only single-phase flow.

Fractured reservoir characterization is highly dependent upon the integration of geology, geophysics, petrophysics, and reservoir engineering. There is a need to characterize fractured reservoirs using a methodology that integrates the reservoir structure, thickness, lithology and petrophysical properties with fracture connectivity (Shen *et al.*, 2005).

Up scaling is a procedure used to represent a fine-grid model or small-scale DFN model in a dual porosity model with either static or dynamic methods. Streamline simulators are faster to run and allow asset teams to quickly validate upscaled reservoir models with dynamic data. According to scale up theory, Gurpinar *et al.* (2000) performed a numerical simulation using a matrix block discretized into gridblocks that

are approximately the size of a core, and then they modified the capillary pressure and relative permeabilities curves using water-oil system, so that the simulation with a coarse grid matched the fine-grid solution. The applicability/validity and rate sensitivity of several conventional up-scaling techniques in a fractured reservoir simulation for an oil-water system is available in the literature (Sanchez-Bujanos *et al.*, 1996; Talukdar *et al.*, 2000). A recent study (Miguel *et al.*, 2004) determined methods of scaling dimensionless variables to simplify the analysis and thus identify the main parameters controlling the gas-oil gravity drainage process in naturally fractured reservoirs.

Geomechanical methods have become increasing popular in recent years. They model the distribution of strain, and hence of likely fracture density. They can range from simple elastic models (Zeno *et al.*, 2002) to more general Mohr Coulomb elastoplastic model.

2.2 Nitrogen injection projects

The limited availability of gas in some countries, besides its price increases, has frequently resulted in the economic unattractiveness of reservoir pressure maintenance or the hydrocarbon enhanced recovery processes. Nitrogen injection has been used in the United States since the mid-1960s at the Devonian Block 31 Field in West Texas (Manrique *et al.*, 2006). During the 1970s and the 1980s the enhanced recovery of hydrocarbons through the injection of non-hydrocarbon gases, such as nitrogen, carbon dioxide, and combustion gases, experienced great activity. During the last 40 years, over 30 nitrogen projects have been initiated in the United States, some of them in carbonate reservoirs in Alabama, Florida, and Texas. Hydrocarbon gas injection projects experienced a decrease from 96 percent value for 1971 to 25 percent for 1990, due mainly to the increase of gas cost and demand in this period. On the other hand, for the same period the nitrogen enhanced recovery projects increased from 0 to 10 percent.

There are now, only two active nitrogen projects in carbonate reservoirs in the United States, the Water-Alternating-Gas in Jay Little Escambia (N2-WAG), which started in 1982, and the pressure maintenance project in Yates Field, which started in the mid-1980s. Based on the expected increment of CO_2 availability in the United States, the number of nitrogen injection projects is not expected to grow. One example is the announcement of a new immiscible CO_2 project in Yates field (Manrique *et al.*, 2006).

The Jay/Little Escambia Creek (LEC) fields were discovered in 1970 and produced oil of 51 ^{o}API from a carbonate reservoir in the Florida panhandle and southern Alabama. The formation is found below 15,000 ft and its average thickness is about 350 ft. It was found that the Jay/LEC cores exhibited mixed wettability characteristics. Original reservoir pressure was 7,850 psia and the saturation pressure of 2,830 psia.

The Water-Alternating-Gas (N2-WAG) in Jay Little Escambia was implemented in 1982. The nitrogen was selected as the principal injection gas rather than methane because of economics, and instead of CO_2 because of both economics and availability. During the N_2-WAG initiation project no free gas existed in the reservoir, since the minimum pressure was 4,800 psia (Christian *et al.*, 1981). The MMP for nitrogen, methane, and CO_2 with JAY/LEC crude at a reservoir temperature of 285 ^{o}F was about 3,600 psia. And the MMP for nitrogen at 100 ^{o}F (reservoir temperature at the vicinity of the waterflood injection wells) was about 5,100 psia, which is considerably below the planned 7,500 psia operating pressure for the project. Current injection rates in LEC fields are $77x10^{6}$ scf/day of nitrogen and 170,000 bb/day of water. Incremental miscible nitrogen injection is estimated to be 7-10 % of OOIP (Lawrence *et al.*, 2002). Several documented WAG projects using low-water-soluble gases observed significant reductions in injectivity, while significant reductions in water injectivity when high-water-soluble gases were used have not been documented (Greenwalt *et al.*, 1982).

Nitrogen flooding has been an effective recovery process for deep, high-pressure, light oil reservoirs. Generally, for these types of reservoirs, nitrogen flooding can reach miscible conditions (Manrique *et al.*, 2006). However, immiscible nitrogen injection has also been used for pressure maintenance, cycling of condensate reservoirs, and as a drive gas for miscible slugs, among other uses. A review of the literature (Clancy *et al.*, 1982) indicates that nitrogen projects in the world can be placed in one or more of the following general categories:

1. Immiscible displacement of the reservoir fluids in the oil zone and/or gas zone by nitrogen.

2. Pressure maintenance that has the purpose of maintaining the pressure of the reservoir at or above its respective dewpoint or bubble-point or at the existing pressure. The use of nitrogen for pressure maintenance presents several advantages; it is economically abundant, easy to obtain, and requires one eighth the energy for its compression than an equivalent volume of gas.

3. Gravity enhancement using the gravity drainage potential of a dipping or thick hydrocarbon zone.

4. Multiple contact miscible displacement of the reservoir hydrocarbon by nitrogen.

5. Displacement of a miscible slug of CO_2, rich natural gas, or other solvents, by using nitrogen as a driving fluid.

Nitrogen injection into fractured reservoirs has been considered an inefficient method for enhancing oil recovery because fractures are highly conductive to gas, and gas is the nonwetting phase in the rock matrix. However, nitrogen injection into the Cantarell field has indicated that the efficiency of nitrogen injection in fractured reservoirs is not as low as expected (Vicencio *et al.*, 2004 and 2006).

Cantarell is a giant naturally fractured complex reservoir under nitrogen injection pressure maintenance. The reservoir fluid is characterized as black oil with 22 ^{o}API. The main pay zones are highly fractured vuggy carbonate formations from the Jurassic, Cretaceous, and Lower Paleocene geological ages. In the overthrust block, the complex is composed of the Akal, Nohoch, and Kutz fields, bounded internally by faults. Akal, a supergiant field, is the largest, most important field in Mexico and the sixth largest in the world. It has original oil in place (OOIP) of 32 billion standard barrels (BSTB) out of the 37 in the complex (Rodriguez *et al.*, 2004). The mechanisms of gravity drainage and gravity force on this field have been studied extensively in this research. In addition, this field has been studied through complex simulation models by other authors (Arevalo *et al.*, 1996, Rodriguez *et al.*, 2004) but this research covers an extensive investigation based on conceptual models using average and heterogeneous properties, thermal models (Vicencio *et al.*, 2004), sensitivity studies based on uncertain properties, and proper matrix grid resolution (Vicencio *et al.*, 2006). In addition, a simple analytical model that describes the movement of nitrogen injected front through fractured system by using basic equations for fluid-flow in permeable media, using the Buckley Leveret theory, was developed during this research.

Miscible experiments have been simulated (Arevalo *et al.*, 1996) and in all case studies the contacts between nitrogen and crude oil always show both liquid and vapor phases, indicating that miscible conditions were not met. Initiation of nitrogen injection in Cantarell resulted in useful pressure maintenance effects (Limon-Hernandez *et al.*, 2001). The pressure maintenance by water injection was discarded based on a review of a water injection project, located southwest of Akal, where there were some indications of substantial risk of water channeling through the fracture system resulting in an early breakthrough (Limon-Hernandez *et al.*, 1999).

The pressure maintenance program in the Cantarell field started with the injection of 300 MMPCD of nitrogen in May 2000, and by December of the same year, injection reached the maximum programmed injection rate of 1,200 MMPCD. Nitrogen is injected in the gas cap through seven wells, drilled and completed at the top of the reservoir (Rodriguez *et al.* 2001, Daltaban *et al.*, 2002). Based on economic analysis, the cryogenic separation of air has been shown to be the more flexible and economical way to produce high nitrogen volumes (Arevalo *et al.*, 1996).

Additional studies of the Cantarell field reported in literature (Gurpinar *et al.*, 2000) use a triple porosity simulation model in order to represent fracture, matrix, and vuggy systems. But future reservoir engineering work on understanding the fluid-flow behavior in triple porosity rocks will make it possible to establish reservoir properties with more certainty.

Due to nitrogen injection availability for pressure maintenance in reservoirs located in Southern Mexico, nitrogen injection at the gas cap has been studied and/or implemented in some naturally fractured reservoirs.

Nitrogen injection also has been evaluated as a way to accelerate gas sales and to increase oil recovery in the Ekofisk field, which is a naturally fractured reservoir located in the Norwegian sector of the North Sea. Simulation results indicated that enhanced oil recovery by nitrogen injection into the upper Ekofisk formation is forecast to be 165×10^6 bbl, through 20 years of nitrogen injection at 200 MMscf/day (Thomas *et al.,* 1991).

Additional studies (Qasem *et al.,* 1994) conclude that the optimization of gas injection in naturally fractured reservoirs requires, as its basis, the initiation process in the early life of the field and recognition of a heterogeneity map of the matrix rock, including the intrinsic properties of various rock types and inter-block connectivity.

CHAPTER 3

DESCRIPTION OF CANTARELL NATURALLY FRACTURED RESERVOIR

3.0 Introduction

A petroleum reservoir system includes the reservoir rock and fluids, gas cap, aquifer, and surface and subsurface facilities. Simulation can incorporate all of these components into a "virtual" reservoir system, having as a result a model ranging from simple to very complex. The complexity of a model is based on the analysis of available data before beginning a simulation study. Users should consider that the more complex the model, the more detailed are the data requirements.

Reservoir modeling can be described as three interdependent components:

1. Geologic modeling
2. Rock characterization
3. Fluid characterization

These three components make up the reservoir model.

The field used in this study corresponds to a highly fractured carbonate reservoir of an offshore complex located in Southern Mexico, which has been modeled previously as a dual porosity system (PEMEX, personal communication). This is the largest oil field in Mexico, discovered in 1976, and the main pay zones are from the Jurassic, Cretaceous and Lower Paleocene geological ages; formations are hydraulically continuous. Production started in 1979 and by 1981 reached a peak of 1.156 MMSTBD. Since then and up to 1995, the field produced at an almost constant rate of 1 MMSTBD by drilling new wells and implementing a gas lift system. Since 1996, production has increased due

to the infill drilling, expanding production facilities, and implementing, in 2000, of a pressure maintenance program by nitrogen injection.

3.1 Geological modeling

The geological model provides a depiction of the distribution of rock types and properties in the reservoir, and is part of the input data for the simulation model. The starting point of this study considers a homogeneous and isotropic permeability system. The average properties for the naturally fractured reservoir shown in Table 3.1 have been obtained from published information (Rodriguez *et al.*, 2001; Limon-Hernandez *et al.,* 2001; Manceau *et al.*, 2000; Arevalo *et al.*, 1996).

The reservoir under study has been represented as a conceptual model, which uses average properties to achieve an idealized representation of the reservoir. The main utility of a conceptual model lies in simple process evaluations; and it helps to compare the results with published analytical models in literature, which become more effective as the system decreases in complexity.

Two zones that form the simple conceptual model are shown in Figure 3.1. The upper zone corresponds to a gas cap where nitrogen has been injected, and a lower zone is formed by the oil zone and is bounded by the oil-water contact.

The dimensions of the conceptual model in x and y directions were defined based on consideration of a cubic geometry for the reservoir under study with a 1.5 x-y length ratio. Based on published information, we have also considered that 20.3% of its original oil-in-place has been produced and 25.5×10^9 stock tank barrels of oil-in-place remained before the initiation of the nitrogen injection (in year 2000). The thickness of both the gas cap and oil zone were obtained by the response of well monitoring data taken during the production time of the field (PEMEX, personal communication). The field configuration illustrated in Figure 3.2 shows the GOC and WOC before nitrogen injection.

The identification of reservoir boundary conditions was obtained by considering a constant pressure at the oil-water contact after nitrogen injection. This consideration is supported by the analysis of monitoring the pressure response taken before and after the nitrogen injection (Rodriguez *et al.*, 2001).

Nitrogen injection occurs through six wells drilled and completed within the gas cap at the top of the field. Injector wells are located in the gas cap at the central top of the reservoir, specifically at 3850 ft of depth, in order to maintain the reservoir pressure at the oil-water contact. A total reservoir gas injection rate of 1,500 MSCFD was obtained by using a black oil model whose description is given in Chapter 4.

Natural depletion of the field has caused a pressure in the oil zone decline from its original average value of 3969 psia in 1979 to 1543 psia in 2000 (before nitrogen injection).

We simulated the reservoir conditions of the field using a simple model; therefore a constant WOC was simulated by considering a constant pressure boundary condition. It was modeled by locating producer wells at the lowest layer of the conceptual model under constant bottomhole pressure and uniformly distributed, as shown in Figure 3.1. Therefore the number of wells used for our conceptual model equals the number of gridblocks per layer. Similar bottomhole pressure values were used for all producer wells by matching the measured oil field production rate before nitrogen injection. The procedure used to define constant bottomhole pressure for all wells is described in Chapter 4.

3.2 Rock reservoir properties

Data obtained from core analysis, such as permeability, porosity, relative permeability curves and capillary pressures are representative, in general, of only the matrix system. But some exceptions could occur in a case where there are microfractures.

Therefore, data from conventional core analysis should not be used in numerical simulators without proper corrections to account for the presence of fractures (Aguilera, 1982).

A dual porosity simulation model should consider two different regions in order to define specific rock-fluid properties for the matrix and fracture systems. Therefore, a set of relative permeability curves, capillary pressure curves and rock compressibility values are necessary input simulation data for each region.

This study assumes that the water phase is not moving through the producer wells and the oil-water contact remains at the same level after nitrogen injection; therefore our problem has been reduced to an oil-gas system with an initial water saturation of 0.15 (by design) in the entire reservoir.

3.2.1 Oil-gas relative permeability

The relative permeability curve is critical in predicting the flow rate of one phase in the presence of another. This study considers that the water phase is not moving through the producer wells and the oil-water contact remains at the same level after nitrogen injection; therefore our problem has been reduced to an oil-gas system. The two-phase relative permeability behavior in the matrix and fractures for our case studies are therefore of considerable importance in effectively estimating the field production rates.

3.2.1.1 Matrix System

Matrix oil-gas relative permeabilities used in our simulation case studies were measured in the laboratory, and they are shown in Figure 3.3. The shape of this set of curves corresponds to the following models:

$$k_{ro} = k_{ro}^{0}\left(\frac{S_o - S_{or}}{1 - S_{or} - S_{wi}}\right)^{e_o} \text{ and } k_{rg} = k_{rg}^{0}\left(1 - \frac{S_o - S_{or}}{1 - S_{or} - S_{wi}}\right)^{e_g}$$

The parameter values of each model are presented in Table 3.2, where e_o and e_g values are the saturation exponents obtained in the laboratory from matrix samples. Oil-gas relative permeability curves represented by these models can be used to define the matrix and fracture saturations presented in Table 3.3.

3.2.1.2 Fracture System

The assumption of fracture relative permeability equal to the phase saturation is often used in numerical simulations (unity slope). Figure 3.4 shows the fracture relative permeability curves used for our simulation case studies. This linear relationship considered suggests no resistance and ideal flow in the fractures, so that inside the fracture the phases can move past each other without hindrance.

Experimental results (Rangel-German *et al*., 1998) utilizing an X-ray Computerized Tomography (CT) scanner on two matrix blocks have shown that the best matches are achieved when a 0.6 slope is used instead of 1.0. But the use of a lower slope of the straight line is an indication of higher resistance flow through the fracture.

In our simulation case studies, the set of relative permeabilities for matrix and fracture remain constant over the life of the reservoir. However, as reservoir pressure declines, there is a reduction in porosity and permeability due to closing of the fractures. This effect produces a continuous change in the fracture relative permeability system that was not considered in our simulation case studies. The aperture changes of fractures during the reservoir exploitation can be described by geomechanical models which integrate all data to estimate in-situ geomechanical rock properties.

3.2.2 Capillary pressure

The capillary pressure represents the pressure differential that must be applied in order for a nonwetting fluid to displace a wetting fluid from the capillary tube. Capillary

pressure is inversely proportional to the radius of the capillary tube and is also a measure of the tendency of a solid to attract or imbibe the wetting phase and repel the nonwetting phase. Therefore, capillary pressure is a function of interfacial tension, permeability, porosity, wettability, saturation and hysteresis.

The numerical flow representation of fluids through a fractured porous media must consider both the matrix and the fracture capillary pressure curves.

3.2.2.1 Matrix System

Since the gas phase displaces the oil phase in our reservoir model, a set of drainage curves has been considered for the capillary pressure data.

Capillary forces are the most important parameter of immiscible gas-liquid flow in fractured reservoirs (Firoozabadi, 1993). Figure 3.5 shows capillary pressure data for the matrix system, which was represented using the following model:

$P_c(atm) = P_c^0 \left(1 - \frac{S_o - S_{or}}{1 - S_{or} - S_{wi}} \right)^{e_{pc}}$, where parameter values are defined in Table 3.2

The shape of this drainage capillary pressure curve shows that the largest pores are connected to the surface because the curve remains essentially flat as the wetting phase saturation is decreased from 85% to 65%. High capillary pressure values at high irreducible oil saturation (40%) can be observed because the rock is extremely fine grained with very low porosity (0.02) and very low permeability (0.2 md), which are characteristic of a tight formation.

Based on the consideration of a capillary tube representation, the pore size probability density function was obtained using $\alpha(r_i) = \frac{P_c}{r_i} \frac{dS_{nw}}{dP_c}$, where r_i was calculated based on $r_i = \frac{2\sigma_{go} \cos\theta}{P_c}$ considering the oil wetting phase ($\cos\theta = 1$), and

$\sigma_{go} = 10\ dynes/cm$ was obtained from the published measured gas-oil interfacial tension of several Iranian reservoirs under reservoir conditions (Saidi, 1987); and $\frac{dS_{nw}}{dP_c}$ was calculated by using a central difference formula.

Figure 3.6 shows that a very small pore radius range from 0.03-0.15 microns represents the tight matrix formation of the field under a capillary tube representation.

3.2.2.2 Fracture System

The starting point of our simulation study considers a capillary discontinuity system; which means no capillary pressure in the fracture system.

In general, several authors (Kazemi *et al*., 1977; Beckner *et al.*, 1991; Gilman *et al.*, 1994) have assumed that fracture capillary pressures are negligible. Others have shown experimentally that capillary continuity can become important (Horie *et al*., 1990; Firoozabadi *et al*., 1990; Labastie *et al*., 1990; Barkve *et al*., 1992; Rangel-German *et al*., 1998).

In his experimental work, Rangel-German (1998) has observed that in a thin fractures system the front is stable. That is to say, capillary continuity is maintained between the fracture and the matrix. However, for the wide fracture system, the imbibition forces are not that strong and the front is not piston like; therefore, in a wide fracture system faster breakthrough times were observed.

Since the effect of fracture capillary pressure generally is more pronounced in gas gravity drainage than in the capillary imbibition process (Firoozabadi *et al*., 1990), we investigated the impact of capillarity continuity with a detailed sensitivity analysis presented in Chapter 5.

The flow of fluids in naturally fractured reservoirs is dependent upon the capillary contact, which exists from block to block. The importance of fracture capillary pressure

in the drainage performance is visualized in the flow of gas from a fracture to a matrix cell in a gas-oil system computed as (Schlumberger simulation software manuals, 2005)

$$F_g = TR * GMOB * (P_{of} - P_{om} + d_{fm}\rho_g g + P_{cogf} - P_{cogm} + \frac{DZ_{mat}(X_G - X_g)(\rho_o - \rho_g)g}{2})$$

where

F_g is the flow of gas from a fracture to a matrix cell

TR is the transmissibility between the fracture and matrix cells,

$GMOB$ is the gas mobility in the fracture cell (upstream),

P_{of} is the oil phase pressure in the fracture cell,

P_{om} is the oil phase pressure in the matrix cell,

d_{fm} is the difference in depth between the fracture and matrix cells (usually zero),

ρ_g is the density of gas at reservoir conditions,

ρ_o is the density of oil at reservoir conditions,

g is the acceleration due to gravity,

P_{cogf} is the capillary pressure of gas in the fracture cell (normally zero),

P_{cogm} is the capillary pressure of gas in the matrix cell,

DZ_{mat} is the matrix block height, and

$\frac{DZ_{mat}(X_G - X_g)(\rho_o - \rho_g)g}{2}$ is the gravity drainage head, where X_G and X_g are the partial volumes of mobile gas in the simulation fracture and matrix cells respectively.

We observed in the above expression that it is not the capillary pressure but the contrast in the matrix medium and fracture medium that strongly influences the two-phase flow behavior.

The low displacement efficiency of gas-oil gravity drainage in the fractured reservoirs is believed to be due to capillary pressure contrast of the matrix and the

fracture; on the other hand, a substantial reduction of fractured capillary pressure or its elimination may provide a condition for a very efficient recovery.

Fracture capillary pressure is practically equivalent to capillary continuity, and when there is continuity, reduction of the capillary pressure by increasing the reservoir pressure may not give a notable extra oil recovery. However, if there is no continuity, the reduction of capillary pressure will give a significant extra oil recovery (Firoozabadi *et al*., 1990). This is demonstrated in Chapter 5.

3.2.3 Pore volume compressibility

Pore volume compressibility defines the fractional change in porosity with a unit change in pressure. The average value considered for the matrix compressibility system is 4.5×10^{-6} $psia^{-1}$, and 3.4×10^{-5} $psia^{-1}$ for the fracture system. This information was obtained from the analysis of a transient pressure test and was provided for the development of this research project (PEMEX, personal communication). Field data indicates that, for this reservoir study, the fracture compressibility factor is eight times higher than the matrix rock. Practically, open or partially mineralized natural fractures are more compressible than host rock.

If this data were not available, a good approximation that has been developed by Aguilera (1999) who has estimated fracture compressibility for three cases, natural fracture mineralization, partial secondary mineralization, and total secondary porosity system including fractures, vugs, and caverns, could be used.

3.3 Fluid properties

A laboratory analysis Pressure-Volume-Temperature (PVT) data set was available for this study (PEMEX, personal communication). A preliminary analysis of that information indicates that the field fluid corresponds to a black oil system. This result is

due to the initial oil formation volume factor of 1.32 reservoir bbl/stb, the initial producing gas-oil ratios of 600 scf/stb, and the gravity of stock-tank oil of 22 ^{o}API.

The black oil model assumes that stock tank oil only exists in the oleic phase but gas can exist in both the oleic and gaseous phases. Also, black oil systems consider that fluid properties are only dependent on pressure.

The oil properties encountered most in reservoir black oil simulation are oil density, oil compressibility, oil formation volume factor, oil viscosity, and solution gas-oil ratio.

3.3.1 Oil density

Density of the stock tank oil is usually measured and reported as specific gravity, γ_o (with respect to water at standard conditions) or degrees API. The reservoir fluid density measured for our simulated case is 22 ^{o}API.

3.3.2 Oil compressibility

Average oil compressibility under saturated pressure is acceptable for most simulation cases. This compressibility value is used at all pressures of the simulation PVT table. A value of 10.96×10^{-6} 1/psia was used for the black oil simulation case studies.

3.3.3 Oil formation factor

The oil formation volume factor is defined as the volume of reservoir oil required to produce one barrel of oil at stock tank conditions. The values used for the black oil simulation case studies are represented in Figure 3.7. In this figure, a value of 2145 psia is also shown as the initial bubble-point pressure of the fluid under consideration.

3.3.4 Oil viscosity

Oil viscosity is usually determined in the laboratory for the particular reservoir fluid under study and is normally reported as one of the results of the PVT test. Like other physical properties of liquids, it is affected by both pressure and temperature. The oil viscosity values used for the isothermal black oil study are illustrated in Figure 3.8.

3.3.5 Solution gas-oil ratio

The quantity of gas dissolved in oil at reservoir conditions is called the solution gas-oil ratio. This ratio is defined in terms of the quantities of gas and oil that appear at the surface during production. It is also called the dissolved gas-oil ratio and occasionally gas solubility. Figure 3.9 shows the solution gas-oil ratio for the black oil simulation study.

3.3.6 Gas properties

Gas properties used in black oil simulation are gas density, the gas formation volume factor, and gas viscosity.

The gas density of simulated fluid at surface conditions is 0.0615 lbm/ft^3. This property is normally measured in the laboratory at each pressure stage in the differential liberation. The stages are below reservoir temperature and should cover the initial reservoir bubble-point pressure through to the surface pressure (14.7 psia). Gas density is required for calculating the gas viscosity (μ_g), gas compressibility and gas deviation factor (z). The behavior of gas-oil ratio, gas formation volume factor and gas viscosity with respect to reservoir pressure are shown in Figures 3.9, 3.10 and 3.11, respectively.

Table 3.1 Average properties of the simulated reservoir model.

Matrix Permeability (md)	0.20
Fracture Permeability (md)	5000
Matrix Porosity (fraction)	0.05
Fracture Porosity (fraction)	0.02
Gas Zone Thickness (ft)	2700
Gas/Oil Contact (ft)	6500
Oil/Water Contact (ft)	8800

Table 3.2 Parameter values used in the matrix relative permeability and matrix capillary pressure models (PEMEX, personal communication).

k_{ro}^{0} ; End-point oil relative permeability	1.00
S_{or} ; Residual oil saturation	0.40
S_{wi} ; Initial (residual) water saturation	0.15
e_o ; Numerical exponent	3.00
k_{rg}^{0} ;End-point gas relative permeability	0.32
e_g ; Numerical exponent	2.00
P_c^0 ; End-point capillary pressure (psia)	6.00
e_{pc} ; Exponent for oil-gas capillary pressure	6.00

Table 3.3 Saturation values of matrix and fracture systems obtained from oil-gas relative permeability curves (PEMEX, personal communication).

Description	Matrix System	Fracture system
Critical gas saturation; Sgc	0.00	0.0
Residual oil saturation; Sor	0.40	0.0
Residual liquid saturation	0.55	0.0
Maximum gas saturation	0.45	1.0
Maximum oil saturation	0.85	1.0

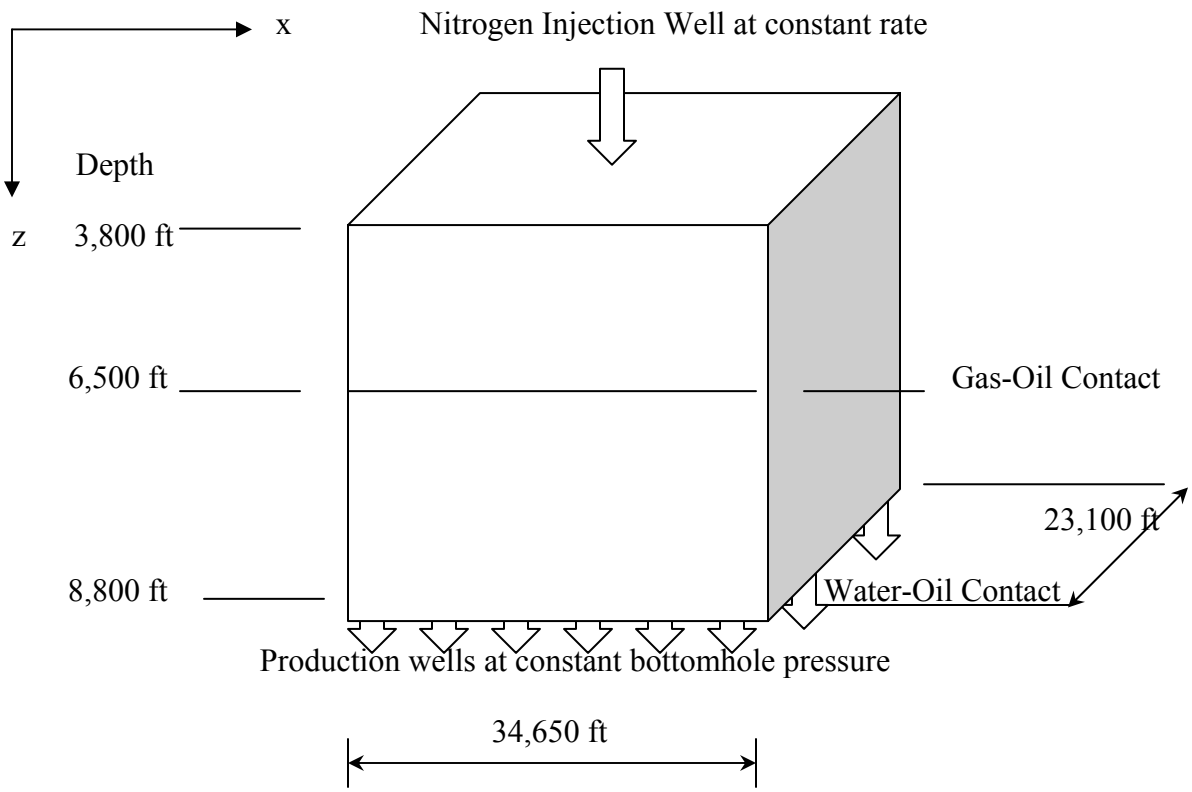

Figure 3.1 The conceptual reservoir model that represents the reservoir under study.

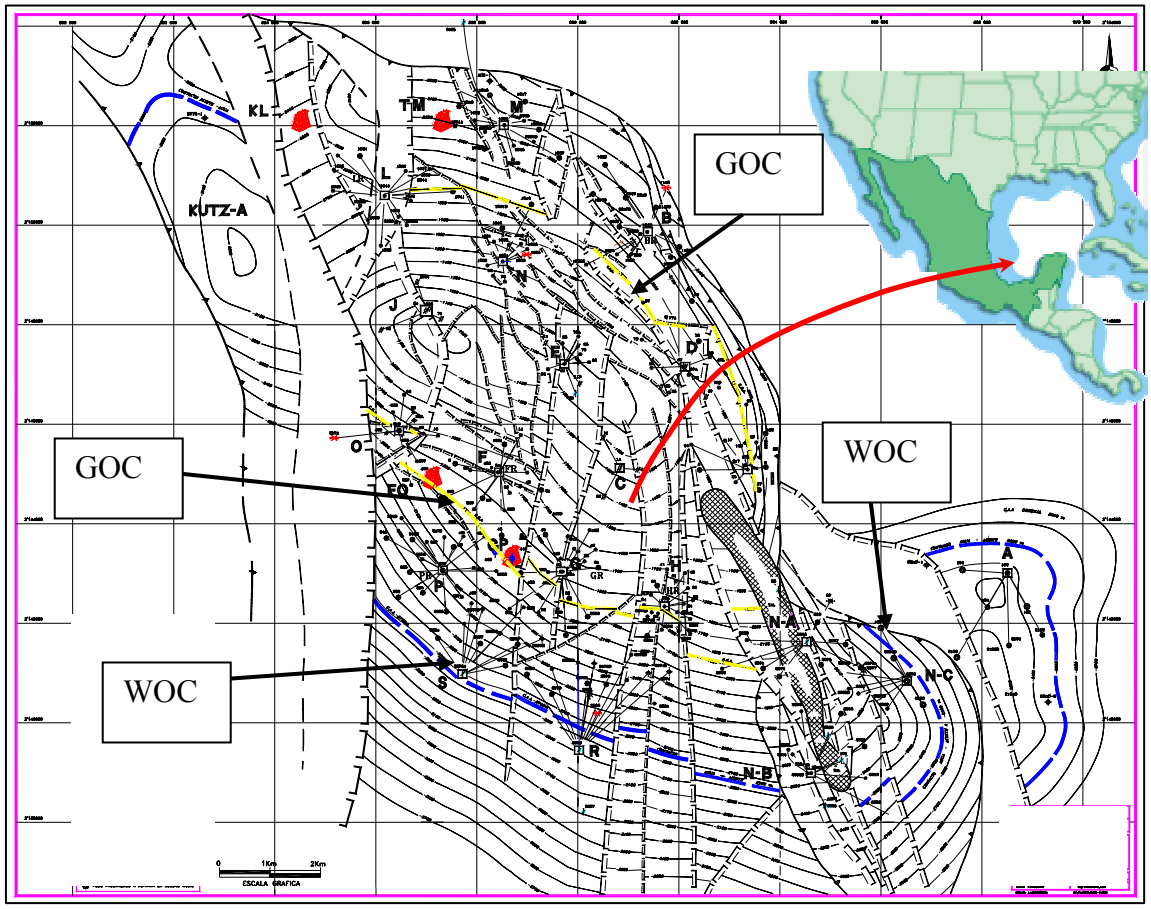

Figure 3.2 Field water oil contact (WOC) and gas-oil contact (GOC) before nitrogen injection.

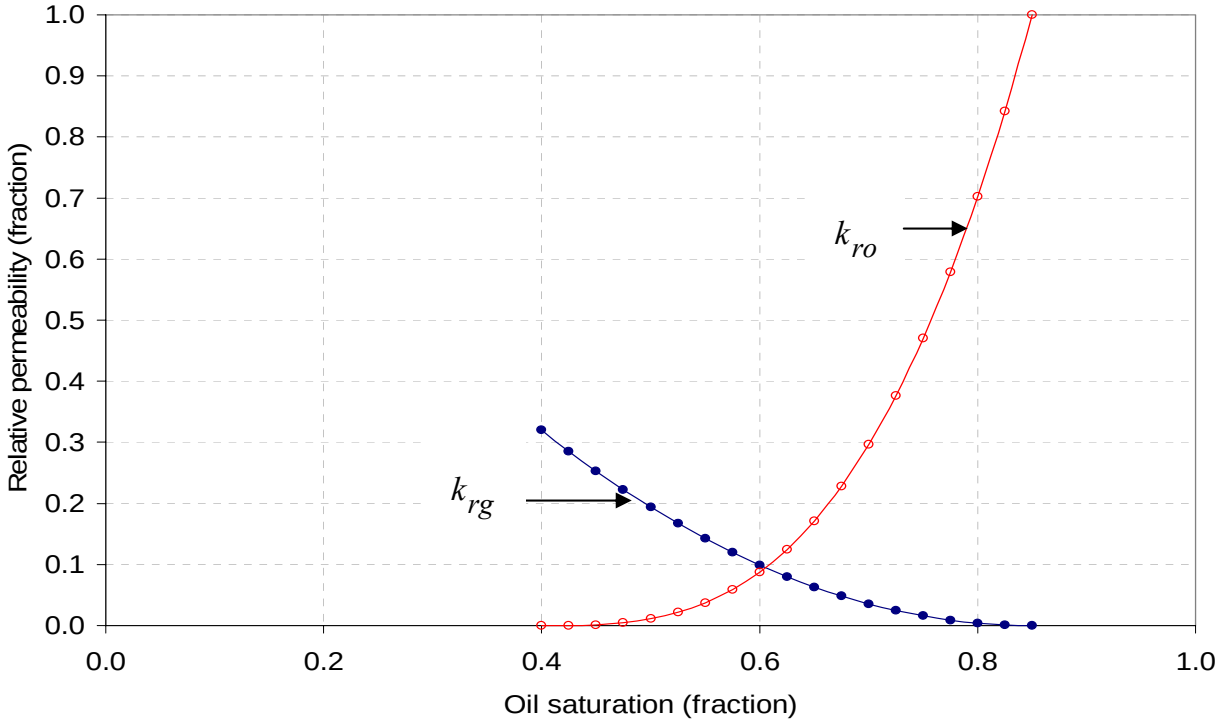

Figure 3.3 Oil and gas relative permeability curves for the matrix system.

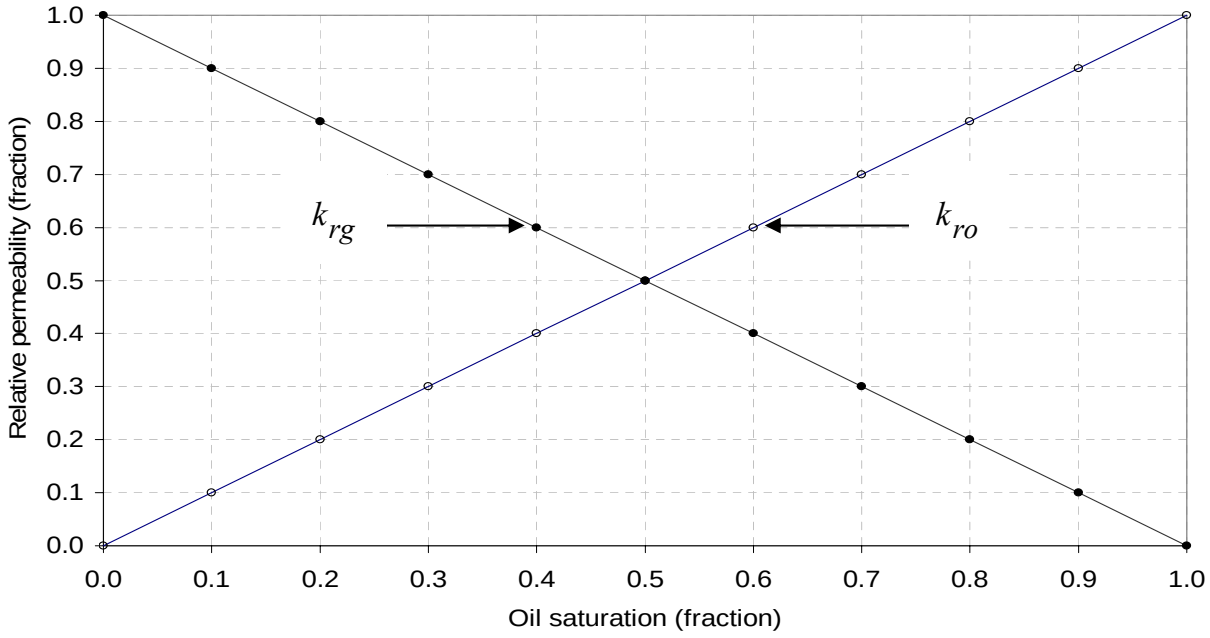

Figure 3.4 Oil and gas relative permeability curves for the fracture system.

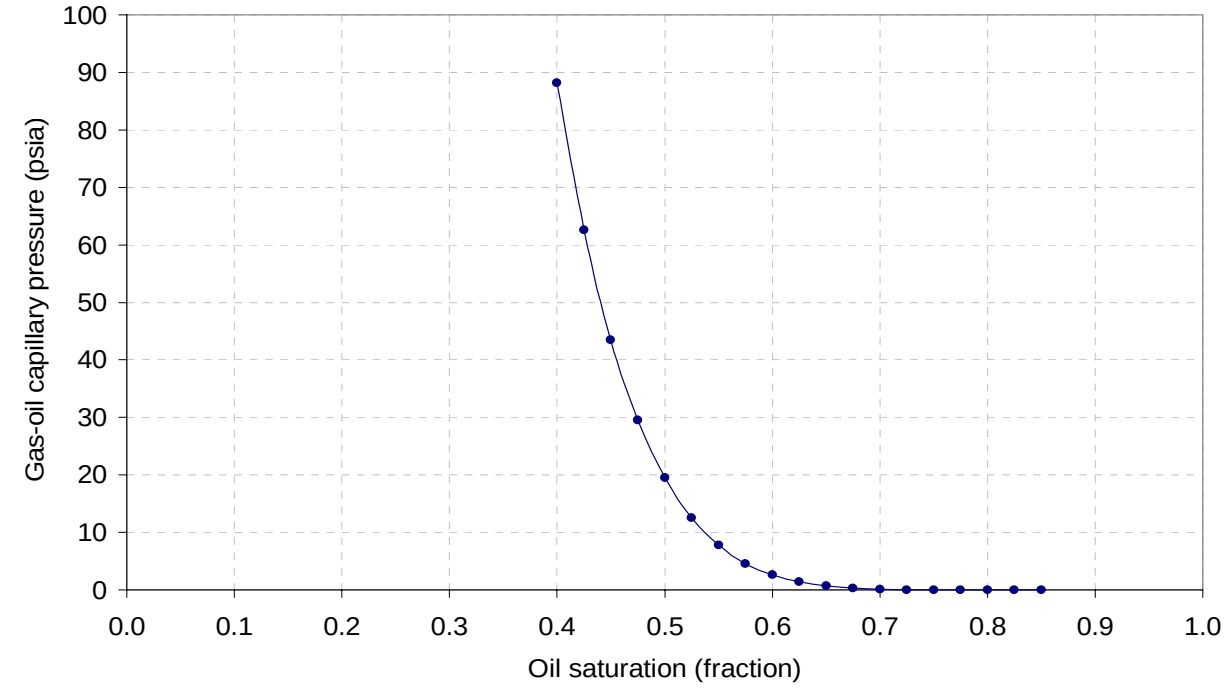

Figure 3.5 Gas-oil capillary pressure curve for the matrix system.

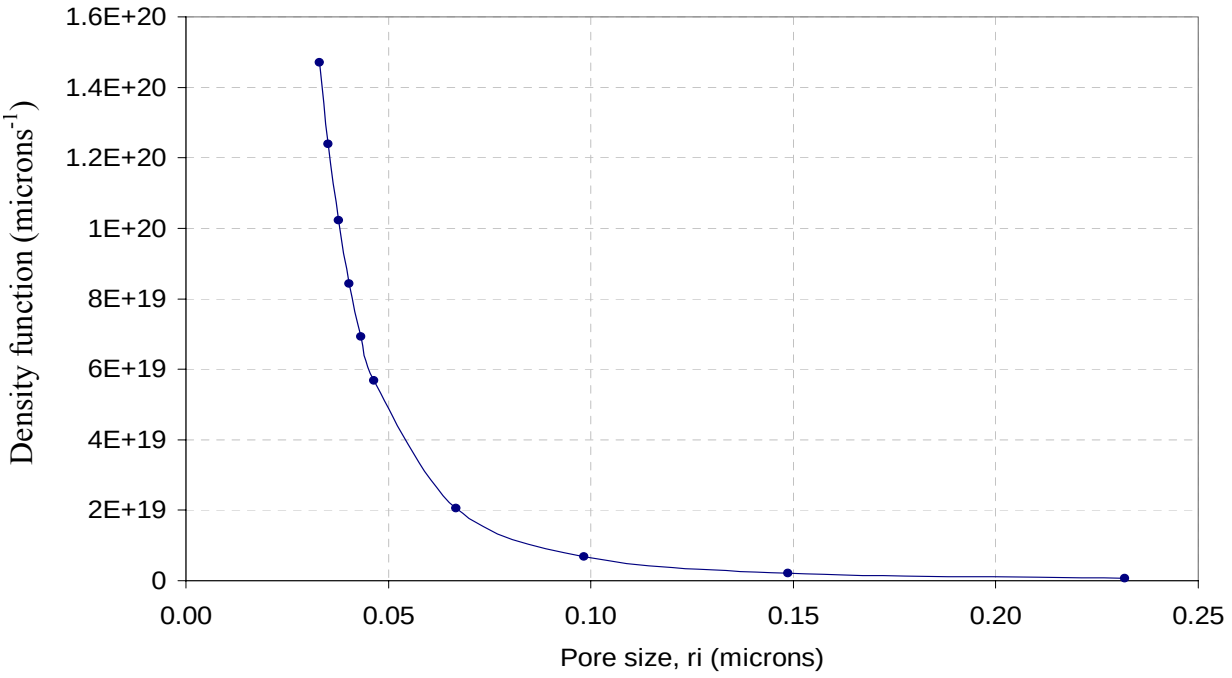

Figure 3.6 Pore size probability density function for the matrix system.

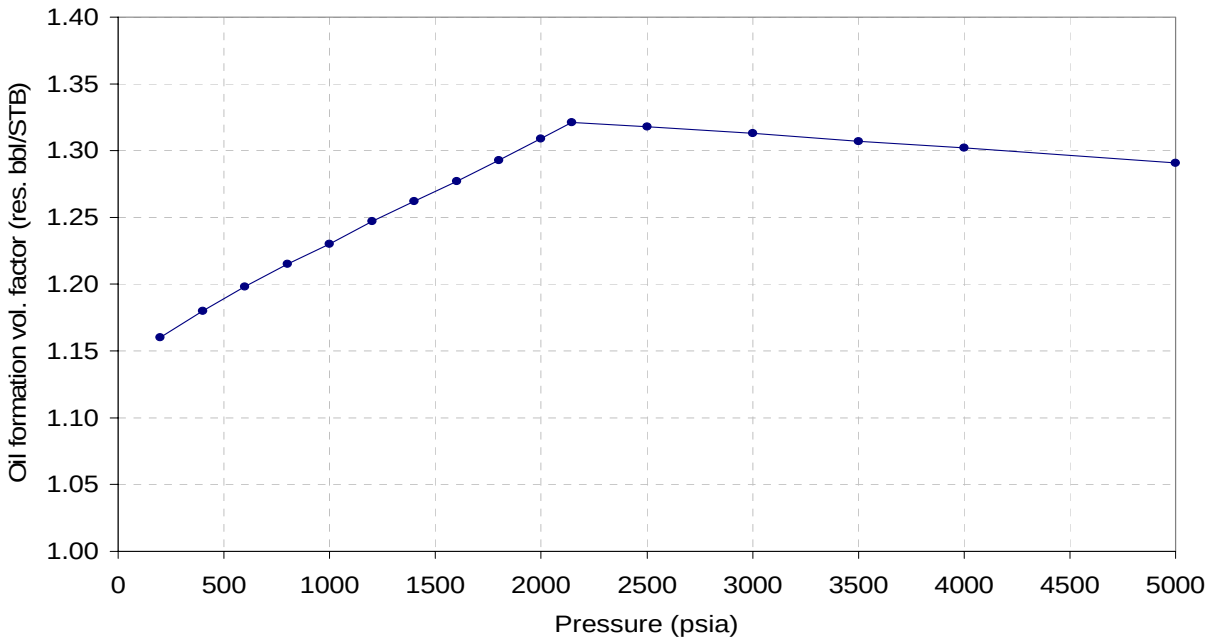

Figure 3.7 Oil formation volume factor used for case studies using the black oil formulation.

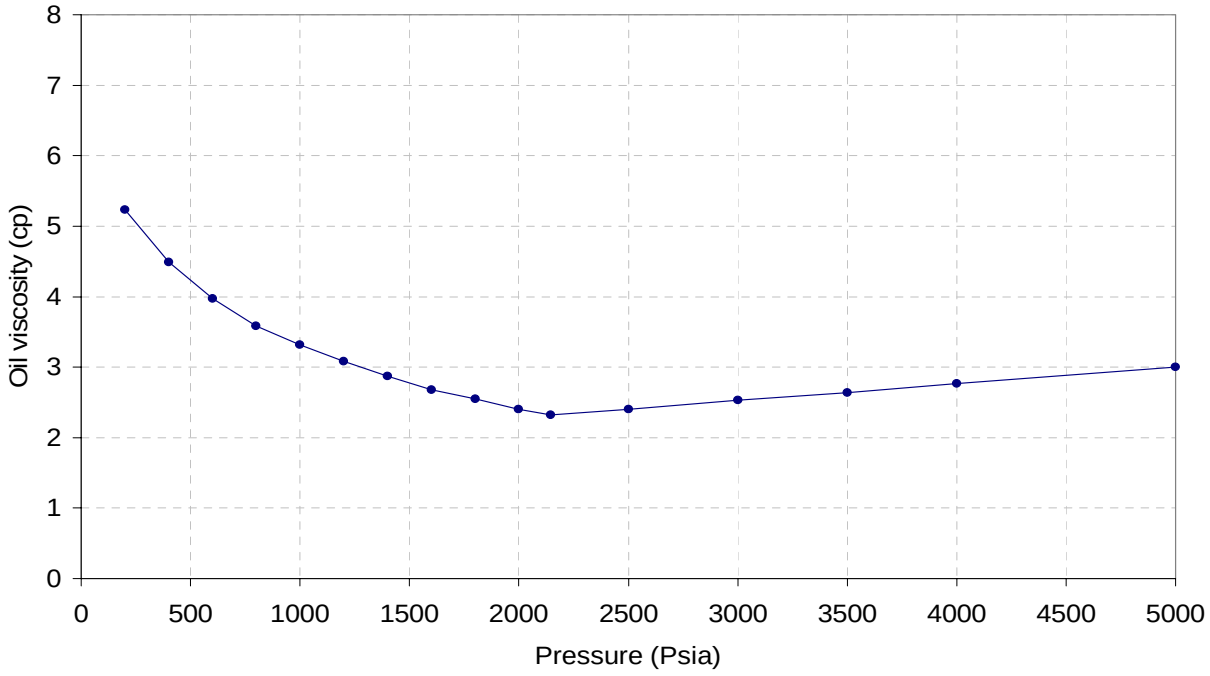

Figure 3.8 Oil viscosity data used for case studies using the black oil formulation.

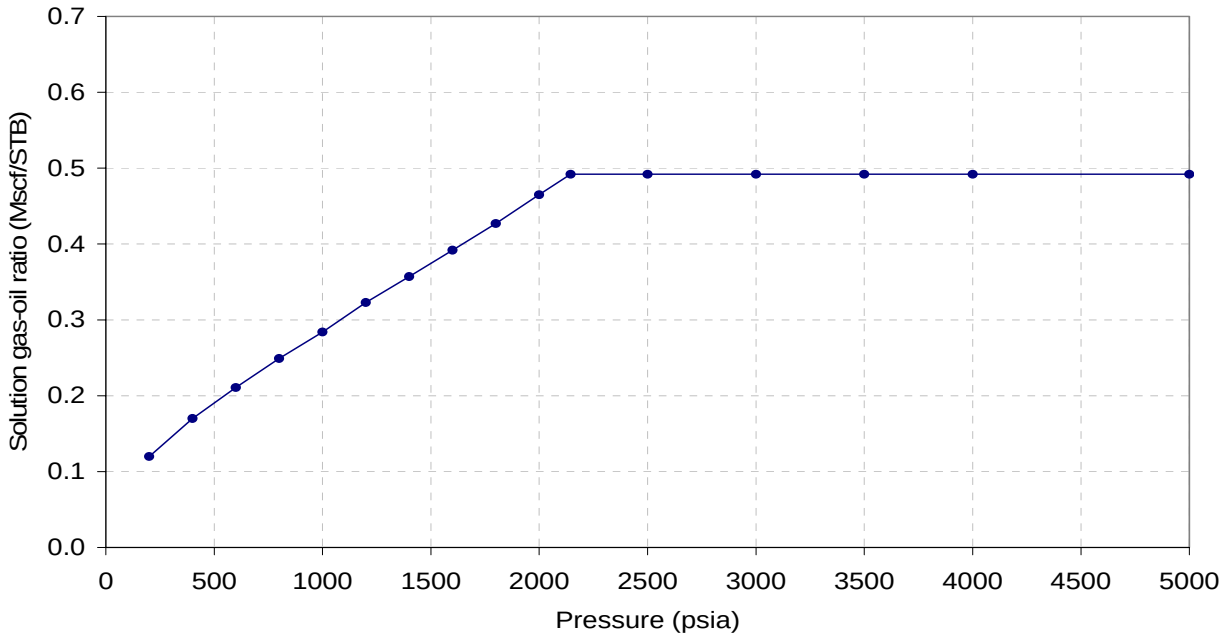

Figure 3.9 Solution gas-oil ratio used for case studies using the black oil formulation.

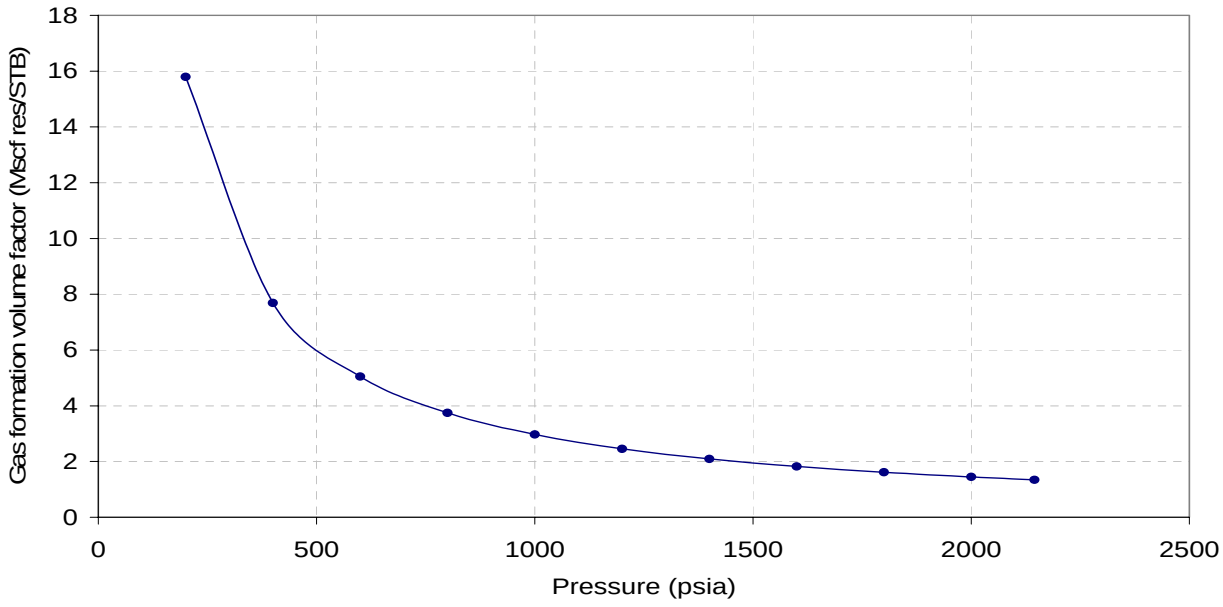

Figure 3.10 Gas formation volume factor for case studies using the black oil formulation.

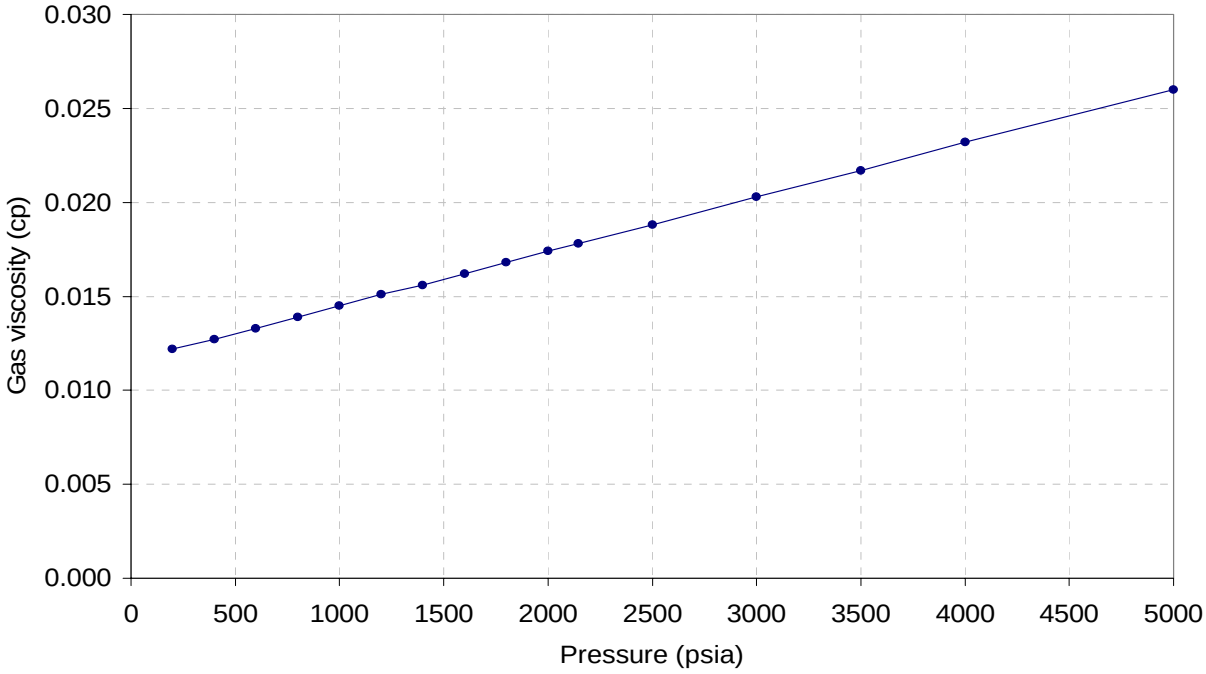

Figure 3.11 Gas viscosity used for case studies using the black oil formulation.

CHAPTER 4

RESERVOIR SIMULATION CASE STUDIES USING HOMOGENEOUS PROPERTIES

4.1 Introduction

Much current practice in predicting oil recovery is based on numerical simulation, because simulation can solve problems that quantitatively describe the flow of multiple phases in a heterogeneous reservoir. A simple modeling is useful for the reservoir performance and may confirm the primary producing mechanism and reduce the computing time.

A recent study (Lake, 2003) indicates that incorporating more data into simulation models leads to greater confidence. But this conclusion has not been proven and, indeed, cannot be true for all cases. Lake (2003), in his presentation, suggests the use of simplified models in predicting reservoir performance. These models are far less general than simulators, but can predict field-wide performance and are well suited for predicting uncertainty. One approach for analyzing oil production mechanisms in naturally fractured reservoirs is to study their behavior by using simplified models, as we did in this research.

In order to achieve our goals in this research project, we used simplified reservoir models because they provide simple process evaluation, consider average properties, give qualitative results, and are useful when lacking data.

We constructed several case studies by using the commercial simulator ECLIPSE 100 (a black oil simulator) and ECLIPSE 300 (a compositional simulator). Such case studies covered a range of modeling complexity, and each added a value to the following complexity in representation. We started with a black oil model in a fracture system.

Subsequently, we increased the complexity by considering the same fluid formulation in a dual porosity system, then we used an isothermal compositional model in a dual porosity system and, finally, we constructed a thermal compositional model in a dual porosity system for our simulation studies.

4.2 Black oil model in a fractured system

Isothermal black oil models have been widely used in reservoir simulations. In this section, we show the results of the first simulation case considering only the fracture system, which is characterized by low pore volume. Fractures themselves typically do not have much fluid volume, but they significantly enhance reservoir permeability. Nelson (2001) classifies this fracture reservoir as type I, where the fracture system provides the essential porosity and permeability. He also suggests an early calculation of fracture porosity because is an important property.

This simulation case study considers no local exchange of fluids between the fracture and the matrix. It was built by considering the average fracture properties illustrated in Table 3.1 and by initially using a coarse grid with $10 \times 10 \times 20$ gridblocks ($2500\ ft \times 2500\ ft \times 250\ ft$). The accuracy of this simulation case using a coarse grid is questionable, but a grid refinement study indicated that the simulated oil production rate did not match the field oil production rate for any refinement case. This was mainly due to the consideration of no matrix-fracture fluids transfer; this fact is explained in detail in Section 4.2.3.

For all our constructed simulation case studies, we simulated the nitrogen injection into a naturally fracture reservoir matching field oil production during the initiation of nitrogen injection implementation.

4.2.1 Modeling constant oil-water contact

In order to model a constant oil-water contact during the gas injection time, we considered 1) the number of producer wells equal to the number of simulation gridblocks per layer located at the bottom of the conceptual model, and 2) the same bottomhole pressure in all producer wells.

As a starting point, we considered a bottomhole pressure equal to the oil-water contact pressure. But the simulation results indicated that this consideration did not adequately represent the field oil production conditions because measured oil field rates were never reached; such behavior is illustrated in Figure 4.1.

As an alternative to solve this problem, we performed a sensitivity analysis with the bottomhole pressure to match the oil field production rate during the initiation of nitrogen injection implementation. After several simulation runs, we found that a bottomhole pressure equal to 1720 psia for all the producer wells adequately matched the field oil production rate, as is illustrated in Figure 4.2.

4.2.2 Fracture porosity effect

The uncertainty of fracture porosity is high since its measurement is complicated. This uncertainty is because the volume of fractures is usually very small and also because fracture porosity values are less than the accuracy range of almost any tool available at this time.

Performing several simulation cases by injecting nitrogen, we observed that fracture porosity is a very sensitive property to maintain a constant field oil production rate; therefore, we incorporated more log porosity data to be integrated into our simplified model, specifically in a vertical direction near the injector wells.

Figure 4.3 shows the porosity variations of both the matrix and fracture systems in a vertical cross section of the total thickness formation at the center of the field simulated.

This information was interpreted and previously utilized by field experts in order to conduct simulation studies (PEMEX, personal communication).

In Figure 4.4, we observed that, considering an average fracture porosity of 0.03, the oil production rate is maintained only during the first 500 days of nitrogen injection. This figure also shows the tendency of the field oil production rate, considering two values of fracture porosity (0.0175 and 0.03).

4.2.3 Simulation results

The oil production rate decline observed in Figure 4.4 is not representative for the field under study. This decline occurs mainly because we are not considering the matrix pore volume, which contains the majority of the reservoir pore volume and acts as a source or sink term to the fractures. It was also observed that the oscillation cycles of the oil production rate are related to the size of the grid cells located below the oil-gas contact. This conclusion was reached after monitoring the simulation reservoir saturation changes below the oil-gas contact using GRAF, an ECLIPSE post-processor.

Based on the above observations, we have concluded that it was necessary to consider the following additional complexities for our next simulation case study:

1) To refine the gridblocks in vertical direction in order to simulate the advancement of the gas-oil contact front adequately, and

2) To construct a black oil case study considering the pore volume of both the matrix and fracture systems. This representation is called a black oil case study with a dual porosity system. Its modeling approach is discussed in the next section of this chapter.

4.3 Black oil model with a dual porosity system

4.3.1 Description of a dual porosity system

A dual porosity simulation model should consider two different regions in order to define specific rock-fluid properties for the matrix and fracture systems. Therefore, a set of relative permeability curves, capillary pressure curves, and rock compressibility values are necessary input simulation data for each region.

Data obtained from core analysis, such as permeability, porosity, relative permeability curves, and capillary pressures, are representative, in general, of only the matrix system. But some exceptions could occur in the case that there are micro-fractures. Therefore, data from conventional core analysis should not be used in numerical simulators without proper corrections to account for the presence of fractures (Aguilera, 1982).

A dual porosity system describes the fluids present in the fracture and matrix systems. To model such systems, two simulation cells are associated with each block in the geometric grid, and each active matrix cell must connect with an active fracture cell.

Flow of fluids occurs primarily through the fractures, which have high permeability and low effective porosity surrounding individual matrix blocks. The matrix blocks contain the majority of the reservoir pore volume with low permeability and act as a source or sink term to the fractures.

The representation of such flow behaviors indicates that simulation of naturally fractured reservoirs is a challenging task from both a reservoir characterization and a numerical standpoint. The commercial simulator ECLIPSE 100 with a dual porosity option was selected for this case study.

Basic data for fracture system was already shown in the previous model (black oil model in a fractured system), but additional information such as shape factors, fracture

description, and simulator restrictions should be considered for the construction of this simulation case study.

4.3.2 Shape Factor

A matrix block is defined by shape, volume, and height. In naturally fractured reservoirs, the shape of the matrix blocks is irregular, but for practical studies the block units are reduced to simplified geometrical volumes, such as cubes or parallelepipeds.

The shape factor, also called sigma, is a geometric factor that accounts for the surface area of the matrix blocks per unit volume and a characteristic length associated with the matrix-fracture flow.

Kazemi *et al*. (1977) proposed the following form for sigma:

$$\sigma = 4\left[\left(\frac{1}{Lx^2}\right)+\left(\frac{1}{Ly^2}\right)+\left(\frac{1}{Lz^2}\right)\right]$$

where L_x, L_y and L_z are typical *X, Y, Z* dimensions of the matrix blocks, respectively.

Sigma could be specified as a single value for the whole field and alternatively it could be treated as a simple history matching factor. Ponting (2004) has indicated that assuming a single value per gridblock may represent a significant oversimplification, particularly when a process such as gravity drainage depends heavily on the values.

Table 4.1 illustrates the geometric average dimensions of the matrix blocks. This information was used only for the homogeneous case studies and it considers each block within the reservoir to be identical.

4.3.3 Fracture description

A recent study (Daly, 2004) indicates that construction of a static reservoir model for a fractured reservoir will typically involve some or all of the following steps:

1) Selection of the fracture sets to be considered

2) Identification of the spatial distribution

3) Modeling of the fractures as objects, and

4) Assignment of appropriate petrophysical properties.

Therefore, adequate flow simulation of fractured reservoirs requires determination of the fracture morphology, fracture width, fracture spacing, fracture porosity, fracture permeability, and fracture compressibility.

4.3.3.1 Fracture morphology

An important factor that dictates fracture porosity and permeability is the morphology of the fractures. Fracture morphology can be observed in cores and outcrops and inferred from some well logs. There are four types of natural fracture plane morphology (Nelson, 2001):

1) Open fractures

2) Deformed fractures

3) Mineral-filled fractures, and

4) Vuggy fractures

For our case studies, we have considered that all fractures are completely open and vuggy porosity is part of the fracture system porosity. We also considered that all fractures possess no deformational or diagenetic material filling the width between the walls of the fracture, and that they are potentially open conduits to fluid-flow. In general, open fractures greatly increase reservoir permeability.

4.3.3.2 Fracture width

The fracture opening at reservoir conditions may depend on depth, pore pressure, and type of rock. Experiments performed in the laboratory (Aguilera, 1999) have indicated how fracture width may change during reservoir depletion. But for our

simulation case studies, a constant fracture width was considered through the entire field production time.

In the literature, subsurface fracture widths (2000-5000 ft) show values less than 0.001 cm (Nelson, 2001). However, statistics have shown that the most frequent range is between 0.001-0.004 cm (Van Golf-Racht, 1982). The average fracture width calculated for our case studies was 0.0007 cm using a permeability of 5000 md. This result was obtained by defining the fracture permeability as $K_f=w^2/12$, and considering the vuggy porosity as a part of the fracture system. Rossen (1992) found that wide fractures may cause segregation of phases, which occurs in the reservoir under study.

4.3.3.3 Fracture spacing

Fracture spacing is defined as the average distance between regularly spaced fractures measured perpendicular to a parallel set of fracture of a given orientation (Parsons, 1966). When fractures occur in sufficient spacing or length, the effect on fluid-flow becomes important. For our case studies a fracture spacing of 0.1 fractures per foot was obtained, considering an average matrix height of 10 ft.

4.3.3.4 Fracture porosity

Fracture porosity, like matrix porosity, is the percentage of a particular void volume in a rock mass compared to its total volume. It accounts only for voids occurring between the walls of the fracture system. We must have accurate knowledge of this volume as early as possible to evaluate the reservoir properly, and this estimation must be updated continuously through the early production history with as many methods of calculation as the data permit. Fracture porosity is generally a small number compared to normal matrix porosity. Most good fracture reservoirs possess less than 1% fracture porosity (Nelson, 2001). However, this small porosity value can be important to

production in thick reservoirs and over large drainage areas. For our case study, average fracture porosity is 2% because the vuggy system was considered as a part of the fracture system.

4.3.3.5 Fracture permeability

Fracture permeability is defined as the permeability of a rock in which the fracture is only responsible for the flow of fluids. For our case studies, an average value of 5000 md was considered.

4.3.4 Brief simulator descriptions

We describe some of the special features of the ECLIPSE simulator that was used for our simulation studies:

1) By default, the ECLIPSE simulator multiplies the input fracture permeabilities by the fracture porosity in order to generate an effective permeability, which is used during the entire simulation run. For our case studies the input fracture permeability represents an effective value, therefore the NODPPM keyword, in the ECLIPSE simulator, should be activated in the grid section of the data file in order to override the permeability modification.
2) For case studies constructed under a dual porosity option using ECLIPSE simulators, the number of layers in the *z* direction should be doubled. This is due to the fact that the ECLIPSE simulator associates the first half of the grid with the matrix blocks, and the second half with the fractures.
3) The ECLIPSE simulator has the restriction that wells connect only to fracture cells and not to matrix cells.

4.3.5 Modeling performance

The modeling performance of the black oil with a dual porosity system was achieved in three stages: First, matching the oil production rate at nitrogen injection initiation; second, calculating the field bubble-point pressure and matching reservoir pressures before nitrogen injection; and third, selecting the best gridblock dimension.

4.3.5.1 Matching the field oil production rate

In order to match the field oil production rate before nitrogen injection, an average field bottomhole pressure of 1511 psia (Rodriguez *et al*., 2001) was considered for all the producer wells. We performed several simulation runs using the connection transmissibility factor as a sensitivity parameter to match the field oil production rate.

The connection transmissibility factor was used as a sensitivity parameter because we were not considering the same number of producer wells in the field, their wellbore radius, and skin factor. All the production wells were located at the WOC level in order to reproduce the field boundary conditions.

The connection transmissibility factor is considered in the ECLIPSE 100 simulator for the calculations of volumetric production rate of each phase at stock tank conditions, as is shown in the following expression:

$$q_{p,j} = T_{wj} M_{p,j} (P_j - P_w - H_{wj})$$

where,

T_{wj} is the connection transmissibility factor,

$M_{p,j}$ is the phase mobility at the connection,

P_j is the nodal pressure in the gridblock containing the connection,

P_w is the bottomhole pressure of the well, and

H_{wj} is the wellbore pressure head between the connection and the well's bottomhole datum depth.

Therefore, this parameter depends on the geometry of the connecting gridblock, net thickness of the connection, wellbore radius, and rock permeability, as is shown in the following expression for a Cartesian grid:

$$T_{w,j} = \frac{\theta Kh}{\ln(r_o / r_w) + S}$$

where,

θ is the angle of the segment connecting with the well,

Kh is the effective permeability times net thickness of the connection,

r_w is the wellbore radius,

S is the skin factor, and

r_o is the pressure equivalent radius of the gridblock defined as

$$r_o = 0.28 \frac{\left[D_x^2 \left(\frac{K_y}{K_x} \right)^{1/2} + D_y^2 \left(\frac{K_x}{K_y} \right)^{1/2} \right]}{\left(\frac{K_y}{K_x} \right)^{1/4} + \left(\frac{K_x}{K_y} \right)^{1/4}}$$

where,

D_x and D_y are the x and y dimensions of the gridblock respectively

K_x and K_y are the x and y directional permeabilities respectively

After performing several simulation case studies, the results indicated that:

1) By using a connection transmissibility factor of 155 md-ft with an average bottomhole pressure of 1511 psia for all producer wells, we adequately matched the field oil production rate of 1,500,000 bpd during the nitrogen injection initiation, as is illustrated in Figure 4.5.

2) By injecting 250 MMscf/day in each of the six-injector wells, the oil production rate was almost constant through four years of nitrogen injection after which it started to decline.

The total gas injection of 1,500 MMscf/day used in our case study was approximated to an equivalent of 1,300 MMscf/day of nitrogen by using a gas compressibility factor ratio of 0.8814. This ratio was calculated by considering a gas compressibility factor of 0.903 at 1000 psia and 220 ^{o}F (top reservoir conditions), and a nitrogen compressibility factor of 1.0245 under the same reservoir conditions (Vargaftik *et al*., 1996). This approximation was confirmed by modeling a compositional dual porosity case and is described in detail in Section 4.4.

4.3.5.2 Calculating field bubble-point pressure and matching reservoir pressures

The field bubble-point pressure corresponds to the reservoir pressure at the gas-oil contact. It was obtained by using a set of different pressure values at the gas-oil contact and by matching the monitoring reservoir pressure of 1504 psia at a reference depth (7765 ft). This reference pressure was monitored in the field before the nitrogen injection initiation.

After several simulation runs, we concluded that a simulated bubble-point pressure of 1080 psia is an adequate representation for our case studies. This conclusion was based on the following facts:

1) A pressure of 1076 psia was monitored at the field gas-oil contact before nitrogen injection.
2) A difference of 28 psia was observed between this simulation case study (1532.86 psia) and the field monitoring pressure (1504 psia) at the reference depth (7765 ft).

3) A pressure of 1929 psia was obtained with the simulation case study at the bottom of the system. This location corresponds to the water-oil contact depth (8685 ft) where a field monitoring pressure of 1920 psia was registered before nitrogen injection.

The final reported results were obtained by performing an iterative matching process. First, we matched the pressure distribution; then we re-calculated the connection transmissibility factor and finally we returned to calculate the pressure distribution. Performing this iterative matching, we finally obtained a good representation of the field data (the initial oil production rate and the monitored reservoir pressures).

Because the ECLIPSE simulator determines the initial distribution considering capillary-gravity equilibrium, the pressure distributions in the gas cap reflected small variations between the matrix and fracture systems. But in the oil zone, the distribution of pressure in both systems is practically the same, as is illustrated in Figure 4.6.

4.3.5.3 Vertical grid refinement

In the previous case studies using a black oil formulation, it was observed that oil production rate oscillations are related to the gridblock sizes below the gas-oil contact. Therefore, by refining the grid cells located at the oil zone in a vertical direction, we adequately represented the main direction of the gaseous phase displacement.

The vertical grid refinement considered several simulation case studies, but a grid dimension of $11\times11\times120$ adequately represented the variation of results in this case study. A detailed analysis based on the distribution of nitrogen concentrations is performed in Section 4.4.

Figure 4.7 shows the small variation between case studies with a fine gridblock dimension $(11\times11\times250)$ and the selected gridblock dimension $(11\times11\times120)$. This figure also illustrates that oil production response behaves by cycling variations in all simulated

cases; each cycle size corresponds to the movement of the gaseous phase into the next layer below the oil-gas contact.

These cycling variations were minimized using a smaller grid size in z direction, but as we know, a smaller grid size corresponds to a longer simulation time.

The computing time consumed for the case study with a dimension of 11x11x250 was 88.75 minutes. On the other hand, for a case study with a dimension of 11x11x120, the computation time was 24.6 minutes, both simulating a nitrogen injection process for 10 years.

4.3.6 Analysis of gravity drainage

In fractured reservoirs, the gravity drainage mechanism plays the major role in hydrocarbon recovery from low permeability matrix blocks, when their height is sufficient (Saidi, 1987). The presence of vertical fractures makes gas-oil contact advancement ahead of the gas-oil contact in the matrix blocks. The difference between the density of the fluids and the elevation of the two contacts causes the hydrocarbons to be produced from the matrix block.

In the ECLIPSE simulator, the fluid exchange between the fracture and matrix due to gravity has been modeled by activating the GRAVDRM keyword, which also allows the re-infiltration of oil into the matrix blocks.

Figure 4.8 shows the oil saturation profiles of matrix blocks located at different depths from 6523 ft to 7857 ft. These saturation changes were obtained after simulating the reservoir gas re-injection for 10 years.

The oil saturation profile located at 6523 ft corresponds to the immediate simulation gridblock located below the gas-oil contact, and the last saturation profile located at 7857 ft corresponds to the deepest simulation matrix gridblock where the gravity drainage mechanism occurred.

As we can observe, the shape of the oil saturation profiles are very similar at any depth, with a shift in time. This is because:

1) Same capillary pressures for all the matrix blocks were considered.
2) Capillary pressure for the fracture system was negligible.
3) The pressure difference in matrix and fracture systems is very small (Figure 4.9).

4.4 Isothermal compositional model with a dual porosity system

Typical oil is composed of many components. For this case study, the characterization of the reservoir fluid considers six components, which adequately represent the PVT laboratory experiment by using the two-parameters Peng-Robinson EOS. The fluid characterization is described in Section 4.4.1.

A large number of compositional models have been developed using different equations, variables, and implicitness levels. However, the correct application of those models and the characterization of fractured reservoirs are ones of the most challenging topics in the oil and gas industry.

Some applications of compositional simulators are:

1) Reservoirs with large compositional variations with depth or *x*-*y* direction
2) Temperature variations with depth
3) Oilfield operations involving gas injection or recycling processes
4) Recovery of condensates, and
5) Enhanced oil recovery processes.

In any of these applications, compositional simulation may improve the decision-making by using simple case studies.

Our goals in performing this simulation case study were; first, to determine the nitrogen injection distribution into the gas zone; second, to determine the arrival time of nitrogen at the gas-oil contact of the field under study; and third, to define the impact of

gravity drainage by injecting nitrogen. The commercial simulator ECLIPSE 300 for compositional modeling was used in order to reach these goals.

Data used for the construction of this case study, such as dimension of the gridblocks, rock properties, and rock-fluid properties were same as those used in the black oil case studies (see Sections 4.2 and 4.3).

4.4.1 Fluid characterization

New information concerning the characterization of the fluid, which includes number of components, critical temperature, critical pressure, critical z values, molecular weights, acentric factors, binary interaction coefficients, and the oil composition is necessary for the performance of this simulation case study. Table 4.2 shows the field fluid characterization resulting from a study project made by IFP, Institute Francais du Petrole (PEMEX, personal communication).

The characterization of the reservoir fluid considers six components, which adequately represent the available PVT laboratory experiments using the two-parameter Peng-Robinson EOS. Component 1 was characterized by pure nitrogen, component 2 by methane, component 3 by ethane and propane, component 4 by butane and pentane, component 5 by hexane, and component 6 by C_7^+. The fluid characterization described was also used in the construction of a simulation model for the nitrogen injection of the field under study.

4.4.2 Construction of the simulation case study

The construction of this simulation case study requires specification of the liquid composition in the gas-oil contact at reservoir pressure. The liquid composition of the reservoir fluid at reservoir conditions, immediately before the nitrogen injection, was determined by performing a flash calculation using the PVTi program, which is an

equation of state based from the laboratory analysis of oil and gas samples integrated into the ECLIPSE 300 simulator (Schlumberger simulation software manuals, 2005).

Calculation of liquid composition was achieved by considering a bubble-point pressure of 1080 psia, which was obtained by performing the simulation case study with a black oil formulation. The results are illustrated in Table 4.3.

In order to adequately represent the field conditions before the nitrogen injection process, we matched the simulation results with monitoring field data (pressure and oil production).

4.4.3 Matching reservoir pressure before nitrogen injection

During this stage, the reference pressure (at 7765 ft) obtained using the compositional simulation case study was 1503.23 psia, and the field-monitoring data measured was 1504 psia. This is an indication that initial distribution of pressure in the fracture systems represents practically the same field conditions at that time. These results were obtained using a bubble-point pressure of 1080 psia.

Comparing the reference pressure obtained from the black oil model simulation (1532 psia) and the compositional model (1503.23 psia) we observed a difference, which could be mainly because fluid samples were taken from different production wells and at different times during the field production life. But from a practical point of view, values are similar and its application in the distribution of pressures in the gas-oil contact, oil zone, and the water-oil contact obtained similar pressure results in both models.

4.4.4 Matching oil production rate before nitrogen injection

As we mentioned in Section 4.3, the connection factor was the parameter used to match the field oil production rate.

Several simulation case study results indicated that a connection factor of 133 md-ft adequately matches the field oil production rate before nitrogen injection.

The difference in results from the black oil case study (155 md-ft) could be due to the fact that we used different gas injection rates, or to the difference in PVT properties between the nitrogen and the reservoir gas injected (gas reservoir re-injected in the black oil model and the nitrogen injection in the compositional model).

Computing simulation time using the compositional case study was increased about 4 times (5.6 hrs. per simulation run) compared with the black oil model (88 minutes), both under the same grid dimensions $(11\times11\times120)$, same simulated production time (10 years), and same production strategy.

4.4.5 Analysis of the field oil production rate after nitrogen injection

The oil production rate obtained through both compositional simulation and black oil case studies adequately matched the field oil production rate reported before nitrogen injection (1,500,000 bpd), as is shown in Figure 4.10.

Based on Figure 4.10, as a first approach, we observed that the re-injection of reservoir gas resulted in a lower oil production rate than nitrogen injection, and also, for some unknown reason, we observed that the oil rate oscillations in the compositional model are smaller than in the black oil model. We did not focus on the last topic in detail but we considered that it is an issue that needs more investigation.

The difference in oil production rates obtained by injecting two different gases at the same reservoir conditions and equivalent injection rates was explained after studying the gravity force mechanism that provides different flow patterns under small density variations. This is explained in detail in Section 4.5.2.

4.4.6 Analysis of the nitrogen distribution

Once the isothermal compositional case study adequately reproduced the field monitoring data, we proceeded to analyze the nitrogen movement mainly into the gas cap, the arrival time of nitrogen at the gas-oil contact, and the nitrogen distribution along the GOC, as it is described throughout the following sections.

4.4.6.1 Nitrogen distribution into gas cap

By using Graf software, a post-processor of the ECLIPSE simulator we observed that, during the first four months of injection, up to 85 % of the nitrogen molar concentration was distributed mainly in a vertical direction between the well injector (3850 ft) and the gas-oil contact (6500 ft), rather than in a horizontal direction, as is illustrated in Figure 4.11.

Figure 4.11 shows the distribution of nitrogen concentrations into the gas cap, specifically in six fracture cells located at a reservoir depth of 3935, 4475, 5015, 5555, 6095 and 6523 ft. These cells are located exactly below the injector wells.

4.4.6.2 Arriving time of nitrogen at GOC

The nitrogen concentration profiles illustrated in Figure 4.11 show that a molar concentration of 96 % of nitrogen reaches the GOC after 200 days of injection using 11x11x120 simulation grid cells. The rapid movement of nitrogen through the gas-oil contact due to the gravity force mechanism occurs during the first four months after the initiation of the injection (Vicencio *et al*., 2004).

4.4.6.3 Nitrogen distribution along the GOC

We also plotted the nitrogen molar concentrations in a horizontal direction along the GOC (6523 ft) in six field locations that are illustrated in Figure 4.12. The first location, P1, corresponds to the fracture cell at the gas-oil contact in a vertical direction

with respect to the injector well; the second, P2, is located at the gas-oil contact separated 2500 ft in a radial distant from P1. The remaining four locations are distributed under the same sequence as P1 and P2.

Nitrogen molar concentrations in the fracture system of the six cells are illustrated in Figure 4.13, which indicates that after the nitrogen concentration reached the gas-oil contact, it is spread mainly in a horizontal direction. This horizontal nitrogen spread occurs more rapidly at the gas-oil contact depth, rather than at the top of the reservoir.

Simulation results indicated that in location P6, (at 12500 ft away from P1), a nitrogen molar concentration of 57% lasted around 1000 days after nitrogen injection initialized; in other words, the highest nitrogen distribution was mainly in the center part of the reservoir at the gas-oil contact.

Figures 4.14 and 4.15 illustrate two cross sections in x and y directions, which show the nitrogen molar concentration profiles in the fracture system after 3600 days of injection.

4.5 A quarter representation of the full isothermal compositional dual porosity case study

The symmetric movement at the front, observed with the full-simulation case study, is mainly due to the consideration of homogeneous and isotropic fracture and matrix permeabilities, and also because of the steady movement of the gas-oil contact. Taking advantage of the symmetry, we reduced our problem size to a quarter of the original model, as is described in our next simulation case study.

The analysis of simulation case studies with a quarter of the full-system representation reduced the computing time not only for the isothermal compositional case but for the first thermal case studies as well. This reduction of the system allowed us to

carry out several additional simulation runs, using grid refinements in order to obtain better computational accuracy.

The quarter full-system representation was constructed by achieving the following modifications based on transmissibility definitions and material balance:

1) Reduction in a quarter of the total field injection rate (54,166.5 MMscf/day/well),

2) Reduction in a half (of its original value) of the well connection transmissibility factor (65.505 md-ft) for cells located at the bottom system along the inside planes.

3) Reduction in a quarter of the well connection transmissibility factor for cells located at the bottom system but towards the well injector (33.2525 md-ft)

4) A transmissibility multiplier of 0.75 in x and y directions for inner cells with no producer wells.

The results obtained with the quarter representation were validated by comparing the results of the full system, as is described below.

First, we compared the variation of nitrogen molar concentrations into the gas cap at 3935, 4475, 5015, 5555, 6095 and 6523 ft, as illustrated in Figure 4.16. These locations correspond to the cells distributed in a vertical direction between the well injector and the gas-oil contact. Figure 4.16 indicates that adequately using a quarter full-system representation, we could simulate the vertical variations of nitrogen molar concentrations in the gas cap.

Second, we compared the variations of nitrogen molar concentrations along the gas-oil contact for the locations P1, P2, P3 and P4, and we observed the same response in both representations, as illustrated in Figure 4.17.

Third, we compared other simulation variables like oil production rate, saturation, and reservoir pressures, which indicated that reducing the full case study by a quarter, we would have the same response.

Simulation time for the quarter of full-system (6x6x120) was 1.343 hrs, which shows a reduction of about four times the simulation time compared with the full system (11x11x120).

A three-dimensional representation of the quarter system is shown in Figure 4.18, which illustrates the nitrogen molar concentrations in the fracture system after injecting nitrogen for 3000 days.

Once we adequately matched the reservoir fluids movement, we reduced the simulation grid size at the center of the reservoir for a better representation of the nitrogen distribution. The analysis of the grid refinement with the quarter representation is described in the next section.

4.5.1 Grid refinement study

We performed a grid refinement study in both x and y directions. After several simulation runs, we observed that smaller grid sizes at the reservoir center caused longer computational time for the simulation to complete. The cell size reduction and increasing number of cells considerably increase the reservoir simulation time, as shown in Figure 4.19. This figure illustrates four representative cases of the grid refinement study. Detailed description about each grid dimension for various cases is shown in Table 4.4.

The results of several simulation case studies were compared to define the best grid representation. Field oil recovery behavior is illustrated in Figure 4.20 and reservoir pressure behavior at 5897 ft in Figure 4.21. Both figures indicate that there is no significant variation of such properties with respect to the grid dimension changes.

During the grid refinement study, we observed that the nitrogen molar distributions behave differently in respect to the reservoir pressure and oil recovery. This is because nitrogen molar concentration and oil matrix saturation are more sensitive to the grid dimension variations.

Figures 4.22 and 4.23 illustrate the nitrogen molar concentration at the gas-oil contact and at the oil zone location (5897 ft), respectively. In Figure 4.22 grid dimensions of $13\times13\times120$, $11\times11\times120$, and $9\times9\times120$ represent practically the same nitrogen concentration behavior. And as was expected, the simulation with the smallest number of gridblocks consumed less computing time. Figures 4.23 and 4.24 show a grid refinement study for nitrogen molar concentration in the oil zone and matrix oil saturation, respectively. As can be seen, the results presented using $11\times11\times120$ and $13\times13\times120$ gridblock dimensions are virtually the same in both cases.

Based on results and computing times, we decided that a grid dimension of $11\times11\times120$ adequately represents the nitrogen distribution and movement of fluids into the quarter full-system. Once we defined the grid dimensions, we were able to study the main mechanism acting during the nitrogen injection into naturally fractured reservoirs.

4.5.2 Gravity force mechanism study

Gravity force is a mechanism that acts when we inject a fluid into a reservoir that has a different density than the fluid that resides in the reservoir. In our simulation case study, the difference in density between the nitrogen injected and the reservoir gas resulted in a nitrogen movement straight to the gas-oil contact because gravity forces destabilize the displacement.

4.5.2.1 Injection of nitrogen at the top of gas cap

The literature review about the gravity force mechanism (Lake, 1989) indicates that nitrogen injection in our simulation case study corresponds to a conditionally stable case, where viscous forces stabilize the displacement and gravity forces destabilize with gravity instability as a result.

The flow stability analysis was obtained after calculating $M^o < 1$ and $\Delta\rho g \sin\alpha < 0$; where

$$M^o = \frac{K^o_{r1}\mu_2}{K^o_{r2}\mu_1}$$

$\Delta\rho = (\rho_1 - \rho_2)$ and $\alpha = -90^0$.

K^o_{r1} is the end point relative permeability of the displacing fluid (nitrogen)

K^o_{r2} is the end point relative permeability of the displaced fluid (reservoir gas)

μ_2 is the displacing fluid viscosity (nitrogen)

μ_1 is the displaced fluid viscosity (reservoir gas)

ρ_1 is the displacing fluid density (nitrogen)

ρ_2 is the displaced fluid density (reservoir gas)

The results are obtained under the condition that relative permeability sets are the same for nitrogen and reservoirs gas. The viscosity ratio of the fluid displaced (gas in reservoir) and gas displacing (nitrogen) at reservoir conditions is

$$\frac{\mu_{reservoir\ gas}(cp)}{\mu_{nitrogen}(cp)} = \frac{0.013}{0.023} = 0.56, \text{ and}$$

$$\Delta\rho g \sin\alpha = (3.79 - 3.421)(lbm/ft^3) \quad Sin(-90) < 0$$

During the initial stage of the simulation (no nitrogen injection), it was observed that under static conditions the density of the gaseous phase in the fracture system at the top of the reservoir (3935 ft) was 3.423 lbm/ft^3 and 3.640 lbm/ft^3 at the gas-oil contact

(6365 ft, Cell 61), and the corresponding cell pressures were 1028.843 psia and 1088.428 psia. After 170 days of nitrogen injection, the nitrogen molar concentrations at both locations were almost 100% (99.99% at 3935 ft and 98.06 % at 6365 ft). At that time, the density of the gaseous phase at the top of the reservoir was 3.9 lbm/ft^3 and 4.23 lbm/ft^3 at the gas-oil contact, as illustrated in Figure 4.25. This density variation occurred due to small changes in the reservoir pressure (1029.911 psia at the top and 1091.602 psia at 6365 ft).

This behavior indicates that small density variations between the reservoir gas and the injected nitrogen have caused the nitrogen to move in a vertical direction toward the gas-oil contact, and then spread horizontally along the gas-oil contact.

Figure 4.25 shows that the variation in densities between nitrogen injected and the gas in the reservoir is a very important parameter that we must consider for an adequate representation of the gas injected into the gas cap.

The cone-shaped distribution of the injected nitrogen in the gas cap fractures has been observed by other authors (Rodriguez *et al*., 2004), who simulated the same field using a complex geologic model.

4.5.2.2 Injecting CH_4, reservoir gas and N_2 at the top of gas cap

In our simulation case study, the gas cap thickness is approximately 2700 ft. Consequently, the gravity force mechanism is very important because it determines if the injected gas is moving straight towards the gas-oil contact, remaining at the top of the reservoir, or following a special geometric distribution. We performed the gas injection simulation under isothermal conditions and at the same reservoir conditions with three different gases: methane (CH4), which has less density than the reservoir gas; reservoir gas (mixture), which has the same density as the gas at reservoir conditions; and nitrogen, which has a density higher than the reservoir gas.

The results indicated that, if the density of the injected gas is less than the reservoir gas, the injected gas will stay at the top of the reservoir and the gravity drainage mechanism will act with in-situ reservoir gas. For gases with the same reservoir gas density, the flow pattern distribution follows a semi-spherical flow pattern since gas frontal movements are the same in *x*, *y* and *z* directions. For nitrogen with a density higher than the reservoir gas, it will move straight to the gas-oil contact rapidly, and the gravity drainage mechanism will act with high nitrogen molar concentrations mainly at the center of the reservoir, and lower nitrogen concentrations away from the injector wells (Vicencio *et al*., 2004).

Figures 4.26, 4.27 and 4.28 show the flow pattern for each case study, considering the same reservoir injection conditions (900,000 Mscf/day) and the same bottomhole pressure (1511 psia). Figure 4.28 also illustrates that once the nitrogen has reached the gas-oil contact, it spreads in a horizontal direction.

The variation of gas phase density at the top of the reservoir during 170 days of injection is illustrated in Figure 4.29. We also observed the different flow pattern distributions by analyzing Figure 4.29, which also indicates the gaseous phase density during the initiation stage of the injection process.

Additional analysis was performed by using the field oil total production of each case. Results have indicated that by injecting nitrogen for four years, the oil recovery is higher than the other two simulated cases. Such results are illustrated in Figure 4.30.

Higher oil production rates were achieved by injecting nitrogen because nitrogen has more contact area with the oil in the field, and this increases the sweep efficiency. The nitrogen movement along GOC in Figure 4.31 shows the expansion of the contact area of nitrogen with reservoir oil during 0, 120, 500, 1000, and 1500 days of injection.

The oil matrix drainage depends on the injected gas properties. Therefore, injection of three different gases (methane, reservoir gas and nitrogen) was also reflected in the oil saturation of the matrix blocks. Figure 4.32 illustrates the oil saturation of a simulation matrix cell located at 6937 ft in the center of the reservoir by injecting different gases. Simulation results have indicated that oil matrix drainage by injecting nitrogen is faster than the other gases, because nitrogen injection increases the sweep efficiency. The flow pattern distribution also impacts the computing time. For nitrogen injection, the computing time was 5.96 hrs, for reservoir gas re-injection, 1.41 hrs, and for methane injection, 1.24 hrs. Each of these three cases simulated 1500 days of injection.

4.6 Compositional thermal dual porosity model

In order to simulate the temperature impact of nitrogen injection at surface conditions, we conducted a thermal compositional case study, in which pressure, saturation, temperature and nitrogen distributions matched the isothermal compositional dual porosity case study under both static and dynamic conditions.

Finding the impact of nitrogen injection at low temperature conditions is one of the main goals of this research. This is because the high-density values of nitrogen could accelerate its movement in the reservoir, causing possible channeling and early breakthrough. This behavior can be observed by analyzing Figure 4.33, which shows the variation of nitrogen density with respect to pressure and temperature.

Figure 4.33 also illustrates the gaseous phase density at reservoir conditions (1100 psia and 220 ^{o}F). We observed that by injecting nitrogen at surface conditions (80 ^{o}F) or lower temperatures, and maintaining the pressure of the reservoir or even increasing it after nitrogen injection, the density differences between the nitrogen injected and the reservoir gas at reservoir conditions become higher.

The ECLIPSE 300 simulator with the thermal dual porosity option was used for our simulation case studies. This simulator enables modeling thermal oil recovery in fractured reservoirs in which there are temperature changes. The limitation of the ECLIPSE 300 simulator for our case study is that EOS is not available with the thermal option. Therefore, we performed K-values calculations by flashing the PVT data at a wide range of reservoir pressures and temperatures. We obtained K-values for each component by using a correlation, as is explained in Section 4.6.2.3.

The construction of a thermal model considering the molar concentration changes is a challenge, since many simulation problems deal with isothermal conditions and also because the development of thermal models in many commercial simulators are used for the simulation of oil reservoir with high viscosity values. The simulation of heavy oil by thermal methods considers correlations for the fluid properties with respect to temperature and pressure, instead of equations of states, to characterize the reservoir fluid. This is also the case for the thermal commercial simulator ECLIPSE 300.

4.6.1 Reservoir rock thermal properties

The data used to construct the thermal case study concerns the thermal properties of the fluids and the rock. The rest has been described in the previously studied cases.

Since most of the thermal data was not provided for our simulation study, we had to use the correlations from the literature and apply them adequately, based on the rock characteristics.

Reservoir rock properties for our simulation thermal case study were rock thermal conductivity, rock heat capacity, and matrix-fracture thermal conductivities.

4.6.1.1 Rock thermal conductivity

The heat transfer in rocks with small porosity is essentially dominated by heat conduction. Heat flow density q for heat conduction is proportional to the temperature gradient: $q = - \lambda * \text{grad } T$ (Fourier law).

Here the constant λ is a measure of the capacity of the investigated rock to conduct heat and is called thermal conductivity. Therefore, the thermal conductivity, λ, is the quantity of heat transmitted, due to the unit temperature gradient, in unit time under steady conditions in a direction normal to a surface of the unit area.

Thermal conductivity of many sedimentary rocks is strongly anisotropic. When no data is available or no direct measurements can be performed, thermal conductivity can be inferred from a number of indirect data: mineralogical composition and fluids saturation, well-log correlations, and correlations with other parameters. While some of these methods are based on well-defined physical models, others are purely empirical.

Rock thermal conductivities are considered to have a constant value at room temperatures to 200 ^{o}F. Prats (1986) presented extensive correlations for reservoir, rock and, mineral types. For a pure mineral calcite, 49.8 Btu/ft/day/^{o}F is an average thermal conductivity value. Coats (1980) assume that thermal conductivity is a function of the gas saturation only. This implies that the thermal conductivity of a rock filled with liquid is independent of whether the liquid is oil or water, and is the same whatever the porosity of the rock. Others (Clauser and Huenges, 1995) show a variation of thermal conductivity with temperature for carbonates, which corresponds to the formation type of our case study. A value of 33.89 Btu/ft/day/^{o}F was used for our thermal case.

4.6.1.2 Rock heat capacity

The amount of energy needed to raise the temperature of a rock is proportional to the temperature increase and to the size of the rock. The amount also depends on what the

rock is made of. Rock heat capacity is the amount of energy needed to raise the temperature by 1 ^{o}F. For our thermal case study, we use a value of 39 Btu/ft^{3}/^{o}F, which is an average value for limestone at 200 ^{o}F (Prats, 1986).

4.6.1.3 Matrix-fracture thermal conductivity

The matrix-fracture thermal conductivity property allows changes of thermal conductivity values surrounding the matrix block. For all matrix blocks, we used the same value as the matrix thermal conductivity (33.89 Btu/ft/day/^{o}F).

4.6.2 Fluid thermal properties

The construction of a thermal simulation case study characterizing the reservoir fluid using several hydrocarbon components requires the thermal properties for each component as input data for the simulator.

For our simulation case studies some thermal properties were specified for each component, but others were defined as an average based on phase behavior. The thermal properties used for our cases were oil specific heat, heat of vaporization, equilibrium constant K, thermal expansion, and fluid (oil and gas) viscosities as a function of temperature.

4.6.2.1 Oil specific heat

The specific heat is the amount of heat per unit mass required to raise the temperature by 1 ^{o}F. By using the ECLIPSE simulator, the specific heat values must be given for each hydrocarbon component in at least one phase.

The oil specific heat was obtained through the literature by using the correlation of Gambill (Prats, 1986), which relates oil specific heat to temperature and oil gravity: $Co = 4.186\left(0.388 + 0.00045T\right)/\sqrt{\gamma_o}$; where, Co is oil specific heat (kJ/kg/^{o}C), T

is temperature (^{o}C) and γ_o is oil gravity. We can observe in this correlation that the higher molecular weight results the lower specific heat in the oil.

For our simulation case study, pure nitrogen (defined as PS1 in Table 4.5) specific heat was obtained by the Shomate equation (National Institute of Standards and Technology, NIST, 2003), which is similar to the correlations given in the literature (Vargaftik *et al*., 1996; Young, 1991, and Sychev *et al*., 2000). The oil specific heat values shown in Table 4.5 were obtained at reservoir temperature conditions (220 ^{o}F) and used for the thermal simulation case studies.

4.6.2.2 Heat of vaporization

The heat of vaporization is the amount of heat required to vaporize one gram of a liquid at its boiling point with no change in temperature. Usually it is expressed in J/g but in our simulation cases it was specified as BTU/lbm. This property is important for obtaining the enthalpy of gaseous components.

The heat of vaporization for each component is defined as $\Delta H(T) = A(1-T/T_c)^B$ for temperature, $T <$ critical temperature, T_c; and $\Delta H(T)=0$ for $T > T_c$.

Heats of vaporization are usually obtained at the normal boiling point. Therefore, the constant A is defined as $A=\Delta H_{nb}/(1-T_{nb}/T_c)^B$, where ΔH_{nb} is the heat of vaporization at the normal boiling point, and T_{nb} is the normal boiling point. The exponent B is usually defaulted to 0.38. For the nitrogen component we used published data (Carlyle, 1998, Winokur, 2004). The heat of vaporization values used for our simulation case studies are illustrated in Table 4.6.

4.6.2.3 Equilibrium constants

Equilibrium constants K_i are defined as $K_i = y_i / x_i$, where y_i and x_i are experimentally determined values of the compositions of the gas and liquid that exist at equilibrium at a given pressure and temperature.

We performed K-value calculations by flashing the PVT data at a wide range of reservoir pressures and temperatures, and then we calculated the K-value for the components using a correlation.

The ECLIPSE 300 simulator with the thermal option provides three methods to calculate oil component K-values: Crookston correlation, Wilson correlation, and entering the K-values as tables.

For our thermal case study, we used the Wilson correlation, which considers the critical properties of the fluid characterization. The Wilson correlation is expressed as

$$K(P,T) = e^{5.372697(1+Ac(1-(T/Tc)))} \frac{P_c}{P}.$$

where,

Ac is the acentric value

Tc is the critical temperature

Pc is the critical pressure.

By plotting K-values against pressure in a semi-log scale for the Wilson correlation and flash calculations, we observed parallel trends for the pressure values in the range of interest, as illustrated in Figure 4.34. Therefore, we decided to adjust the Wilson correlation K-value by changing critical pressure values to obtain a good match with the flash calculations, as illustrated in Figure 4.35. The new critical pressure values that matched the flash calculations are illustrated in Table 4.7.

4.6.2.4 Thermal expansion coefficient

The coefficient of isobaric thermal expansion, β, is defined as the fractional change in volume of a liquid as temperature changes under constant pressure where $\beta = (1/V)(\partial V/\partial T)_p$; this definition in terms of density follows $\beta = (-1/\rho)(\partial\rho/\partial T)_p$. The thermal expansion coefficient is usually assumed to be constant over a limited range of temperatures. For a small change in temperature, such expression can be approximated by $V_2=V_1(1+\beta(T_2-T_1))$. Petroleum reservoir engineers rarely use this liquid property since petroleum reservoirs are normally operated at constant temperature, but in our simulation case study it is important to define the thermal expansion coefficient because we need to know the gas and oil density changes with respect to temperature.

The literature (Prats, 1986) provides a correlation based on the crude density at 60 ^{o}F. But the PVT fluid studied shows a good approximation by using Farouq Ali correlation (Prats, 1986), which indicates that a value of $5x10^{-4}$ $^{o}F^{-1}$ can be used for our case study.

The oil density calculation at any pressure and temperature in ECLIPSE 300 is a function of the thermal expansion coefficient, β, the component isothermal compressibility , C_P, and the oil reference density, ρ_{ref} . Oil density is calculated based on the following expression:

$$\rho_{oil} = \frac{\rho_{ref}}{\left(1+\beta\left(T-T_{ref}\right)\right)\left(1-C_P\left(P-P_{ref}\right)\right)}$$

where,

ρ_{ref} is the oil reference density at reference temperature T_{ref} and reference pressure P_{ref}.

In our simulation cases, reference points were considered at surface conditions. A value of $6.9x10^{-6}$ was considered for the isothermal oil compressibility and an oil reference density of 54 lbm/ft^3.

4.6.2.5 Oil viscosity as a function of temperature

The oil viscosity for all oil pseudo-components was considered equal. It was obtained for a correlation based on the oil phase (McCain Jr., 1998). Figure 4.36 illustrates the oil viscosity variations with respect to temperature.

4.6.2.6 Gas viscosity as a function of temperature

The literature (Prats, 1986) provides gas viscosity correlation for each pseudo-component, as illustrated in Figure 4.37.

Because 80% of gas composition corresponds to methane, which is the pseudo-component PS2, the gas viscosity at reservoir conditions before nitrogen injection is 0.013 cp, a similar value to methane gas viscosity.

During nitrogen injection, the gaseous phase viscosity changed because nitrogen has 44% higher viscosity (0.023) than the gas in place at the same reservoir temperature (221 ^{o}F).

4.6.3 Reservoir simulation study

4.6.3.1 Well injector simulation constrains

Since it is necessary to define the thermal boundary conditions in the injector wells, we studied the nitrogen properties to define the state conditions of such gas at the injecting pressure in the bottom of the wells. By using the nitrogen vapor pressure illustrated in Figure 4.38, we found that nitrogen injection at reservoir pressure (1000 psia or higher) and at reservoir temperature (60 ^{o}F or higher) stays in the gaseous phase. Therefore, we defined the following constraints in the nitrogen well injectors:

1) A constant injection temperature at the bottom well and
2) Nitrogen quality equal to 1.0

4.6.3.2 Verification of the thermal case study

The analysis of reservoir temperature distribution was performed with the full system in order to consider the total energy available in the reservoir. For practical purposes, the verification of the thermal case study with respect to the isothermal case study was performed by using a quarter of the original thermal representation. The thermal case study was tested by comparing the static and dynamic flow models under isothermal and thermal conditions for the quarter of full-system, as described in the following sections.

4.6.3.2.1 Calibration of thermal case study under static conditions

The case study considering thermal compositional option with a dual porosity in a quarter full-system representation was simulated for 100 days with no nitrogen injection. The variations of pressure, temperature, gas density, and oil density with respect to depth in the fracture system are illustrated in Figures 4.39, 4.40, 4.41 and 4.42, respectively. The figures show similar trends in the thermal model under static conditions and in the isothermal compositional model.

4.6.3.2.2 Calibration of thermal case study under dynamic conditions

The simulation results of a thermal compositional case study by injecting the nitrogen at reservoir temperature can be compared with the isothermal compositional results, if both are under the same dynamic conditions.

The simulation results of our thermal and isothermal compositional case studies, with a dual porosity in a quarter of full-system representation, are illustrated in Figures 4.43, 4.44, 4.45 and 4.46, which show the nitrogen vertical distributions, nitrogen horizontal distributions, reservoir pressures and gas saturations, respectively. These simulations considered a nitrogen injection at 220 ^{o}F over 1500 days.

These figures illustrate a similar flow behavior between both case studies. The results can be confirmed visually or by animation in Figure 4.47, which shows the nitrogen distribution during 100, 1000 and 1500 days of nitrogen injection in the fracture system.

4.6.3.3 Reservoir temperature variations by injecting nitrogen at standard conditions

Gas temperature injection in fractured reservoirs plays an important role in the flow pattern distribution especially when the differences in densities for the injected gas and resident gas become significant.

The injection of nitrogen at 60 ^{o}F during 1500 days indicates that the temperature changes mainly occur close to the injector well, particularly in the center of the reservoir, and that negligible temperature changes occur in the oil zone.

Figure 4.48 illustrates the temperature profiles by injecting nitrogen at 60 ^{o}F. We also observed that, after injecting the nitrogen at 60 ^{o}F for 300 days, the reservoir temperature around the injector wells dropped close to 60 ^{o}F. Reservoir gas temperature then slowly increases following a linear trend. This temperature behavior was observed at all depths. Figure 4.49 shows the temperature variations; as we can observe, the area affected by injecting nitrogen at low temperatures is small and it is only in the gas cap zone.

Since significant temperature changes occur mainly in the gas cap, a possible convection phenomenon could occur only within this zone, and could be present mainly between the injector well and the GOC. However, Rodriguez (2004) indicated that thermal convection does not seem to play a role in the dynamics of the flow of fluids in the field study.

4.6.3.4 Nitrogen molar concentrations by injecting the gas at higher temperatures

The injection of nitrogen at a higher temperature (900 ^{o}F) decreases the reservoir gas density. The temperature changes occur also in the upper part of the gas cap as seen in Figure 4.50. Due to these temperature changes, the injected gas density becomes less than the gas reservoir density, therefore nitrogen density changes affect the gravity force mechanism.

The results indicated that the variations of the nitrogen molar concentrations occur mainly in the gas cap at the top of the reservoir, as we observe in Figure 4.51. Since, from a practical point of view, the flow pattern at 900 ^{o}F is similar to the flow pattern for the isothermal compositional case, we concluded that injection at higher temperature does not impact nitrogen distribution in the reservoir. The effect of temperature on nitrogen distribution, in this case, is limited due to the fact that large variations in gas densities occur mainly in a small part of the gas zone in the reservoir.

Table 4.1 Geometric dimension of matrix blocks used for dual porosity case studies.

L*x* (ft)	L*y* (ft)	L*z* (ft)	Sigma $(ft)^{-2}$
5	5	10	0.36

Table 4.2 Fluid characterization based on Peng-Robinson EOS used for compositional dual porosity case studies.

Property	Pseudo-components					
	PS1	PS2	PS3	PS4	PS5	PS6
	N_2	C_1H_4	C_2H_6-C_3H_8	C_4H_{10}-C_5H_{12}	C_6H_{14}	C_7^+
Critical temperature (^oF)	-227.00	343.10	598.92	795.12	913.00	1420.0
Critical pressure (psia)	492.00	667.40	669.18	519.38	431.00	220.0
Critical *Z* values	0.30	0.30	0.30	0.30	0.30	0.31
Molecular weight	28.01	16.04	36.03	64.72	86.18	323.0
Acentric factor	0.040	0.008	0.121	0.213	0.296	0.590
Binary interaction coefficients	0.100					
	0.140	0.010				
	0.160	0.020	0.000			
	0.180	0.030	0.010	0.000		
	0.240	0.090	0.030	0.010	0.000	

Table 4.3 Liquid composition at reservoir conditions obtained from flash calculations using PVTi program.

Pseudo-component	PS1	PS2	PS3	PS4	PS5	PS6
Liquid composition	0.0008	0.1747	0.1415	0.0962	0.0370	0.5498

Table 4.4 Grid refinement data with cell dimension variations in *x* and *y* directions for four representative case studies.

Case	Gridblock Dimension	X Cell Size (ft) at the center of reservoir Cells: (1-11,11,1-120)	X Cell Size (ft) at reservoir edge Cells: (1-11,1,1-120)	Y Cell Size (ft) at the center of reservoir. Cells: (11,1-11,1-120)	Y Cell Size (ft) at reservoir edge Cells: (1,1-11,1-120)
CASE I	6x6x120	1050	2100	1575	3150
CASE II	9x9x120	525	2100	787	3150
CASE III	11x11x120	150	2100	150	3150
CASE IV	13x13x120	150	2100	150	3150

Table 4.5 Oil specific heat data for each pseudo component at 220 ^{o}F used for thermal dual porosity case studies.

Pseudo-Component	Components	Oil specific heat (Btu/lbm/^{o}F)
PS1	N_2	0.5418
PS2	C_1H_4	0.8899
PS3	C_2H_6-C_3H_8	0.8000
PS4	C_4H_{10}-C_5H_{12}	0.6600
PS5	C_6H_{14}	0.6100
PS6	C_7^+	0.5000

Table 4.6 Heat of vaporization of each pseudo component for thermal dual porosity case studies.

Pseudo-Component	Components	Heat of vaporization (BTU/lbm)
PS1	N_2	122.82
PS2	C_1H_4	306.99
PS3	C_2H_6-C_3H_8	286.114
PS4	C_4H_{10}-C_5H_{12}	240.438
PS5	C_6H_{14}	220.474
PS6	C_7^+	-

Table 4.7 Critical pressure values from flash calculations and adjusted Wilson correlation.

Pseudo-component	Components	Critical pressure by EoS (psia)	Critical pressure adjusted (psia)
1	N_2	492.00	240.00
2	C_1H_4	667.40	350.00
3	C_2H_6-C_3H_8	669.18	669.18
4	C_4H_{10}-C_5H_{12}	519.38	1200.00
5	C_6H_{14}	431.00	1600.00
6	C_7^+	220.00	2500.00

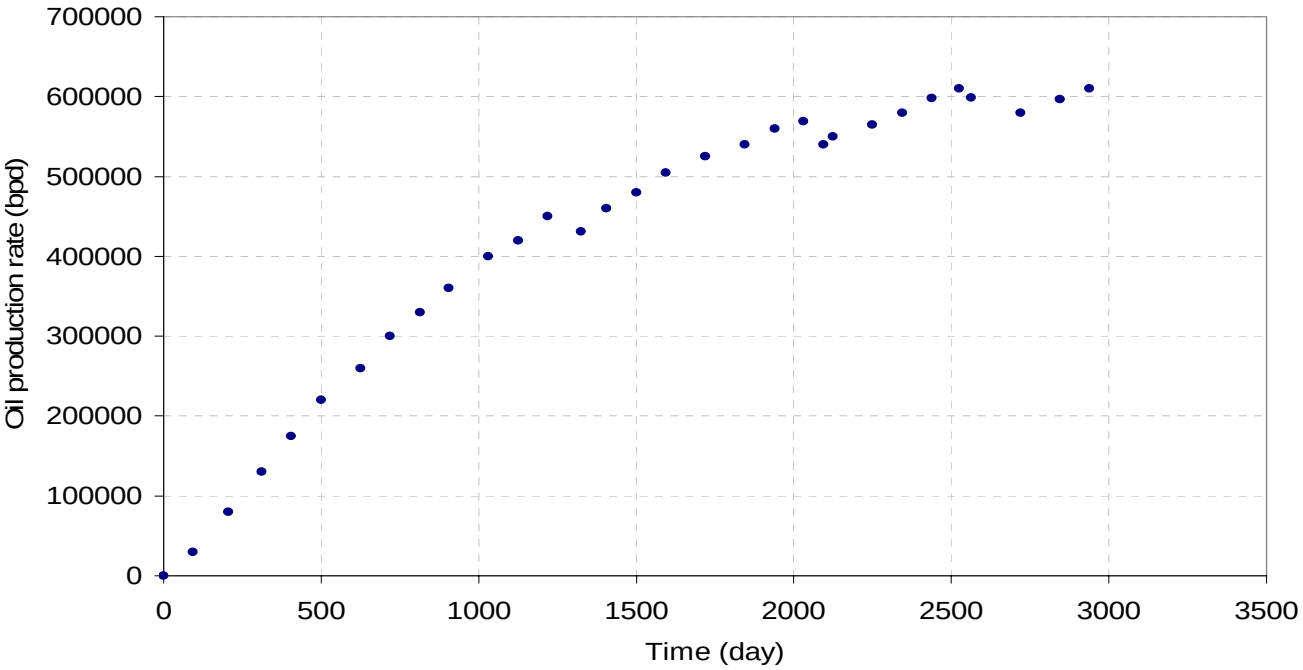

Figure 4.1 Oil production rate trend considering a BHP of all producer wells similar to WOC pressure for the black oil fractured system.

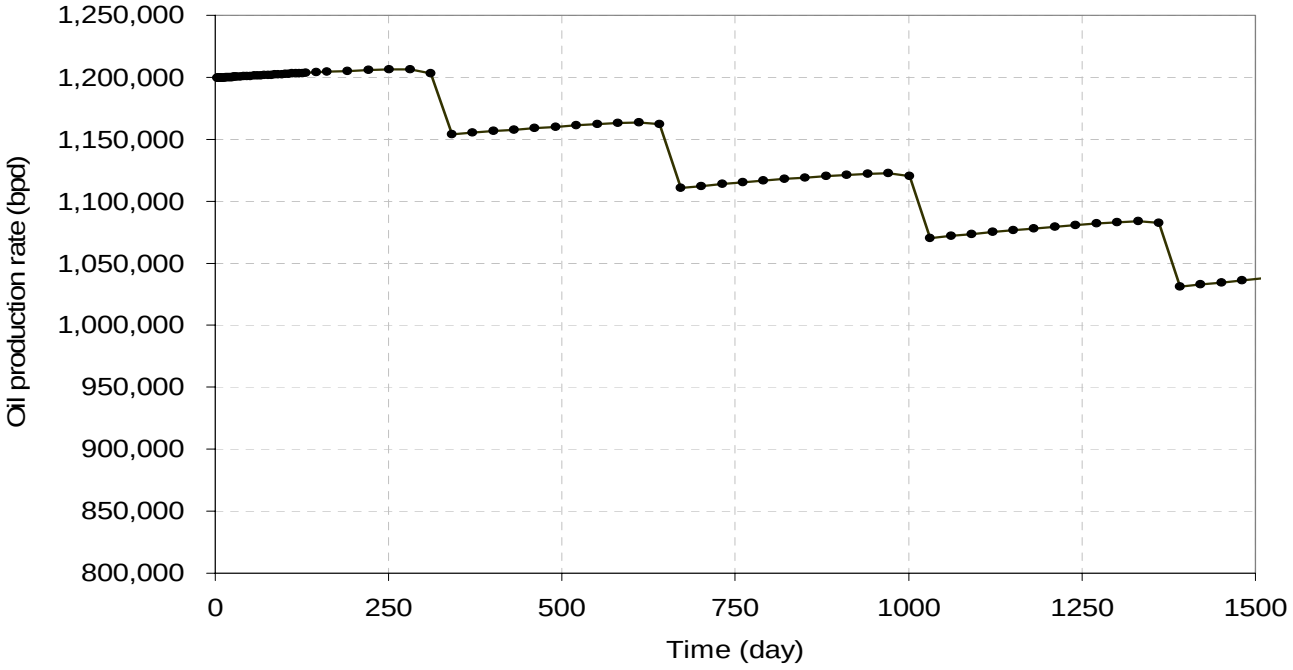

Figure 4.2 Oil production rate trend considering BHP=1720 psia for the black oil fractured system.

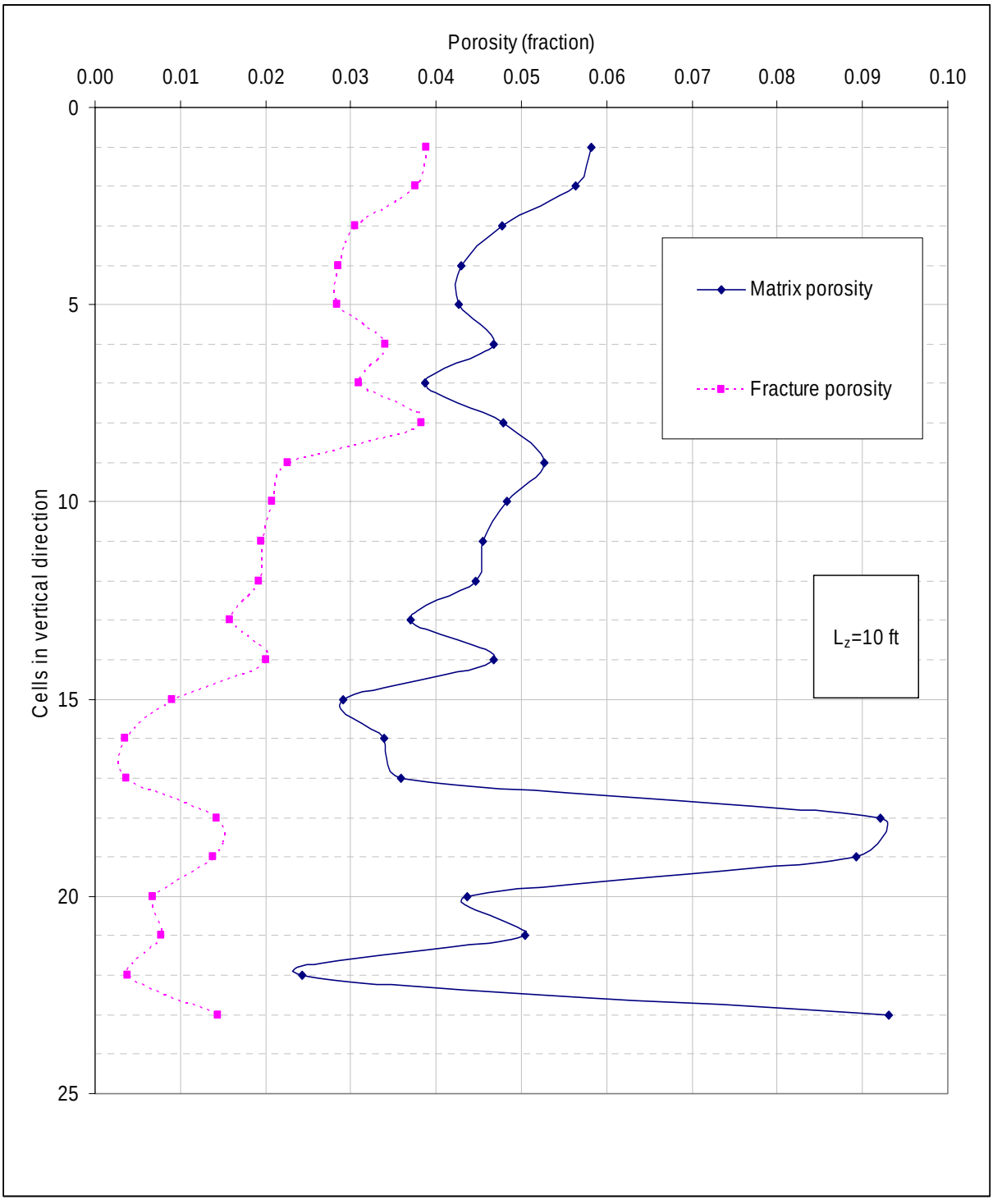

Figure 4.3 Matrix and fracture porosities of a vertical cross section at the center of the field under study.

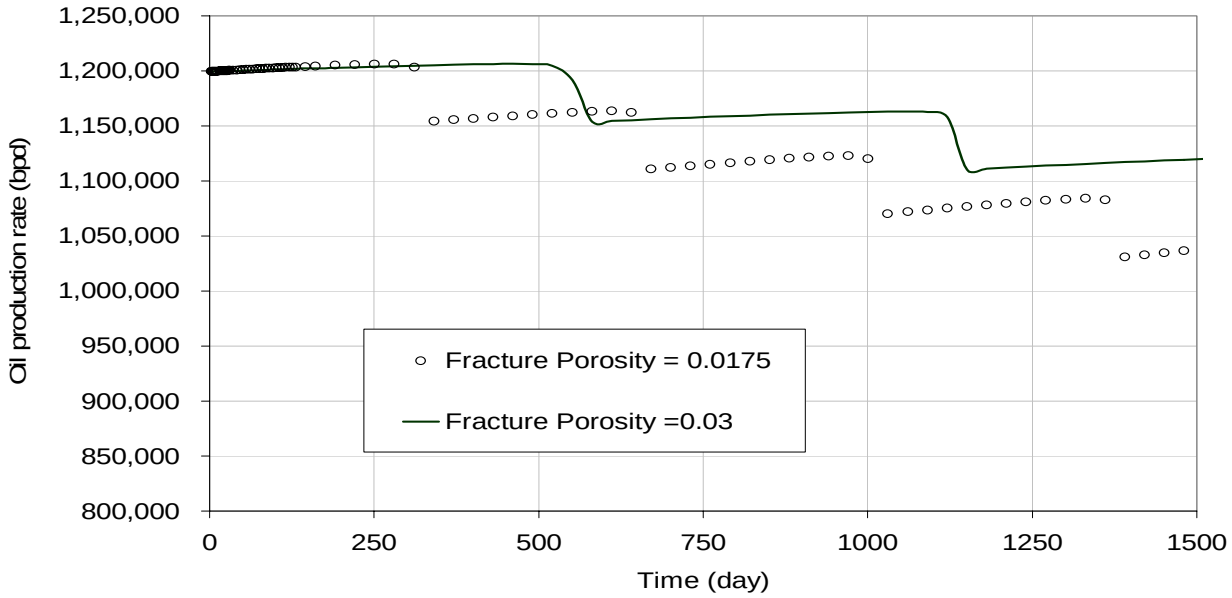

Figure 4.4 Oil production rate trend with two average fracture porosity values (0.0175 and 0.03) for the black oil fractured system.

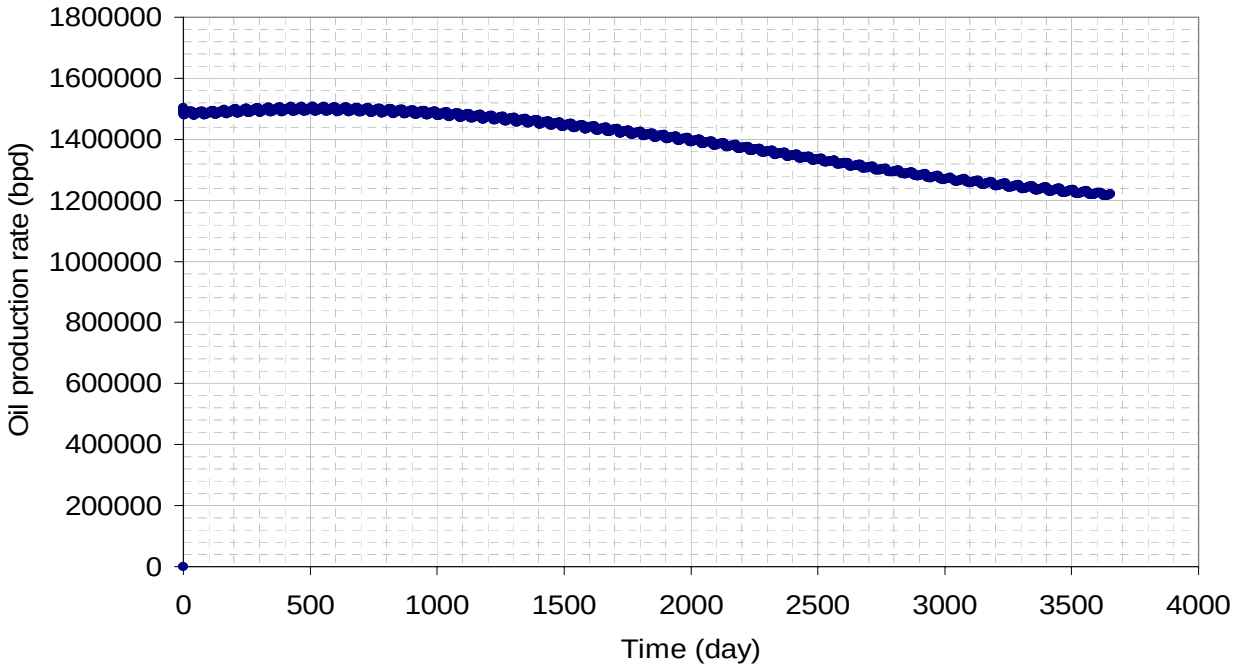

Figure 4.5 Oil production rate trend for a black oil dual porosity system.

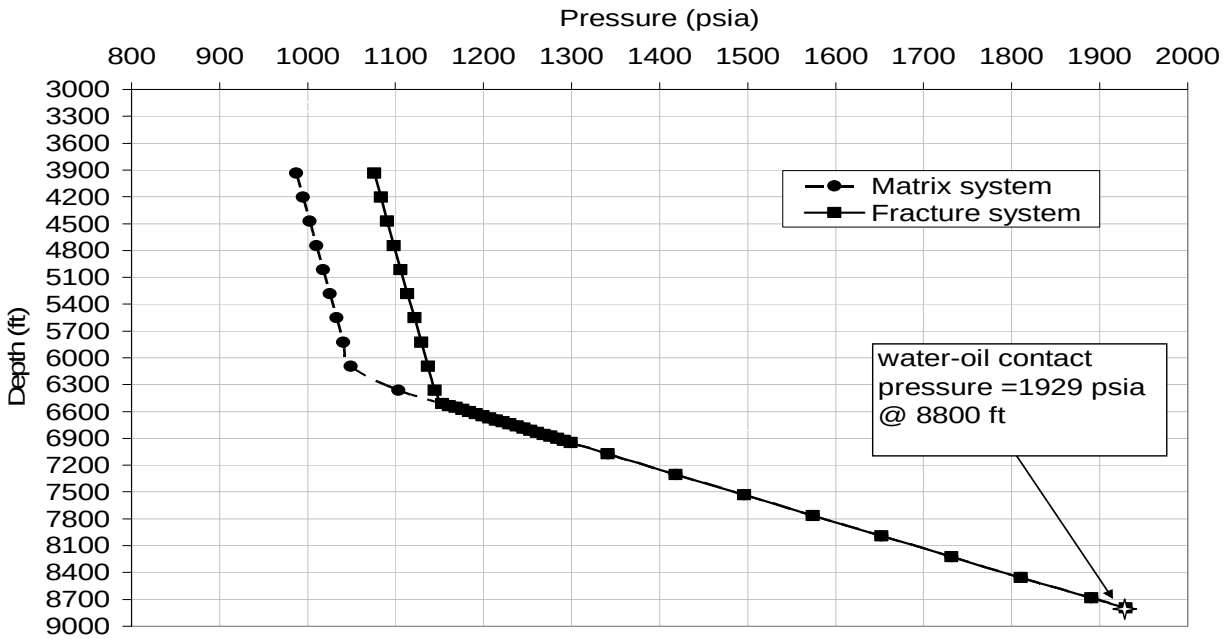

Figure 4.6 Pressure distribution trend for black oil system dual porosity.

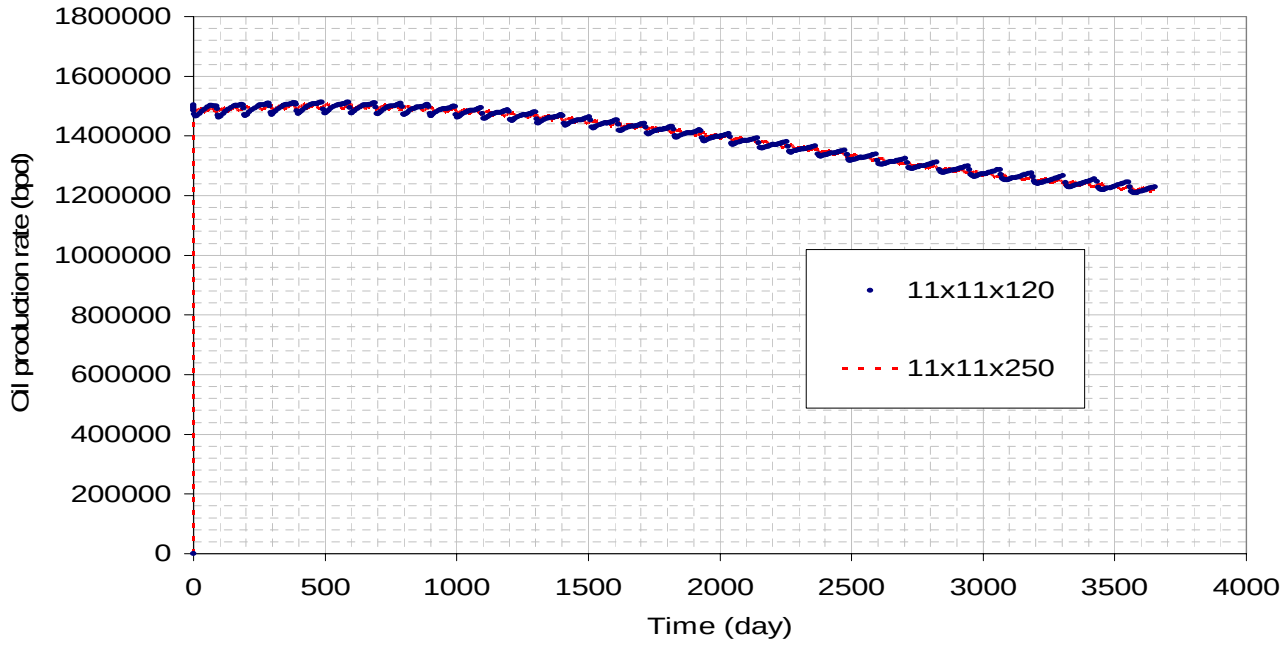

Figure 4.7 Vertical grid refinement for black oil dual porosity system.

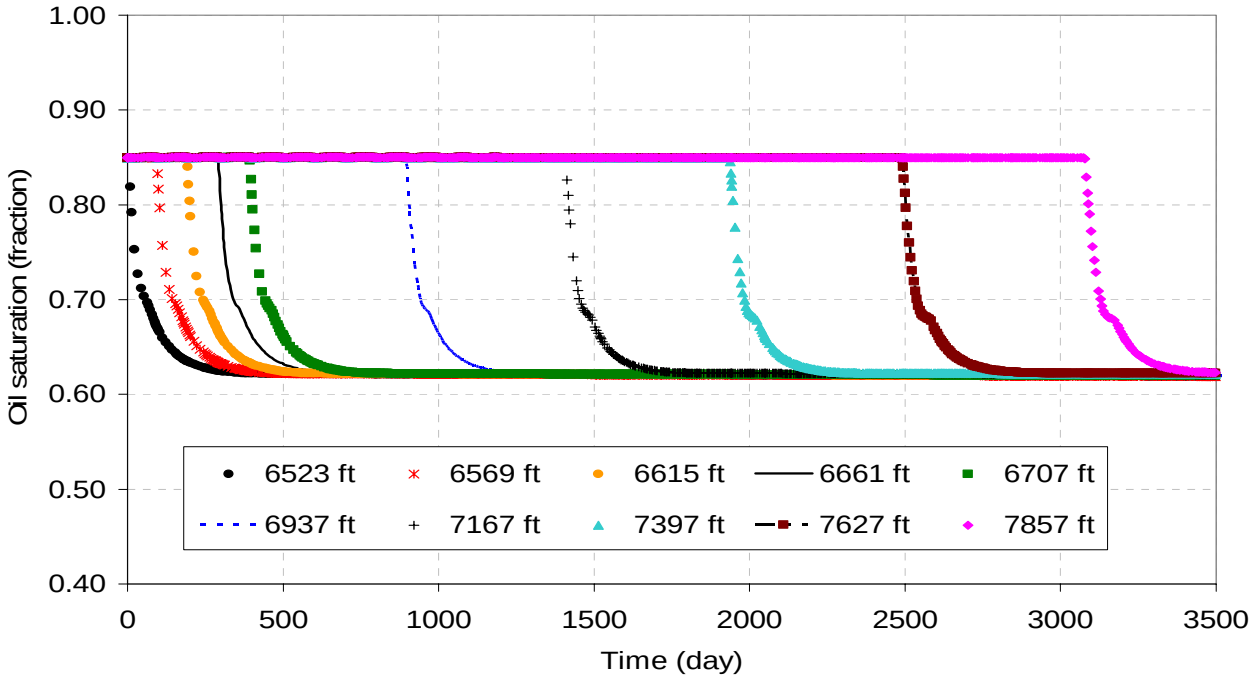

Figure 4.8 Oil saturation profiles of matrix blocks after reservoir gas re-injection for a black oil dual porosity system.

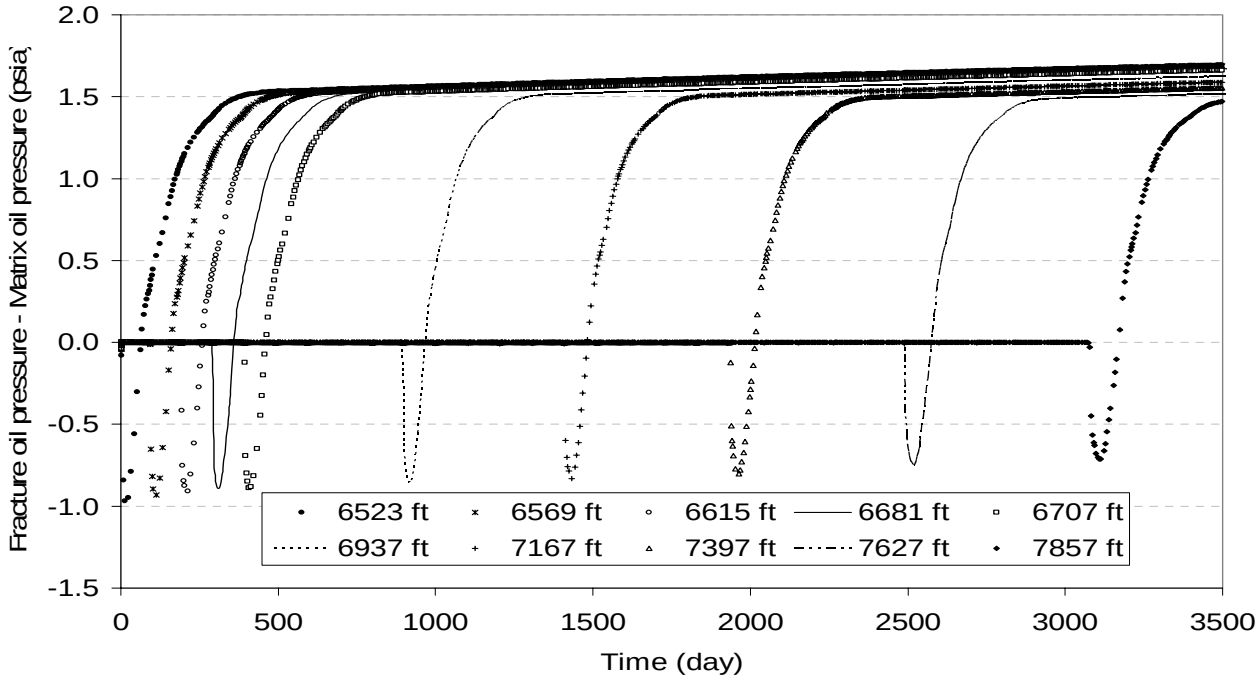

Figure 4.9 Matrix and fracture pressure difference after nitrogen injection for a black oil dual porosity system.

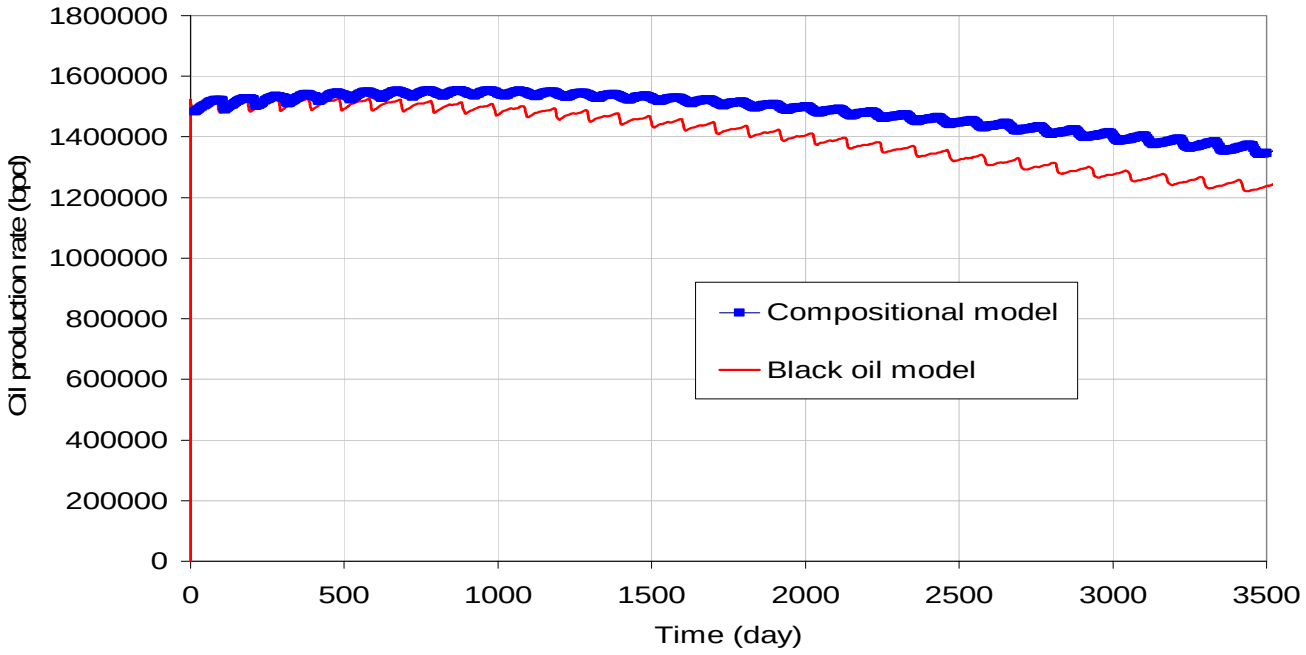

Figure 4.10 Oil production rate vs. time comparing black oil and a compositional case studies.

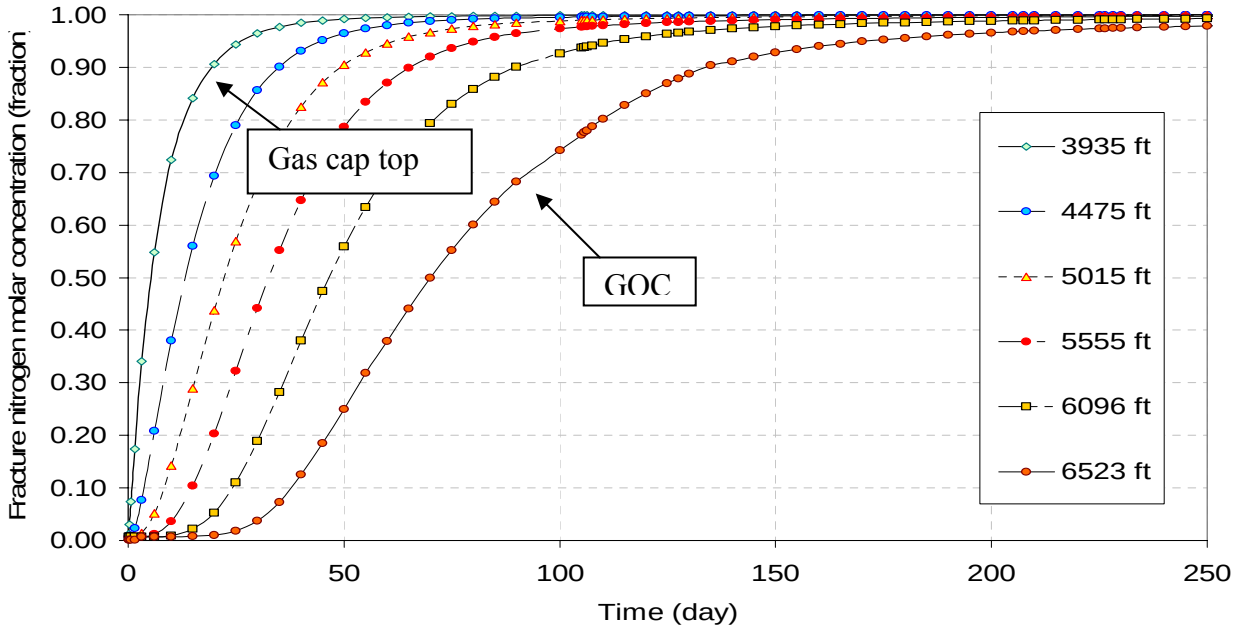

Figure 4.11 Nitrogen molar concentration profiles in gas cap for a compositional dual porosity system.

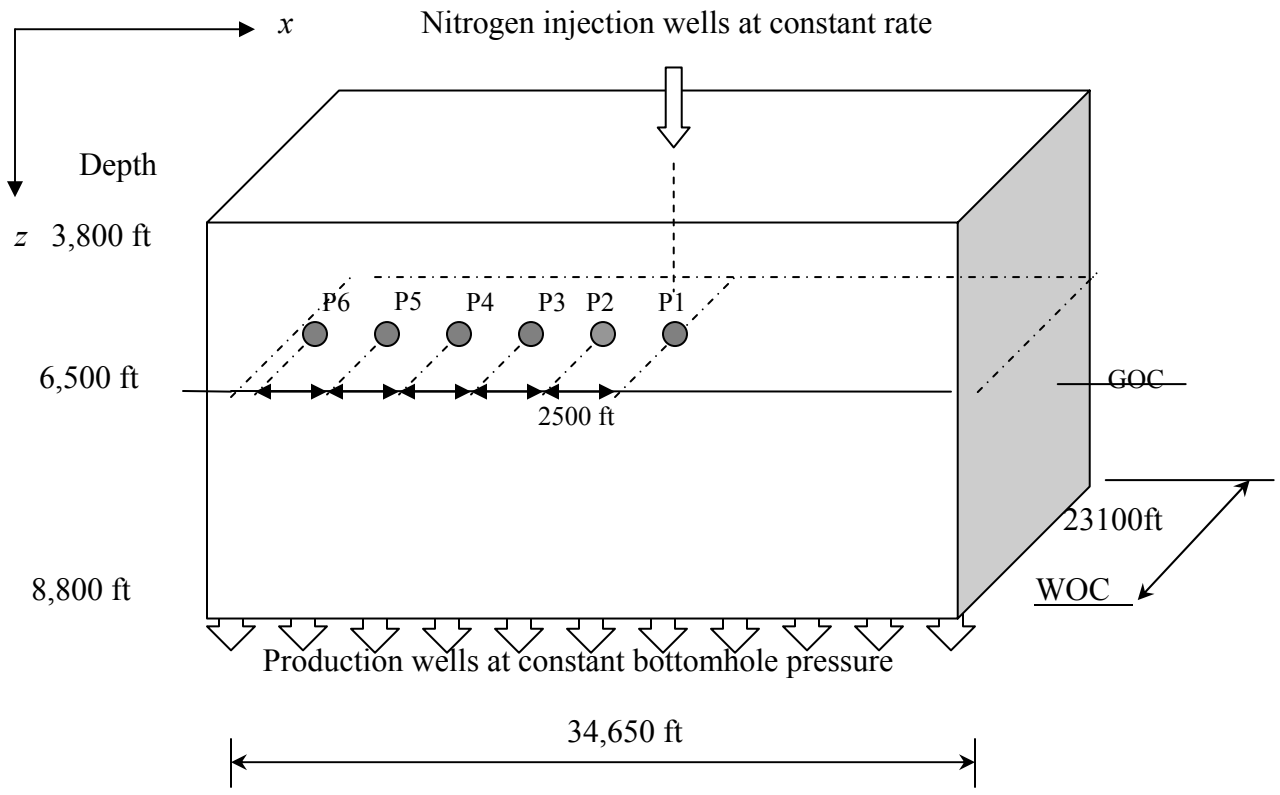

Figure 4.12 Location of six fracture grid cells along the GOC used to analyze the distribution of nitrogen molar concentrations.

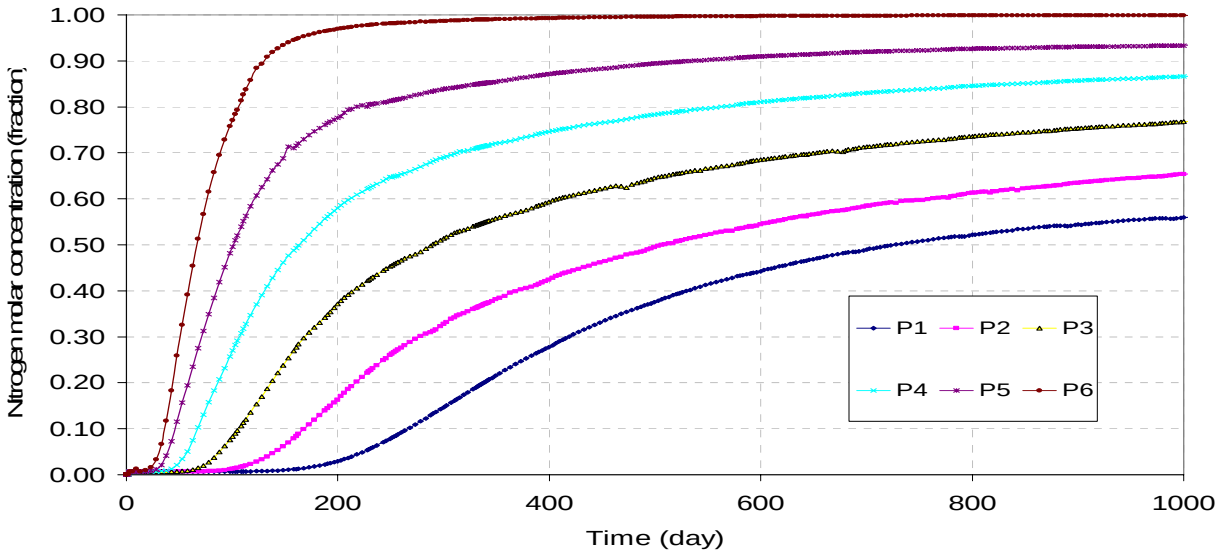

Figure 4.13 Distribution of nitrogen molar concentration profiles along GOC for six fracture grid cells.

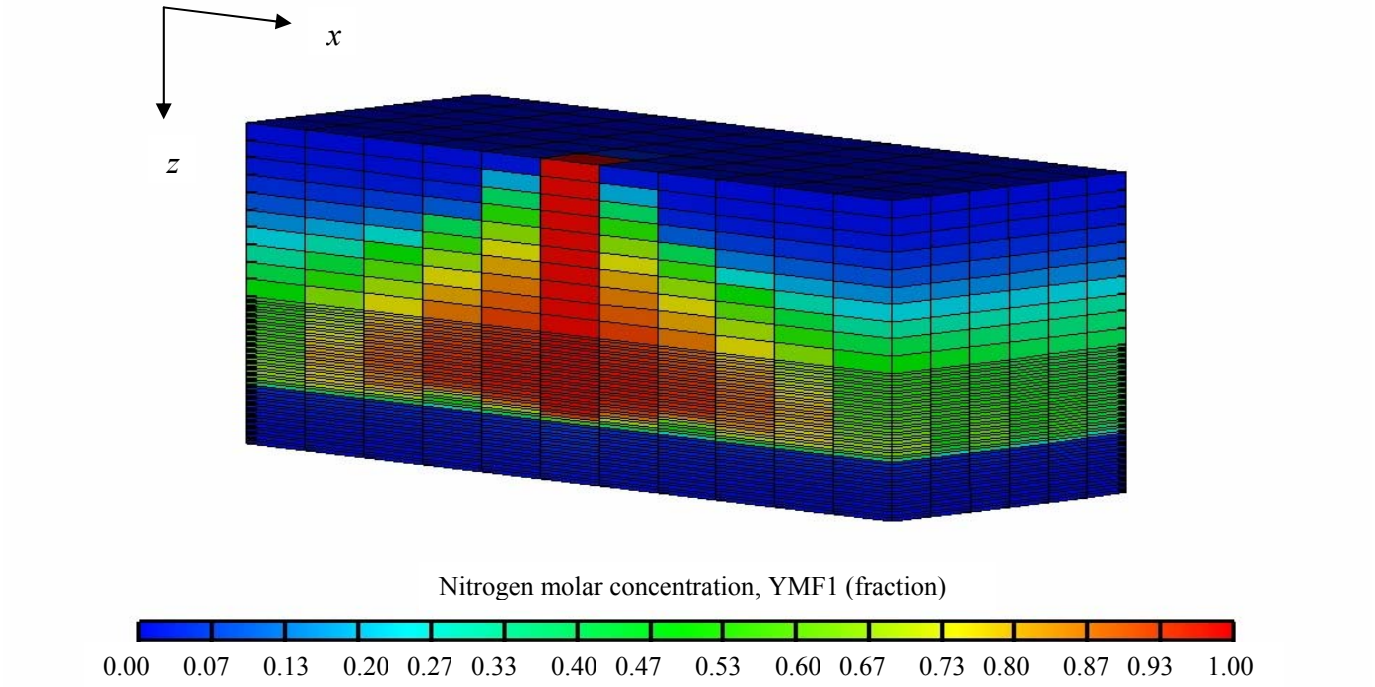

Figure 4.14 Nitrogen molar concentrations in *x-z* cross section.

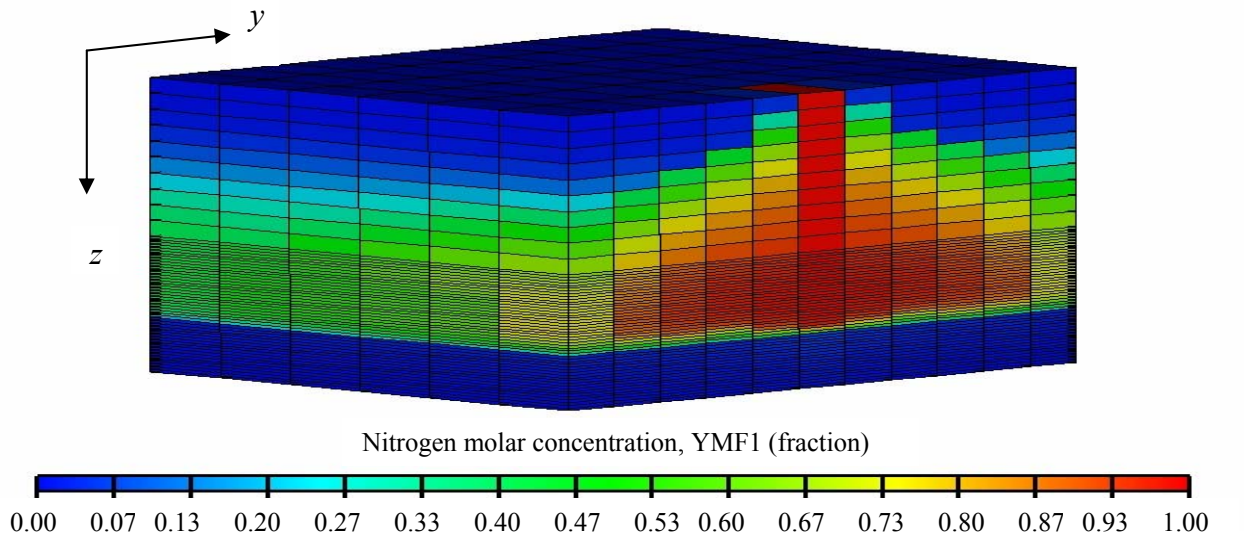

Figure 4.15 Nitrogen molar concentrations in *y*-*z* cross section.

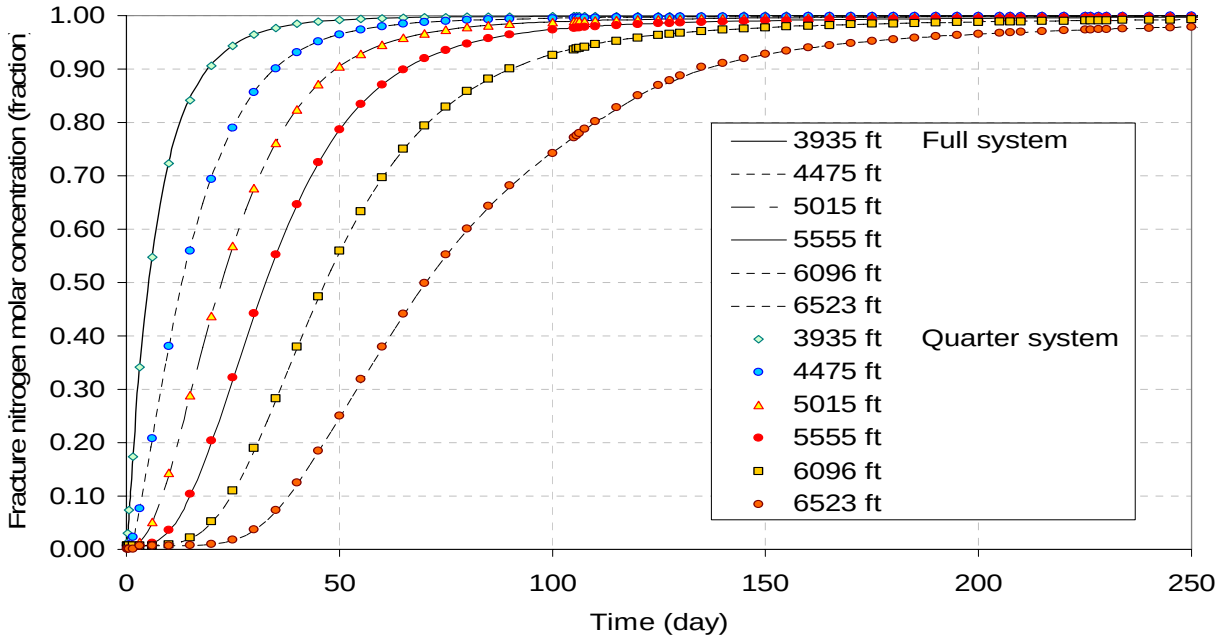

Figure 4.16 Vertical profiles of nitrogen molar concentrations at six different depths for full and quarter systems.

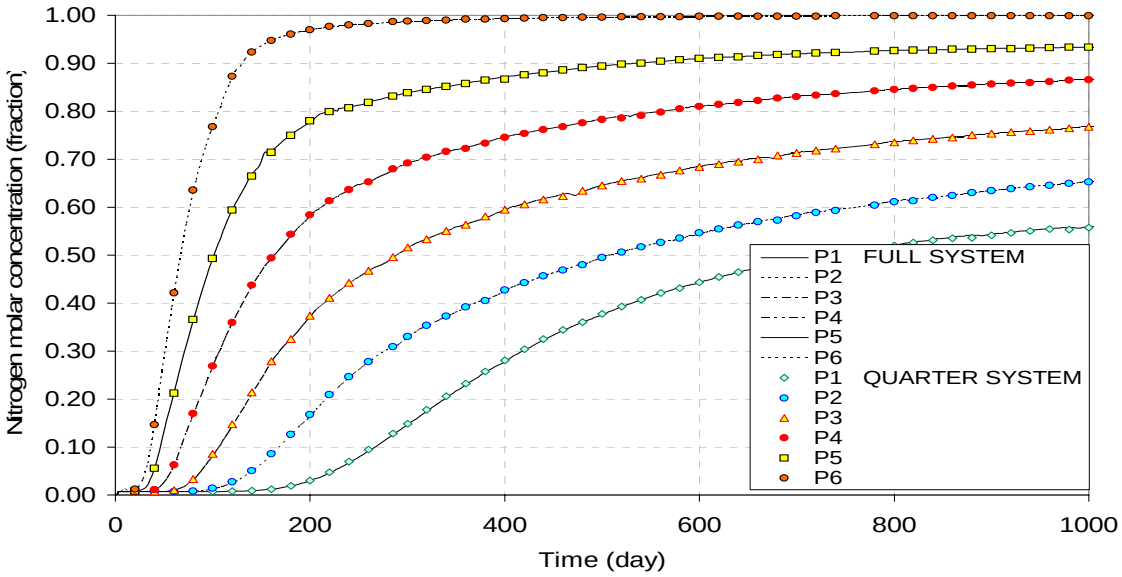

Figure 4.17 Horizontal profiles of nitrogen molar concentrations of six locations along the GOC for full and quarter systems.

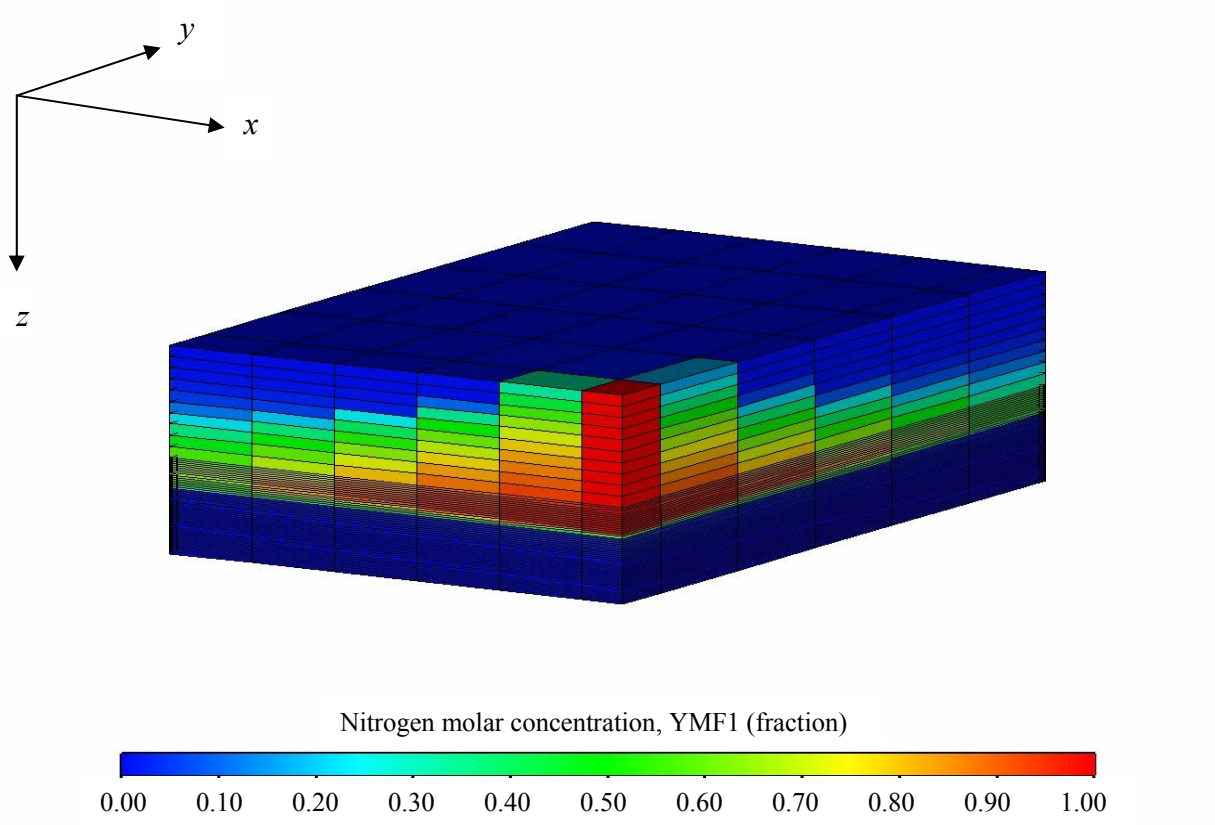

Figure 4.18 Nitrogen molar concentrations for quarter system.

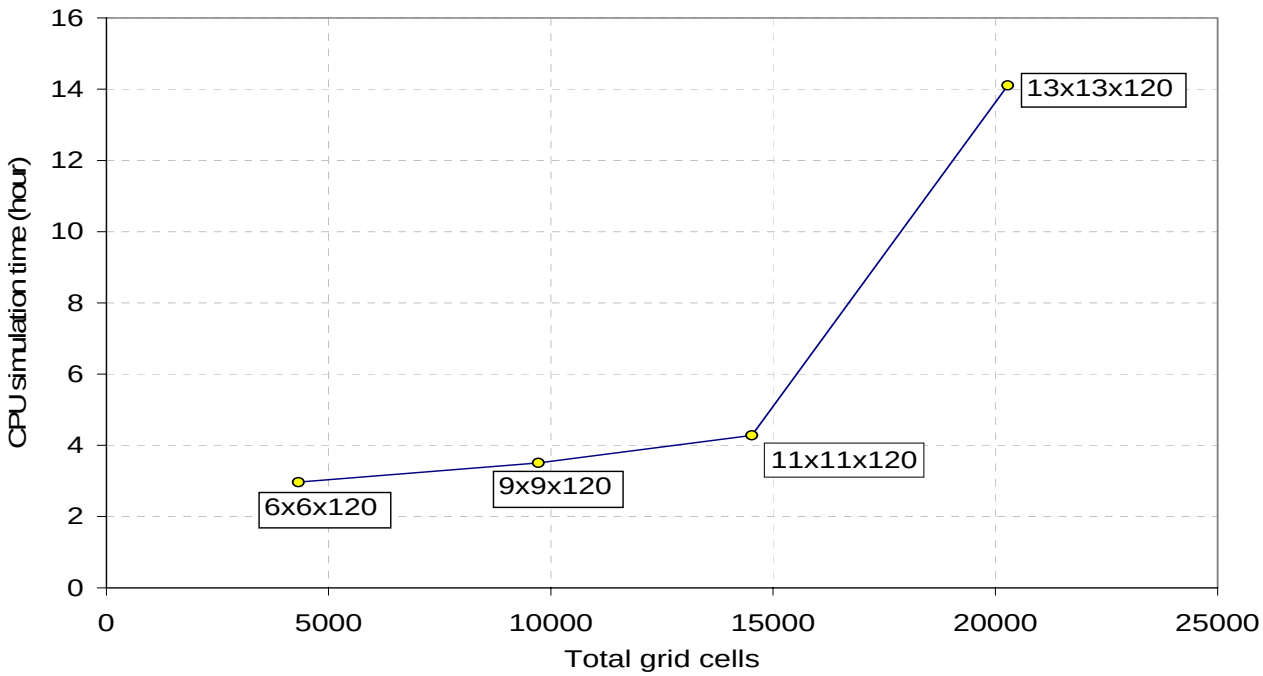

Figure 4.19 Computing time for grid refinement study for quarter system.

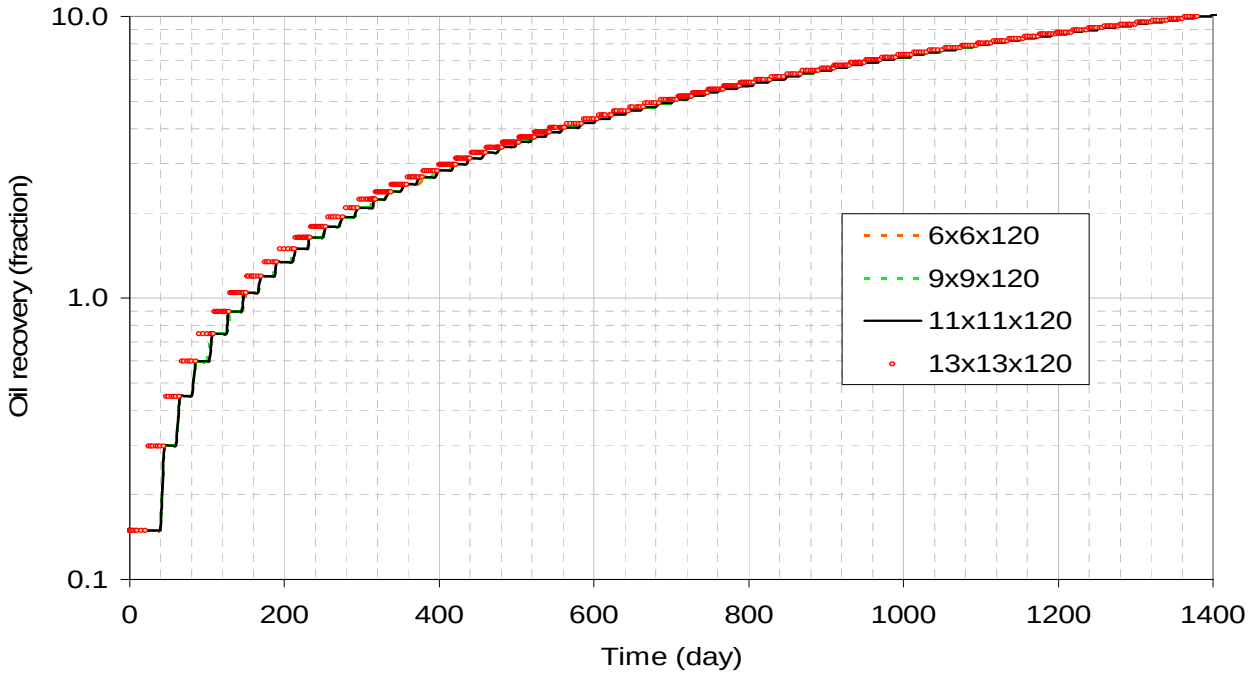

Figure 4.20 Oil recoveries vs. time for grid refinement study for quarter system.

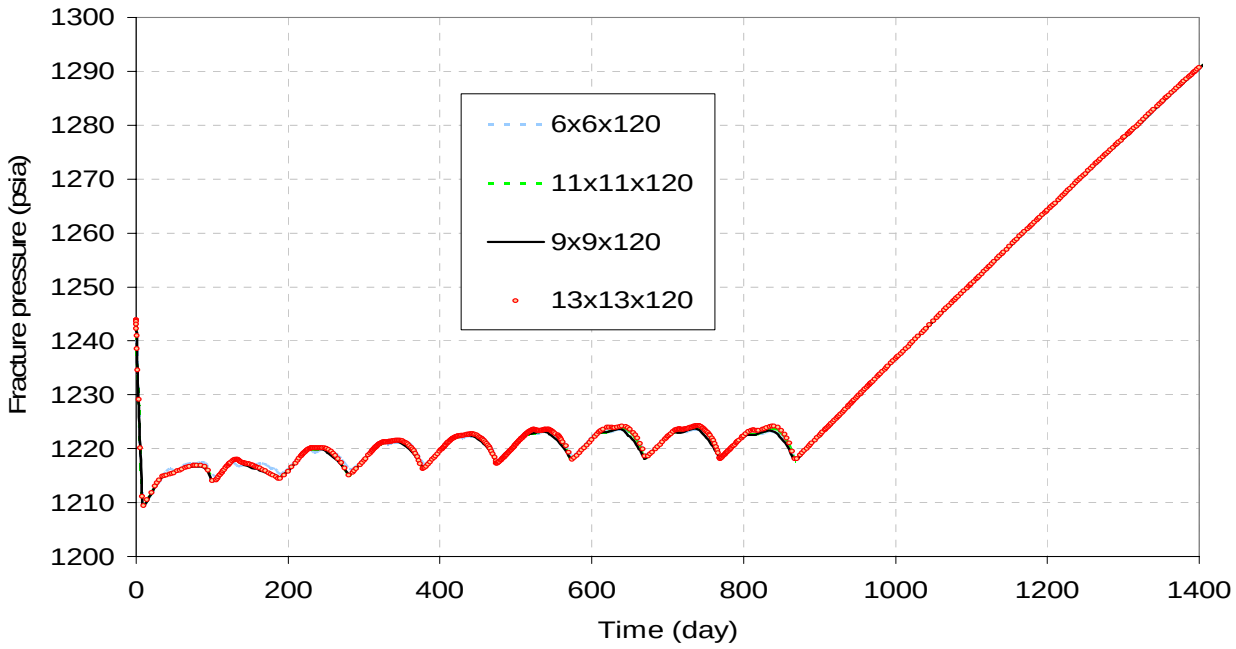

Figure 4.21 Pressure vs. time for grid refinement study.

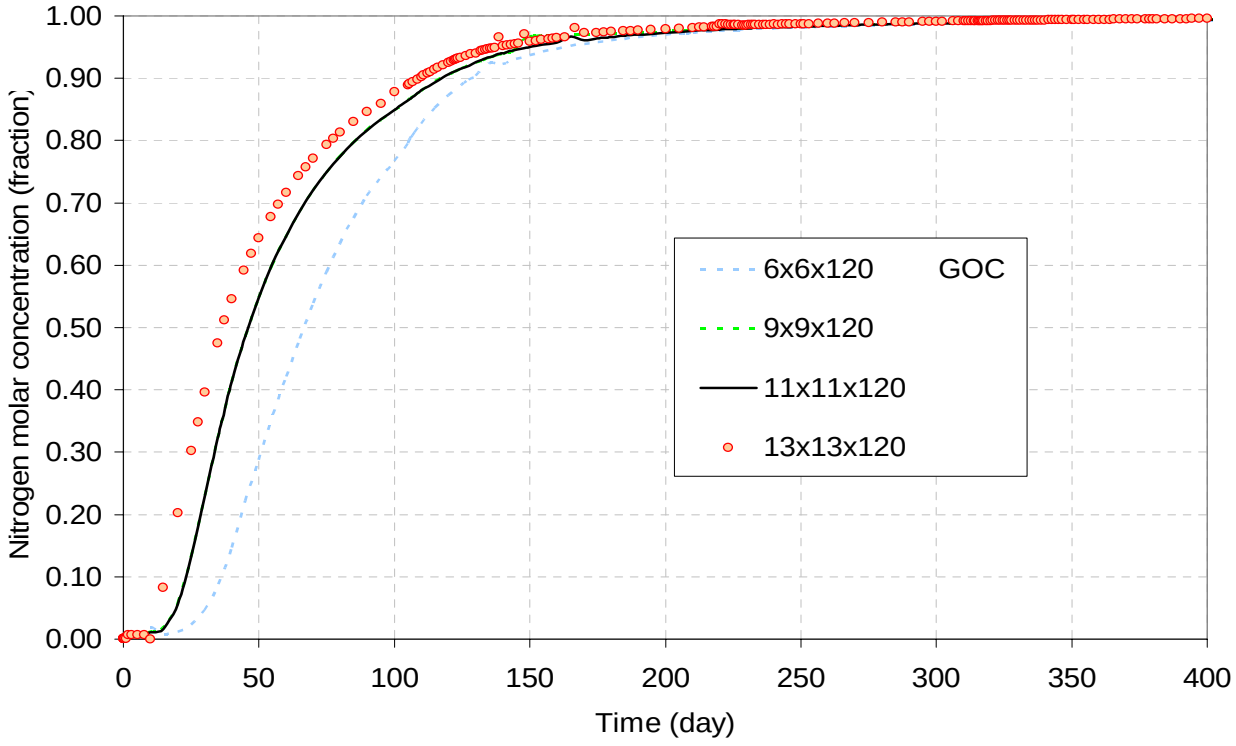

Figure 4.22 N_2 molar concentrations at GOC vs. time for grid refinement study.

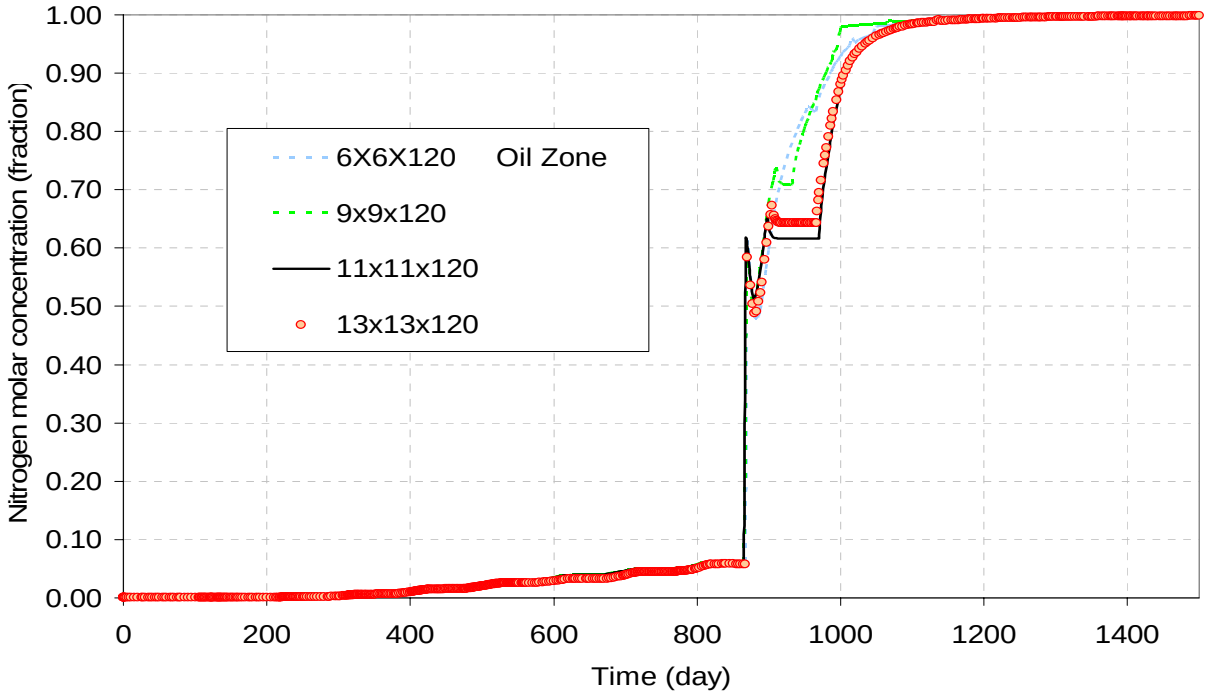

Figure 4.23 N_2 molar concentrations at oil zone vs. time for grid refinement study.

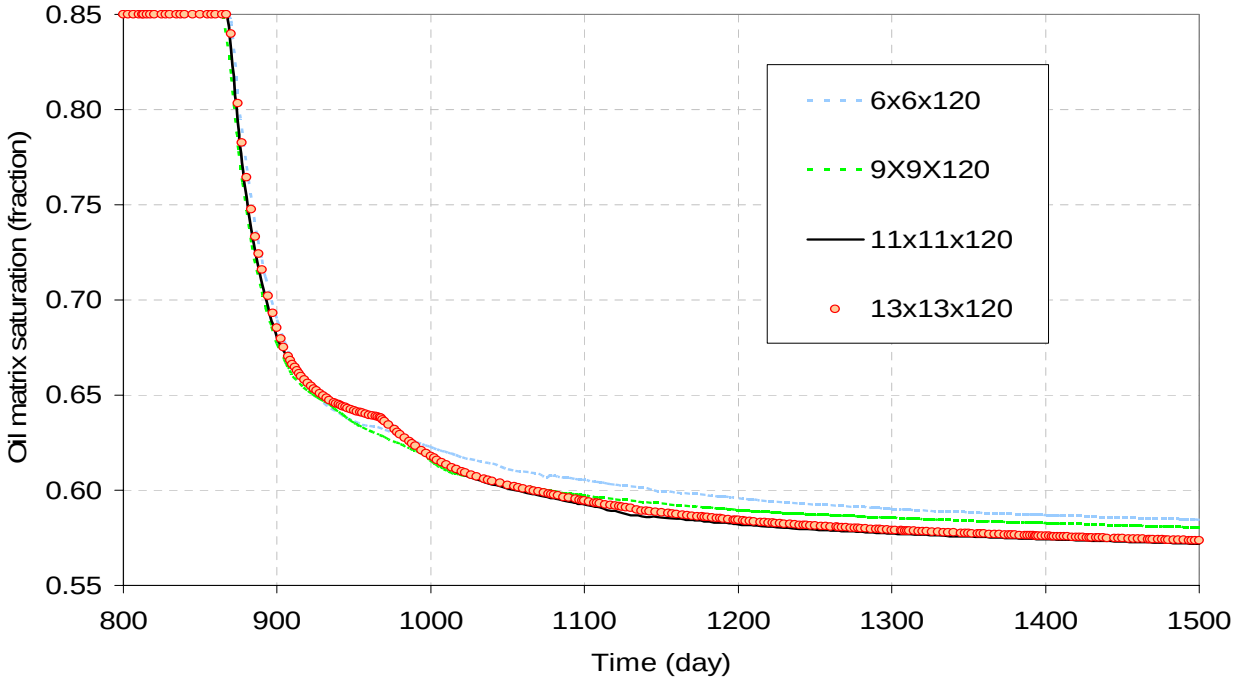

Figure 4.24 Oil matrix saturations vs. time in oil zone for grid refinement study.

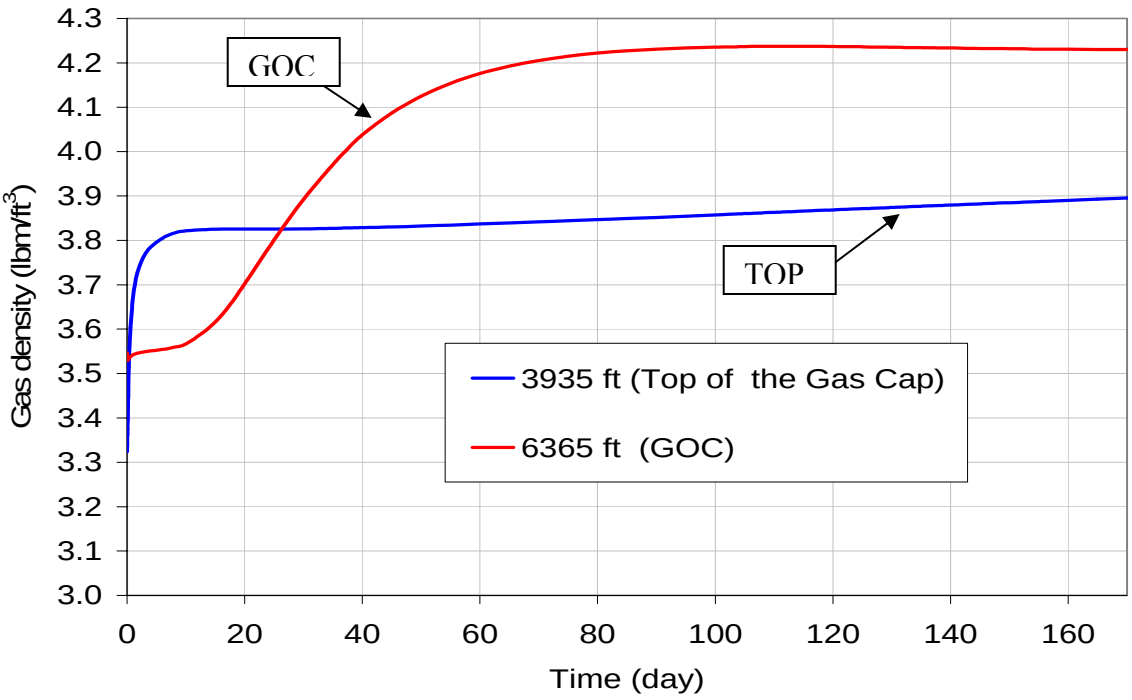

Figure 4.25 Gaseous phase density variations at the top and GOC after injecting nitrogen at the top of the reservoir.

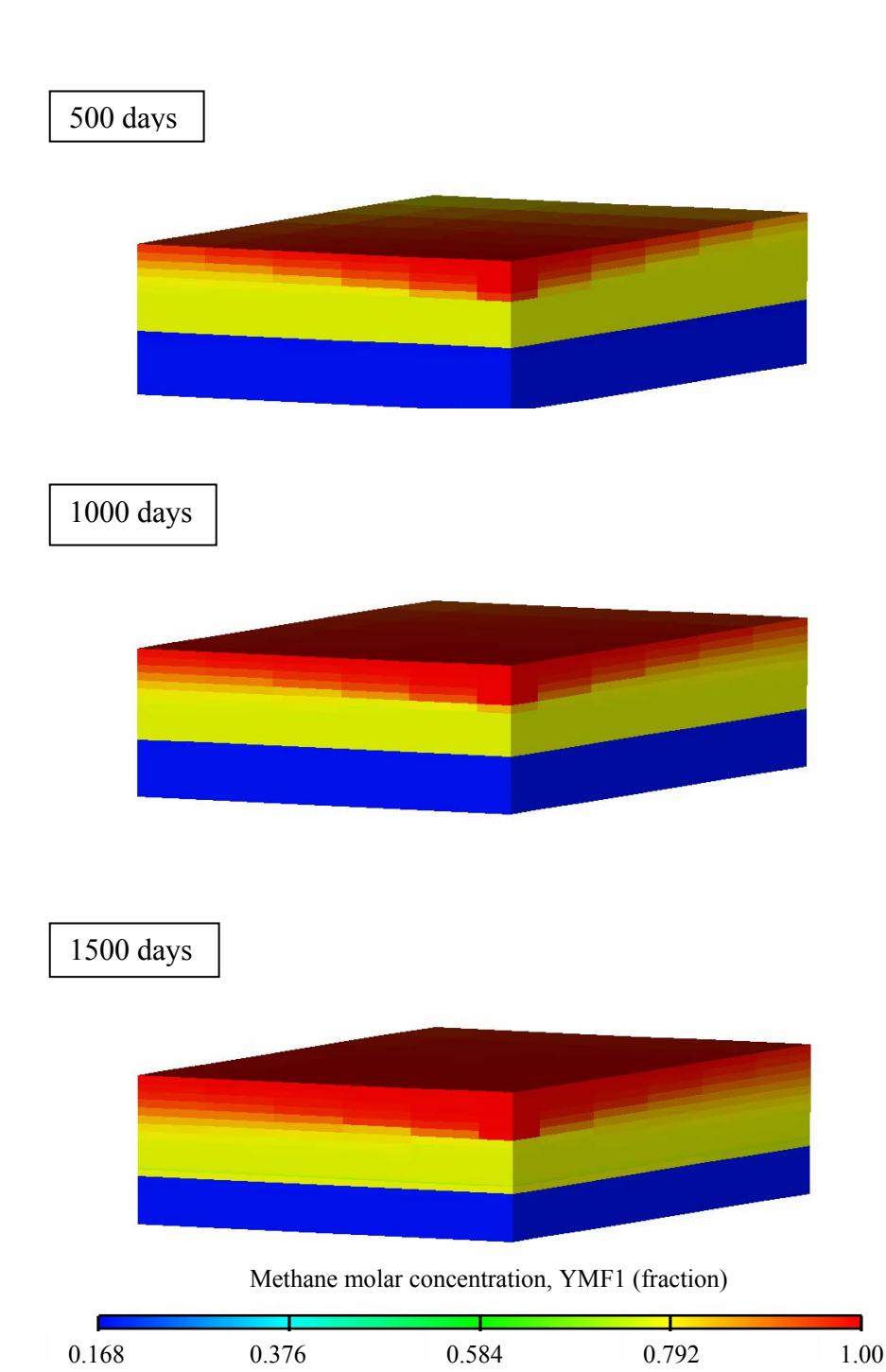

Figure 4.26 Methane molar concentrations for quarter system (500, 1000 and 1500 days).

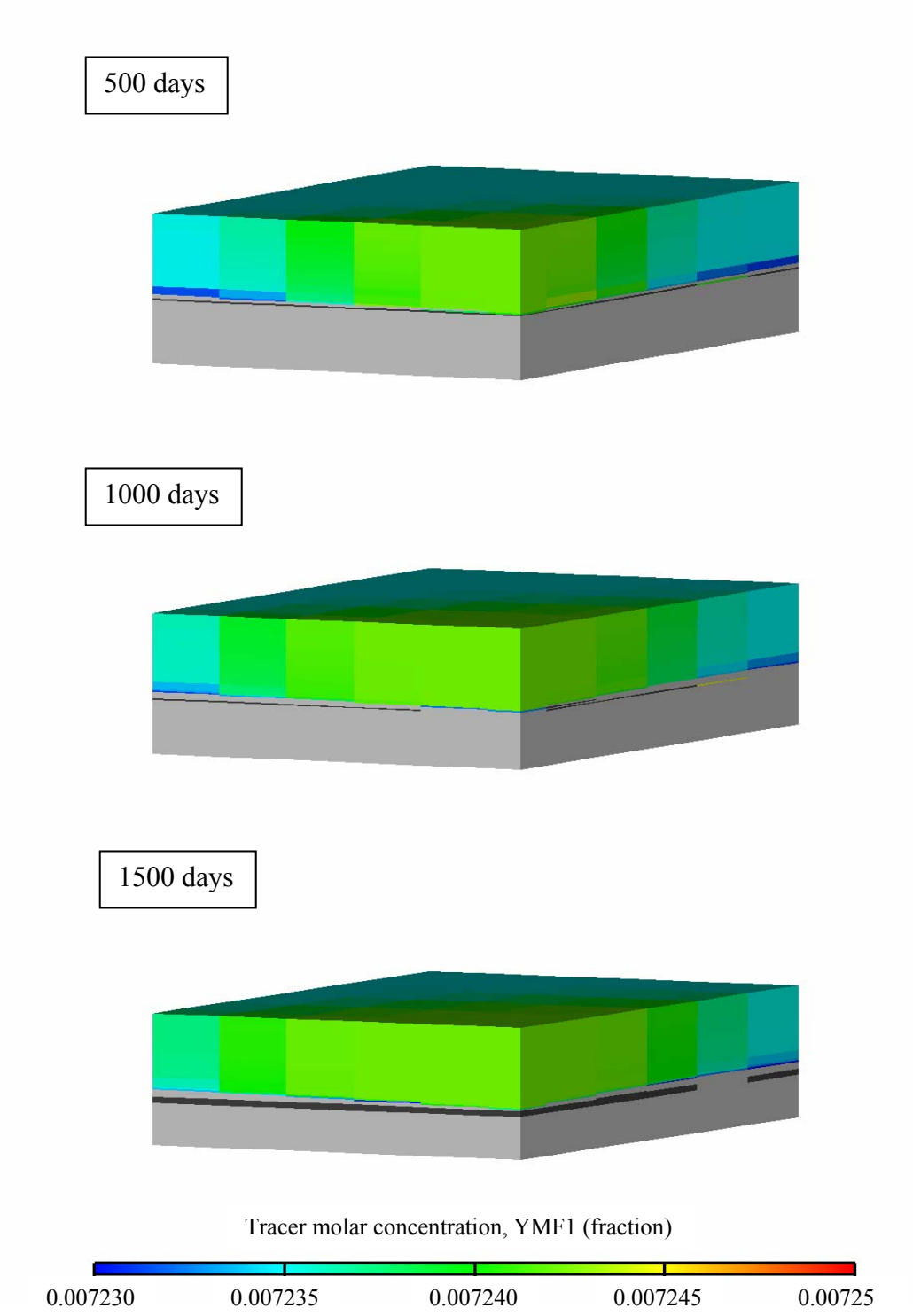

Figure 4.27 Tracer distribution of gas re-injected for quarter system (500, 1000 and 1500 days).

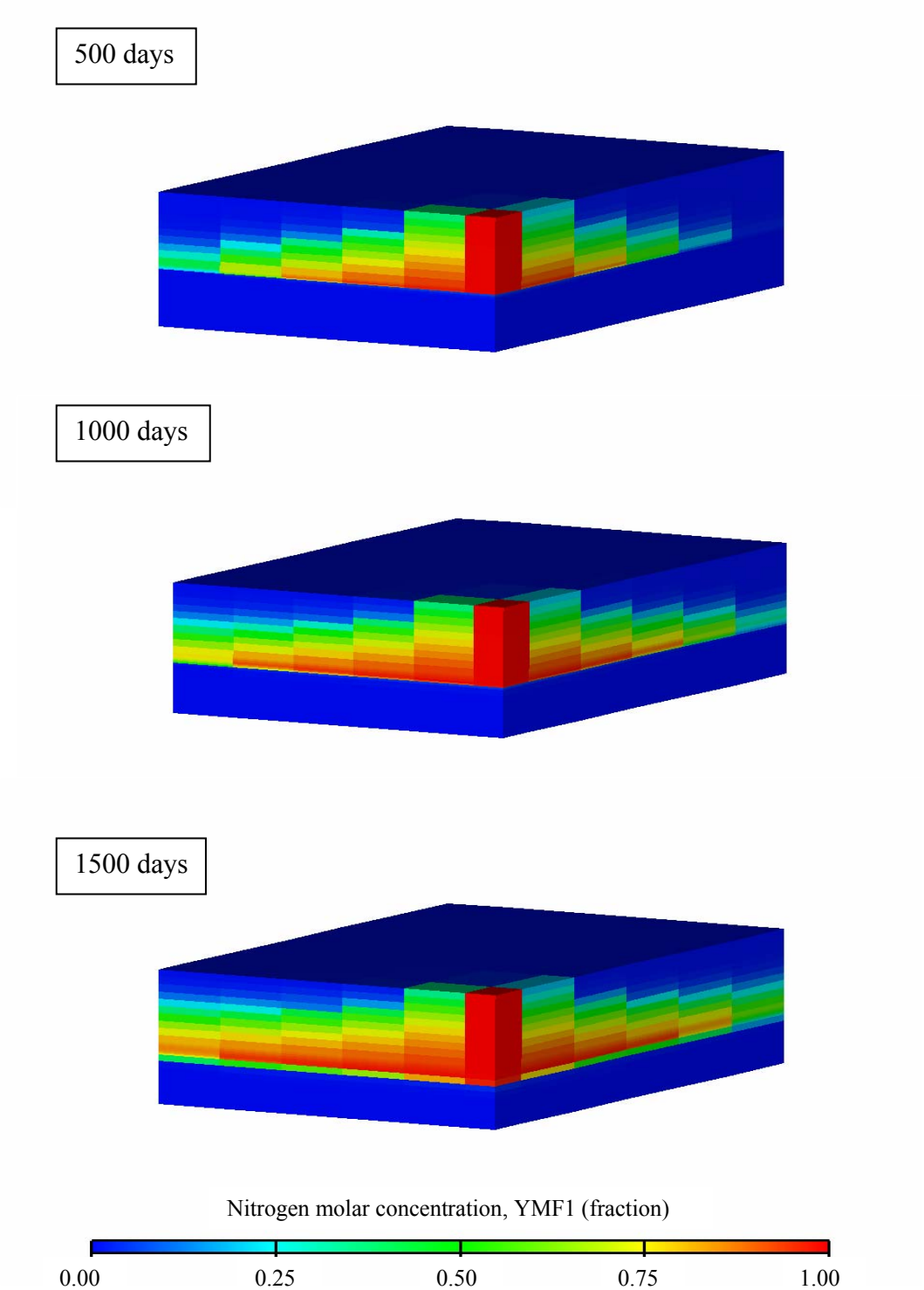

Figure 4.28 Nitrogen molar concentrations for quarter system (500, 1000 and 1500 days).

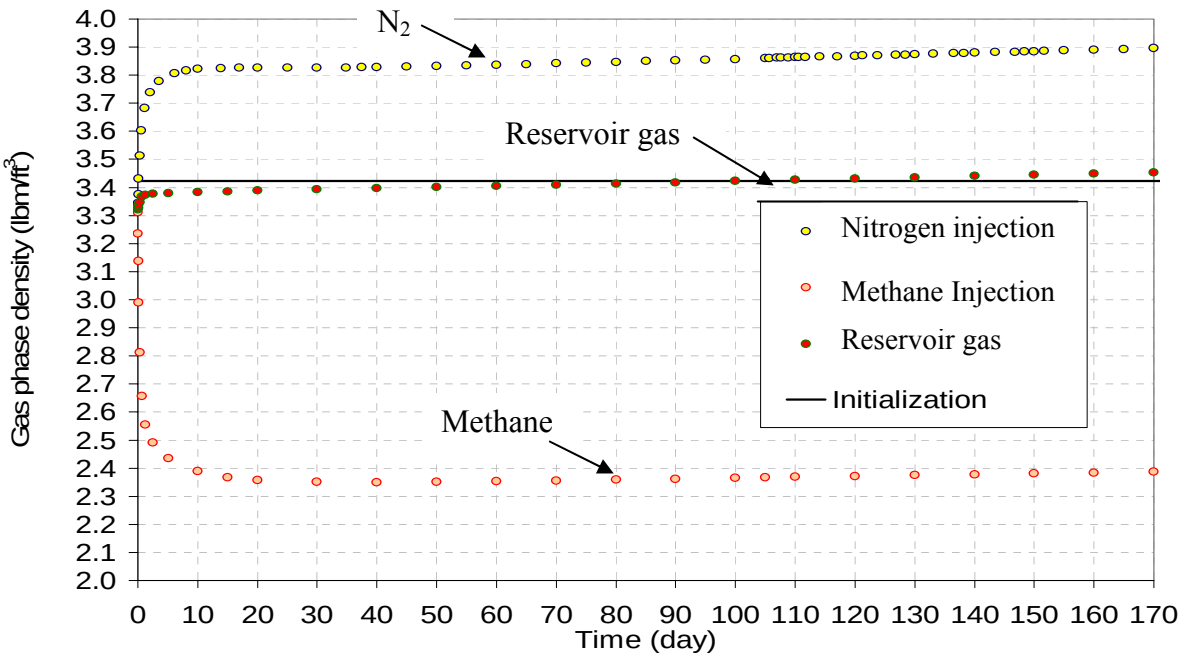

Figure 4.29 Gas phase density variations at the top reservoir after injecting methane, reservoir gas, and nitrogen.

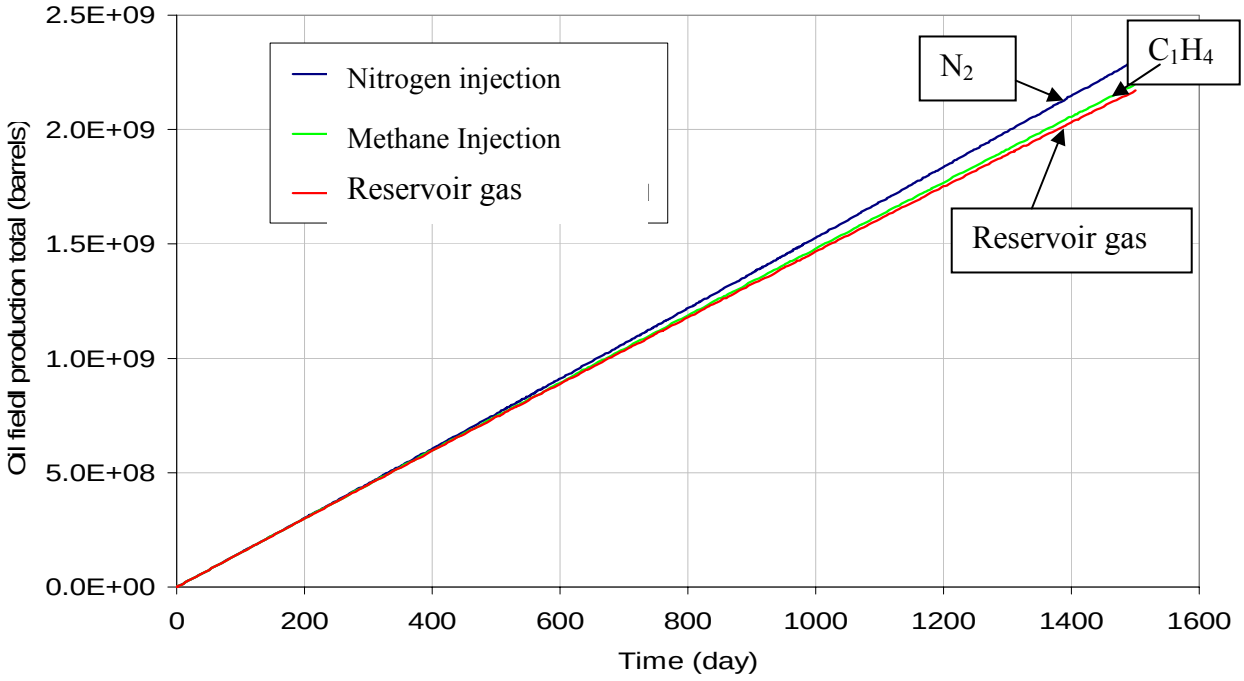

Figure 4.30 Total oil field production during injection of CH_4, reservoir gas, and N_2.

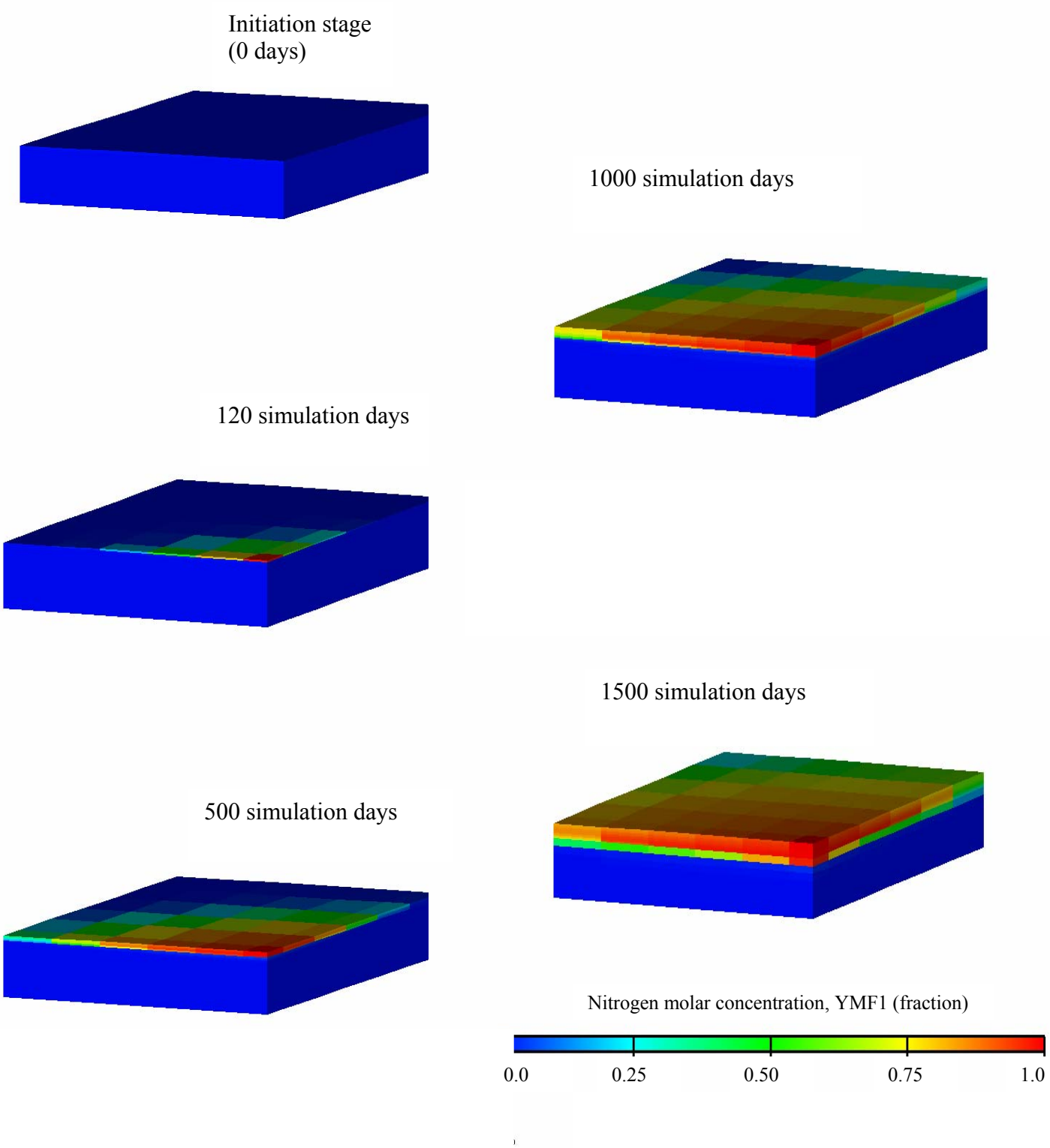

Figure 4.31 Nitrogen molar concentrations along GOC at 0, 120, 500, 1000 and 1500 days of injection.

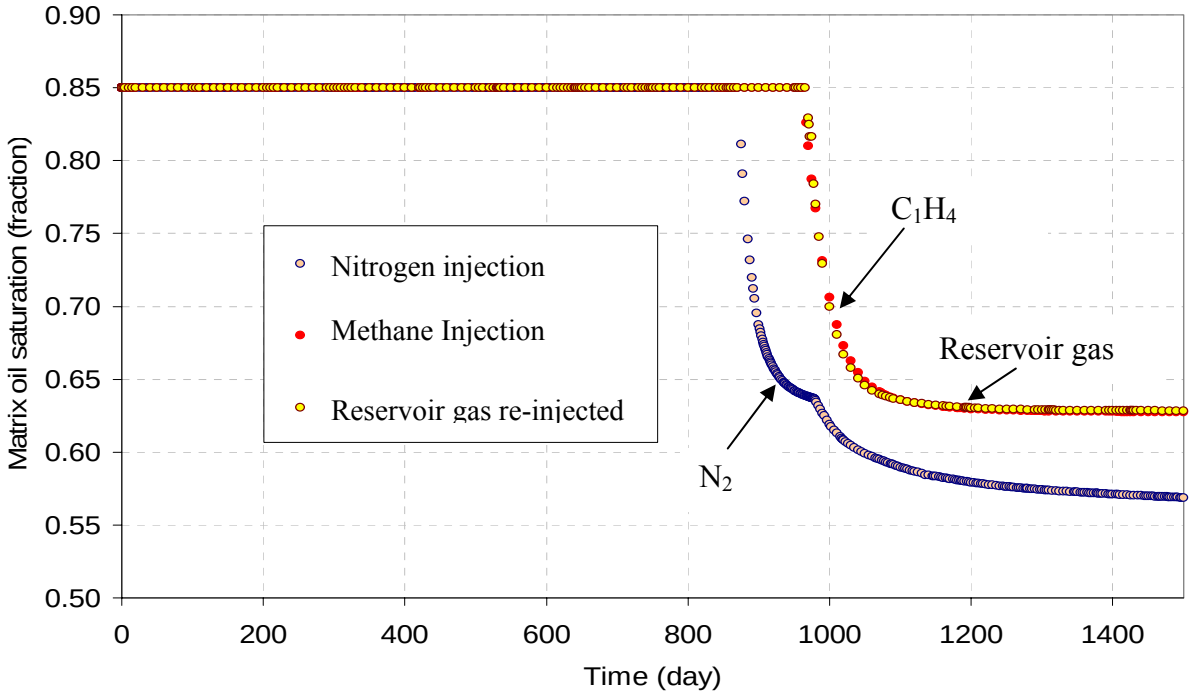

Figure 4.32 Matrix oil saturation vs. time for three different injected gases.

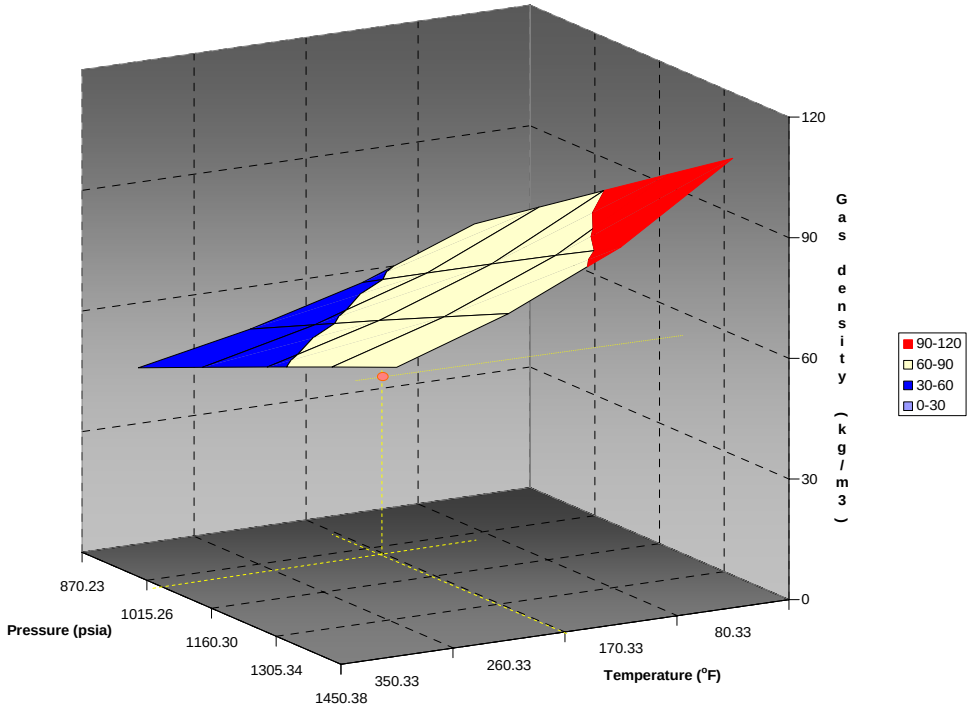

Figure 4.33 Nitrogen density behavior vs. pressure and temperature.

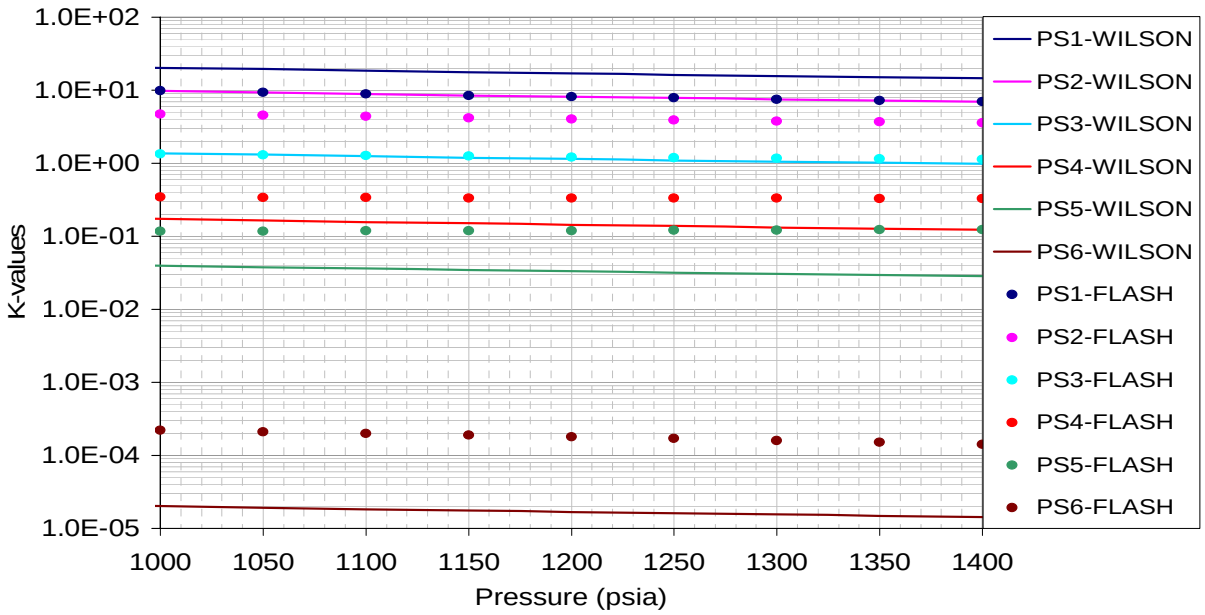

Figure 4.34 K-values using Wilson correlation and flash calculations.

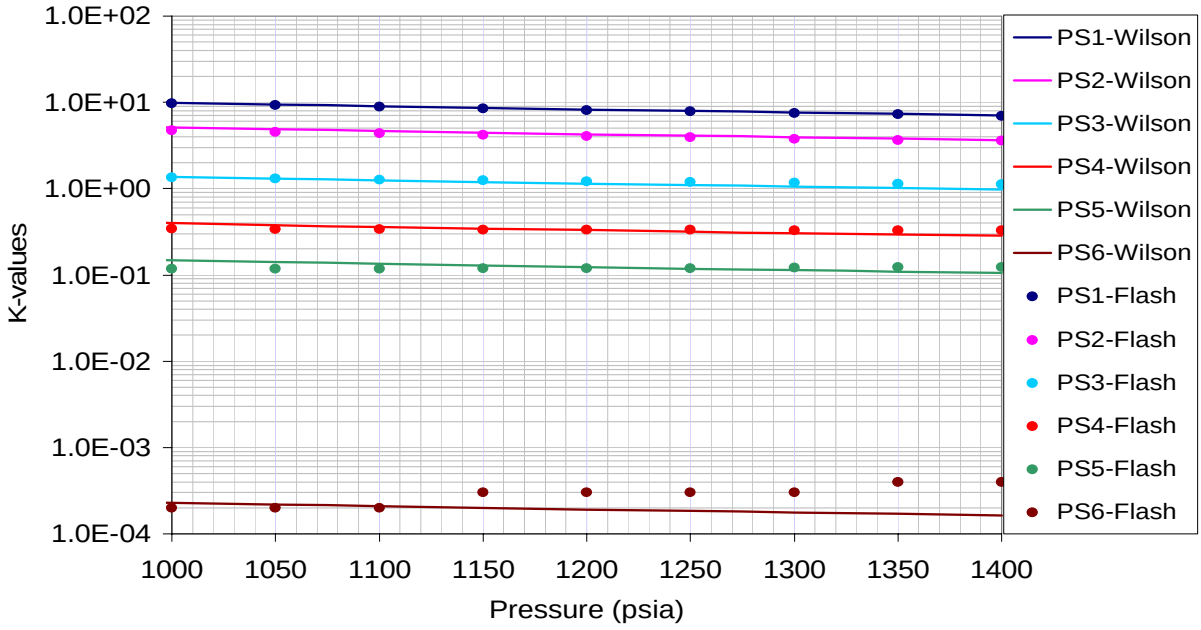

Figure 4.35 K-values using adjusted Wilson correlation and flash calculations.

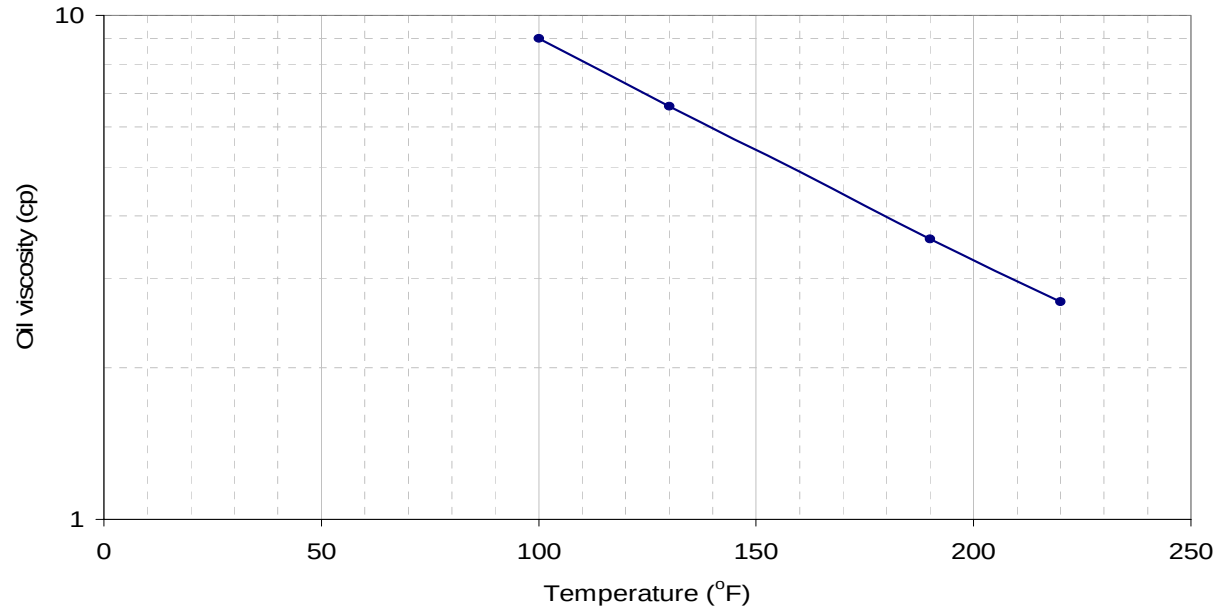

Figure 4.36 Oil viscosity as a function of temperature for thermal case study.

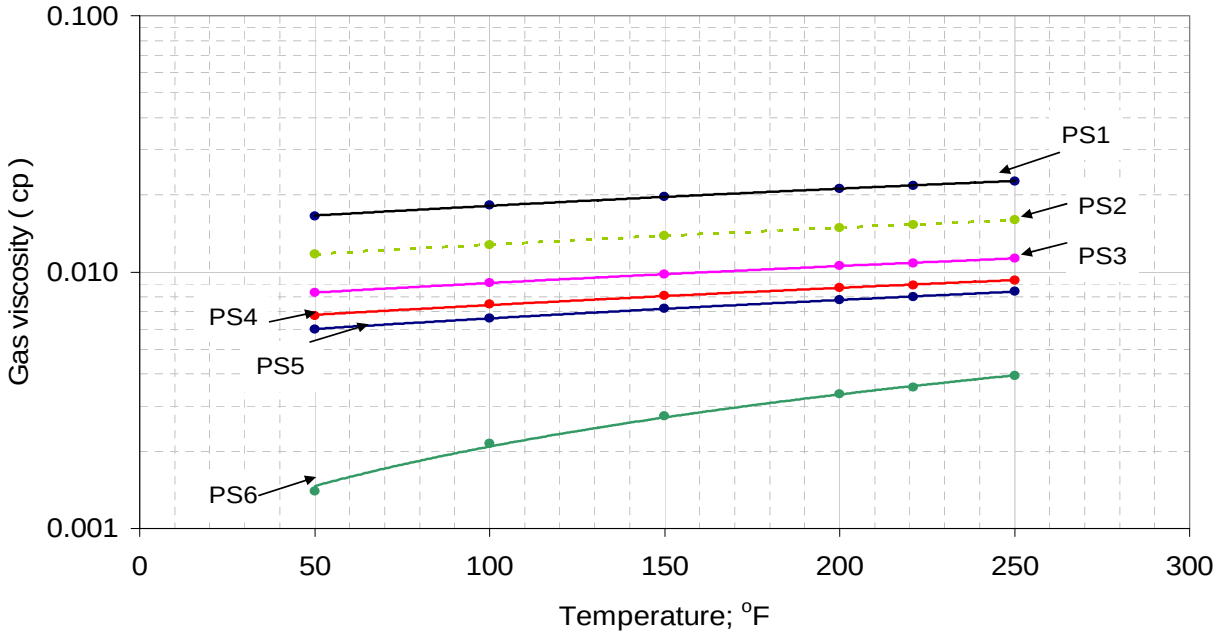

Figure 4.37 Gas viscosities as a function of temperature for thermal case study.

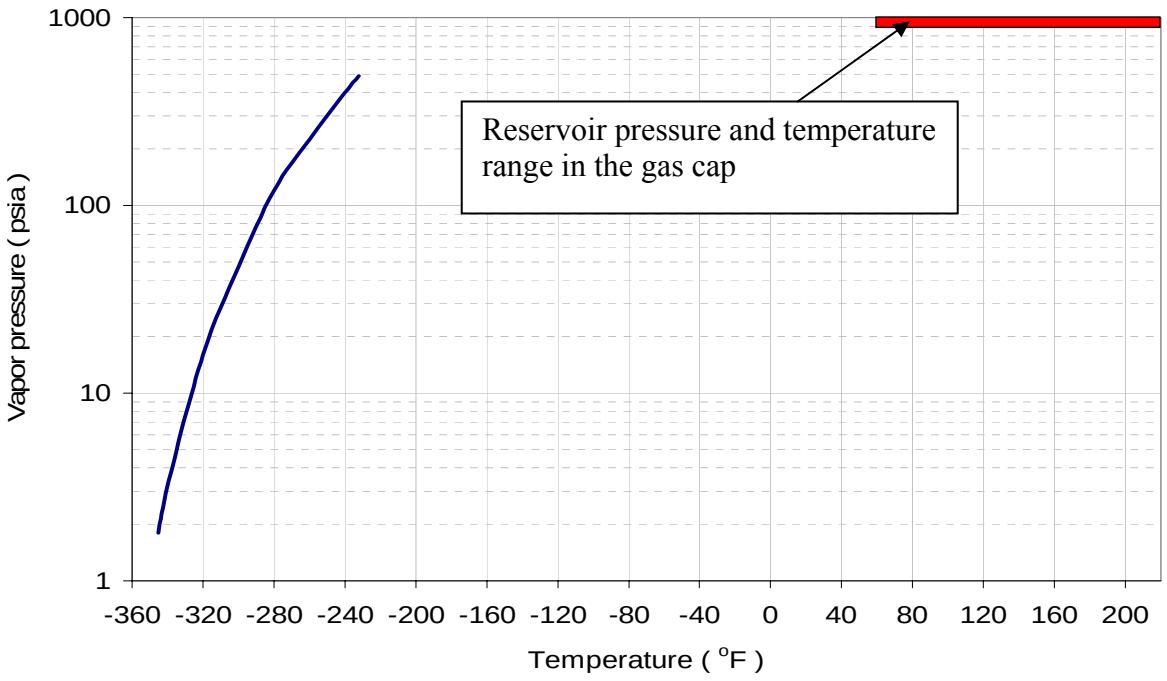

Figure 4.38 Nitrogen vapor pressure behavior as a function of temperature.

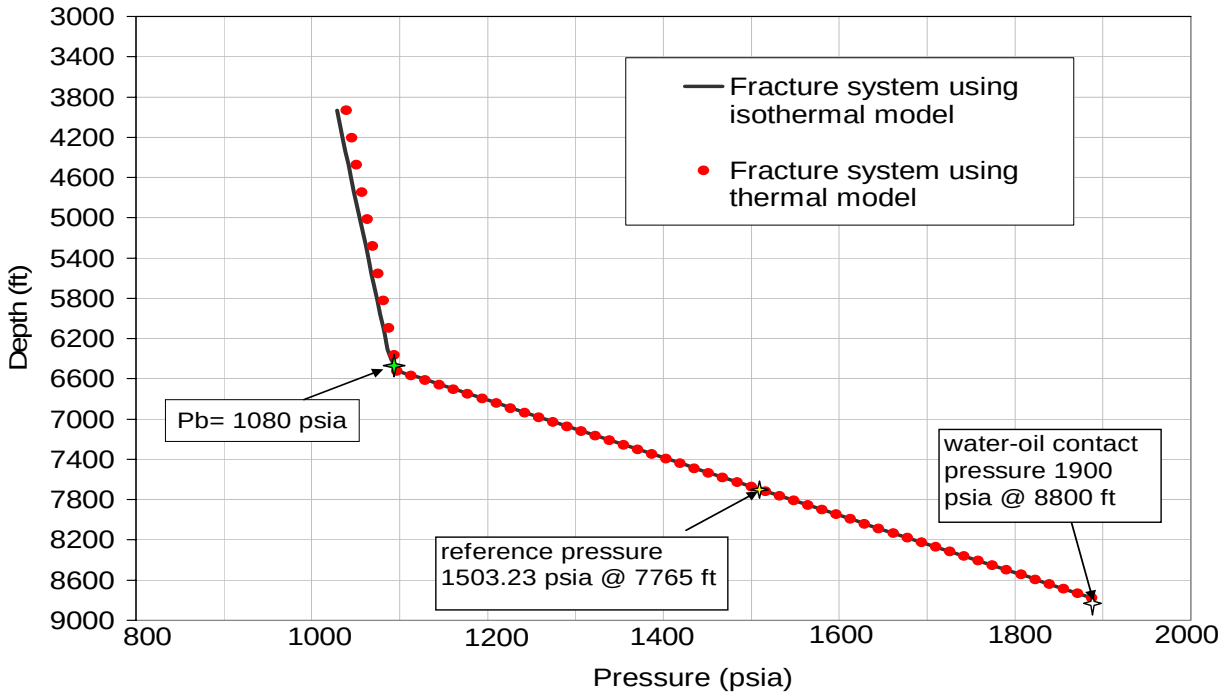

Figure 4.39 Pressure profiles in fracture system for isothermal and thermal case studies with dual porosity in quarter system under static conditions.

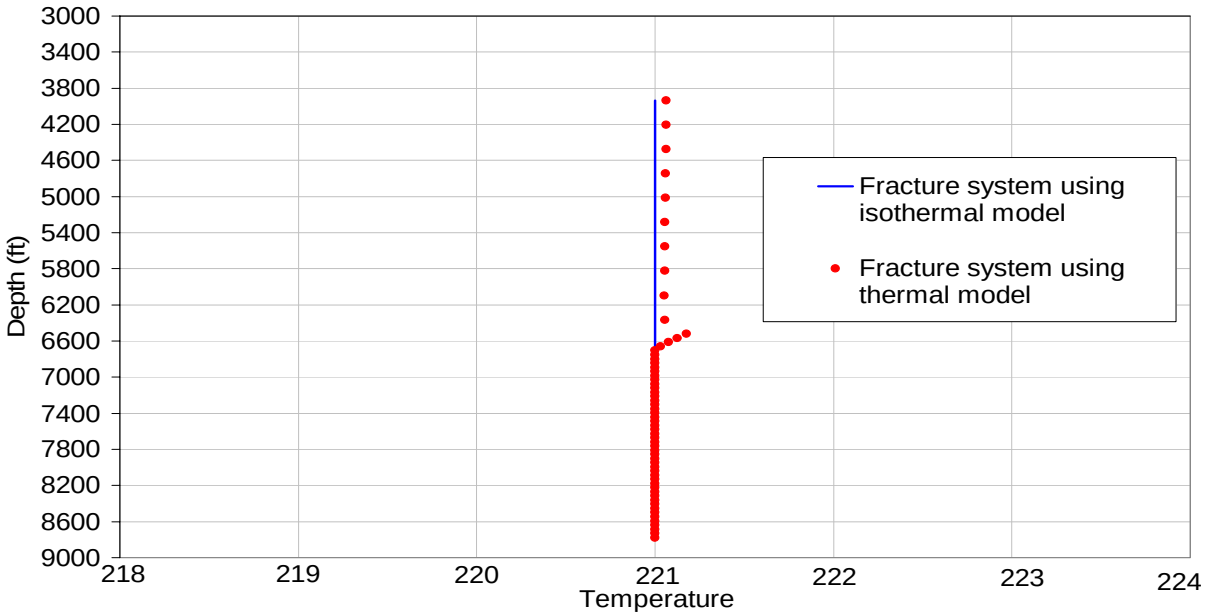

Figure 4.40 Temperature profiles in fracture system for isothermal and thermal case studies with dual porosity in quarter system under static conditions.

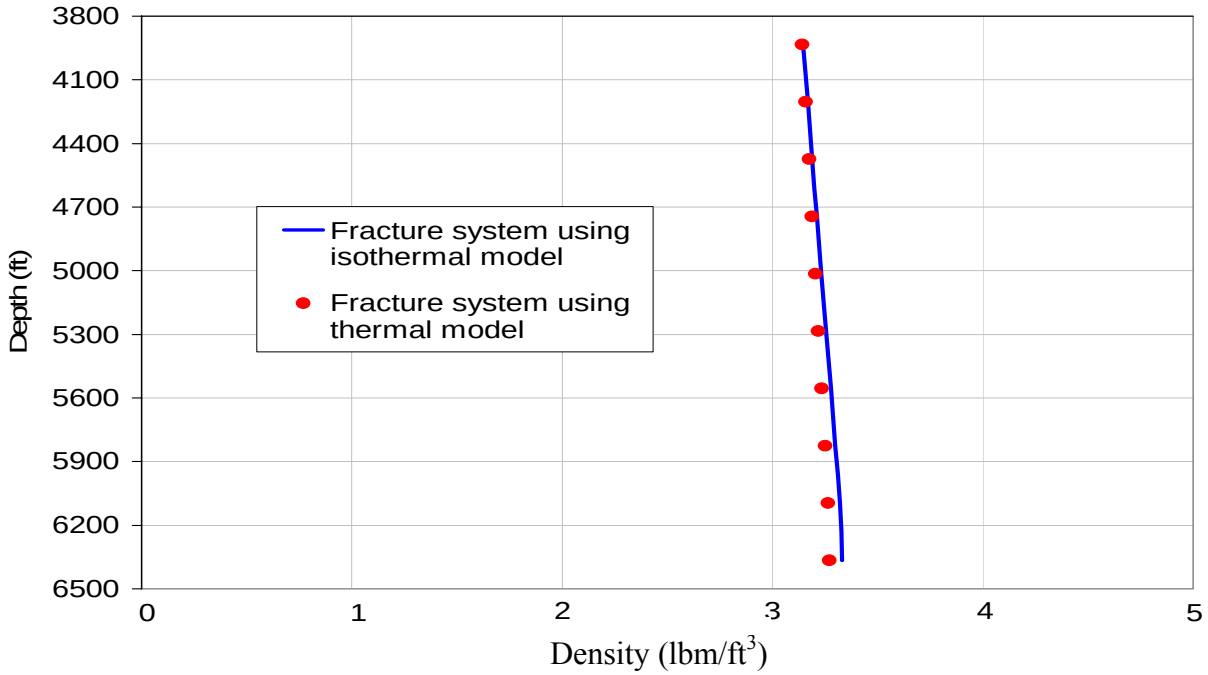

Figure 4.41 Gas density profiles in fracture system for isothermal and thermal case studies with dual porosity in quarter system under static conditions.

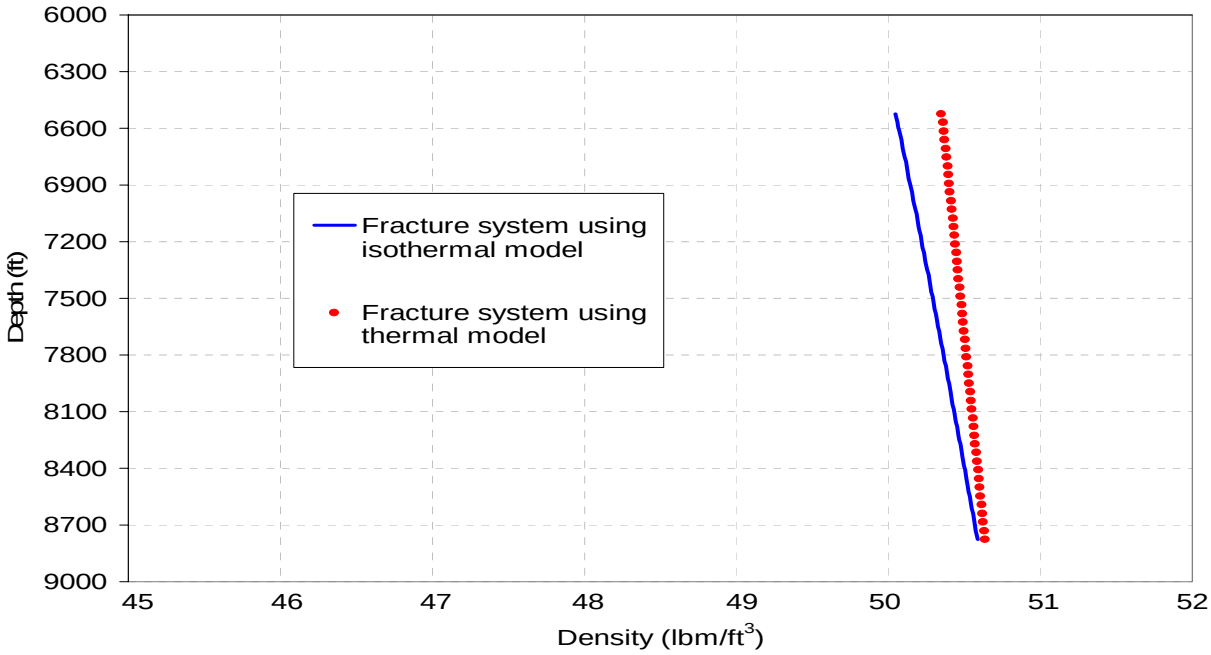

Figure 4.42 Oil density profiles in fracture system for isothermal and thermal case studies with dual porosity in quarter system under static conditions.

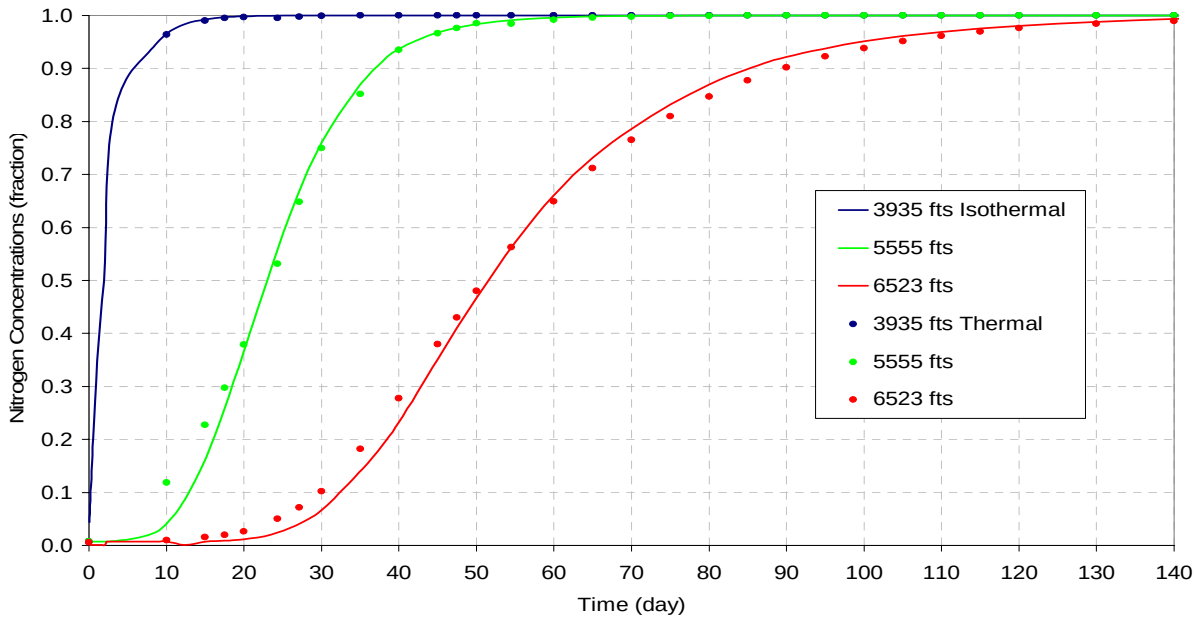

Figure 4.43 Nitrogen vertical distributions for isothermal and thermal case studies with dual porosity in quarter system under dynamic conditions.

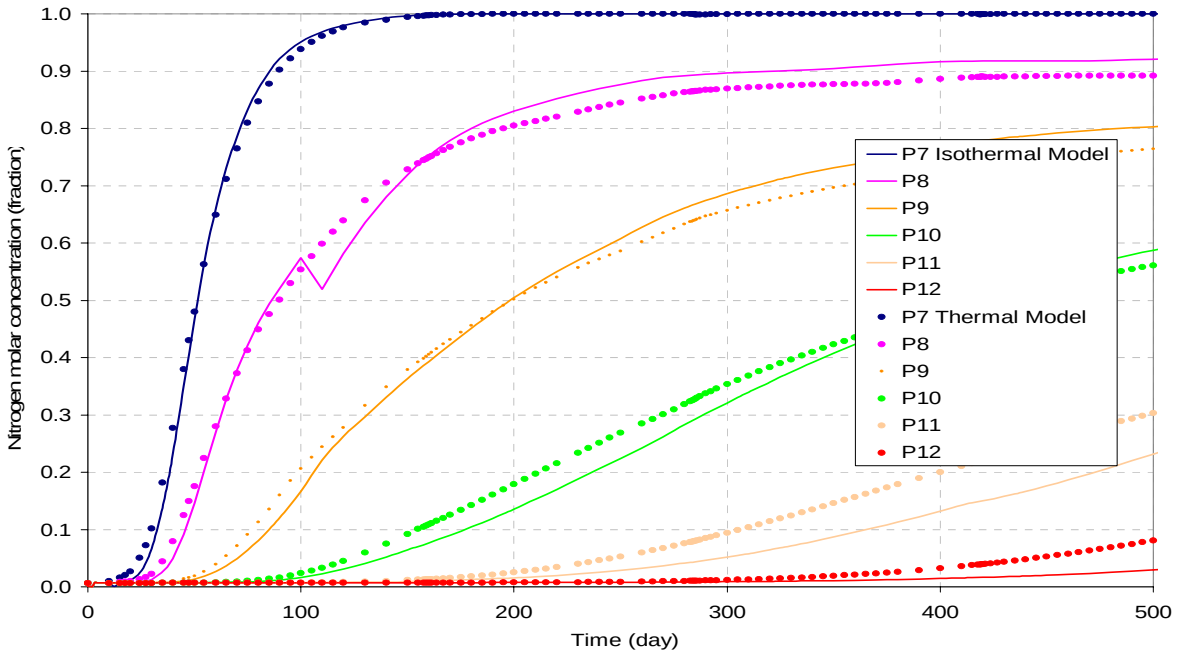

Figure 4.44 Nitrogen horizontal distributions for isothermal and thermal case studies with dual porosity in quarter system under dynamic conditions.

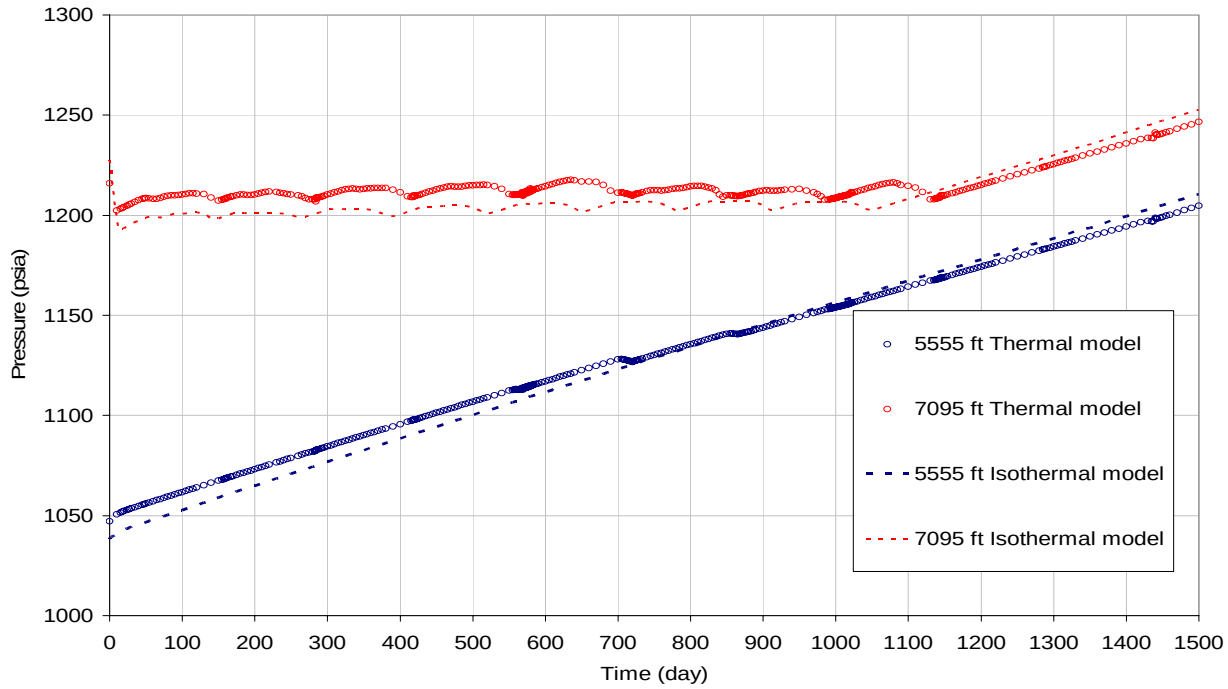

Figure 4.45 Reservoir pressure distributions for isothermal and thermal case studies with dual porosity in quarter system under dynamic conditions.

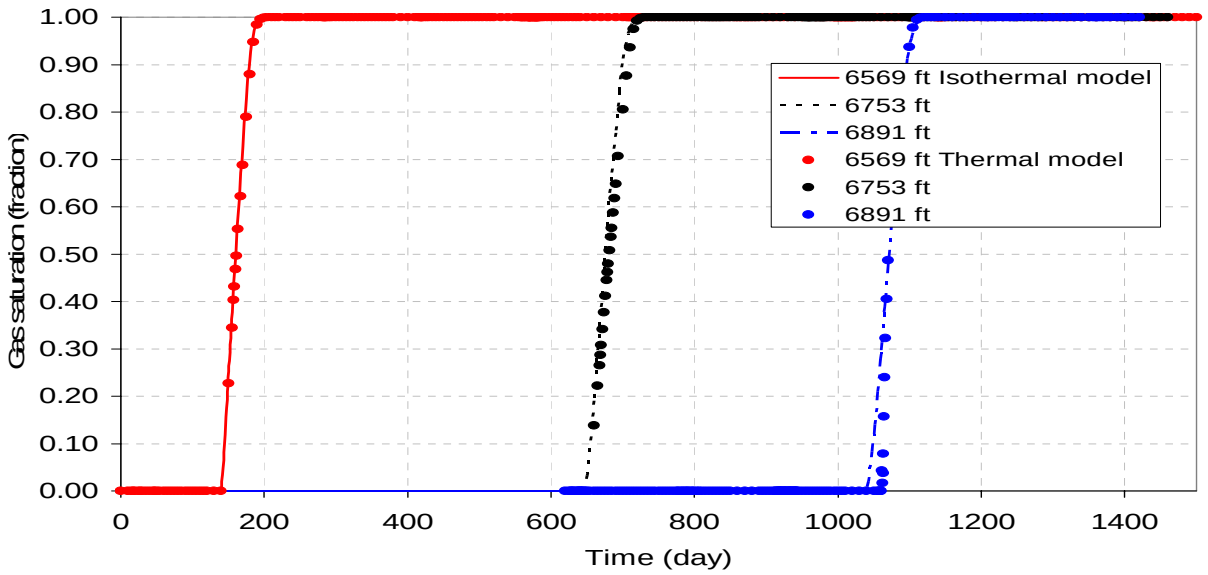

Figure 4.46 Gas saturations in isothermal and thermal case studies with dual porosity in quarter system under dynamic conditions.

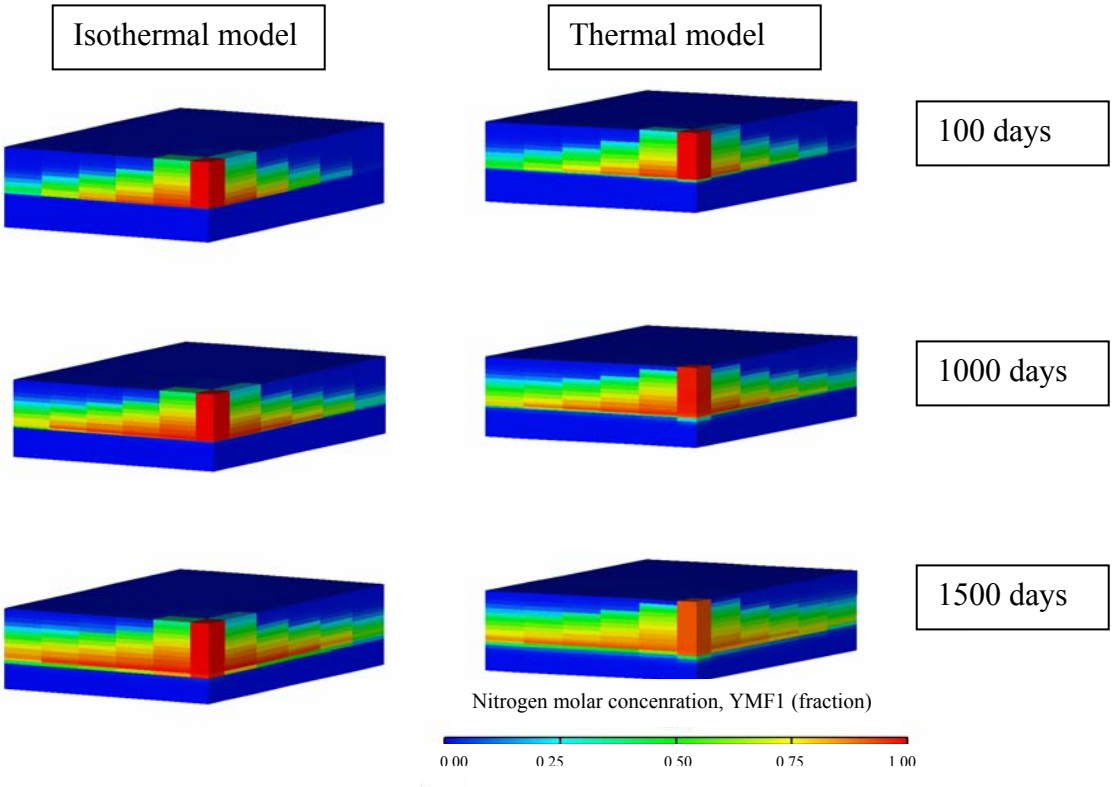

Figure 4.47 Nitrogen molar concentrations for isothermal (left) and thermal (right) case studies during 100, 1000 and 1500 days of injection.

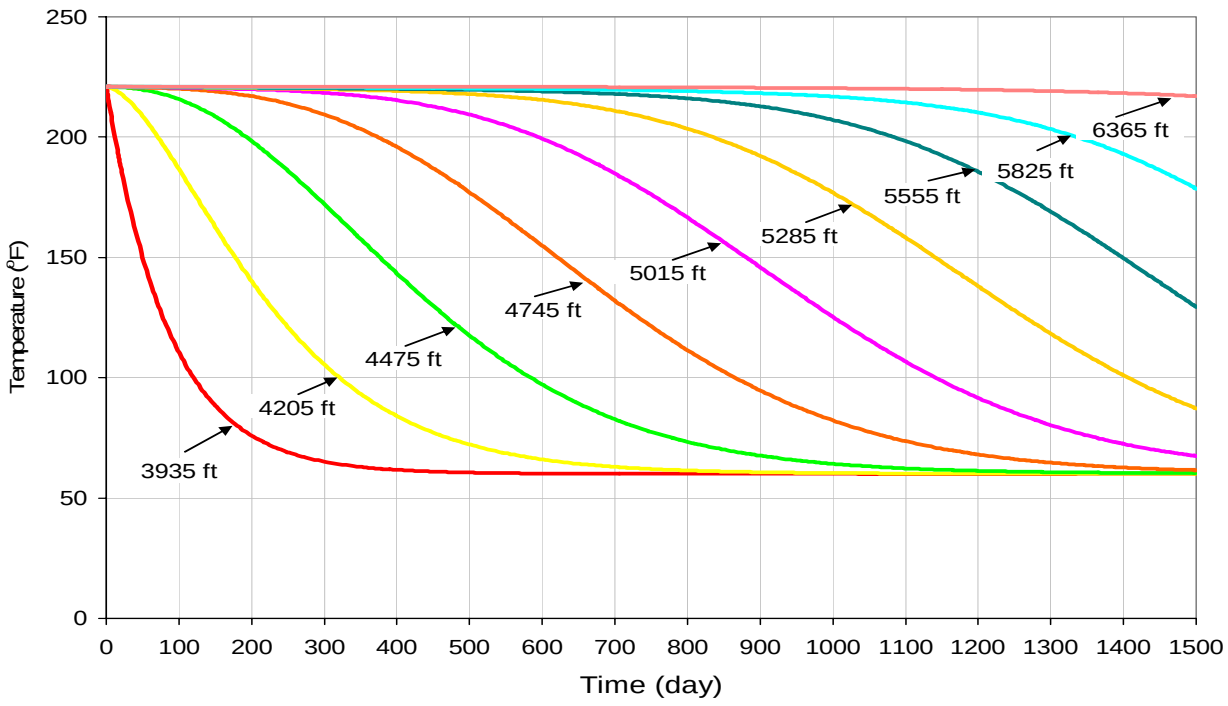

Figure 4.48 Temperature distributions in *z* direction at the center of the field studied using full system and injecting N_2 at 60 °F.

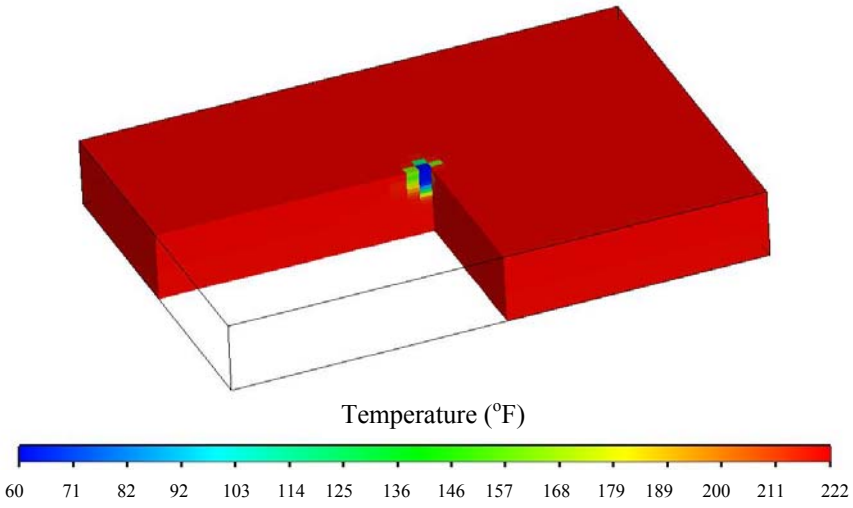

Figure 4.49 Temperature distribution using full system and injecting nitrogen at 60 °F.

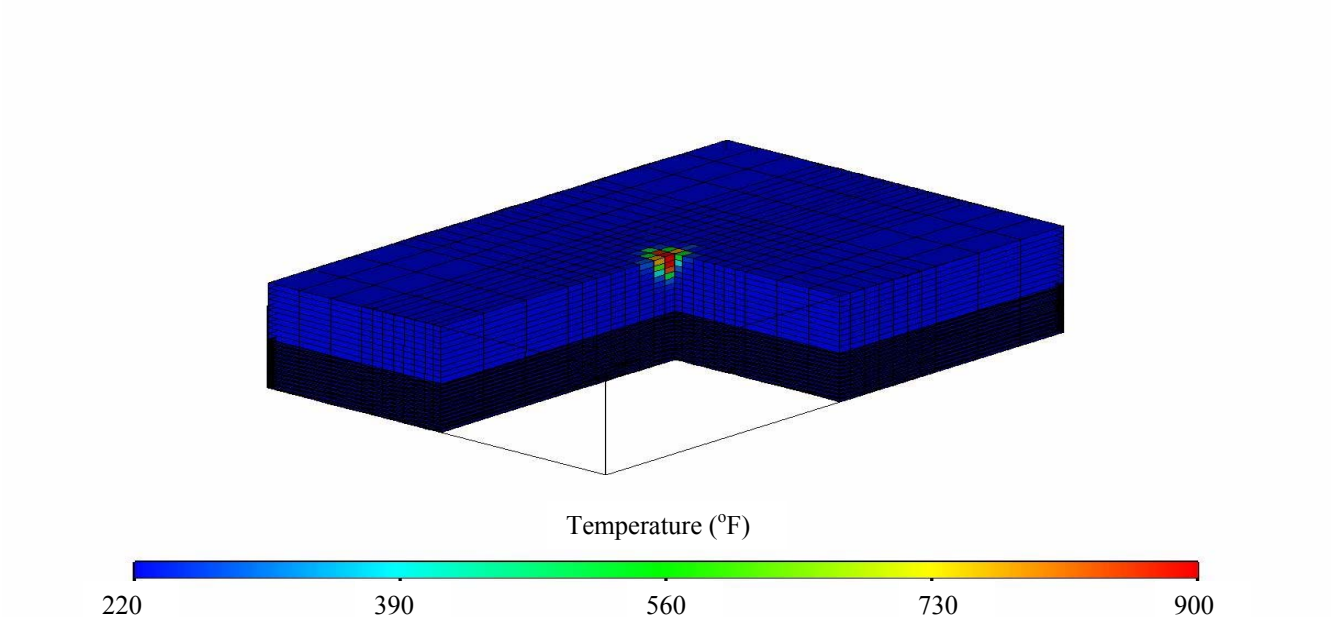

Figure 4.50 Temperature distributions by injecting nitrogen at high temperature (900 °F).

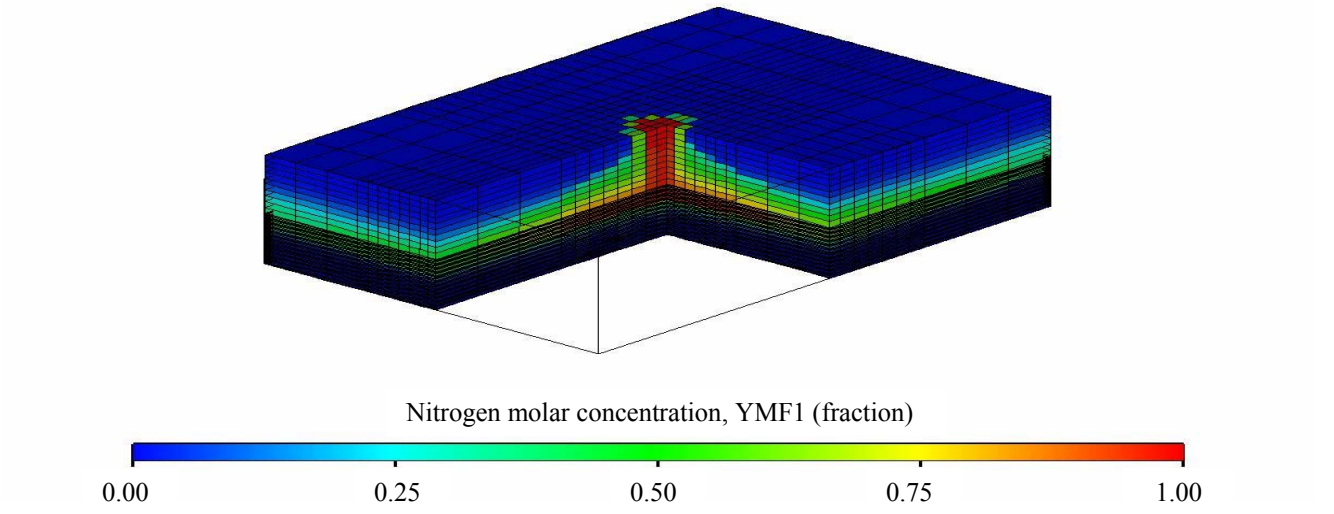

Figure 4.51 Distribution of nitrogen molar concentrations by injecting at high temperature (900 °F).

CHAPTER 5

RESERVOIR SIMULATION CASE STUDIES CONSIDERING HETEROGENEITIES

5.1 Introduction

This chapter addresses the simulation of nitrogen injection in the field under study through different scenarios, considering heterogeneities in order to study their impact on nitrogen distribution and oil recovery. As a starting point, we considered the variation of properties, such as matrix and fracture permeabilities, matrix and fracture porosities, and matrix block dimensions. We performed sensitivity studies based on matrix block size and capillary continuity data to assess their impact on the gravity drainage mechanism.

Heterogeneity and anisotropic properties were considered only for the isothermal compositional model, and the range of values used corresponds to an actual naturally fractured reservoir characterized as a dual porosity system.

Our simulation case studies considered the nitrogen injection for pressure maintenance, the same fluid characterization and conceptual model described in Chapter 4. Therefore, by using the ECLIPSE commercial simulator, we constructed several compositional dual porosity simulation case studies under isothermal conditions in order to adequately represent the production conditions of the field and the monitoring field data before nitrogen injection. The characterization of the reservoir fluid for these case studies considered six components, which adequately represented the available PVT laboratory data (Table 4.2). The main mechanisms in our case studies are: 1) the gravity force mechanism, which occurs in the gas cap and is mainly due to the difference in densities of injected gas and reservoir gas; and 2) the gravity drainage mechanism, which occurs mainly in the oil zone when the fractures are full or partially saturated with gas. In

a fractured reservoir, gravity drainage is an important recovery mechanism and plays a major role in hydrocarbon recovery.

Some authors (Jensen *et al.*, 1997) define heterogeneity as a property of reservoirs that causes the flood front to distort and spread as the displacement proceeds. But heterogeneity is always present in all reservoirs. It is difficult to define and usually has the largest effect on vertical sweep efficiency (Lake, 1989).

In the following section, we show the porosity and permeability data sets, measures of heterogeneity, and simulation results for the reservoir under study by using field data (PEMEX, personal communication). This information provides a good understanding of the impact of heterogeneity on the field under study.

5.2 Heterogeneity and isotropic properties

Table 5.1 displays the input data for the reservoir under study and also shows the values of porosity and permeability for the matrix and the fractured systems. This data indicates that permeability values in the x and y directions for both systems (matrix and fracture) are equivalent and higher than permeability values in the z direction. In addition, we observed that the range of properties considered for the heterogeneous and anisotropic reservoir varies on a small scale.

Figures 5.1 through 5.5 show the property variations of matrix permeability in x direction, matrix porosity, fracture permeability in x direction, fracture porosity, and vertical matrix block sizes, respectively (PEMEX, personal communication). This data set is part of the input data used for the construction of our isothermal, compositional, dual porosity, and heterogeneous case study.

5.2.1 Porosity and permeability histograms of the fractured system.

In order to extract summary information and determine average values for the reservoir properties, we started with the construction of porosity and permeability histograms of the fractured system. We focused our averaging procedure on fracture properties mainly because, for a dual porosity system, the flow occurs mainly through fractures, and the matrix system is considered as a porous medium that stores the hydrocarbons.

The data set used indicated that fracture porosity values followed a normal distribution as shown in Figure 5.6, and fracture permeability values follow a shifted log-normally distribution. These distributions give an understanding of average properties and provide the bridge between property values and statistics, but they do not include any information about spatial arrangement and tend to ignore most of the reservoir structures.

The shape of porosity and permeability histograms can be used to help diagnose the presence of units (e.g., facies) and confirm their geological identification (Jensen *et al.*, 1997). But for our case study, the histograms in Figures 5.6 and 5.7 were used to determine the average field properties. In performing averaging for the reservoir properties, we should keep in mind that in summarizing variability, a considerable amount of information is lost (Jensen *et al.*, 1997).

A measure of variability is a common reservoir engineering practice that can be applied to any reservoir property. Because fracture permeability varies far more than other properties that affect flow and displacement in a dual porosity system, our next analysis focused on the heterogeneity of the fractured system, as described in the following section.

5.2.2 Measures of heterogeneity

5.2.2.1 Lorenz coefficient

Common measures of reservoir heterogeneity are the Lorenz and Dykstra Parsons coefficients. The Lorenz coefficient varies between 0 (homogeneous) and 1 (infinitely heterogeneous) and it is defined as L_C. In order to compute this coefficient for our reservoir under study, we first arranged the permeability values in decreasing order of K/ϕ and then calculated the partial sums.

$F_j = \dfrac{\sum_{j=1}^{J} K_j h_j}{\sum_{i=1}^{I} K_i h_i}$, $C_J = \dfrac{\sum_{j=1}^{J} \phi_j h_j}{\sum_{i=1}^{I} \phi_i h_i}$, where $1 \le J \le I$ and there are I data points, K is the absolute fracture permeability, ϕ is the fracture porosity, and h is the average aperture fracture calculated by $h_i = \sqrt{\dfrac{K_i * 12}{\phi_i}}$. This expression was obtained by equating the Darcy equation $\left(\dfrac{K\,\Delta p}{\mu L}\right)$ and the Poiseuille equation $\left(\dfrac{h^2 \phi\,\Delta p}{12\mu L}\right)$, where μ represents the fluid viscosity, L the radial length of fracture, Δp the pressure drop, and K the absolute permeability.

Fracture aperture values obtained with $h_i = \sqrt{\dfrac{K_i * 12}{\phi_i}}$ ranged from 8 up to 377 microns for our reservoir, and Nelson (2001) reports that fracture aperture values ranged from 1 up to 500 microns for shallowly buried natural fractures. These values are for shallow depths (several hundred meters). However, fracture aperture values obtained for the reservoir under study (3800 ft) were smaller than values reported by Nelson (2001). We expected such results because natural fracture apertures change with depth and during reservoir depletion. On the other hand, the fractured system of the reservoir under study

includes vugs and caverns that have considerable impact on the calculation of average fracture apertures.

Figure 5.8 shows the histogram of fracture apertures for the reservoir under study and indicates that the average value is around 250 microns. This value is an important calculation that will be useful for the analysis of capillary continuity described in Section 5.3.2.

The Lorenz coefficient was obtained by plotting *F* (fraction of total flow capacity) versus *C* (fraction of total volume) on a linear graph and connecting the points to form the flow capacity plot, where *F* represents the fraction of the total flow passing a fraction *C* of the reservoir volume (Jensen *et al*., 1997).

For our heterogeneous case study, we used vertical fracture permeability values in the range of 6000 md up to 7000 md. Other permeability values outside this range were ignored due to their scarcity. By using this information with the corresponding aperture fracture, the calculated Lorenz coefficient was 0.03; and by using vertical matrix permeability values with their corresponding average matrix height, we obtained a Lorenz coefficient of 0.26. The calculation of L_C for the fractured system was obtained using $L_C = \frac{Area.\overline{ABCA}}{Area.\overline{ADCA}}$, where the $\overline{ABCA}$ and $\overline{ADCA}$ are the points that define both areas, as is illustrated on the flow capacity plot of Figure 5.9. Areas $\overline{ABCA}.$ and $\overline{ADCA}$, were calculated by fitting a polynomial function through data and subsequently integrating such polynomial function. L_C for the matrix system was obtained in the same manner, using $L_C = \frac{Area.\overline{AB'CA}}{Area.\overline{ADCA}}$.

Our calculation of L_C, which considered the variation of permeability in a vertical direction resulted in small values for both systems (matrix and fracture), it was a first indication that both systems can be represented using averaged properties. This was also

confirmed by performing numerical simulations using average reservoir properties and heterogeneous reservoir properties respectively, using the same formulation and the same conceptual reservoir model.

We also performed a L_C calculation using horizontal permeability data for matrix and fracture systems; results indicated that both flow capacity curves followed a very similar behavior such as a 45^o line $(\overline{AC})$, which also indicates that the variation of properties in a horizontal direction can be represented by averaged properties for both matrix and fracture systems.

It is important to point out that L_C calculations provide a basic understanding of data but it is necessary to confirm the use of averaged properties by performing numerical simulations, since different permeability distributions can give the same value as the Lorenz coefficient.

5.2.2.2 Dykstra-Parsons coefficient

A second, and perhaps more common, measure that lies between the same limits as L_C is the Dykstra-Parsons coefficient, defined as $V_{DP} = \frac{k_{0.50} - k_{0.841}}{k_{0.50}}$ (Peters, 2004), where $K_{0.50}$ is the median permeability and $K_{0.841}$ is the permeability one standard deviation up $K_{0.50}$ on a log-probability plot. The Dykstra-Parsons coefficient is computed from a set of permeability data ordered in decreasing value. $K_{0.50}$ and $K_{0.841}$ values were taken from a best fit line when data was plotted on a log-probability paper. For our case study using fracture permeability in a vertical direction, the probability plot for the calculation of the Dykstra-Parsons coefficient is illustrated in Figure 5.10. The probability scale used in Figure 5.10 was constructed by using DISTR.NORM.INV, a statistic function of Microsoft Office Excel, where $K_0 = K_{0.50}$ and $K_1 = K_{0.841}$.

Since most of data in Figure 5.10 follow a horizontal line trend, $K_{0.50}$ and $K_{0.841}$ values were very similar (6500 and 6400, respectively), therefore the Dykstra-Parsons coefficient calculated was a small value (V_{DP}=0.015). V_{DP} and L_C coefficients resulted in small values because there are not a lot of variations in the vertical permeability values of the field under study, and also because variation of permeability data followed a shifted log-normal distribution.

Some authors (Jensen *et al*., 1997) have indicated that many studies show a small sensitivity of models to variations in the Dykstra-Parsons coefficient when $V_{DP} \leq 0.5$, while for large-heterogeneities ($V_{DP} \geq 0.5$) they observed a large sensitivity. These results were verified for the reservoir under study by performing numerical simulations.

The numerical simulation results and the measured heterogeneities indicated that by having small values for the Lorenz and Dykstra-Parsons coefficients in a process with a strong gravity drainage mechanism, reservoir modeling can be represented by averaging reservoir properties. This is described in detail in Section 5.3.2.

5.3 Numerical simulation

5.3.1 Modeling approach

We considered that two zones form the conceptual model as shown in Figure 3.1. An upper zone corresponds to a gas cap where nitrogen has been injected, and an oil lower zone limited by the oil-water contact. Therefore our case study has been reduced to an oil-gas system with an initial water saturation of 0.15 (by design) in the entire reservoir. All oil production wells were geometrically distributed at the bottom of the system and constrained by a constant bottomhole pressure. This design allowed simulation of a constant pressure boundary condition at the oil-water contact after nitrogen injection was initiated. The identification of this boundary condition is supported

by both the analysis of the monitoring pressure response taken before and after nitrogen injection and the steady movement of the gas-oil contact through the exploitation of the field studied. Six injector wells were drilled and completed within the top center of the field in the gas cap and were constrained by a constant nitrogen injection rate. The grid dimension was 11x11x120. The minimum grid sizes in *x*, *y* and *z* directions were 525, 787 and 46 ft, respectively. A constant field nitrogen injection rate of 1,300 MMscf/day with a constant bottomhole pressure in all producer wells was used for all our simulation cases. A good match of the oil field production (1,500,000 bpd) and the reservoir pressure distribution was obtained before the nitrogen injection initialization.

5.3.2 Numerical simulation results

Simulation results considering heterogeneous and anisotropic properties indicated that nitrogen molar concentrations followed almost the same flow pattern typical of average reservoir properties, as illustrated in Figure 5.11. Similar nitrogen distribution resulted because the range of reservoir properties considered for the heterogeneous and anisotropic reservoir varies on a small scale. The simulation result is consistent with the calculations obtained for the Lorenz and Dykstra-Parsons coefficients.

The results of numerical simulations considering the heterogeneous case study confirmed that although, to best of our knowledge, there is no reservoir that has homogeneous properties. This does not imply that all reservoirs are dominated by their heterogeneity, since in many cases one mechanism is so strong that it completely overshadows all others (Lake, 1989). Therefore, the representation of the reservoir under study using average reservoir properties is a good assumption.

In all our case studies, the gravity drainage mechanism is very pronounced, and the impact of the oil production rate for heterogeneous and averaged cases occurred in a similar manner, as illustrated in Figure 5.12. This figure illustrates small changes in oil

production rates due to heterogeneity effects, and we also observed that the cycling behavior of the oil production rate for the heterogeneous case study is less than in the homogeneous case study.

Table 5.2 illustrates the arrival time of a 90% nitrogen molar concentration at different depths for both heterogeneous and homogenous case studies; such locations correspond to the center of the reservoir under study where nitrogen is injected. This table shows that nitrogen fronts move at a similar velocity near the GOC through the fractured system in both cases.

Since gravity drainage is the main mechanism that occurs in the reservoir under study, we performed several sensitivity studies on geological uncertainties in order to study their impact on the production forecasting. The simulation studies are presented in Section 5.4.

5.4 Sensitivity study

In this section, we focus on sensitivity studies based on matrix block sizes and capillary continuity to access their impact on the gravity drainage mechanism. The ECLIPSE commercial simulator with a compositional formulation and a dual porosity option was used for the field simulation case studies. Furthermore, our sensitivity studies for capillary continuity were performed using several fracture apertures considering a block size with 10 ft height.

The purpose of this study was to focus on the impact of uncertain properties based on production forecasting and nitrogen distribution during nitrogen injection in naturally fractured reservoir under a strong gravity drainage mechanism. We performed several sensitivity studies based on matrix block sizes and capillary continuity properties because of their high impact on the gravity drainage mechanism. The sensitivity cases considered the conceptual model used in Chapter 4.

5.4.1 Sensitivity study on matrix block size

Matrix block sizes affect production rate and oil recovery during gas gravity drainage under secondary and tertiary conditions in naturally fractured reservoirs. This observation resulted from a work comprised of analyzing reported laboratory experiments under reservoir conditions by Saidi *et al.* (1993). The results of these experiments were also reproduced by using a compositional simulator.

Matrix block size is an uncertain parameter that is difficult to obtain for the entire reservoir and affects production rate and oil recovery during gas gravity drainage under secondary and tertiary conditions in naturally fractured reservoirs. The block size dimensions are used for the shape factor of the Kazemi formulation: $\sigma = 4\left(\frac{1}{L_x^2}+\frac{1}{L_y^2}+\frac{1}{L_z^2}\right)$, where $L_{x,}L_y$ and L_z are typical *x*, *y* and *z* matrix dimensions that are not related to the simulation grid dimensions. Matrix geometry is one of the main factors in evaluating oil recovery for a dual porosity model, and its distribution in the entire reservoir is very important.

Saidi (1987) recommends several methods that may be used to determine this important parameter, such as outcrop studies, flowmeter survey, gradiomanometer, magnetic resonance scanner, tracer injection, log interpretation, and diffusion.

Recently, modern techniques using geomechanic models, statistics, and seismic data (Galarraga *et al.*, 2005, Al-Qahtani *et al.*, 2001, Araktingi *et al.*, 1992) have been developed to aid in determing the distribution of the fracture network, and therefore determining the shape of matrix blocks. The combination of these methods and techniques can result in a better interpretation and integration of all available data to determine a matrix block size distribution for naturally fractured reservoirs.

When information is not available, a common simulation practice is to define an average shape factor as a matching parameter for the entire reservoir, but generally this practice impacts the geometry of matrix blocks when we define L_z then try to obtain a history matching by changing shape factors. For our sensitivity study, we used five different geometries of matrix blocks by using the same shape factor ($0.36/ft^2$) with different block heights and the same dimension L_x and L_y using Kazemi's formulation (Figure 5.13).

The simulation cases were performed on a quarter representation of a homogeneous, compositional, isothermal, and dual porosity case study with a constant matrix block size.

The simulation results of all cases which considered variations in matrix block sizes indicated that the gravity drainage mechanism has different behaviors with respect to depth; therefore we analyzed two cases, one at a depth near the GOC (at 6523 ft) and other far from the GOC (at 6891 ft).

5.4.1.1 Gravity drainage sensitivity analysis with variations in matrix block sizes located near and far from GOC

At the same depth, near the GOC (6523 ft), the gravity drainage mechanism behaves differently, as illustrated in Figure 5.14. This figure shows that the arrival time of nitrogen is similar in all case studies. This is mainly because injected nitrogen moves straight to the GOC, due to the gravity force mechanism, which occurs in the gas cap and is mainly dependent on the difference between densities of injected gas and reservoir gas. Figure 5.14 also shows that the highest oil recovery was obtained for slabs with the biggest matrix block height. On the other hand, for matrix blocks located far from the GOC (6891 ft), matrix oil saturations behave differently from matrix blocks located near the GOC, as shown in Figure 5.15.

Figure 5.15 illustrates that gravity drainage far from the GOC initiated early in matrix blocks with smaller height ($L_z = 4$ ft); this occurs mainly because the nitrogen arrival time is faster in small matrix block heights than in large matrix heights. Besides, as it was observed on blocks near the GOC, the lowest oil recovery is obtained for the smallest matrix block height because they reach a faster equilibrium between gravity and drainage forces than bigger matrix block heights.

We also compared the gravity drainage behavior at different depths for two block sizes (4 ft and 46 ft). The gravity drainage behavior for a matrix block of a 4 ft height at different reservoir locations is illustrated in Figure 5.16, and for a matrix block of a 46 ft height in Figure 5.17. Simulation results indicated that the gravity drainage mechanism for the same matrix block size at different depths has a similar impact on gravity drainage behavior with a shift in time because of nitrogen arrival time. Figure 5.18 illustrates the impact of the gravity drainage mechanism within two matrix block sizes (L_z = 4 ft and L_z = 46 ft) shifting curves at the same time. Figures 5.18 (matrix oil saturation versus time) and 5.19 (cumulative oil production versus time) show that higher oil recoveries were obtained with matrix blocks with the bigger matrix height (L_z = 46 ft). Computing time by performing case studies in matrix blocks with 46 ft height is longer (by a factor of 9) than a case with smaller matrix height (see Figure 5.20).

The results from the sensitivity study on the matrix block size indicated that:

1) The gravity drainage mechanism in nitrogen injection into a naturally fractured reservoir depends not only on the matrix block height but also on reservoir depth and nitrogen arrival time. Therefore, total oil production is not linearly dependent on the matrix block height.

2) Common simulation practices, such as matching shape factor for the entire reservoir by defining matrix height, impacts matrix block geometry and therefore affects

the total oil recovery, mainly when gravity drainage is the dominant reservoir mechanism.

3) The gravity drainage mechanism for the same matrix block size at different depths has a similar impact on gravity drainage behavior with a shift in time because of nitrogen arrival time.

5.4.2 Sensitivity study on capillary continuity

We investigated the impact of capillary continuity to assess the impact of the major forces (gravity and capillarity) during nitrogen injection into naturally fractured reservoirs, and also because, in practice, very often the performance predictions of fractured petroleum reservoirs have been based on the assumption of capillary discontinuity between matrix blocks. For all our case studies we used several averaged reservoir properties for a quarter, compositional, isothermal, and dual porosity system.

When gravity drainage is the main mechanism, the effect of fracture capillary pressure is generally more pronounced than in a capillary-imbibition process (Firoozabadi *et al.*, 1989) and oil recovery strongly depends on capillary continuity (Labastie *et al.*, 1990).

The existence of capillary continuity between blocks is supported by very little reliable experimental data. Some authors (Firoozabadi *et al.*, 1990) confirmed, in their experiments with a stack of small matrix blocks, the validity of a porous-medium model with fracture capillary pressure. Others (Labastie *et al.*, 1990) have found that oil recovery strongly depends on capillary continuity by designing several series of gravity drainage experiments with a stack of two matrix blocks in contact through bridges made either of porous and permeable media of various characteristics, or non-porous material.

The experimental results of Horie *et al.* (1988) have shown capillary interaction (capillary continuity) between the neighboring blocks, and the authors believe that

incorporation of the capillary-continuity concept in dual porosity models will result in more realistic simulation of naturally fractured reservoirs. Saidi (1987) often assumed capillary discontinuity between a stack of matrix blocks, and he argues that if the fracture aperture is about 0.05 mm (50 microns) or more, capillary continuity between a stack of blocks cannot be realized. The problem of capillary continuity between the matrix blocks of a naturally fractured reservoir is still quite controversial and it very likely always exists (Labastie *et al.*, 1990).

Very often, the performance predictions of fractured petroleum reservoirs have been based on the assumption of capillary discontinuity between matrix blocks, but in naturally fractured reservoirs the matrix blocks are not isolated, as in some idealized representations.

The characteristics of a fractured medium expected to influence the fracture capillary pressures are fracture aperture, fracture surface roughness, and the number of contact points between the fracture faces. For our capillary continuity sensitivity analysis, a set of fracture capillary pressure curves was generated for various fracture apertures based on the Firoozabadi and Hauge model (1989). They developed a phenomenological model based on the Young-Laplace equation of capillarity, $P_c = \gamma\left[\left(\frac{1}{r_1}\right)+\left(\frac{1}{r_2}\right)\right]$, where P_c is the pressure difference across the interface, r_1 and r_2 are radii of curvature of the curved interface at any point, and γ is the surface tension.

We used ($P_{cfD} = \frac{b_o P_c}{\gamma}$) to generate a set of fracture capillary pressure curves to study the impact of gravity drainage, where P_{cfD} is the derived fracture capillary pressure converted to a dimensionless form, b_o is the mean fracture half-width, γ is the interfacial tension, and P_c is the fracture capillary pressure. The numerical values of the dimensionless capillary pressure P_{cfD}, as a function of wetting phase saturation, are listed

in Table 5.3; this information was obtained from a recent published paper (De la Porte *et al.*, 2005).

Our sensitivity study on capillary continuity was performed by several average fracture apertures considering an average block size with a 10 ft height. Fracture capillary pressure data was calculated by considering a gas-oil interfacial tension of 10 dynes/cm and a dimensionless capillary pressure P_{cfD} already shown in Table 5.3. A set of fracture capillary pressure data used for our simulation case studies is shown in Table 5.4.

A recent study on capillary continuity (De la Porte *et al.*, 2005) has shown that in gas-oil systems with gas invading the fractures, use of non-zero gas-oil capillary pressure in narrow fractures, that is, fractures that are 100 microns or less in width, is necessary to predict the oil recovery. Also this recent investigation indicated that oil recovery from the matrix blocks could be underestimated by a factor of almost two when fracture capillary pressure is set at zero.

Our sensitivity study results on capillary continuity in a gas-oil conceptual model, where gravity drainage is the main mechanism during nitrogen injection into naturally fractured reservoirs, indicated that for smaller fracture apertures (high fracture capillary pressure), oil recovery has a considerable impact. Figure 5.21 illustrates important variations on total oil production for cases considering fracture apertures that range from 10 up to 300 microns, and also for a case study considering a zero fracture capillary pressure.

Simulation results suggest that when performing a simulation study for a naturally fractured reservoir it is necessary to reduce the uncertainty of fracture apertures and therefore uncertainty in fracture capillary pressure curves. This is because fracture aperture strongly impacts the oil recovery. For our case studies, oil recovery is affected by a factor that ranges from 1 to 2.2 by considering fracture apertures between 10 to 300

microns, respectively. Table 5.5 shows the ratios of oil recovery factors for the cases with fracture capillary pressure over the case using capillary discontinuity.

Figure 5.21 shows that considering capillarity discontinuity is a good approximation for fracture apertures near or up to 300 microns. Since the fracture aperture histogram for the reservoir under study (Figure 5.8) averaged about 250 microns, capillarity discontinuity is a good assumption to use for the reservoir under study.

In order to confirm such approximations, we constructed Figure 5.22, which illustrates the gravity drainage behavior for two gridblocks located at 6707 ft and 6937 ft. We then compared a simulation case study considering a fracture aperture of 300 microns versus a simulation case study using capillary discontinuity. The results indicate similar gravity drainage behaviors for both cases, as we expected.

Table 5.1 Statistic values for matrix and fractured systems used in the construction of an isothermal, dual porosity, compositional and heterogeneous case study.

Property	Min. Value	Max. Value	Range	Mean	Medium	Standard Deviation
MATRIX SYSTEM						
Porosity (fraction)	0.004	0.110	0.1062	0.039	0.0400	0.0153
Permeability in *x* direction (md)	0.070	6.000	5.9300	2.367	1.6770	2.0550
Permeability in *y* direction (md)	0.070	6.000	5.9300	2.367	1.6770	2.0550
Permeability in *z* direction (md)	0.06	4.800	4.7400	1.894	1.3410	1.6440
Height of matrix block (ft)	10	60	50	37.49	40.00	21.44
FRACTURE SYSTEM						
Porosity (fraction)	0.003	0.17	0.167	0.0298	0.0305	0.0124
Permeability in *x* direction (md)	8000	15000	7000	8097	8000	643
Permeability in *y* direction (md)	8000	15000	7000	8097	8000	643
Permeability in *z* direction (md)	6400	12000	5600	6477	6400	514

Table 5.2 Arrival time of 90% nitrogen molar concentrations through fractured system for homogeneous and heterogeneous case studies.

Cell number below injector well	Depth (ft)	Arrival time of nitrogen front (days)	
		Homogeneous case study	Heterogeneous case study
10	2565	116	120
15	2772	495	573
20	3002	997	1200

Table 5.3 Dimensionless fracture capillary pressure (De la Porte *et al*., 2005).

Saturation of wetting phase	$P_{cfD}=b_oP_c/\gamma$
0.00	17.240
0.01	4.7400
0.02	3.8070
0.04	3.0160
0.06	2.5850
0.08	2.4420
0.10	2.2980
0.12	2.1540
0.14	2.0110
0.16	1.8670
1.00	0.8619

Table 5.4 Fracture capillary pressure data for different fracture apertures.

Sg	PcfD	Pcf (psia) (300 microns)	Pcf (psia) (100 microns)	Pcf (psia) (50 microns)	Pcf (psia) (20 microns)	Pcf (psia) (10 microns)
0.00	17.2400	0.0833	0.2500	0.5000	1.2499	2.4998
0.01	4.7400	0.0229	0.0687	0.1375	0.3437	0.6873
0.02	3.8070	0.0184	0.0552	0.1104	0.2760	0.5520
0.04	3.0160	0.0146	0.0437	0.0875	0.2187	0.4373
0.06	2.5850	0.0125	0.0375	0.0750	0.1874	0.3748
0.08	2.4420	0.0118	0.0354	0.0708	0.1770	0.3541
0.10	2.2980	0.0111	0.0333	0.0666	0.1666	0.3332
0.12	2.1540	0.0104	0.0312	0.0625	0.1562	0.3123
0.14	2.0110	0.0097	0.0292	0.0583	0.1458	0.2916
0.16	1.8670	0.0090	0.0271	0.0541	0.1354	0.2707
1.00	0.8619	0.0042	0.0125	0.0250	0.0625	0.1250

Table 5.5 Ratio of oil recovery factors for cases with fracture capillary pressure and for a case considering capillary discontinuity.

Case study	$R = \dfrac{Oil\ recovery\ factor\ for\ cases\ with\ P_{cf}}{Oil\ recovery\ factor\ for\ a\ case\ considering\ capillary\ discontinuity}$
10 microns	2.2
20 microns	2.0
50 microns	2.0
100 microns	1.4
300 microns	1.0

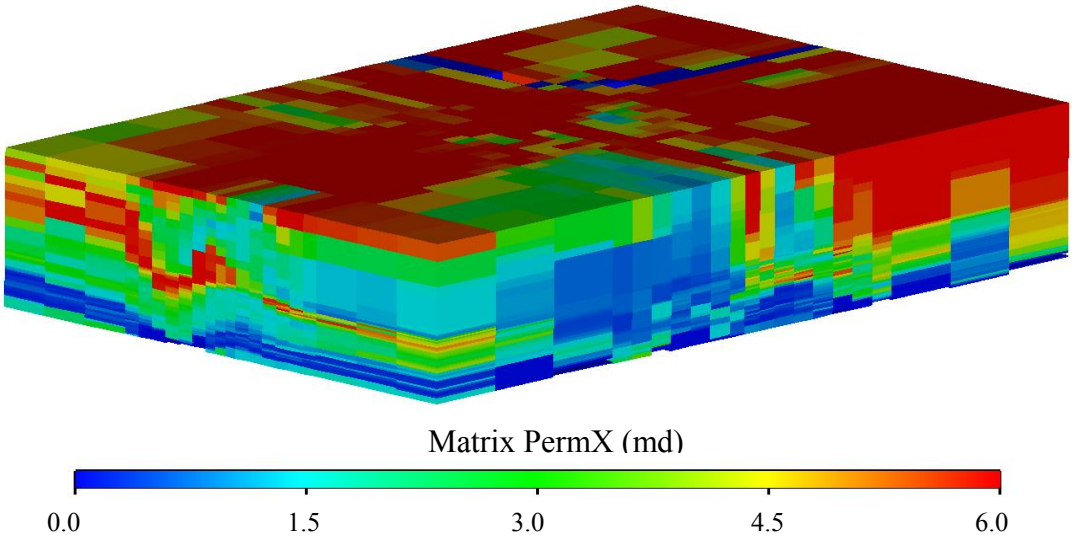

Figure 5.1 Matrix permeability values in *x* direction for an isothermal, compositional, heterogeneous dual porosity case study.

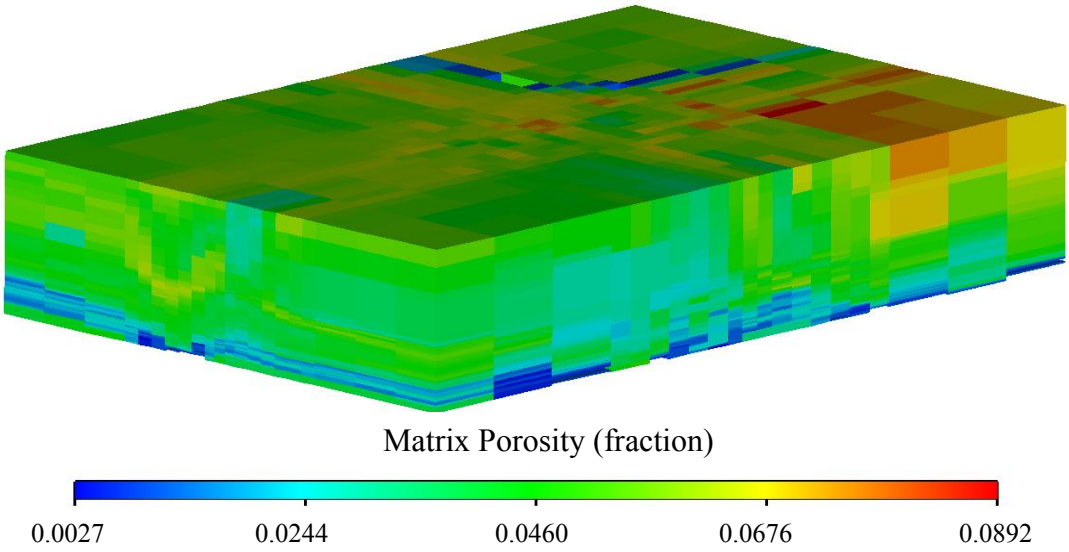

Figure 5.2 Matrix porosity values for an isothermal, compositional, heterogeneous dual porosity case study.

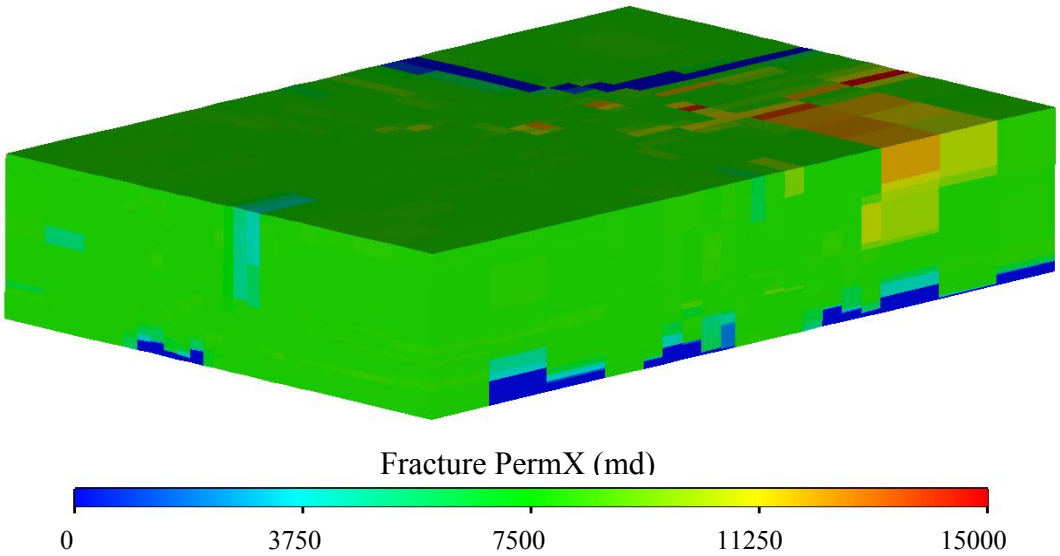

Figure 5.3 Fracture permeability values in *x* direction for an isothermal, compositional, heterogeneous dual porosity case study.

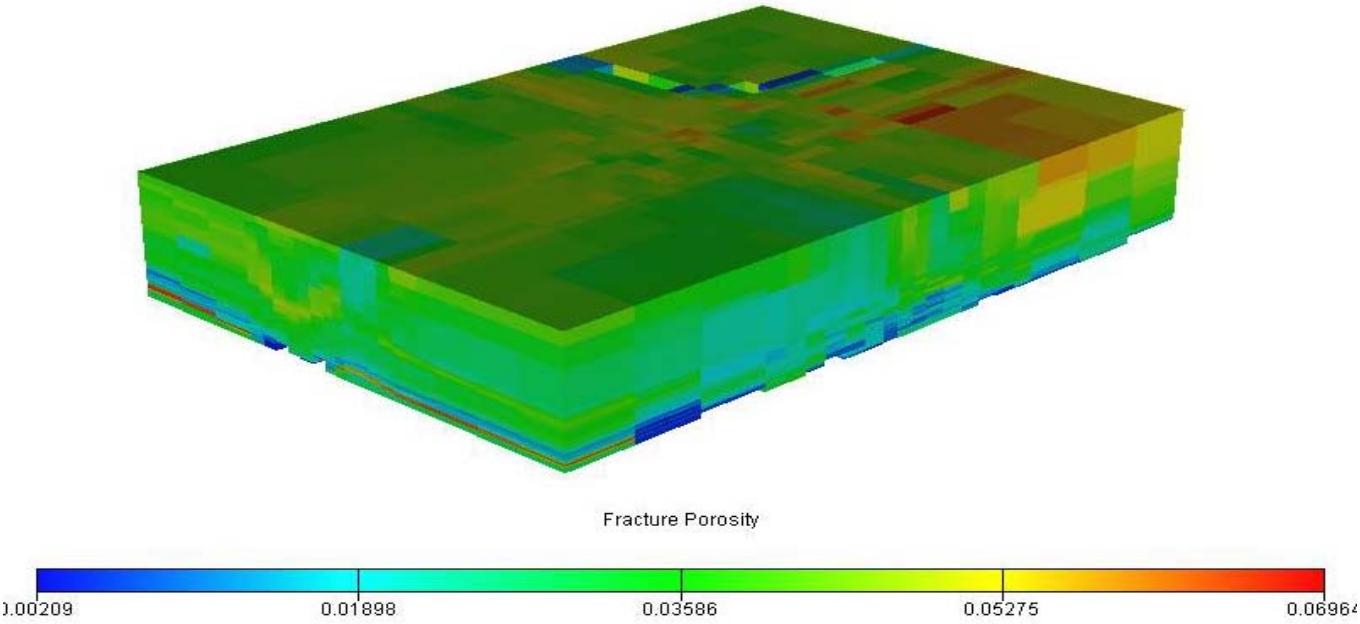

Figure 5.4 Fracture porosity values for an isothermal, compositional, heterogeneous dual porosity case study.

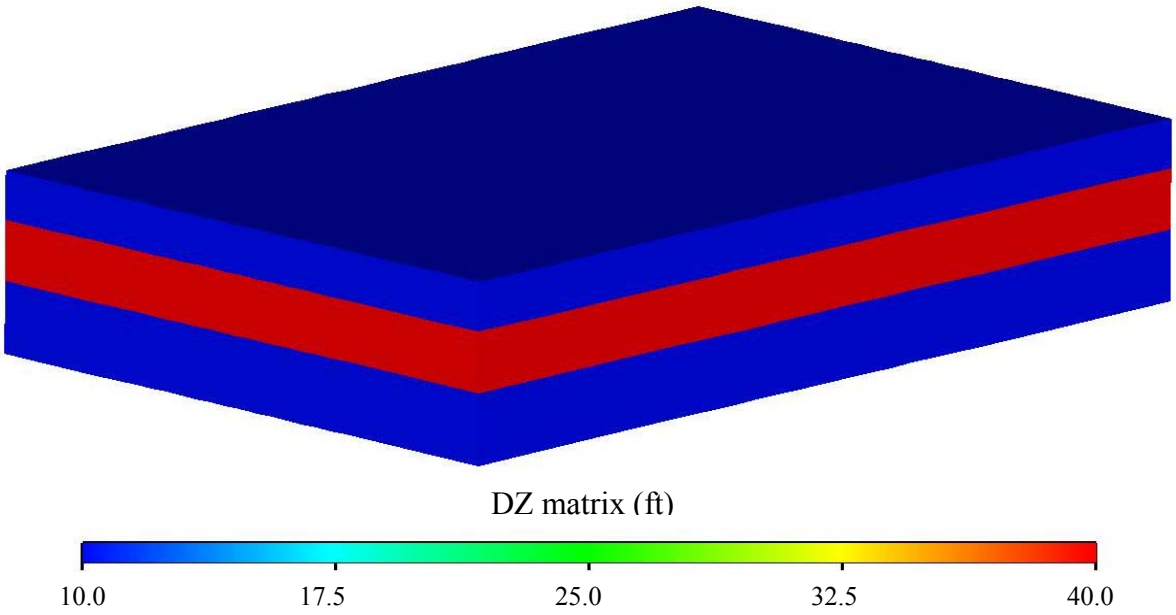

Figure 5.5 Vertical matrix block sizes for an isothermal, compositional, heterogeneous dual porosity case study.

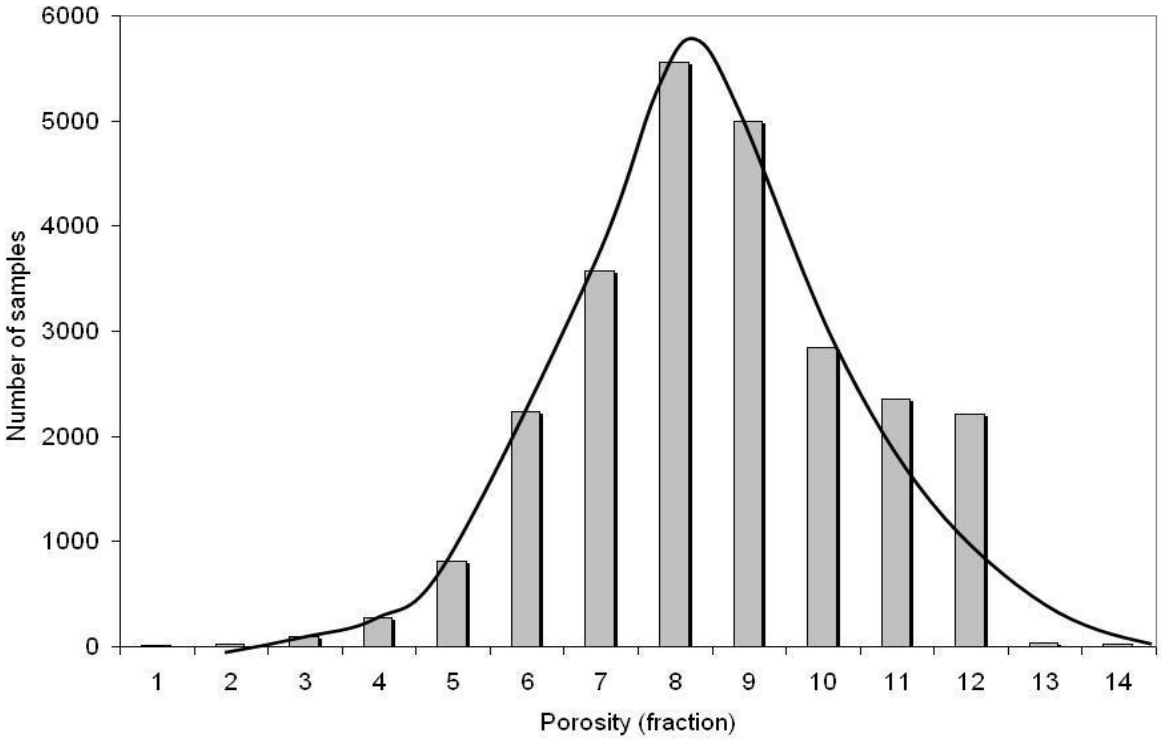

Figure 5.6 Histogram of fracture porosity values for the reservoir under study.

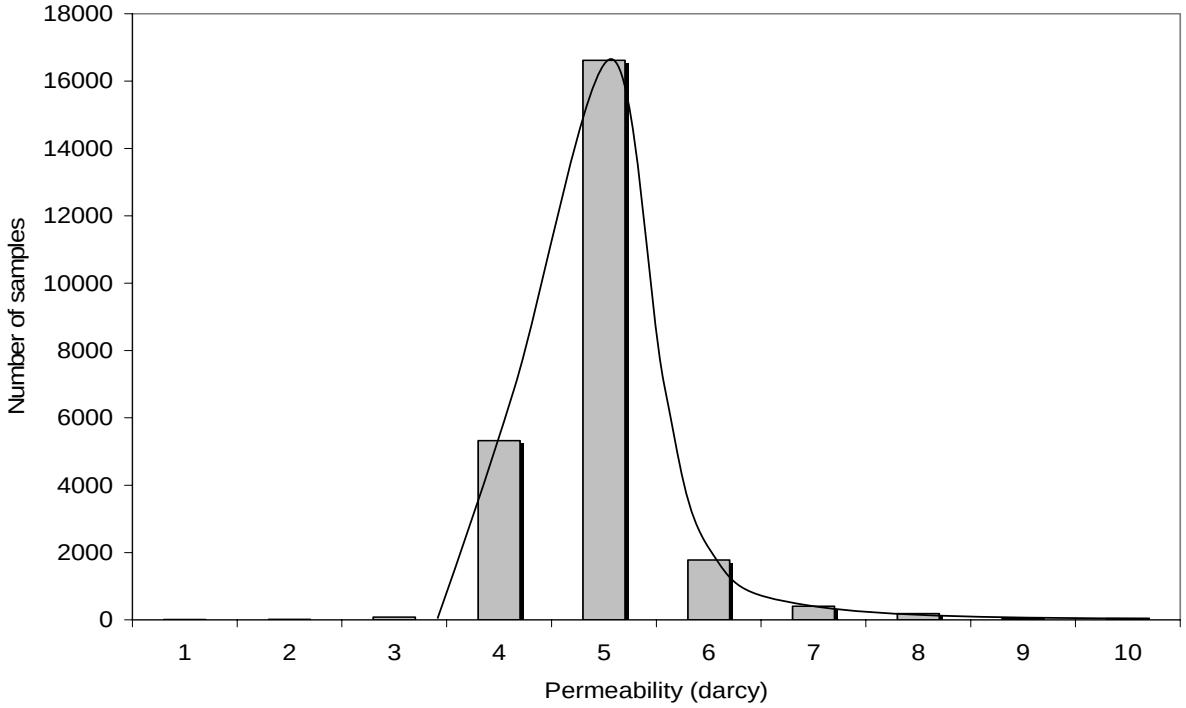

Figure 5.7 Histogram of vertical fracture permeability values for the reservoir under study.

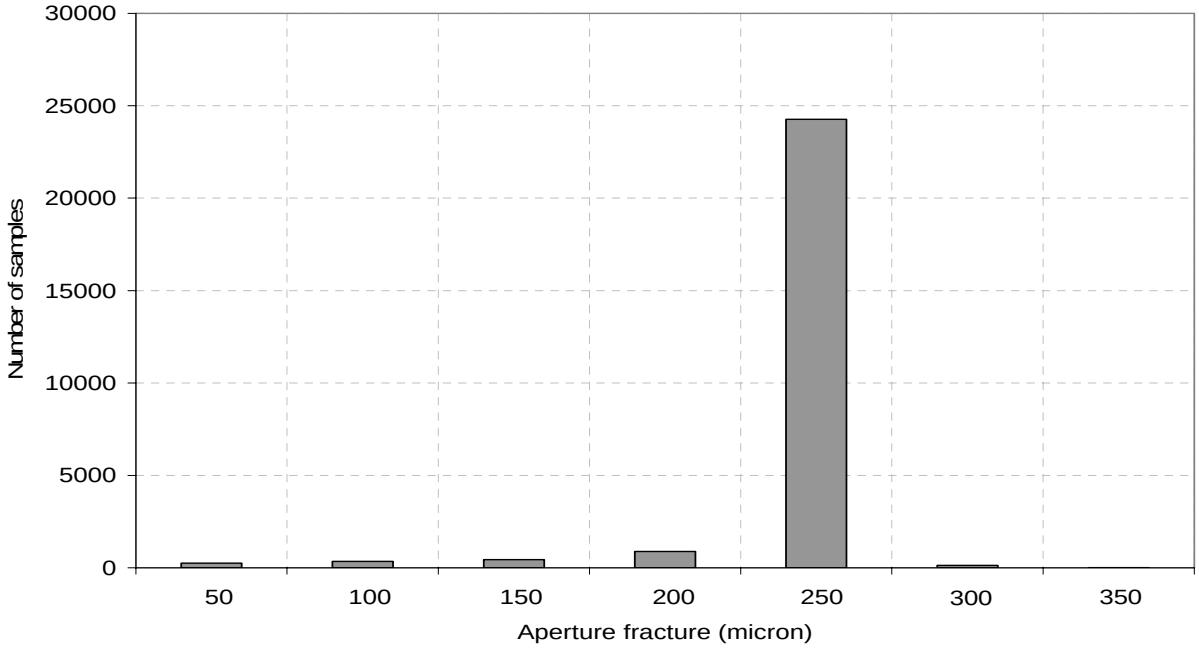

Figure 5.8 Histogram of fracture aperture values calculated by an expression resulted from equating Darcy and Poiseuille equations.

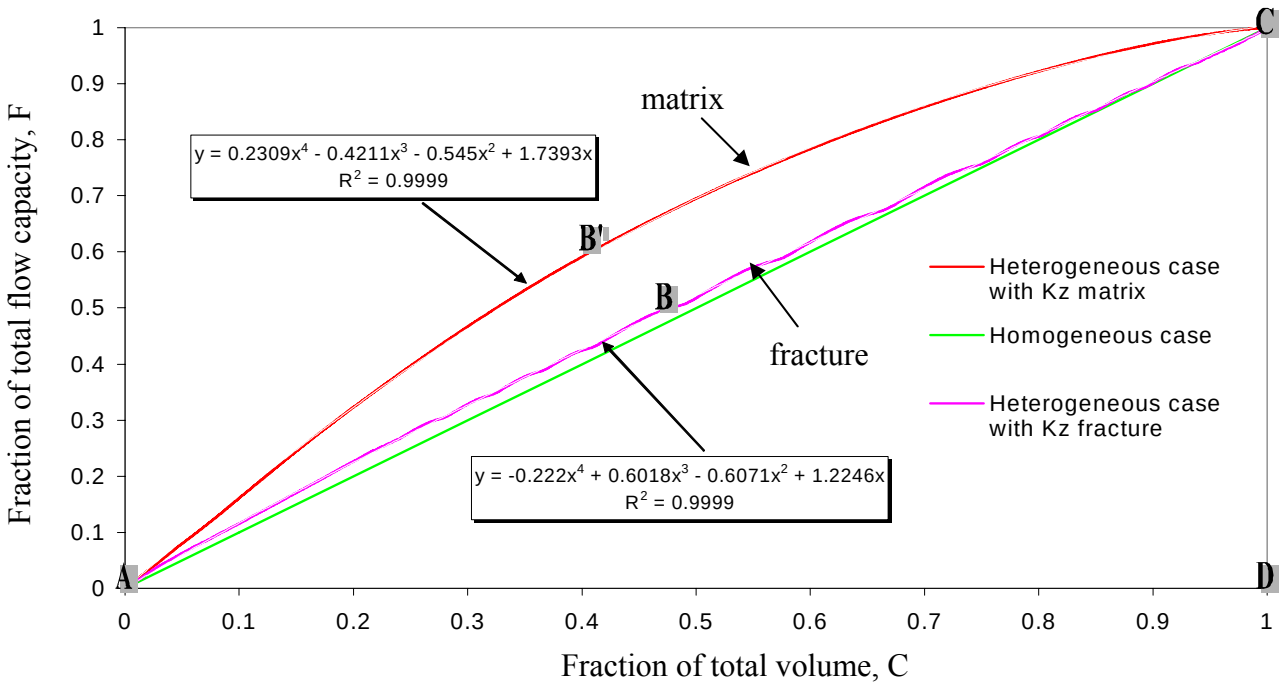

Figure 5.9 Flow capacity plot using vertical permeability for matrix and fractured systems.

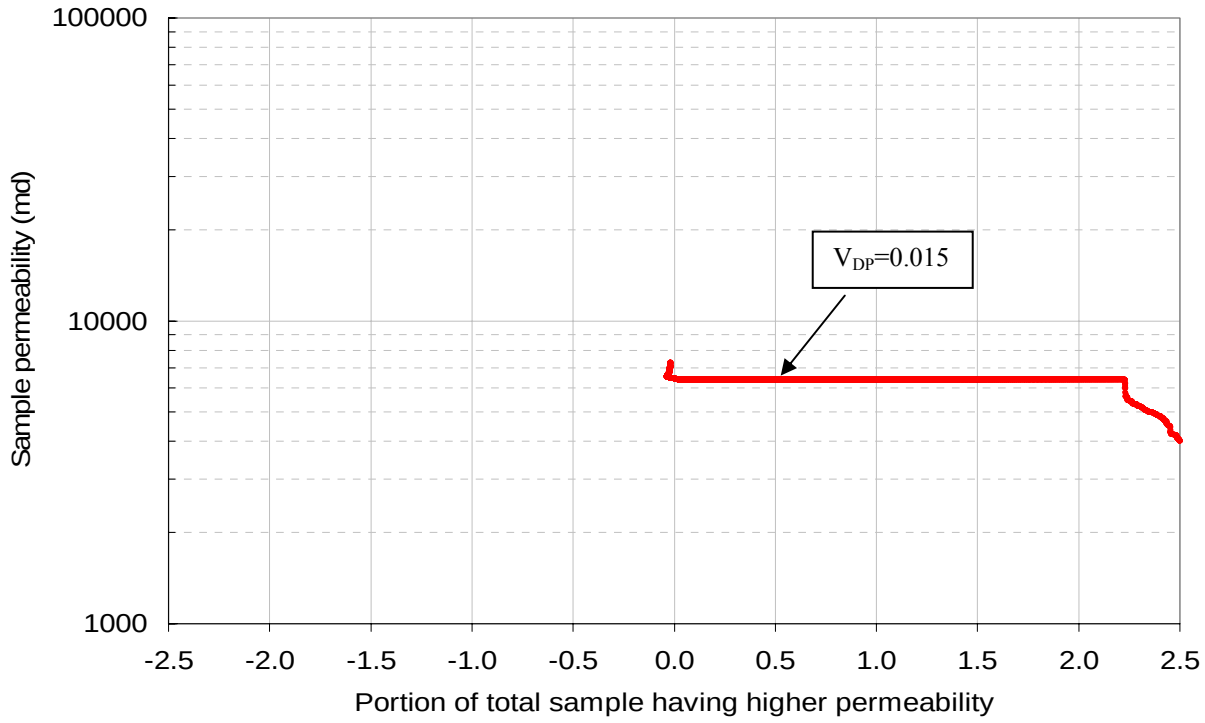

Figure 5.10 Probability plot for Dykstra-Parsons coefficient calculation.

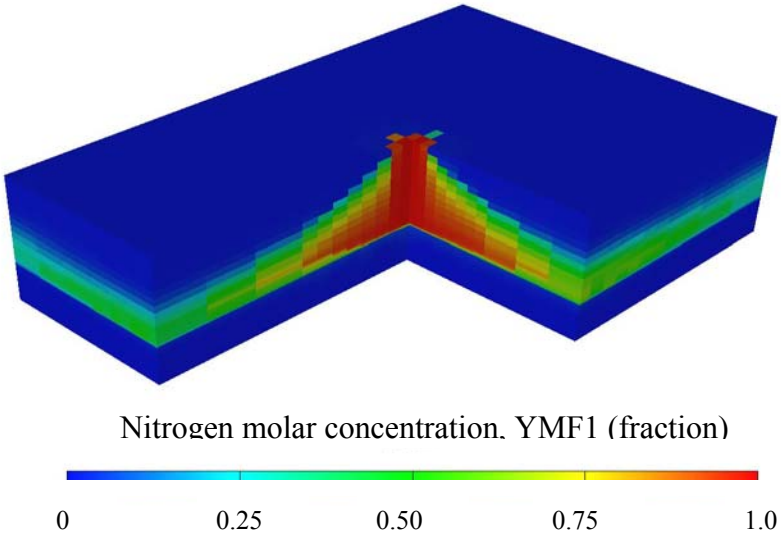

a) Case study using averaged reservoir properties.

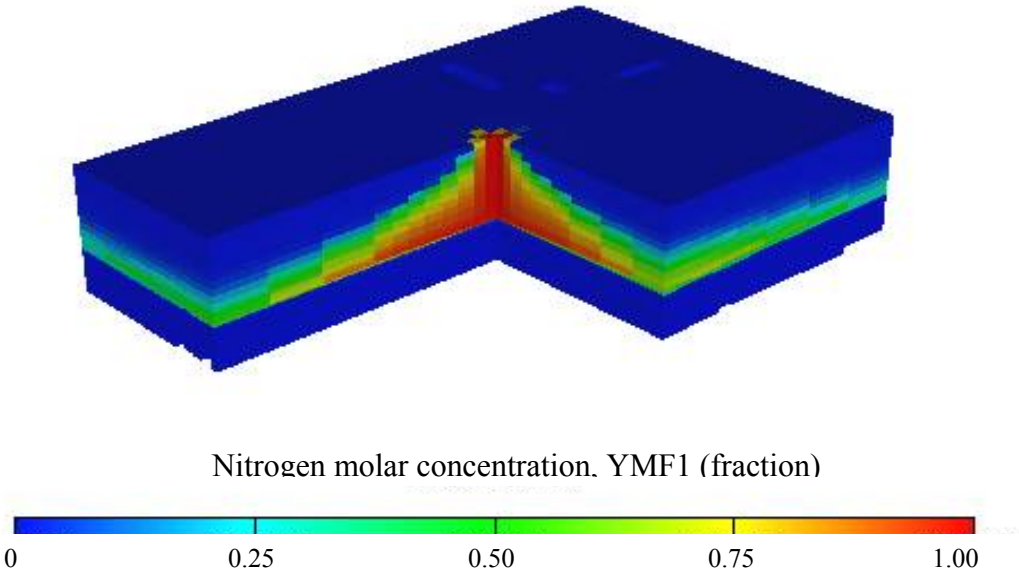

b) Case study using heterogeneous reservoir properties.

Figure 5.11 Nitrogen distributions after 1500 days of injection for averaged and heterogeneous reservoir property case studies.

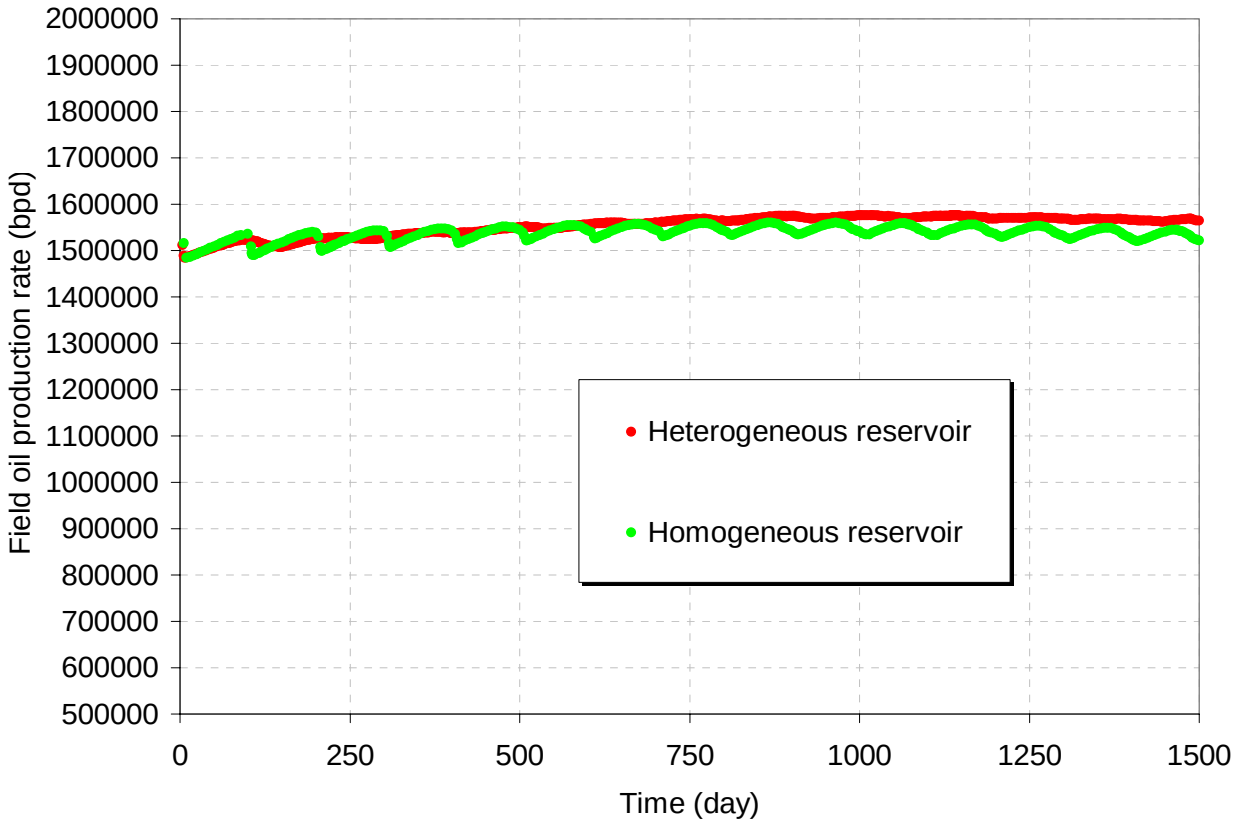

Figure 5.12 Oil production rate behaviors for heterogeneous and homogeneous reservoir property case studies.

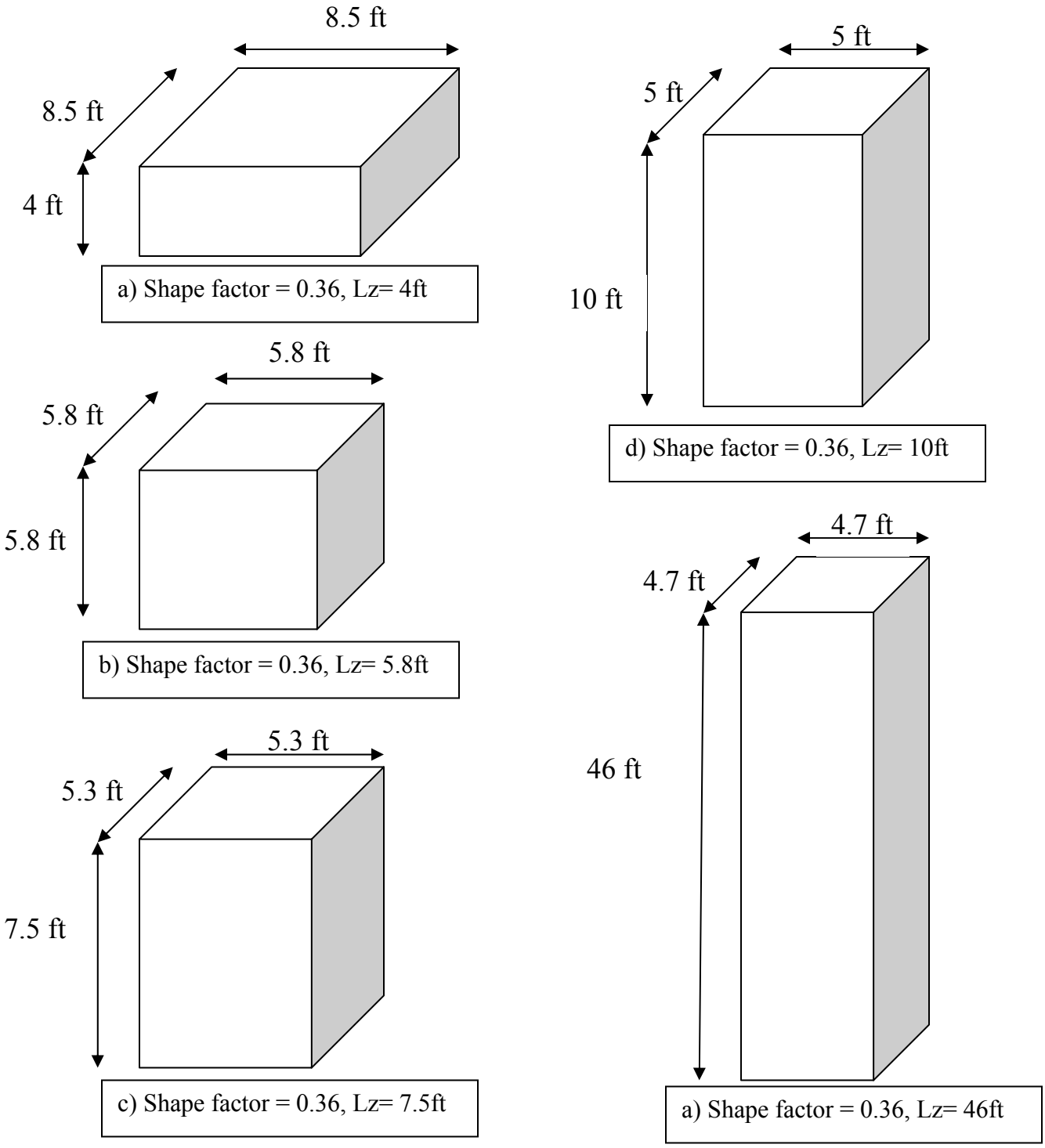

Figure 5.13 Matrix block sizes with same shape factor (σ =0.36/ft^2) and different matrix block heights (Lz).

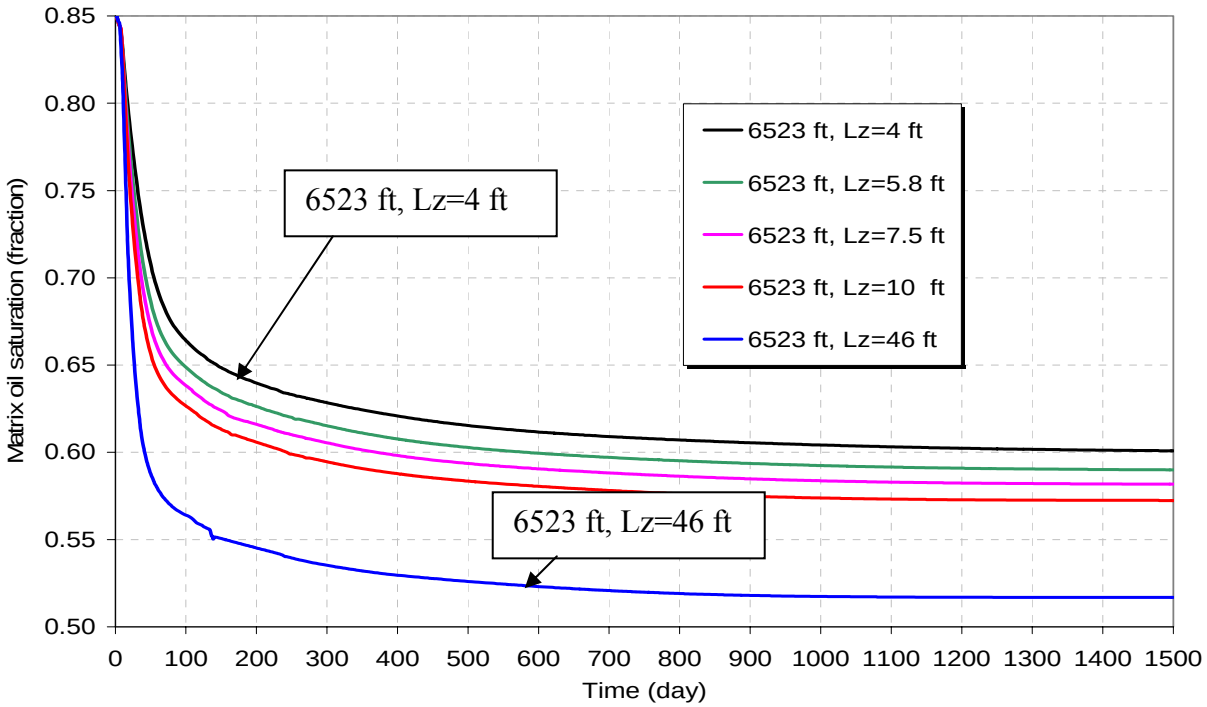

Figure 5.14 Matrix oil saturations for different matrix block geometries near the GOC (6523ft).

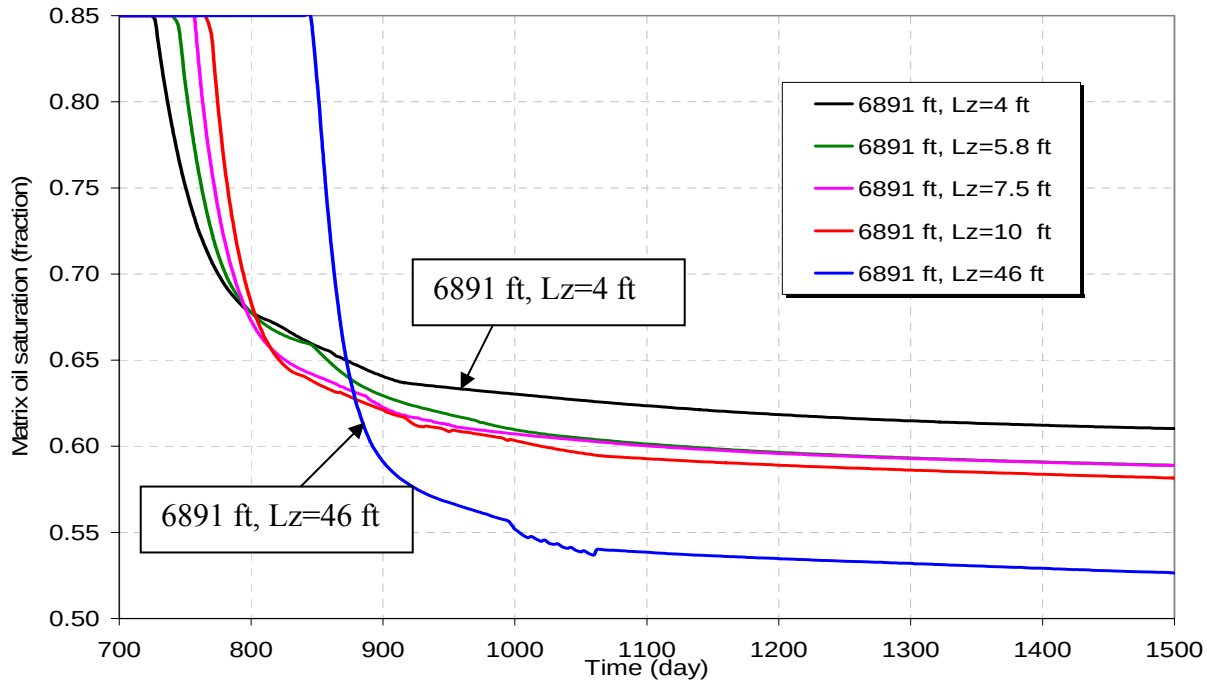

Figure 5.15 Matrix oil saturations for different matrix block geometries far from the GOC (6891ft).

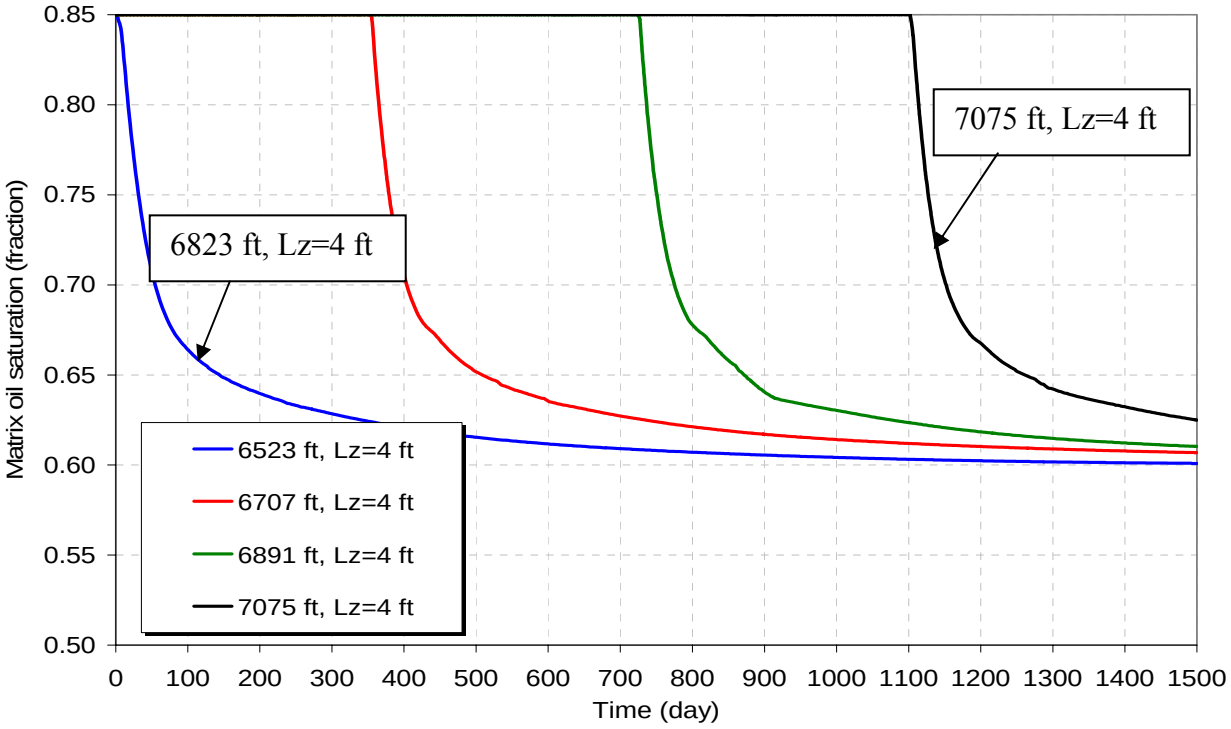

Figure 5.16 Matrix oil saturations for a block with 4 ft height at different vertical reservoir locations.

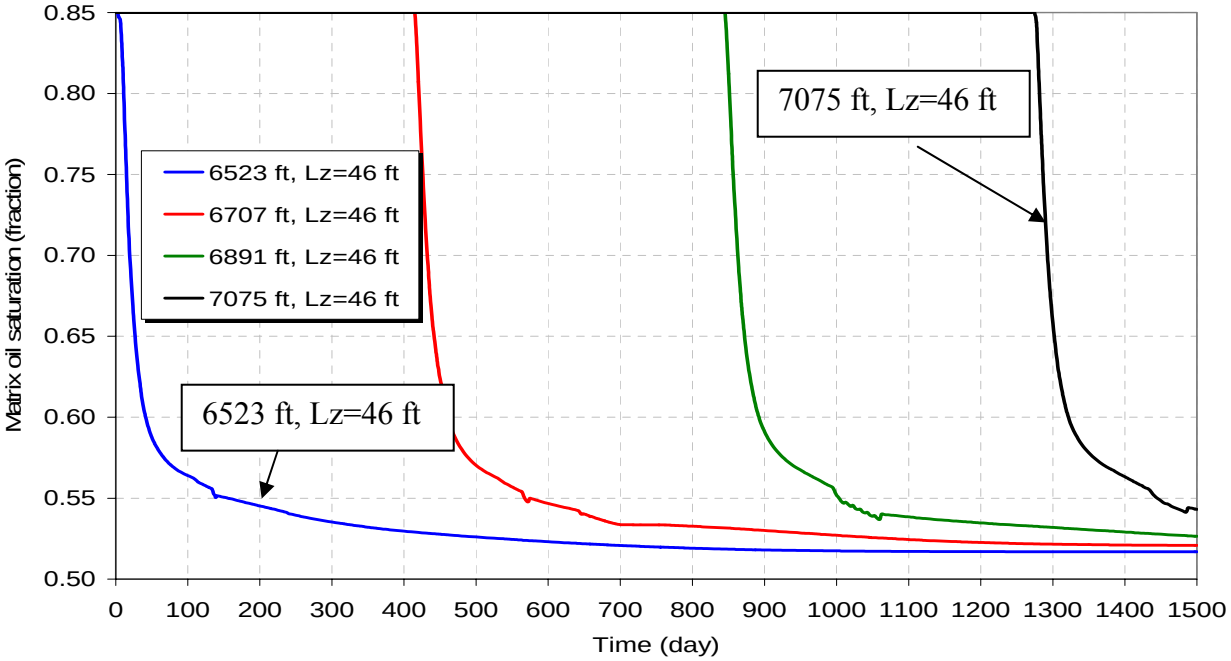

Figure 5.17 Matrix oil saturations for a block with 46 ft height at different vertical reservoir locations.

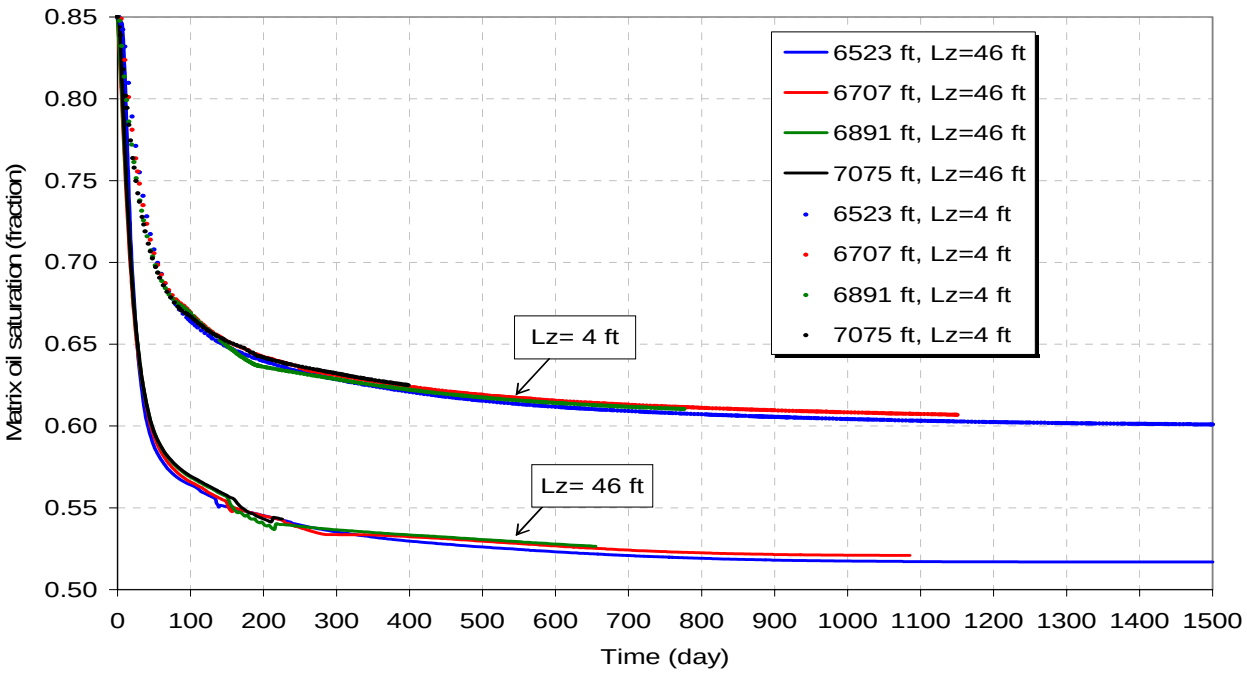

Figure 5.18 Matrix oil saturations for two matrix block heights at different reservoir locations.

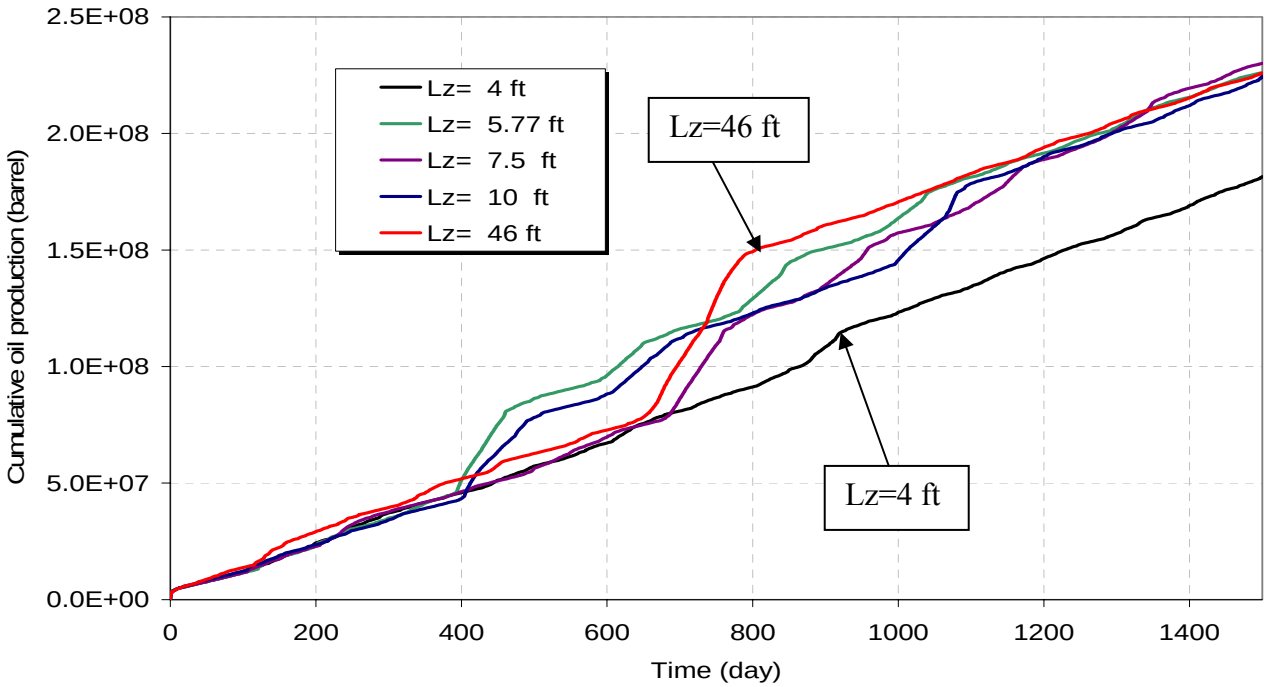

Figure 5.19 Cumulative oil productions for different matrix block heights.

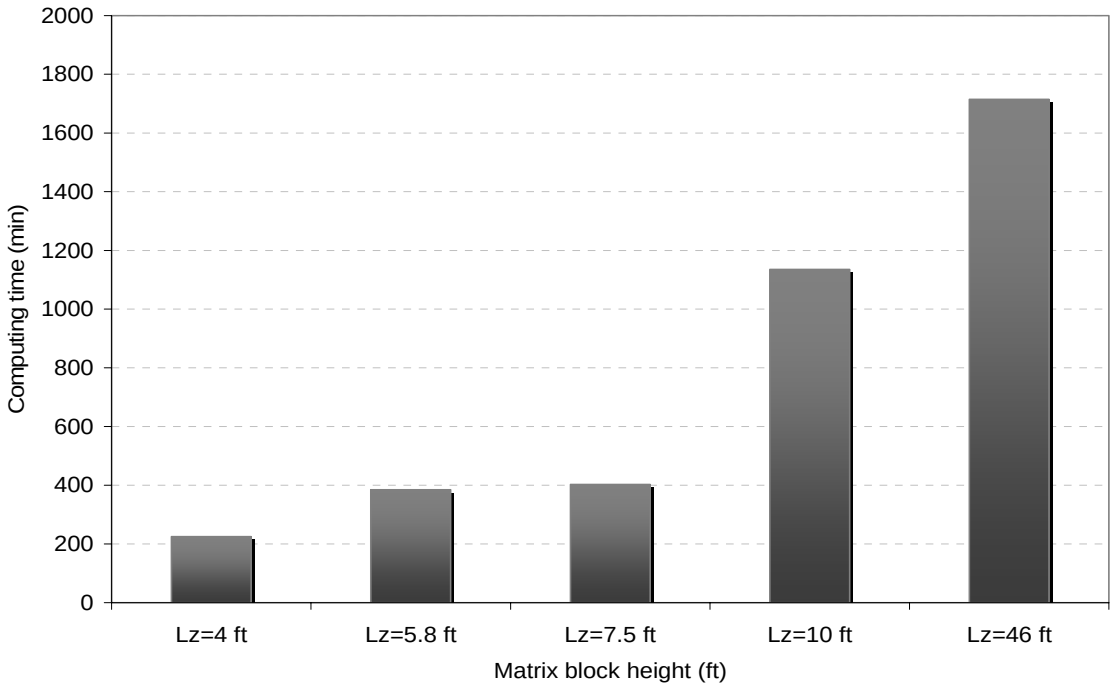

Figure 5.20 Computing times for different matrix block heights.

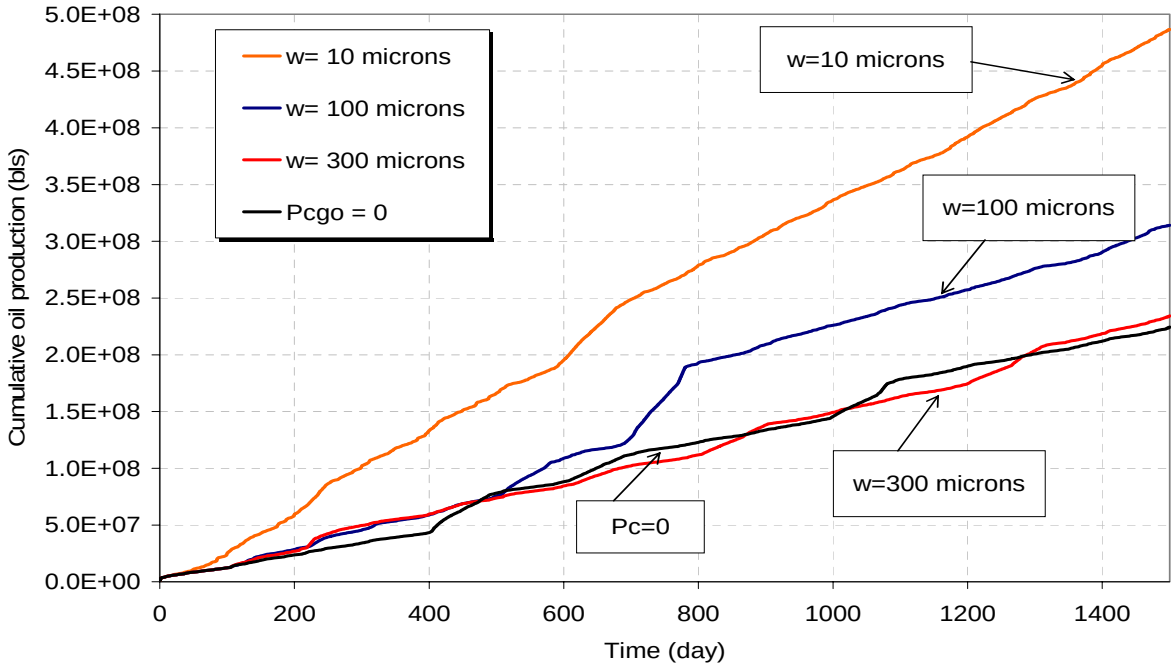

Figure 5.21 Cumulative oil productions for several case studies considering capillary continuity and a case considering a capillary discontinuity.

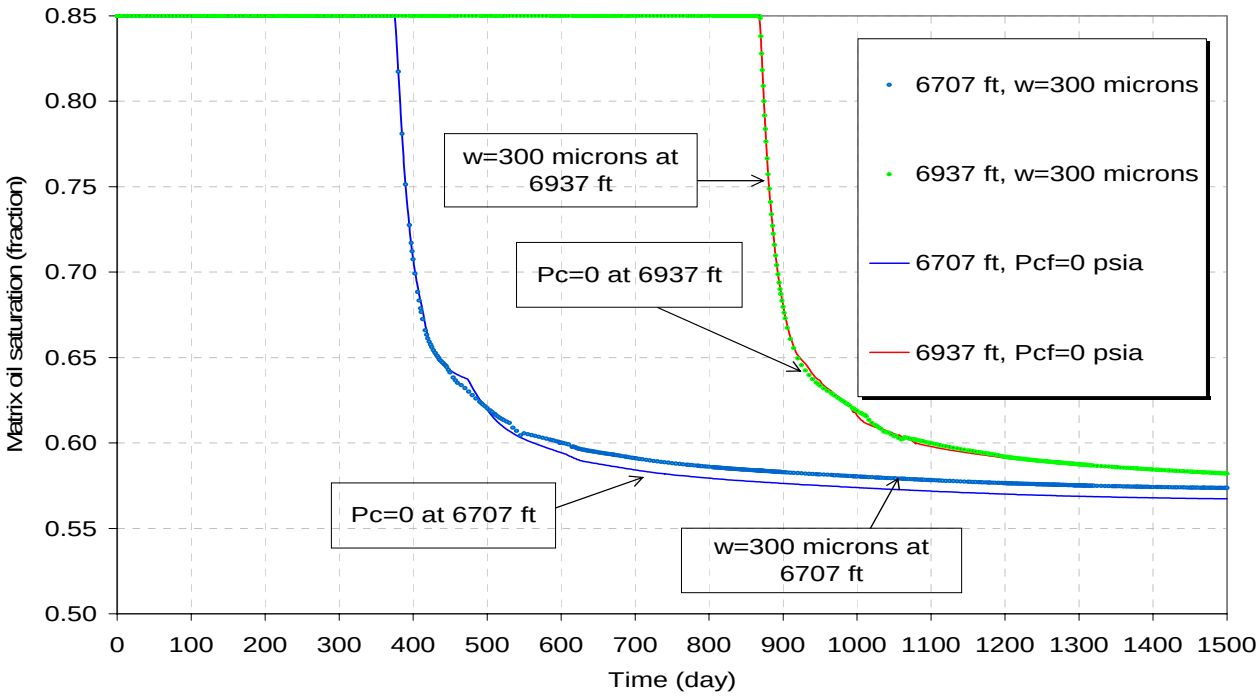

Figure 5.22 Matrix oil saturations in two gridblocks located at different depths for a case study considering 300 microns fracture aperture and a case study considering capillarity discontinuity.

.

CHAPTER 6

SUBGRIDDING SENSITIVITY STUDIES

6.1 Introduction

One of the biggest challenges with simulators using a dual porosity formulation is the accurate representation of fluid exchange between matrix blocks and fractures. Traditionally, dual porosity models assume that the matrix-to-fracture flow is in a steady state, but in some cases, the transient nature of flow can be important.

In order to perform an accurate and efficient simulation of the matrix-fracture fluids transfer, we should consider a proper matrix grid resolution, which subdivides each matrix block into a series of sub-cells, allowing the simulator to predict the transient behavior. In many cases, those effects are not included due to the simulator's use of a conventional approach for the transfer term, which is directly related to the shape factor, fluid mobility, and potential difference between the matrix blocks and fractures (Gilman and Kazemi, 1982).

The focus of this study is matrix subgridding in both vertical and horizontal directions, based on production forecasting and nitrogen distribution during nitrogen injection in naturally fractured reservoirs, under a strong gravity drainage mechanism.

Since gravity drainage is the main recovery mechanism in all of our case studies, and capillary and gravity are usually the major forces in fractured reservoirs, the use of a conventional approach for the transfer term can imply that:

1) Gravity has no explicit effect on the fluid exchange between the matrix and the fractures because matrix block heights are assumed to be at the same depth as the corresponding fracture blocks, and

2) Fluid saturation distributions in the matrix blocks are not considered because the saturation evaluation is performed at the center of a gridblock and it represents an average value for that block.

Therefore, the simulation runs using the conventional approach could produce unrealistic results for naturally fractured reservoirs under strong gravity drainage.

In most commercial dual-porosity simulators (including ECLIPSE 100 and 300), the matrix block heights are assumed to be at the same depth as the corresponding fracture blocks, and therefore, gravity has no explicit effect on the fluid exchange between the matrix and the fractures. To solve this problem, pseudo-capillary pressure curves are used to account for the effect of gravity (Thomas *et al*., 1980). Also, the gravity-segregation concept is used to compute the fluid levels in the matrix and fractures to account for the gravity contribution (Litvak, 1985; Sonier *et al*., 1986).

Most commercial simulators evaluate saturations at the center of a gridblock, and represent an average value for that block. In addition, since substantial changes in pressure, saturation, and concentrations occur in matrix blocks near the fractures, they are not accounted for when no matrix subgridding approach is applied. To solve this problem, the pseudo-capillary pressure concept has been used to account for both gravity effects and non-uniform saturations within a matrix block (Thomas *et al*., 1980; Rossen and Shen, 1987; Dean and Lo, 1986). In addition, the method of subgridding discretization has also been applied to solve this problem (Saidi, 1983; Pruess and Narasimhan, 1982; and Naimi-Tajdar *et al*., 2005).

A study (Naimi-Tajdar *et al*., 2006) applying subgridding sensitivity analysis using the dual porosity option with a GPAS simulator (Wang *et al.*, 1999; Marcondes *et al*., 2005; Han *et al*., 2005, and Naimi-Tajdar *et al*., 2006) was recently carried out. The results of this investigation considering the effects of vertical and horizontal subgridding

showed major impacts on the oil recovery, oil production, and water cut. The investigation was performed for one dimensional waterflood with an explicit gravity effect, and also for two dimensional waterflood with no explicit gravity effect. Naimi-Tajdar (2005) found in his investigation that in some circumstances the results of simulators without matrix subgridding generated a 50% error in oil-recovery calculations.

For our case studies with a dual porosity formulation, a matrix grid refinement is necessary in order to simulate a better fluid-flow representation; therefore, we investigated a matrix subgridding analysis where gravity drainage mechanism dominates oil production and nitrogen is injected at the top of the reservoir.

We used a conceptual model of a stack of two matrix blocks surrounded by fractures, then divided the matrix and fractured systems into a number of Cartesian sub-grids. We used the compositional single porosity model of the ECLIPSE 300 simulator to perform our simulations. By using a single porosity formulation, we specified rock-fluid properties for each system, and as a result, pressures, saturations, and compositions were obtained for each sub-grid.

Figure 6.1 illustrates the stack conceptual model with its corresponding inner and outer constant pressure boundary conditions, while Table 6.1 shows the matrix and fracture properties used for all our case studies. A constant pressure injection of 1092.85 psia and a constant bottomhole pressure of 1091.16 psia for the producer well located at the bottom of the fractured system were used. Under such boundary conditions, average pressure was maintained constant for all the cases under study. The lower matrix block was considered inactive in order to avoid boundary effects of the producer well on the upper block, and injector wells were located at the top of the fracture cells in order to allow nitrogen to flow through fractures.

We investigated the effects of vertical and horizontal subgridding on the matrix oil recovery, gas saturation, oil saturation, and nitrogen molar concentrations, as is described in the following sections.

6.2 Vertical subgridding analysis in a stack of two matrix blocks

We started our matrix and fracture subgridding sensitivity analysis in *z* direction using a cartesian gridcell. Table 6.2 gives the cases studied for our vertical subgridding sensitivity analysis. The main variations of the input simulation files for each case study were *z* dimensions, the gridcell size in *z* direction, the distribution of matrix and fracture properties such as porosity and permeability in *x*, *y* and *z* directions, saturation function regions, and equilibration regions to which each grid cell belongs. We also defined the correct number of injector wells and their locations in order to maintain similar boundary conditions for all cases.

Figure 6.2 shows that for cases with dimensions from 3x3x36 up to 3x3x132, the simulated oil production rates were similar.

The total oil production versus time from the case studies is illustrated in Figure 6.3, which shows that grid refinements using 3x3x132 and 3x3x68 have similar results. The same result was observed by plotting the total oil production response versus the inverse of the matrix grid cell sizes in a vertical direction, as is shown in Figure 6.4.

Figure 6.4 shows that total oil production for a grid refinement case study using 3x3x68 gridblocks is higher by a factor of 1.124 than the base case using 3x3x5. The trend shown in Figure 6.4 illustrates that substantial differences were observed between simulation results. The vertical matrix subgriddings study gave us a better understanding about the necessity of using higher resolution matrix gridblocks, specifically when gravity drainage is the dominant mechanism of oil production. We obtained the same conclusions analyzing the results for matrix oil saturation and matrix gas saturation.

Figure 6.5 illustrates the matrix oil saturation profiles for three cases, by using 3x3x5, 3x3x68, and 3x3x132 gridblocks after 1500 days of nitrogen injection. The curves illustrated in Figure 6.5 show the impact of the gravity drainage mechanism as we performed our matrix grid refinement study. We observed that case studies using 3x3x68 and 3x3x132 gridblocks have similar results. On the other hand, a considerable difference was observed when comparing both cases (3x3x68 and 3x3x132 gridblocks) with a case using 3x3x5 gridblocks. Figure 6.6 illustrates the matrix oil saturation profile after 1500 days of nitrogen injection for case studies using 3x3x132 and 3x3x5 gridblocks, and Figure 6.7 shows the matrix gas saturation profile for the same three case studies in Figure 6.5. The matrix gas saturation values observed in Figure 6.7 correspond to the same oil recovery values for the matrix block because the matrix contains only oil and irreducible water saturations before nitrogen injection. Figure 6.7 illustrates the same trends for case studies using 3x3x68 and 3x3x132 gridblocks after 1500 days of nitrogen injection, and it also shows that the results are considerably different for case studies using 3x3x132 and 3x3x5 gridblocks. Figure 6.8 illustrates the matrix gas saturation profile after 1500 days of nitrogen injection for case studies using 3x3x132 and 3x3x5 gridblocks.

The behavior of matrix nitrogen molar concentrations after injecting nitrogen for 1500 days was similar in the three cases described above. Based on the results of variations in the matrix oil saturations, gas saturations, and production oil rates illustrated above, we concluded that the case study using 3x3x68 gridblocks captures most of the vertical variations for the nitrogen injection. The matrix resolution for the vertical dimension will be the starting point for the horizontal matrix subgridding analysis, which is explained in the following section.

6.3 Horizontal subgridding analysis in a stack of two matrix blocks

After we defined the matrix vertical dimension that adequately captures property variations during 1500 days of nitrogen injection, we started our subgridding sensitivity analysis in horizontal directions for both matrix and fractured systems. We then performed several simulation runs with the same dimension variations in x and y directions considering a constant matrix vertical dimension using a cartesian grid.

Table 6.3 shows the case studies that were used for our horizontal subgridding sensitivity analysis. This study included cases with smaller matrix grid cells near to the fractures in order to capture matrix changes in saturation, pressure, and nitrogen molar concentrations.

Simulation results indicated that, for case studies using 3x3x68 up to 9x9x68 gridblocks, the oil production rate trends were similar, as illustrated in Figure 6.9. This result gave us an indication that gravity drainage has more impact in a vertical direction than in a horizontal direction.

The total oil production resulting from our simulation runs is illustrated in Figure 6.10., which indicates that grid refinements of 5x5x68 and 9x9x68 produce similar results. This figure shows that total oil production for a case using 9x9x68 gridblocks is higher by a factor of 1.09, in comparison with the case using 3x3x5 dimensions. This result corresponds to a difference of 9 % between the two simulation cases.

Based on the oil saturations, gas saturations, and oil productions illustrated above, we concluded that a case study with dimensions of 5x5x68 captures most of the vertical and horizontal matrix variations during 1500 days of nitrogen injection. Therefore, in order to perform an accurate and efficient simulation of the matrix-fracture fluids transfer, it is necessary that simulators using dual porosity formulation consider a proper

matrix grid resolution to better simulate the gravity drainage mechanism, which is present in naturally fractured reservoirs.

The simulation results of all matrix resolution studies suggest that matrix subgridding is especially important when we have gravity drainage as the main recovery mechanism. We investigated the effects of vertical and horizontal subgridding based on matrix oil recovery, gas saturation, oil saturation, and nitrogen molar concentrations. We concluded that 1) a case study using 3x3x68 gridblocks captures most of the vertical variations during the nitrogen injection, and 2) a vertical matrix subgridding study gave us a better understanding of the necessity to use higher resolution matrix gridblocks, especially when gravity drainage is the dominant mechanism of oil production. The simulation results of horizontal matrix subgridding indicated that for case studies using 3x3x68 up to 9x9x68 gridblocks, the horizontal variations on oil production rate behavior, matrix oil recovery, gas saturation, oil saturation, and nitrogen molar concentrations were similar. The results gave us an indication that gravity drainage has more impact in a vertical direction than in a horizontal direction.

Table 6.1 Matrix and fracture properties used for the matrix subgridding study.

Property	Upper block	Lower block
MATRIX SYSTEM		
Porosity (fraction)	0.05	0.0
Permeability in *x* direction (md)	0.20	0.20
Permeability in *y* direction (md)	0.20	0.20
Permeability in *z* direction (md)	0.20	0.20
Height of matrix block (ft)	10	10
Lx and Ly distance (ft)	5	5
FRACTURED SYSTEM		
Porosity (fraction)	1.0	1.0
Permeability in *x* direction (md)	5000	5000
Permeability in *y* direction (md)	5000	5000
Permeability in *z* direction (md)	5000	5000

Table 6.2 Input data used for the vertical subgridding sensitivity studies.

Number of cells in *x,y,z*	Matrix grid cell size, ft ($Dm_{X,Y,Z}$)	$1/(Dm_Z)$ (1/ft)	Number of Cells
3x3x5	5x5x10.0000	0.1	45
3x3x8	5x5x2.50000	0.4	72
3x3x12	5x5x1.25000	0.8	108
3x3x36	5x5x0.31250	3.2	324
3x3x68	5x5x0.15625	6.4	612
3x3x132	5x5x0.078125	12.8	1188

Table 6.3 Input data used for the horizontal subgridding sensitivity studies.

Number of cells in *x,y,z*	Matrix grid cell size, $Dm_{X,Y,Z}$ (ft)	$1/(Dm_X)$ (1/ft)	Number of Cells
3x3x36	5x5x0.3125	0.2000	324
5x5x36	1.667x1.667x0.3125	0.5998	900
9x9x36	0.555x0.555x0.3125	1.8000	2916

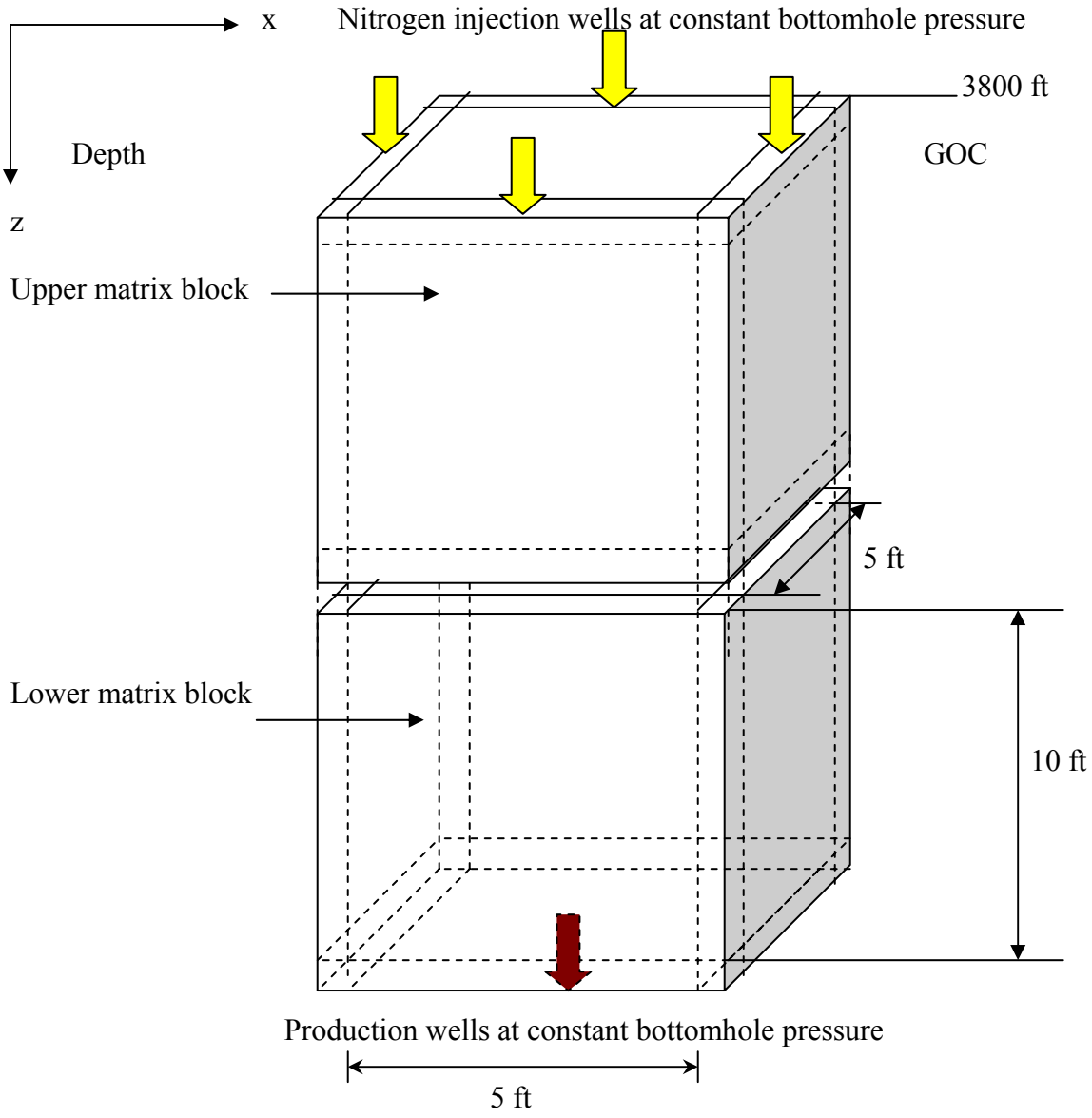

Figure 6.1 A conceptual model used for subgridding sensitivity analysis with a stack of two matrix blocks surrounded by fractures.

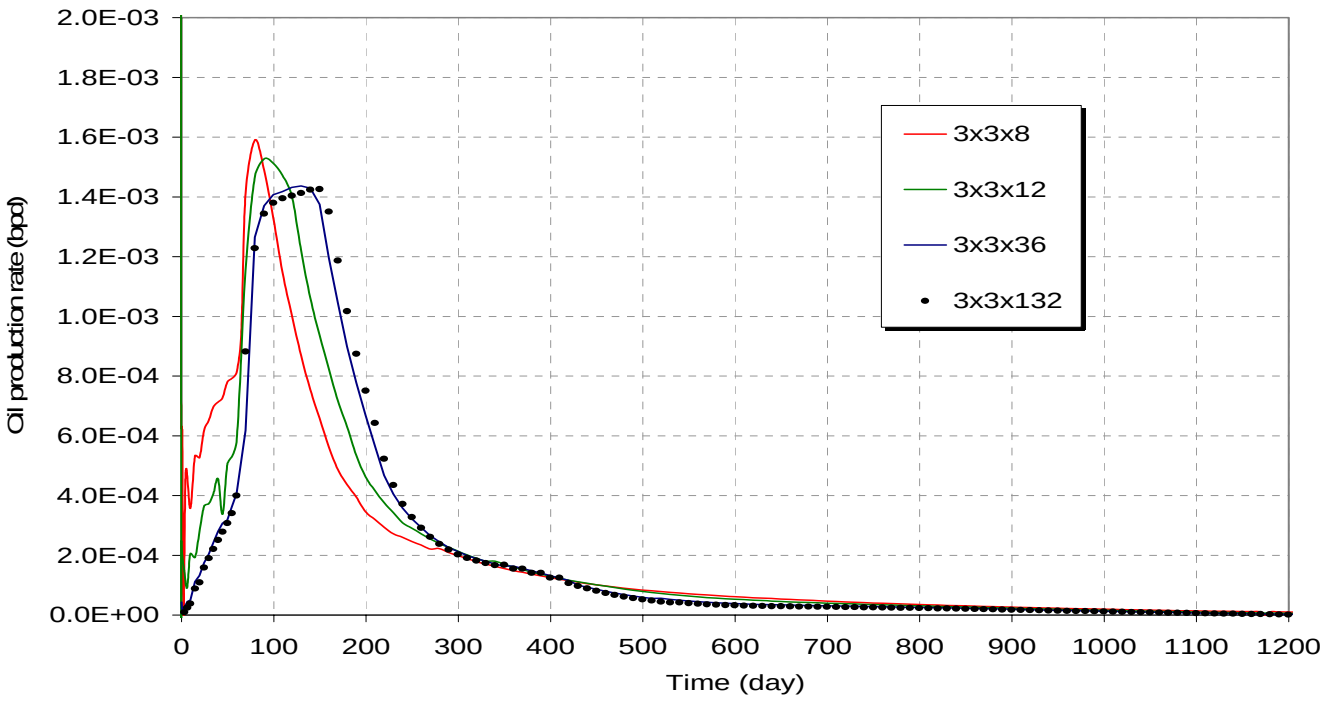

Figure 6.2 Oil production rates for subgridding sensitivity studies in vertical direction.

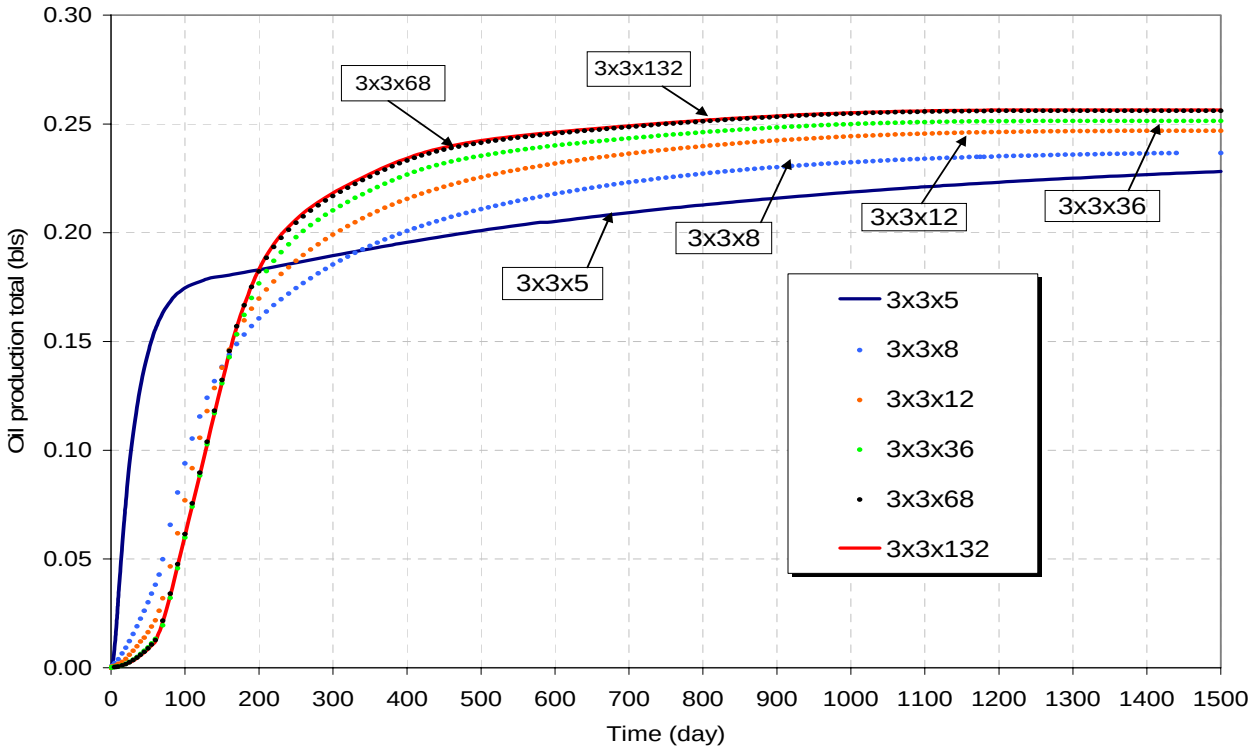

Figure 6.3 Total oil production for subgridding sensitivity studies in vertical direction.

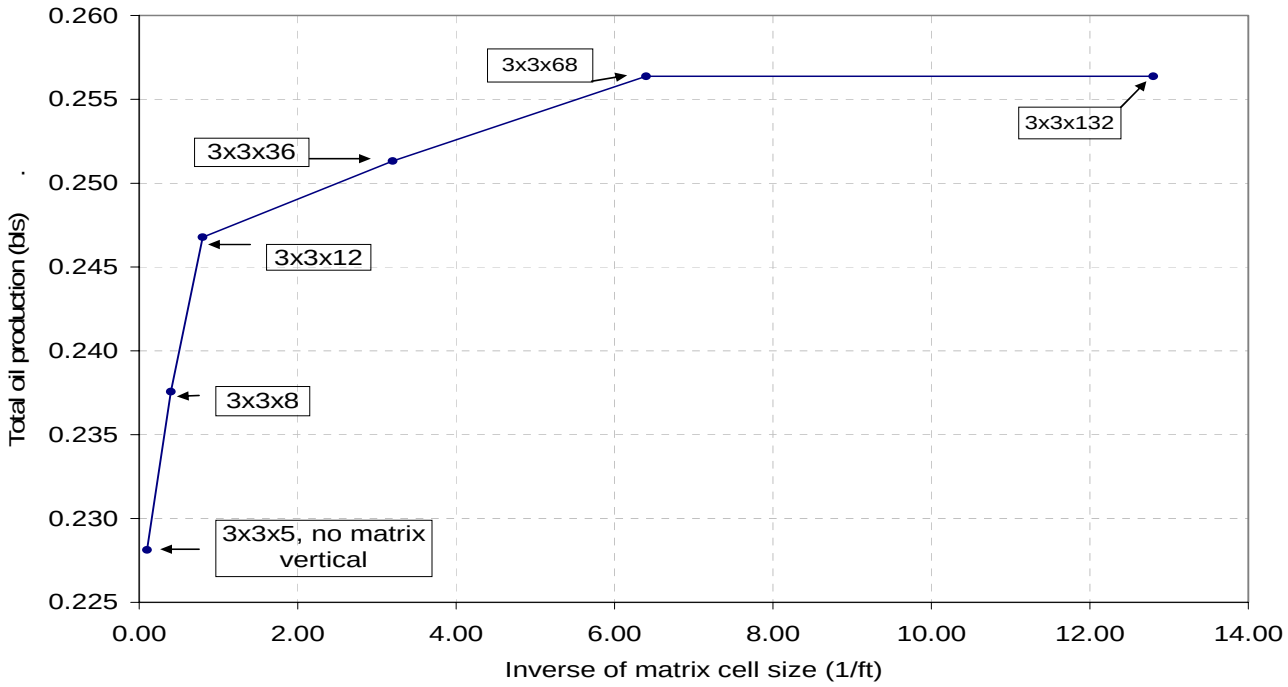

Figure 6.4 Oil production rates vs. inverse matrix cell size for subgridding sensitivity studies in vertical direction.

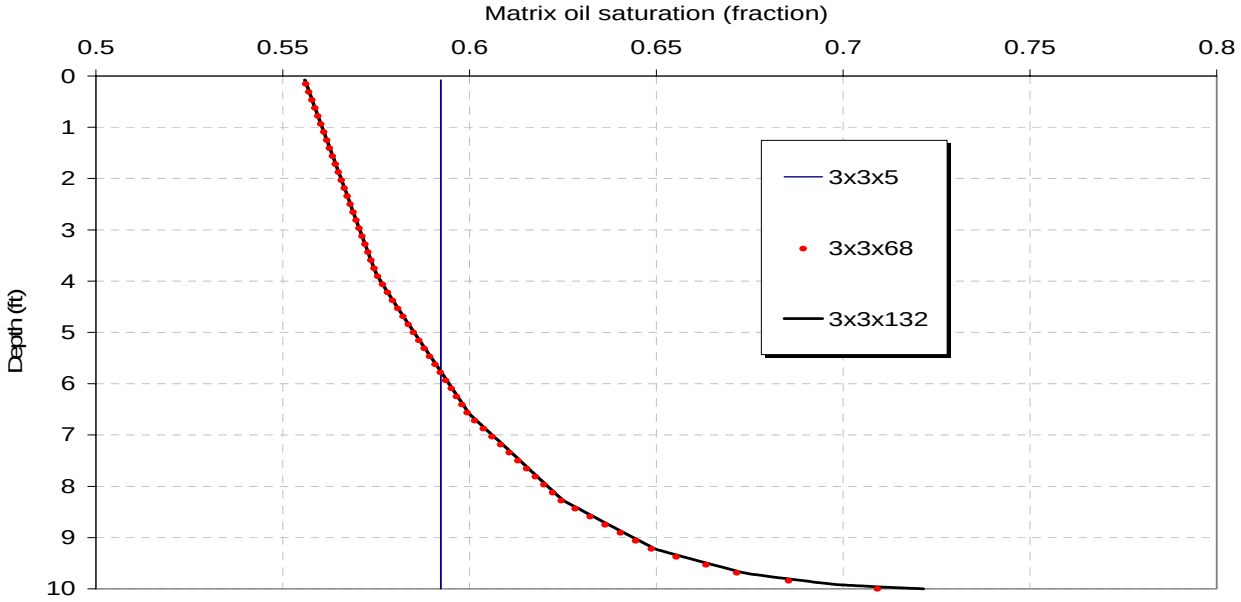

Figure 6.5 Matrix oil saturation versus matrix height for a 10 ft block using subgridding sensitivity studies in vertical direction.

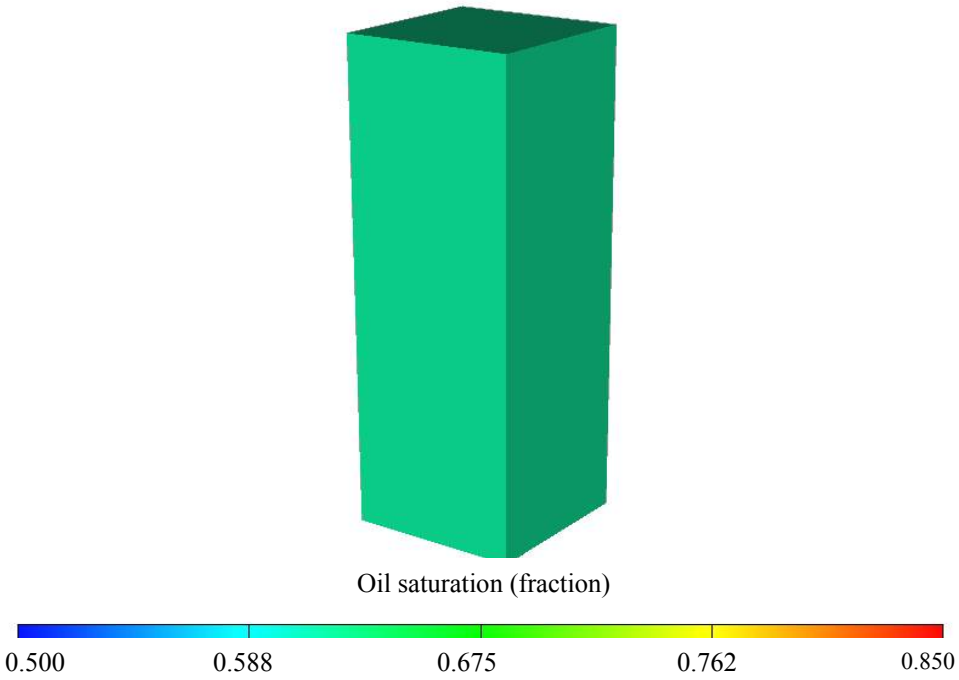

a) Case study with no matrix vertical grid refinement (3x3x5)

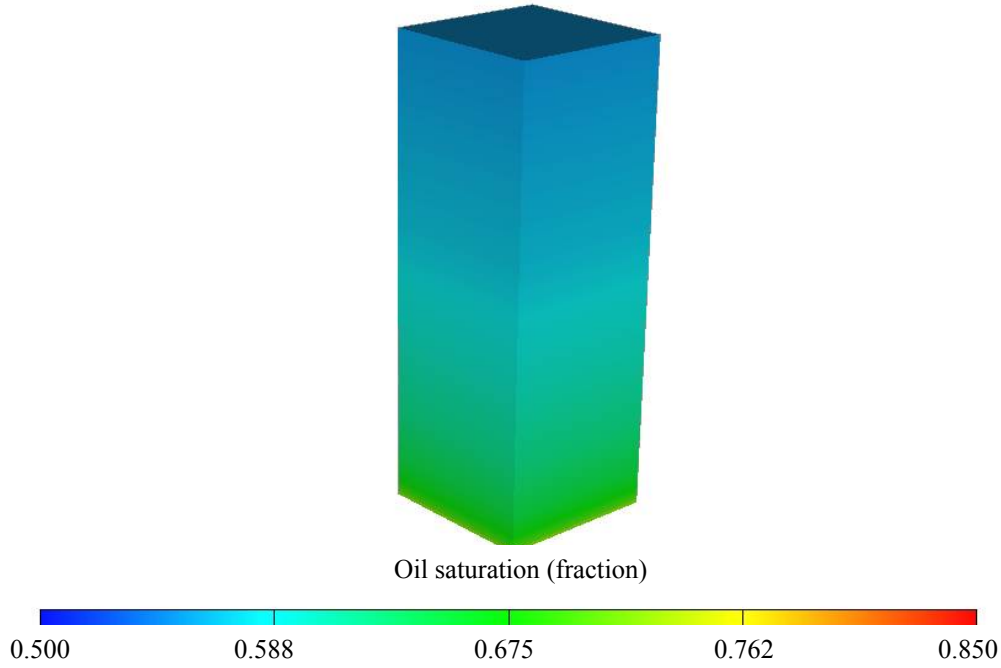

b) Case study with vertical grid refinement (3x3x132)

Figure 6.6 Matrix oil saturation after 1500 days of nitrogen injection for two case studies (with and without vertical grid refinement).

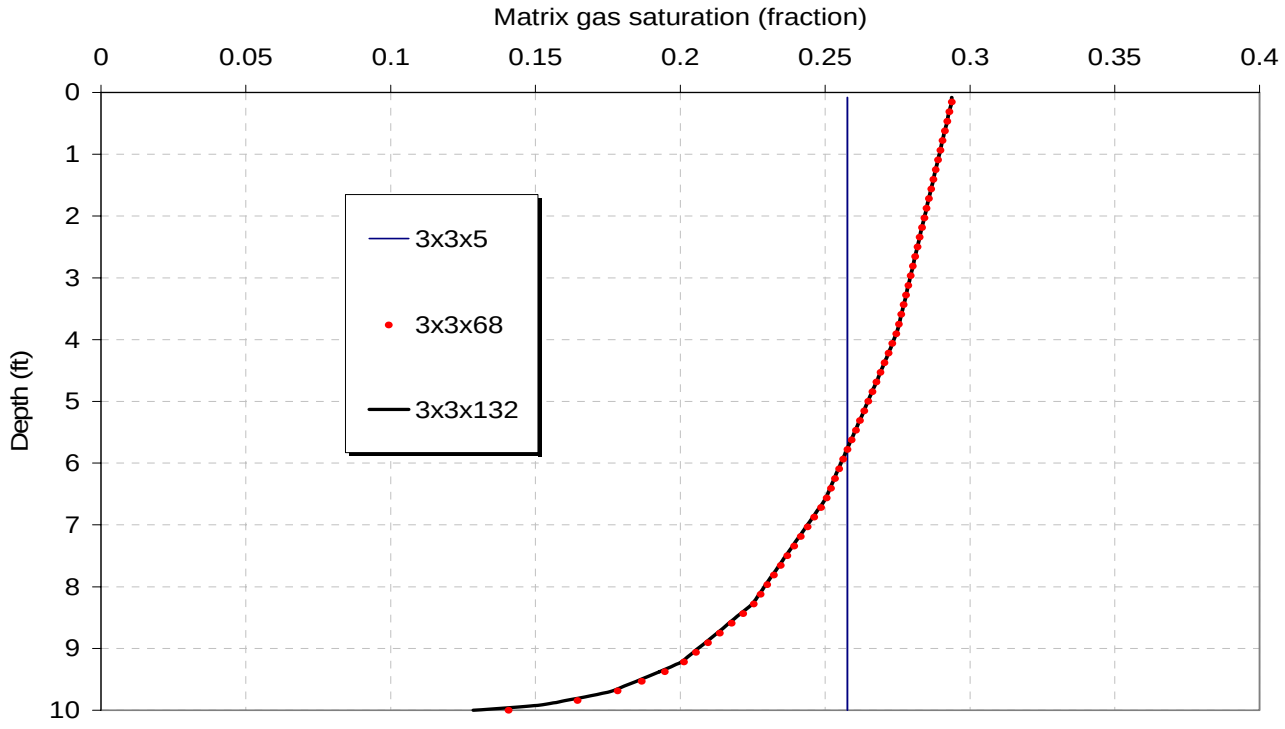

Figure 6.7 Matrix gas saturation vs. matrix height for a 10 ft block using subgridding sensitivity studies in vertical direction.

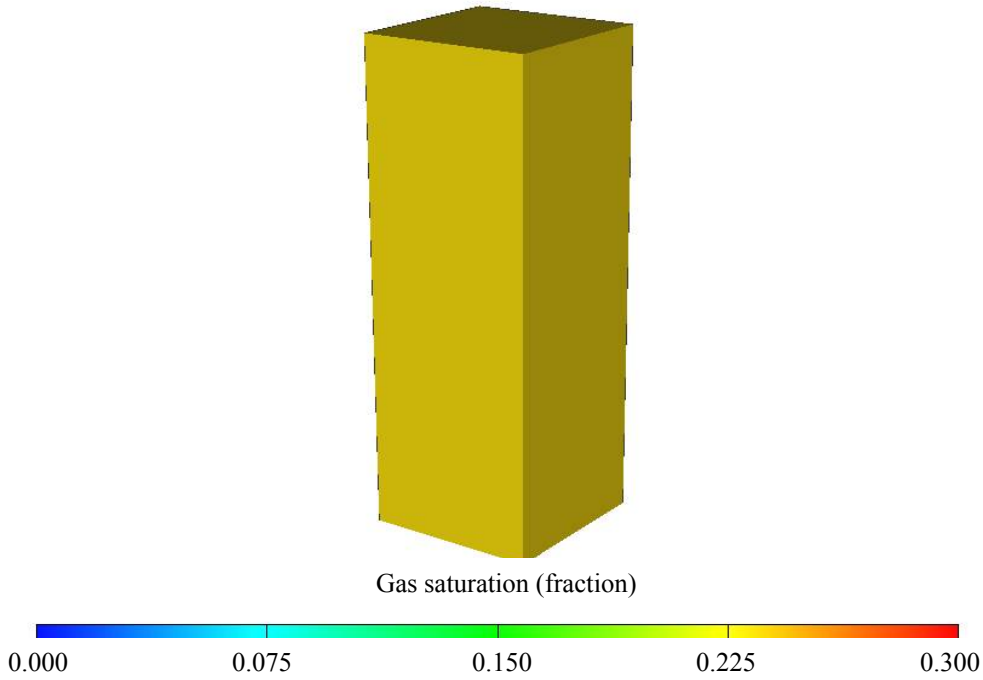

a) Case study with no matrix vertical grid refinement (3x3x5).

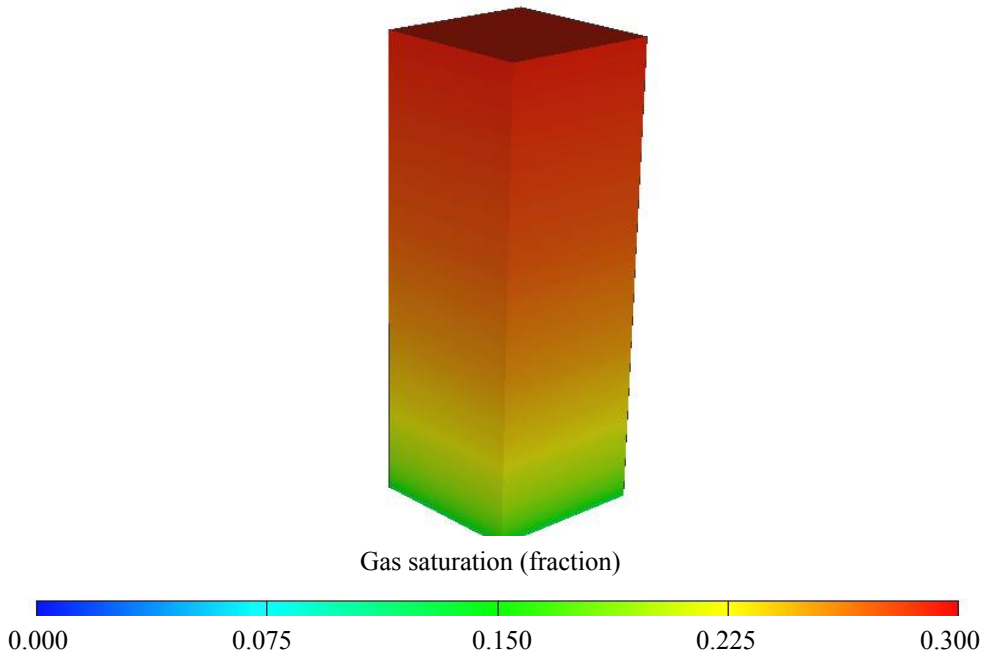

b) Case study with vertical grid refinement (3x3x132).

Figure 6.8 Matrix gas saturation after 1500 days of nitrogen injection for two case studies (with and without vertical grid refinement).

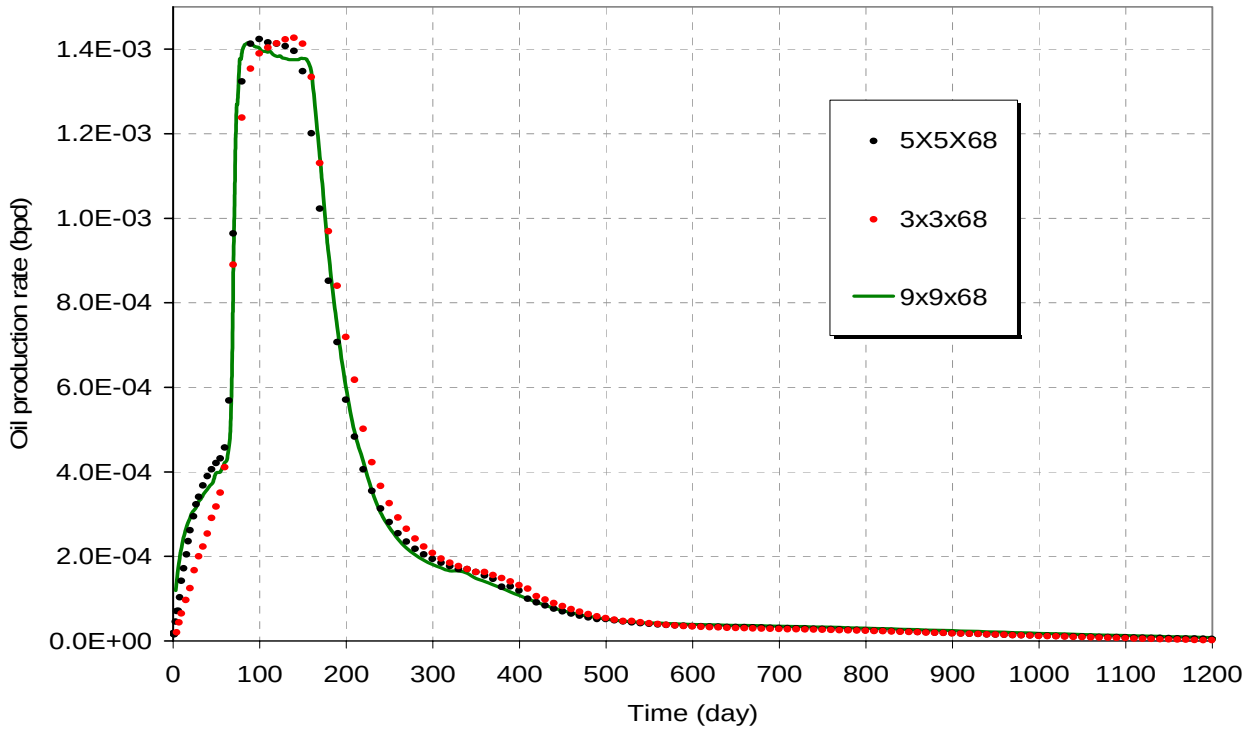

Figure 6.9 Oil production rates for subgridding sensitivity studies in horizontal direction.

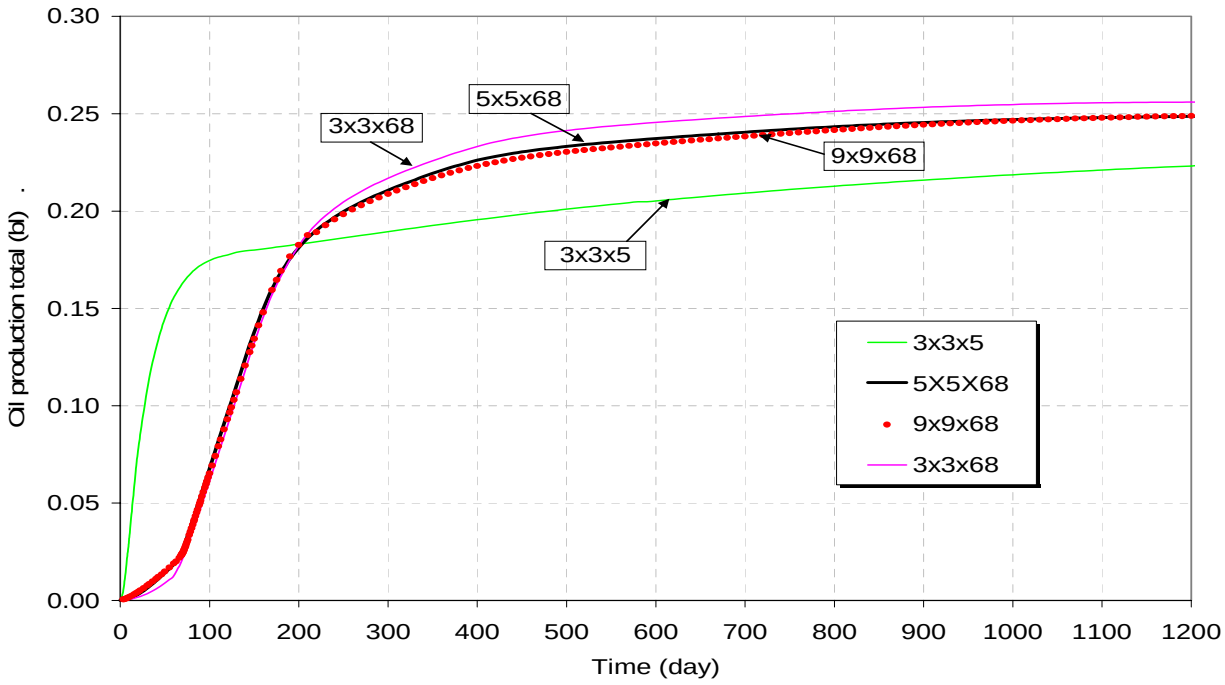

Figure 6.10 Total oil production for subgridding sensitivity studies in horizontal direction.

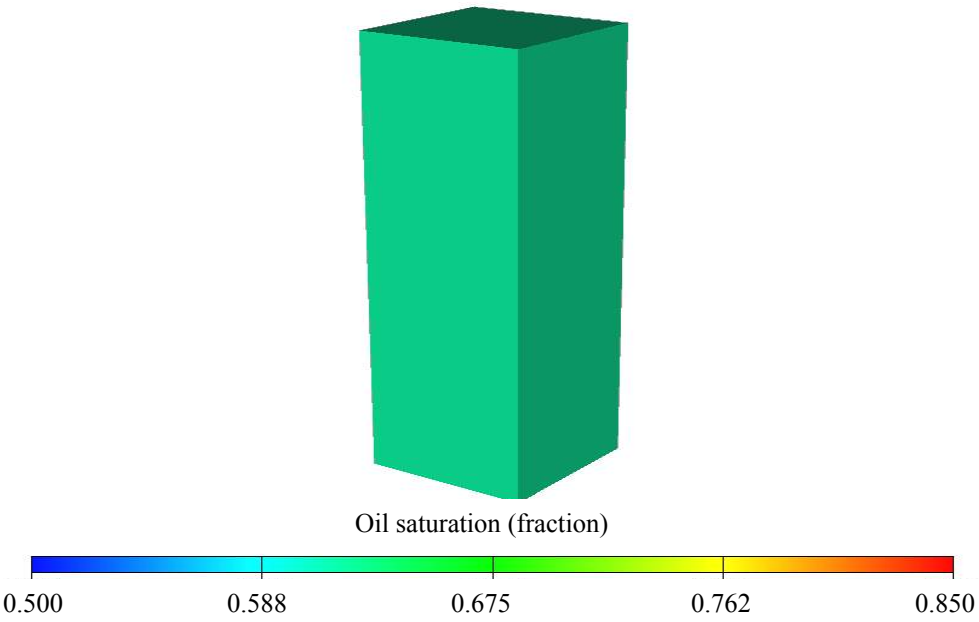

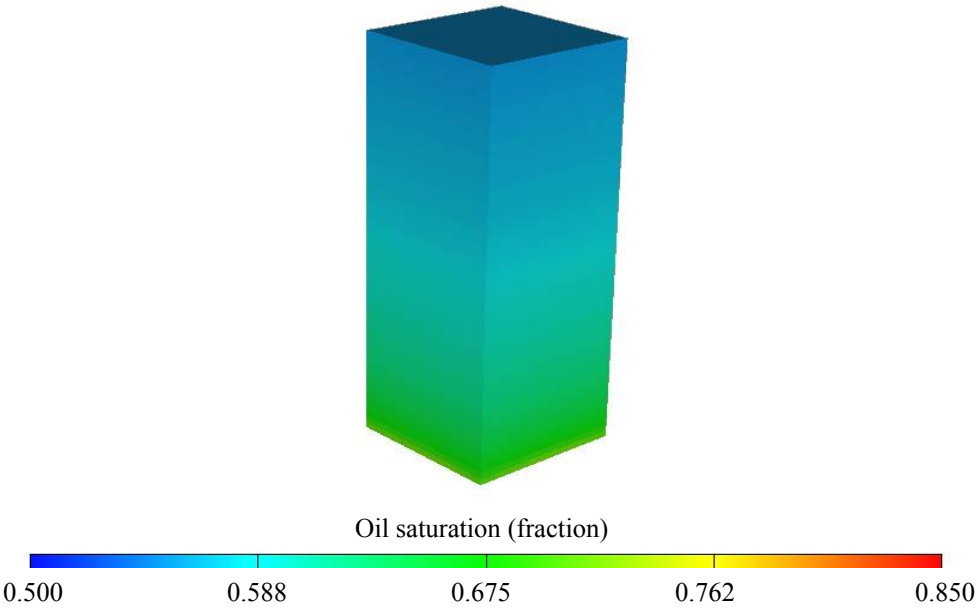

b) Case study with vertical grid refinement (3x3x132).

Figure 6.11 Matrix oil saturation after 1500 days of nitrogen injection for two case studies (with and without vetical grid refinement).

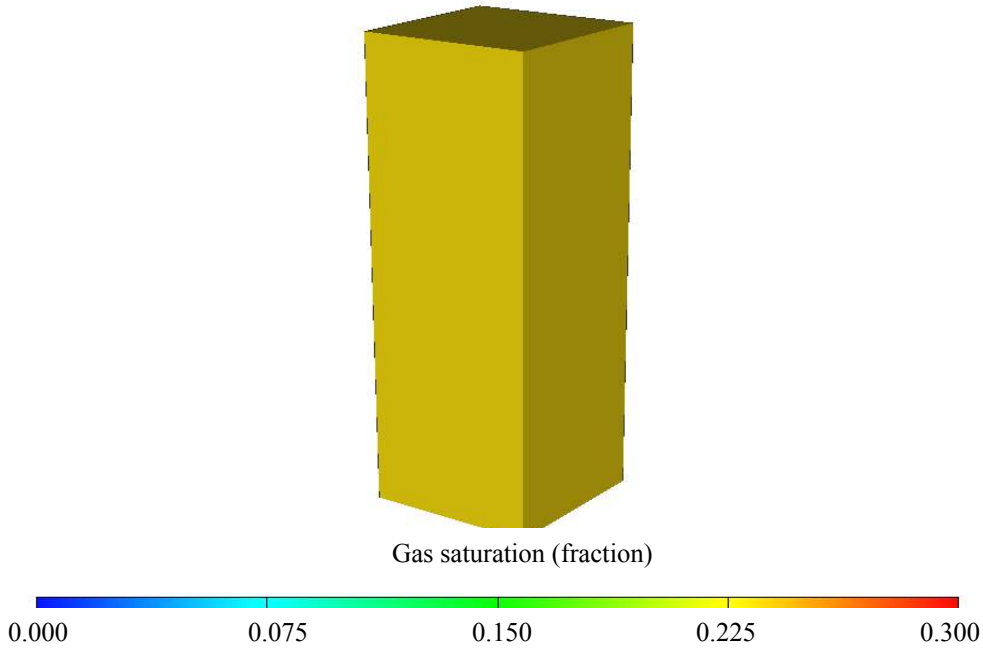

a) Case study with no matrix vertical grid refinement (3x3x5).

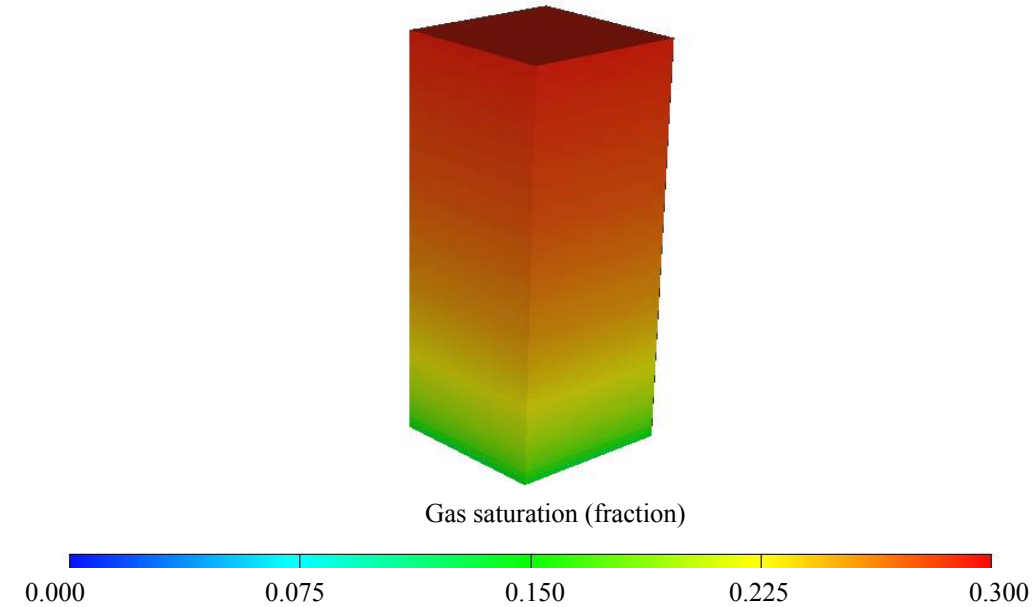

b) Case study with vertical grid refinement (3x3x132).

Figure 6.12 Matrix gas saturation after 1500 days of nitrogen injection for two case studies (with and without vertical grid refinement).

CHAPTER 7

ANALYTICAL MODEL FOR NITROGEN INJECTION FRONT INTO NATURALLY FRACTURED RESERVOIRS

7.1 Introduction

Naturally fractured reservoirs consist of a network of interconnected fractures surrounding porous matrix blocks. Most of the porosity of naturally fractured reservoirs is contained in the matrix blocks. The fractures normally have little pore volume but are orders-of-magnitude more permeable than the matrix blocks.

In some fractured carbonate reservoirs located in Southern Mexico, the primary porosity (matrix) tends to be occluded or has extremely small permeability, and consequently does not contribute to hydrocarbon storage. But a large number of small fractures are present in the matrix, and they play an important role in the "pseudo" matrix properties of a dual porosity representation.

The integration of fracture data from all scales provides a vehicle for achieving good history matching in the simulation of naturally fractured reservoirs. Usually, we characterize a micro fracture system through cores by calibrating fracture properties with well data, constrained, as far as possible, by outcrop observations, geomechanical modeling, and structural analysis. An intermediate fracture system is characterized by using image well logs and by interpreting transient and interference pressure tests between wells. A macro fracture system is characterized through seismic data interpretation. Basically, macro fractures define the main features of the fractured system of a dual porosity model, and the integration of micro and intermediate fracture scales defines the "pseudo" matrix system. This modeling practice is used when primary porosity does not contribute to hydrocarbon storage.

The impact of gravity drainage on oil recovery of a naturally fractured reservoir under nitrogen injection was studied in detail in this research using a three dimensional conceptual field model in this research. We found that when nitrogen is injected into a naturally fractured reservoir, and when primary porosity does not contribute to hydrocarbon storage to maintain the reservoir pressure, gravity drainage plays the major role in hydrocarbon recovery (Chapters 4 through 6). Since gravity drainage is the dominant oil production mechanism, the presence of vertical fractures (the macro system) makes the gas-oil contact advancement ahead of the matrix gas-oil contact, and the difference between the density of the fluids and the elevation of the two contacts makes the oil to be produced from the "pseudo" matrix blocks.

Since tracking the path of the nitrogen front is important for reservoir engineers, to prevent early nitrogen breakthrough into producer wells and to avoid the loss of reservoir energy, we developed a simple analytical model that describes the movement of a nitrogen injected front through the fractured system by using basic equations for fluid-flow in permeable media, such as the Buckley Leveret theory. This basic flow equation was applied successfully when nitrogen displaces oil during an immiscible process into naturally fractured reservoirs under a strong gravity drainage mechanism and when no water phase flow occurs.

The development of the analytical model will help reservoir engineers to understand the problem of gravity drainage in fractured carbonate reservoirs and also to comprehend the dynamics of fluid-flow in naturally fractured reservoirs. Our main objective is to describe the advancement of the nitrogen front through a fracture system of a gas-oil phase equilibrium system under reservoir pressure maintenance, where nitrogen is injected at a constant rate and oil is produced at a constant bottomhole pressure.

A stacked simulation model was used to validate the analytical model; it is described in Section 7.2. The development of the analytical model is described in Section 7.3; a comparison of results between a simulation case study and the analytical model is presented in Section 7.4. Finally, a sensitivity analysis was performed to validate the results of the analytical model, which is described in Section 7.5.

7.2 Stacked simulation model

The stacked simulation model used to validate the analytical model is illustrated in Figure 7.1. It was constructed with the field data shown in Table 7.1; its main assumptions were:

1) There are no variations in the fracture porosity or permeability during the nitrogen injection.
2) Nitrogen is injected at the top of the stacked matrix block at a constant rate.
3) Oil is produced at the bottom of the stacked matrix block under constant bottomhole pressure.
4) The stacked simulation model is composed of matrix blocks surrounded by fractures; it is characterized as a dual porosity system.
5) No oil re-infiltration into the matrix blocks is allowed, to simplify the analytical model.
6) There is no capillary pressure in the fracture ($P_{cf} = 0$).
7) There are no variations in matrix or fracture properties throughout the entire conceptual stacked simulation model.
8) The oil properties are as described in Chapter 4. The reservoir fluid was characterized using a compositional formulation using the Peng Robinson EOS.
9) There is no movement of water phase.

10) The water-oil contact (WOC) remains at the same level after nitrogen injection; therefore our problem was reduced to a gas-oil system, with an initial water saturation of 0.15 (by design) in the entire stacked matrix blocks.

11) The fracture relative permeability equals the gas phase saturation (unit slope).

12) We used $1\times1\times320$ gridblocks. The upper gridblocks (1 to 130) have the same size as the matrix blocks ($5\times5\times10$ ft) and the rest (130 to 160) have sizes of $5\times5\times170$ ft. The sizes of the lower gridblocks were larger than the upper gridblocks because grid refinement was not necessary since the gas saturation front advanced only through the first 50 gridblocks during four years of the nitrogen injection.

Capillary pressure and relative permeability curves for the matrix system were represented by the following models:

$$P_c = P_c^0\left(1-\frac{S_o-S_{or}}{1-S_{or}-S_{wi}}\right)^{e_{pc}}$$

$$k_{ro} = k_{ro}^0\left(\frac{S_o-S_{or}}{1-S_{or}-S_{wi}}\right)^{e_o}$$

$$k_{rg} = k_{rg}^0\left(1-\frac{S_o-S_{or}}{1-S_{or}-S_{wi}}\right)^{e_g}$$

where all parameters are given in Table 7.2 and the behaviors of P_c, k_{ro} and k_{rg} vs. S_o are illustrated in Figures 7.2 through 7.4, respectively.

The lower boundary condition in the stacked simulation model was defined by considering a constant pressure at the WOC during nitrogen injection.

To simulate a constant WOC, we located a producer at the lowest layer of the conceptual stacked model operating under a constant bottomhole pressure. We observed that the oil production rate is almost constant (before nitrogen breakthrough) under the upper and lower boundary conditions defined for the simulation case study.

7.3 Analytical model description

A special case of the general conservation equation written in terms of a gas fractional flow function for the fracture system considering 1) one-dimensional linear flow, 2) isothermal flow of oil and gas in two immiscible phases, 3) rock and fluid properties with no sorption, 4) the matrix-fracture mass transfer term, 5) constant pressure at the water-oil contact (WOC) during nitrogen injection, and 6) vertical flow of nitrogen in a stack of "pseudo" matrix blocks surrounded by fractures (dual porosity system) can be written as

$$\phi_f \frac{\partial S_{g,f}}{\partial t} + u_f \frac{\partial f_{g,f}}{\partial z} = r_{mt} \tag{7.1}$$

for gas phase, where

ϕ_f = fracture porosity, fraction
$S_{g,f}$ = fracture gas saturation, fraction
t = time, t
u_f = volumetric gas flux at reservoir conditions, L^3/tL^2
$f_{g,f}$ = gas fractional flow in the fracture system, fraction
z = length in the direction of flow, L
r_{mt} = rate of mass transfer between matrix and fracture systems, L^3/tL^2L

In the matrix, gas flow is negligible; a special case of the general conservation equation can be written as

$$\phi_m \frac{\partial S_{g,m}}{\partial t} = -r_{mt} \tag{7.2}$$

For the gas phase, where

ϕ_m = matrix porosity, fraction.
$S_{g,m}$ = matrix gas saturation, fraction.

Adding equations 7.1 and 7.2, we obtain

$$\phi_f \frac{\partial S_{g,f}}{\partial t} + u_f \frac{\partial f_{g,f}}{\partial z} + \phi_m \frac{\partial S_{g,m}}{\partial t} = 0 \tag{7.3}$$

Since $f_{g,f}$ depends on gas saturation in the fracture only, we must define a function $F(S_{g,f})$ such as $S_{g,m} = F(S_{g,f})$; therefore, equation 7.3 can be written as

$$\phi_f \frac{\partial S_{g,f}}{\partial t} + u_f \frac{\partial f_{g,f}(S_{g,f})}{\partial z} + \phi_m \frac{\partial F(S_{g,f})}{\partial t} = 0$$

or,

$$\phi_f \frac{\partial S_{g,f}}{\partial t} + u_f \frac{\partial f_{g,f}(S_{g,f})}{\partial z} + \phi_m \frac{dF(S_{g,f})}{dS_{g,f}} \frac{\partial S_{g,f}}{\partial t} = 0 \tag{7.4}$$

Grouping terms, equation 7.4 can be rewritten as

$\frac{\partial S_{g,f}}{\partial t}\left[\phi_f + \phi_m \frac{dF(S_{g,f})}{dS_{g,f}}\right] + u_f \frac{\partial f_{g,f}(S_{g,f})}{\partial z} = 0$, which is a Buckley Leveret type equation $\phi \frac{\partial S_1}{\partial t} + u \frac{\partial f_1}{\partial x} = 0$. The solution of the Buckley Leveret type, where dissipative effects are neglected, is given by $x_1 = \frac{u\,t}{\phi}\frac{\Delta f_1}{\Delta S_1}$. By analogy to the solution of the Buckley Leveret type equation, the solution of the partial differential equation $\frac{\partial S_{g,f}}{\partial t}\left[\phi_f + \phi_m \frac{dF(S_{g,f})}{dS_{g,f}}\right] + u_f \frac{\partial f_{g,f}(S_{g,f})}{\partial z} = 0$ is given by

$$Z_{sg,f}(ft) = \frac{\left(u_{g,f}\ t\right)}{\left[\phi_f + \phi_m \dfrac{\Delta F(S_{g,f})}{\Delta S_{g,f}}\right]}\left[\frac{\Delta f_{g,f}(S_{g,f})}{\Delta S_{g,f}}\right] \tag{7.5}$$

where $Z_{sg,f}$ is the location of gas saturation front in the fracture system.

7.3.1 Determination of fracture volumetric gas flux, $u_{g,f}$

$u_{g,f}$ is defined as the fracture volumetric gas flux evaluated at reservoir conditions, which can be obtained by

$$u_{g,f} = \frac{q_{g,f}}{A_f} \tag{7.6}$$

where

$q_{g,f}$ = volumetric gas rate through the fracture system at reservoir conditions.

A_f = flow area of the fracture system.

Applying a material balance under steady state conditions and with no oil re-infiltration in a gas-oil system (Figure 7.5), we found that the oil production rate at reservoir conditions $\left(q_{o,f}B_o\right)_{rc}$ can be obtained by summing the gas flow rate through the fracture system $\left(q_{g,f}\right)_{rc}$ plus the gas flow rate that enters into matrix system $\left(q_{g,f-m}\right)_{rc}$, which expels the oil from the matrix through the fracture system. The gas material balance can then be expressed as

$$\left(q_{o,f}B_o\right)_{rc} = \left(q_{g,f}\right)_{rc} + \left(q_{g,f-m}\right)_{rc} \tag{7.7}$$

where

$q_{o,f}$ = oil production rate at standard conditions.

$q_{g,f}$ = gas flow rate through the fracture system at reservoir conditions.

$q_{g,f-m}$ = gas flow rate from fracture to matrix system at reservoir conditions.

B_o = oil volume factor at the average pressure system.

From equation 7.7, we can obtain

$$q_{g,f} = q_{o,f} B_o - q_{g,f-m} \tag{7.8}$$

For our case, nitrogen injection maintains the reservoir pressure constant and the oil production rate is approximately constant during four years of nitrogen injection. Simulation results for our case study showed average values of $q_{o,f} = 0.041$ *bpd* and $B_o = 1.19$ (barrels at reservoir conditions/barrels at standard conditions).

Since the matrix system is a source term where no bulk fluid-flow occurs, the gas flow rate from the fracture into the matrix at reservoir conditions $\left(q_{g,f-m}\right)$ can be obtained by

$$q_{g,f-m} = \frac{V_{g,m}}{t} \tag{7.9}$$

where

$V_{g,m}$ = Cumulative gas volume flowed from fracture into the matrix system

t = time.

The gas volume in matrix system can be determined by

$$V_{g,m} = \overline{S_{g,m}}\ Z_{g,f}\ L_x\ L_z\ \phi_m \tag{7.10}$$

where

$\overline{S_{g,m}}$ = average matrix gas saturation.

$Z_{g,f}$ = gas saturation front location in the fractured system.

$L_x L_z$ = area of flow between fracture and matrix.

ϕ_m = matrix porosity.

Substituting equations 7.10 into equation 7.9, the gas flow rate from the fracture into the matrix at reservoir conditions $\left(q_{g,f-m}\right)_{rc}$ can be obtained by

$$q_{g,f-m} = \frac{\overline{S_{g,m}}\ Z_{g,f}\ L_x\ L_z\ \phi_m}{t} \tag{7.11}$$

Substituting equation 7.11 into equation 7.8, the gas flow rate though the fracture system at reservoir conditions $\left(q_{g,f}\right)_{rc}$ can be expressed as

$$q_{g,f} = q_{o,f}B_o - \left(\frac{\overline{S_{g,m}}\ Z_{g,f}\ L_x\ L_z\ \phi_m}{t}\right) \tag{7.12}$$

Substituting 7.12 into equation 7.6, the fracture volumetric gas flux evaluated at reservoir conditions can be obtained by

$$u_{g,f} = \frac{q_{o,f}B_o - \left(\frac{\overline{S_{g,m}}\ Z_{g,f}\ L_x\ L_z\ \phi_m}{t}\right)}{A_f} \tag{7.13}$$

Finally, substituting 7.13 into 7.5, the location of gas saturation front in the fracture system $\left(Z_{sg,f}\right)$ can be expressed as

$$Z_{sg,f} = \frac{\left(\frac{q_{o,f}B_o - \left(\frac{\overline{S_{g,m}}\ Z_{g,f}\ L_x\ L_z\ \phi_m}{t}\right)}{A_f}\ t\right)}{\left[\phi_f + \phi_m \frac{\Delta F(S_{g,f})}{\Delta S_{g,f}}\right]}\left[\frac{\Delta f_{g,f}(S_{g,f})}{\Delta S_{g,f}}\right] \tag{7.14}$$

Grouping and eliminating terms, we obtained

$$Z_{sg,f} + \left(\frac{\overline{S_{g,m}}\ Z_{g,f}\ L_x\ L_z\ \phi_m}{A_f\left(\phi_f + \phi_m \frac{\Delta F(S_{g,f})}{\Delta S_{g,f}}\right)}\left[\frac{\Delta f_{g,f}(S_{g,f})}{\Delta S_{g,f}}\right]\right) = \frac{q_{o,f}B_o\ t}{A_f\left[\phi_f + \phi_m \frac{\Delta F(S_{g,f})}{\Delta S_{g,f}}\right]}\left[\frac{\Delta f_{g,f}(S_{g,f})}{\Delta S_{g,f}}\right]$$

$$Z_{sg,f}\left(1 + \frac{\overline{S_{g,m}}\ L_x\ L_z\ \phi_m}{A_f\left(\phi_f + \phi_m \frac{\Delta F(S_{g,f})}{\Delta S_{g,f}}\right)}\left[\frac{\Delta f_{g,f}(S_{g,f})}{\Delta S_{g,f}}\right]\right) = \frac{q_{o,f}B_o\ t}{A_f\left[\phi_f + \phi_m \frac{\Delta F(S_{g,f})}{\Delta S_{g,f}}\right]}\left[\frac{\Delta f_{g,f}(S_{g,f})}{\Delta S_{g,f}}\right]$$

$$Z_{sg,f}\left[\frac{A_f\left(\phi_f+\phi_m\frac{\Delta F(S_{g,f})}{\Delta S_{g,f}}\right)+\overline{S_{g,m}}\ L_x\ L_z\ \phi_m\left[\frac{\Delta f_{g,f}(S_{g,f})}{\Delta S_{g,f}}\right]}{A_f\left(\phi_f+\phi_m\frac{\Delta F(S_{g,f})}{\Delta S_{g,f}}\right)}\right]=\frac{q_{o,f}B_o\ t}{A_f\left[\phi_f+\phi_m\frac{\Delta F(S_{g,f})}{\Delta S_{g,f}}\right]}\left[\frac{\Delta f_{g,f}(S_{g,f})}{\Delta S_{g,f}}\right]$$

$$Z_{sg,f}=\frac{q_{o,f}B_o\ t}{A_f\left[\phi_f+\phi_m\frac{\Delta F(S_{g,f})}{\Delta S_{g,f}}\right]}\left[\frac{\Delta f_{g,f}(S_{g,f})}{\Delta S_{g,f}}\right]\left[\frac{A_f\left(\phi_f+\phi_m\frac{\Delta F(S_{g,f})}{\Delta S_{g,f}}\right)}{A_f\left(\phi_f+\phi_m\frac{\Delta F(S_{g,f})}{\Delta S_{g,f}}\right)+\overline{S_{g,m}}\ L_x\ L_z\ \phi_m\left[\frac{\Delta f_{g,f}(S_{g,f})}{\Delta S_{g,f}}\right]}\right]$$

$$Z_{sg,f}=\frac{\left(q_o\ \ B_o\ \ \ t\right)\left[\frac{\Delta f_{g,f}(S_{g,f})}{\Delta S_{g,f}}\right]}{A_f\left[\phi_f+\phi_m\frac{\Delta F(S_{g,f})}{\Delta S_{g,f}}\right]+\overline{S_{g,m}}L_xL_z\phi_m\left[\frac{\Delta f_{g,f}(S_{g,f})}{\Delta S_{g,f}}\right]} \tag{7.15}$$

7.3.2 Determination of fracture area, A_f

Considering the matrix block as a slab with sides L_x, L_y and L_z surrounded by a fracture of thickness T/2, as shown in Figure 7.6. The relationship between fracture porosity (ϕ_f) as a function of fracture aperture ($w = T/2$) and matrix block size (L_x, L_y and L_z) for a slab is

$$\phi_f=\frac{volume\ of\ fracture}{volume\ of\ matrix+volume\ of\ fracture}$$

$$\phi_f=\frac{\left(L_x+T\right)\left(L_y+T\right)\left(L_z+T\right)-L_xL_yL_z}{\left(L_x+T\right)\left(L_y+T\right)\left(L_z+T\right)}$$

Expanding terms

$$\phi_f=\frac{L_xL_yL_z+TL_yL_z+TL_xL_z+TL_z+TL_yL_x+T^2L_y+T^2L_x+T^3-L_xL_yL_z}{\left(L_x+T\right)\left(L_y+T\right)\left(L_z+T\right)}$$

Eliminating terms and grouping

$$\phi_f = \frac{T(L_y L_z + L_x L_z + L_y L_x) + T^2(L_z + L_y + L_x) + T^3}{(L_x + T)(L_y + T)(L_z + T)}$$

Considering $T << L_x, L_y$ and L_z then

$$T^2(L_z + L_y + L_x) \approx 0$$

$$T^3 \approx 0$$

$$(L_x + T)(L_y + T)(L_z + T) \approx L_x L_y L_z$$

Substituting these three approximations

$$\phi_f \approx \frac{T(L_y L_z + L_x L_z + L_y L_x)}{(L_x)(L_y)(L_z)}$$

Expanding terms

$$\phi_f \approx \frac{TL_y L_z}{L_x L_y L_z} + \frac{TL_x L_z}{L_x L_y L_z} + \frac{TL_y L_x}{L_x L_y L_z}$$

Eliminating and grouping

$$\phi_f \approx T\left[\frac{1}{L_x} + \frac{1}{L_y} + \frac{1}{L_z}\right] \tag{7.16}$$

From equation 7.16, $T \approx \frac{\phi_f}{\left[\frac{1}{L_x} + \frac{1}{L_y} + \frac{1}{L_z}\right]}$. The area for a vertical fracture surrounded a matrix block is obtained by $A_f \approx \frac{TL_x}{2} \approx \frac{\frac{\phi_f L_x}{\left[\frac{1}{L_x} + \frac{1}{L_y} + \frac{1}{L_z}\right]}}{2} \approx \frac{\phi_f L_x}{2\left[\frac{1}{L_x} + \frac{1}{L_y} + \frac{1}{L_z}\right]}$ (7.17)

Substituting equation 7.17 into equation 7.15, the gas saturation front in the fracture system can be obtained

$$Z_{sg,f} = \frac{\left(q_o \;\; B_o \;\; t\right)\left[\dfrac{\Delta f_{g,f}(S_{g,f})}{\Delta S_{g,f}}\right]}{\left[\dfrac{\phi_f L_x}{2\left(\dfrac{1}{L_x}+\dfrac{1}{L_y}+\dfrac{1}{L_z}\right)}\right]\left[\phi_f + \phi_m \dfrac{\Delta F(S_{g,f})}{\Delta S_{g,f}}\right] + \overline{S_{g,m}} L_x L_z \phi_m \left[\dfrac{\Delta f_{g,f}(S_{g,f})}{\Delta S_{g,f}}\right]} \tag{7.18}$$

7.3.3 Determination of the Δ terms

To determine the Δ terms, we considered the following approximations:

$$\left[\frac{df_{g,f}}{dS_{g,f}}\right] \approx \left[\frac{\Delta f_{g,f}}{\Delta S_{g,f}}\right] \approx \lim_{S\to o} \frac{f(S_0+\Delta S)-f(S_0)}{\Delta S}$$

$$\left[\frac{dF}{dS_{g,f}}\right] \approx \left[\frac{\Delta F}{\Delta S_{g,f}}\right] \approx \lim_{S\to o} \frac{F(S_0+\Delta S)-F(S_0)}{\Delta S}$$

Then the calculation of the derivative terms is described in the following Sections 7.3.3.1 and 7.3.3.2.

7.3.3.1 Derivative of gas fractional flow with respect to gas saturation for the fracture system, $\left[\dfrac{df_{g,f}(S_{g,f})}{dS_{g,f}}\right]$

To study the fractured medium using a dual porosity system, we considered zero capillary pressure in the fracture system. This is a valid assumption since the vertical fracture permeability (5000 md) and fracture apertures (250 microns) are large values for our case study.

An important point is that, in the absence of capillary pressure in the fracture system, the gas fractional flow function is uniquely determined as a function of gas saturation through gas and oil relative permeabilities as described in the following equation (Lake, 1989):

$$f_{g,f} = \frac{1 - \left[\frac{kA(\rho_{oil} - \rho_{gas})\sin\alpha}{\mu_{oil}}\right]\left(\frac{k_{ro,f}}{qt}\right)}{\left[1 + \frac{k_o}{k_g}\frac{\mu_g}{\mu_o}\right]}$$

where

$f_{g,f}$ = gas fractional flow in fracture system, fraction

k = absolute permeability, L^2

A = flow area, L^2

ρ_{oil} = oil density, m/L^3

ρ_{gas} = gas density, m/L^3

α = inclination angle, degrees

μ_{oil} = oil viscosity, m/Lt

$k_{ro,f}$ = fracture oil relative permeability, fraction

k_o = effective oil permeability, L^2

The values of $f_{g,f}(S_{g,f})$ for the case study are illustrated in Figure 7.7 (blue line). This figure illustrates that the $f_{g,f}(S_{g,f})$ curve is less than zero for a large S_o range, which indicates a flow where gravity forces are very strong (Lake, 1989).

Welge (1952) showed that the gas front can be obtained by drawing a secant line from the origin, as is illustrated in Figure 7.7 (red line). This secant line showed a value of $\left[\frac{df_{g,f}(S_{g,f})}{dS_{g,f}}\right] = 1.0$ for our case study. When we applied our result to equation 7.18, we obtained

$$Z_{sg,f} = \frac{\left(q_o \;\; B_o \;\; t\right)}{\left[\frac{\phi_f L_x}{2\left(\frac{1}{L_x} + \frac{1}{L_y} + \frac{1}{L_z}\right)}\right]\left[\phi_f + \phi_m \frac{\Delta F(S_{g,f})}{\Delta S_{g,f}}\right] + \overline{S_{g,m}} L_x L_z \phi_m} \qquad (7.19)$$

7.3.3.2 Derivative of matrix gas saturation with respect to fracture gas saturation, $\left[\frac{dS_{g,m}}{dS_{g,f}}\right]$

To determine the derivative of matrix gas saturation with respect to the fracture gas saturations $\left[\frac{dS_{g,m}}{dS_{g,f}}\right]$, it was necessary to make a detailed analysis of the simulation results. In addition, this analysis also helps to explain the dynamic of fluids flowing into naturally fractured reservoirs.

First, we plotted the matrix and fracture gas saturations up to 1000 days of nitrogen injection for 40 blocks, as is illustrated in Figure 7.8. This figure shows the matrix gas saturation, $S_{g,m}$, versus fracture gas saturation, $S_{g,f}$ on the same curve for almost all gridblocks located further from the injection well. This behavior was not observed for the first two gridblocks, which are located near the gas injection well, because of the inner boundary effects. In addition, this figure indicates that the behavior of matrix versus fracture gas saturation can be divided into two stages: the first fluid-flow stage begins when injected gas starts moving through the fracture until it fully saturates the fractured system ($0 < S_{g,f} < 100\%$); this stage occurs approximately when the matrix gas saturation changes from 0 to 16%. The second fluid-flow stage begins once fractures reach 100% gas saturation until no oil is able to flow from the matrix through fractures. During this stage, the matrix gas saturation changes from approximately 16 to 28%.

Second, we analyzed the average time that each fluid-flow stage occurs after 1000 days of nitrogen injection. Figure 7.9 shows that each fracture gridblock reached 100% gas saturation 24 days (on average) after nitrogen arrival. Therefore full gas saturation in the fracture gridblocks occurs quickly. On the other hand, the second fluid-flow stage

dominates the whole nitrogen injection process (large matrix saturation changes approximately during 200 days), as illustrated in Figure 7.10.

Third, we identified the number of gridblocks for each fluid-flow stage by plotting the simulation results in Figures 7.11 through 7.13. They showed that the first fluid-flow stage occurs only through the two blocks near the gas-oil contact, while the second fluid-flow stage covers most of the gridblocks behind the fractured gas saturation front.

Based on the results illustrated in Figures 7.11 through 7.13, we observed small variations in matrix gas saturations during the second fluid-flow stage; therefore, the term $\left[\frac{dS_{g,m}}{dS_{g,f}}\right]$ is small$\left[\frac{dS_{g,m}}{dS_{g,f}} \approx \frac{0.27-0.21}{1-0} \approx 0.06\right]$. Since $\left[\frac{dS_{g,m}}{dS_{g,f}}\right]$ multiplies the matrix porosity $\left(\phi_m = 0.05\right)$ in equation 7.19, we neglect it as is illustrated in the following equation:

$$Z_{sg,f} = \frac{\left(q_o \;\; B_o \;\; t\right)}{\left[\frac{\phi_f L_x}{2\left(\frac{1}{L_x}+\frac{1}{L_y}+\frac{1}{L_z}\right)}\right]\phi_f + \overline{S_{g,m}} L_x L_z \phi_m} \tag{7.20}$$

Equation 7.20 was the final expression found for the analytical model developed. This equation, in general terms, can also be expressed as

$$Z_{sg,f} = \frac{\left(q_o \;\; B_o \;\; t\right)}{A_f \phi_f \overline{S_{g,f}} + \overline{S_{g,m}} A_m \phi_m} \tag{7.21}$$

where $\overline{S_{g,f}}$ is the gas saturation of the fracture system which is ≈ 1, $A_f \approx \frac{\phi_f L_x}{2\left[\frac{1}{L_x}+\frac{1}{L_y}+\frac{1}{L_z}\right]}$ and $A_m = L_x L_z$ is the matrix block surface which is in contact with

the fracture system and the fluid transfer occurs. This general expression was also found considering a different approach with an overall (weak form) material balance, as described in Appendix A.

7.4 Analytical model results

The movement of the nitrogen injection front through the fracture system versus time was used to compare the analytical model with the simulation case study. The analytical model results are illustrated in Figure 7.14, which shows the position of four nitrogen injection fronts (cases I through IV) applying equation 7.20. Cases I, II and III used the matrix gas saturation resulting from the simulation case study (described in Section 7.2). The main difference between each case was the $\overline{S_{g,m}}$ term calculation. The nitrogen injection front obtained with cases I-III and the simulation case study showed small variations, as illustrated in Figure 7.14. For case IV, the $\overline{S_{g,m}}$ term was calculated based on the shape of matrix capillary pressure profiles versus time (Figure 7.15) and the matrix-fracture oil flow rate profiles versus time (Figures 7.16) obtained by simulation of the case study (described in Section 7.2). These considerations made the analytical model (case IV) adequately reproduce the simulation results for all practical point of view, as is illustrated in Figure 7.17.

The above cases are described in the following:

a) The analytical case I considers that the $\overline{S_{g,m}}$ term is an arithmetic average value of upper and lower matrix gridblocks, such as $\overline{S_{g,m}} = \frac{S_{g,m}^{upper\ block} + S_{g,m}^{lower\ block}}{2}$. These matrix blocks correspond to the upper and lower gridblocks of the second fluid-flow stage, which are illustrated in Figures 7.11 through 7.13. Table 7.3 shows the values used for $\overline{S_{g,m}}$ term calculation.

b) The analytical case II considers that the $\overline{S_{g,m}}$ term is constant, such as $\overline{S_{g,m}} = S_{g,m}^{upper\ block}$. Table 7.3 shows values used for the $\overline{S_{g,m}}$ term calculation.

c) The analytical case III uses the $\overline{S_{g,m}}$ term obtained with $\overline{S_{g,m}} = \dfrac{\int_0^{Z_{sg,f}} S_g(z)\ dz}{Z_{sg,f}}$ as shown in Table 7.4. The calculation of $\overline{S_{g,m}}$ using $\overline{S_{g,m}} = \dfrac{\int_0^{Z_{sg,f}} S_g(z)\ dz}{Z_{sg,f}}$ resulted in a better approximation of the gas saturation front $\left(Z_{sg,f}\right)$ than cases I and II, as is illustrated in Figure 7.13.

d) The analytical case IV uses the $\overline{S_{g,m}}$ values resulted from analysis of matrix capillary pressure profiles versus time and matrix-fracture oil flow rate profiles versus time; therefore simulation results were not necessary for the $\overline{S_{g,m}}$ term calculation. The procedure we applied is described as follows:

First, we calculated the matrix gas saturation value considering equilibrium between capillary and gravity drainage forces, which occurs mainly in matrix gridblocks located at the top of the case study. To estimate this matrix gas saturation, we analyzed the simulation results of the oil flow rate between matrix and fracture systems and found that oil flow transfer is almost negligible at the top of the matrix gridblock, especially after a lot of nitrogen injection, as illustrated in Figures 7.16. This behavior occurs mainly because capillary and gravity forces dominate at the displacement and reach equilibrium. This consideration implies that

$$P_{c,m} = Gravity\ drainage \tag{7.22}$$

Substituting

$P_{c,m} = P_c^0 \left(1 - \frac{S_o - S_{or}}{1 - S_{or} - S_{wi}} \right)^{e_{pc}}$ and $Gravity\ drainage = (\rho_{liquid} - \rho_{gas})\ g\ L_z$ in equation 7.22,

we obtain

$$P_c^0 \left(1 - \frac{1 - S_{g,m} - S_{wi} - S_{or}}{1 - S_{or} - S_{wi}} \right)^{e_{pc}} = (\rho_{liquid} - \rho_{gas})\ g\ L_z \qquad (7.23)$$

We applied equation 7.23 with information used for the case study, and found that the matrix gas saturation $(S_{g,m})$ reaches a value of 0.25 (which corresponds to a matrix capillary pressure of 2.65 psia) when oil flow between the matrix and fracture systems ceases. Subsequently, we considered that the matrix gas saturation calculated corresponds to the upper gridblock and is maintained constant during the entire nitrogen injection. This consideration is acceptable since the simulation results showed small variations in the $S_{sg,m}^{upper\ block}$ between 0.23 up to 0.28, as illustrated in Table 7.3.

Second, we plotted matrix capillary pressure profiles at different times using a simulation case study, as illustrated in Figure 7.15, which showed a quasi-linear trend during the second fluid-flow stage. As an approximation, we considered a linear behavior using $P_{c.m} = 0$ at a guess nitrogen injection front $(Z_{sg,f})$ and $P_{c.m} = 2.65$ psia at $Z_{sg,f} = 0$. After that, we calculated matrix gas saturation profiles based on capillary pressure model and then we applied $\overline{S_{g,m}} = \frac{\int_0^{Z_{sg,f}} S_g(z)\ dz}{Z_{sg,f}}$.

Third, we substituted $\overline{S_{g,m}}$ in equation 7.20 to calculate $Z_{sg,f}$ and if the guess $Z_{sg,f}$ differ from the calculated $Z_{sg,f}$, we will use a trial and error procedure until results converge. The gas saturation front results obtained through similar calculations are shown in Figure 7.17.

An example of the $Z_{sg,f}$ term calculation is illustrated in Tables 7.5 and 7.6. The calculations were performed using EXCEL worksheets with the following input data: 1) a calculation of matrix gas saturation, $S_{g,m} = 0.25$, which corresponds to a matrix capillary pressure of 2.65 psia when oil flow between matrix and fracture systems ceases, and 2) an initial value of the gas saturation front location ($Z_{sg,f}$). The initial guess value of $Z_{sg,f}$ was 30 ft for 100 days of nitrogen injection.

For this exercise, we first defined capillary pressure values in a range of 0-2.65 psia with intervals of 0.01 psia, as is shown in column 1 of Table 7.5. Second, a calculation of matrix gas saturation for each matrix capillary pressure was performed by using $P_{c,m} = P_c^0 \left(1 - \frac{S_o - S_{or}}{1 - S_{or} - S_{wi}}\right)^{e_{pc}}$; the results are illustrated in column 2. Third, in column 3 we calculated the depth for each interval by using $Z = -\left(\frac{Z_{sg,f}^{guess}}{2.65}\right) P_{c.m} + Z_{sg,f}^{guess}$ based on the consideration of linear matrix capillary pressure with depth. Fourth, a calculation of $\overline{S_{g,m}}$ was performed using $\overline{S_{g,m}} = \frac{\int_0^{Z_{sg,f}} S_g(z)\, dz}{Z_{sg,f}}$ as is shown in column 4, and finally after the calculation of the $\overline{S_{g,m}}$ term, we calculated $Z_{sg,f}$ using equation 7.20. The results are shown in column 5. If the difference between the guess $Z_{sg,f}$ and the calculated $Z_{sg,f}$ is less than a tolerance (0.001 ft), we concluded the calculation; otherwise, we used a trial- and-error procedure until $Z_{sg,f}$ converged. Table 7.6 illustrates that at $Z_{sg,f} = 41.8$ ft, the results converged for 100 days of nitrogen injection.

The calculation of the gas saturation front through a fracture system using an analytical model (case IV) is less accurate than cases I-III but its advantage is that no simulation results are needed. As we have described, the analytical case IV includes

many assumptions that should be studied in detail to enhance a better representation of the simulated case study. One of our limitations was the adequate representation of matrix fluid distributions because the ECLIPSE 300 simulator does not include an option for matrix grid refinement in the vertical direction for a dual porosity option.

7.5 Validation of the analytical model based on sensitivity studies

The motivation of this study was to validate the results of the analytical model based on a sensitivity study. We performed several sensitivity studies based on "pseudo" matrix capillary pressure, fracture porosity, and fracture permeability, because of their impact on the advancement of the gas front through fracture system. All of our case studies considered the same conceptual model, boundary conditions, and fluid characterization described in Section 7.2. And all of the simulated gas front advancements of each case study were compared with equation 7.20 by using the analytical case III.

A sensitivity study based on "pseudo" matrix capillary pressure is described in Section 7.5.1, for the fracture porosity in Section 7.5.2, and for the fracture permeability in Section 7.5.3.

7.5.1 Sensitivity study on "pseudo" matrix capillary pressure

The sensitivity study based on matrix capillary pressure used values that ranged from 1 to 20 for the gas-oil capillary pressure exponent, e_{pc}, which is considered in the capillary pressure model. The set of "pseudo" matrix capillary pressure curves used for this study are illustrated in Figure 7.19.

The simulation results for all case sensitivity studies indicated that oil production rate (0.041 bpd) and average pressure (2250 psia) have no significant variations during

1000 days of nitrogen injection, therefore the same constant oil production rate and oil formation volume factor were used for the analytical model validation.

The analytical model (Equation 7.20) adequately reproduced the simulation gas front advancement versus time for all studied cases, as illustrated in Figure 7.20. In addition, both the analytical and the simulation models showed that at a smaller oil-gas capillary pressure exponent, e_{pc}, less gas entered into the matrix system. In other words, large matrix capillary pressure values prohibit oil from being expelled from the matrix through the fracture system and prohibit injected gas from entering the matrix system. We also observed in Figure 7.20 that, for larger gas flow from the fracture into the matrix system (high e_{pc} values), the advancement of the gas front was slower.

For all of our case studies, the final matrix gas saturation simulated could not be predicted by using the end-points of the relative permeabilities or capillary pressure curves because the equilibrium of gravity and capillary forces in the matrix occurs before reaching the relative permeabilities' end-points. For the reservoir under study ($e_{pc} = 6$), the final matrix gas saturation simulated was 0.28 and the final matrix oil saturation was 0.57 after 1000 days of nitrogen injection.

7.5.2 Sensitivity study on fracture porosity

The sensitivity study based on fracture porosity used values ranging from 0.0088 to 0.025. The simulation results of all case studies ($\phi_f = 0.0088,\ 0.0175$ and 0.0250) indicated that oil production rate (0.041 bpd) and average stack pressure (2250 psia) have no significant variations during 1000 days of nitrogen injection. On the other hand, the analytical model developed adequately reproduced the movement of the gas front for all cases, as is illustrated in Figures 7.21. Both the analytical and simulation models showed that, at small fracture porosity values, the advancement of the gas front was faster than for higher fracture porosity values, as Figure 7.21 illustrates.

7.5.3 Sensitivity study on fracture permeability

The sensitivity study based on fracture permeability used values that ranged from 50 to 5000 md. We studied five cases: $k_f = 50,\ 100,\ 500,\ 1000$, and $5000\ md$. The simulation results for all the case studies indicated that the oil production rate and average stack pressure have no significant variations during 1000 days of nitrogen injection except for $k_f = 50\ md$ case. On the other hand, the developed analytical model adequately reproduced the advancement of the gas front for all the case studies, as illustrated in Figure 7.22. This figure also shows similar behavior for case studies in which k_f ranged from 500 to 5000 md. It also illustrates that for case studies with lower fracture permeability values (less than 500 md), the movement of gas front was slower than higher fracture permeability case studies.

Table 7.1 Matrix and fracture properties used for the stacked simulation model and the developed analytical model.

Property	Value
MATRIX SYSTEM	
Porosity (fraction)	0.05
Permeability in *x* direction (md)	0.4
Permeability in *y* direction (md)	0.4
Permeability in *z* direction (md)	0.4
Height of matrix block, L_z (ft)	10
L_x and L_y distance (ft)	5
FRACTURE SYSTEM	
Porosity (fraction)	0.0175
Permeability in *x* direction (md)	50
Permeability in *y* direction (md)	50
Permeability in *z* direction (md)	5000

Table 7.2 Values used for the relative permeability and capillary pressure models (PEMEX, personal communication).

k_{ro}^0 : End-point oil relative permeability	1.00
S_{or} : Residual oil saturation	0.40
S_{wi} : Initial (residual) water saturation	0.15
S_{gr} : Residual gas saturation	0.00
e_o : Numerical exponent	3.00
k_{rg}^0 :End-point gas relative permeability	0.32
e_g : Numerical exponent	2.00
P_c^0 : End-point capillary pressure	6.00
e_{pc} : Exponent for oil-gas capillary pressure	6.00

Table 7.3 Matrix gas saturations of upper and lower gridblocks used for the $\overline{S_{g,m}}$ calculation in cases I and II.

Time (day)	$S_{sg,m}^{lower\ block}$	$S_{sg,m}^{upper\ block}$	$\overline{S_{g,m}}$
100	0.22	0.23	0.22
250	0.21	0.26	0.23
500	0.22	0.27	0.24
750	0.22	0.28	0.25
1000	0.22	0.28	0.25

Table 7.4 $\overline{S_{g,m}}$ values used to calculate $Z_{sg,f}$ for the analytical case III.

Time(day)	$\overline{S_{g,m}}$	$Z_{sg,f}$ (ft)
100	0.23	46.95
250	0.24	111.66
500	0.24	227.96
750	0.26	316.88
1000	0.27	409.87

Table 7.5 Calculation of gas saturation front in the fracture system after 100 days of nitrogen injection using a guess $Z_{sg,f}$=30 ft.

Pc (psia)	Sg_m (fraction)	$Z_{sg,f\ guess}$ (ft)	$\overline{S_{g,m}}$ (fraction)	$Z_{sg,f\ calc}$ (ft)	$Z_{sg,f\ guess}$- $Z_{sg,f\ calc}$ (ft)
2.655	0.251	0.0000	0.2617	41.82	-11.82
2.640	0.251	0.2031			
2.630	0.251	0.3357			
2.620	0.250	0.4683			
2.610	0.250	0.6008			
2.600	0.250	0.7334			
2.590	0.250	0.8660			
2.580	0.250	0.9986			
2.570	0.250	1.1312			
2.560	0.249	1.2638			
2.550	0.249	1.3964			
2.540	0.249	1.5290			
2.530	0.249	1.6616			
2.520	0.249	1.7941			
2.510	0.249	1.9267			
0.09	0.143	28.9832			
0.08	0.140	29.0962			
0.07	0.137	29.2091			
0.06	0.133	29.3221			
0.05	0.129	29.4351			
0.04	0.125	29.5481			
0.03	0.119	29.6611			
0.02	0.111	29.7740			
0.01	0.099	29.8870			
0.00	0.000	30.0000			

Table 7.6 Calculation of gas saturation front in the fracture system after 100 days of nitrogen injection using a guess $Z_{sg,f} = 41.82$ ft.

Pc (psia)	Sg_m (fraction)	$Z_{sg,f\ guess}$ (ft)	$\overline{S_{g,m}}$ (fraction)	$Z_{sg,f\ calc}$ (ft)	$Z_{sg,f\ guess}$- $Z_{sg,f\ calc}$ (ft)
2.655	0.251	0.0000	0.2617	41.82	0.0004
2.640	0.251	0.2412			
2.630	0.251	0.3987			
2.620	0.250	0.5562			
2.610	0.250	0.7137			
2.600	0.250	0.8712			
2.590	0.250	1.0287			
2.580	0.250	1.1862			
2.570	0.250	1.3437			
2.560	0.249	1.5012			
2.550	0.249	1.6587			
2.540	0.249	1.8162			
2.530	0.249	1.9737			
2.520	0.249	2.1312			
2.510	0.249	2.2887			

0.09	0.143	40.4025			
0.08	0.140	40.5600			
0.07	0.137	40.7175			
0.06	0.133	40.8750			
0.05	0.129	41.0325			
0.04	0.125	41.1900			
0.03	0.119	41.3475			
0.02	0.111	41.5050			
0.01	0.099	41.6625			
0.00	0.000	41.8200			

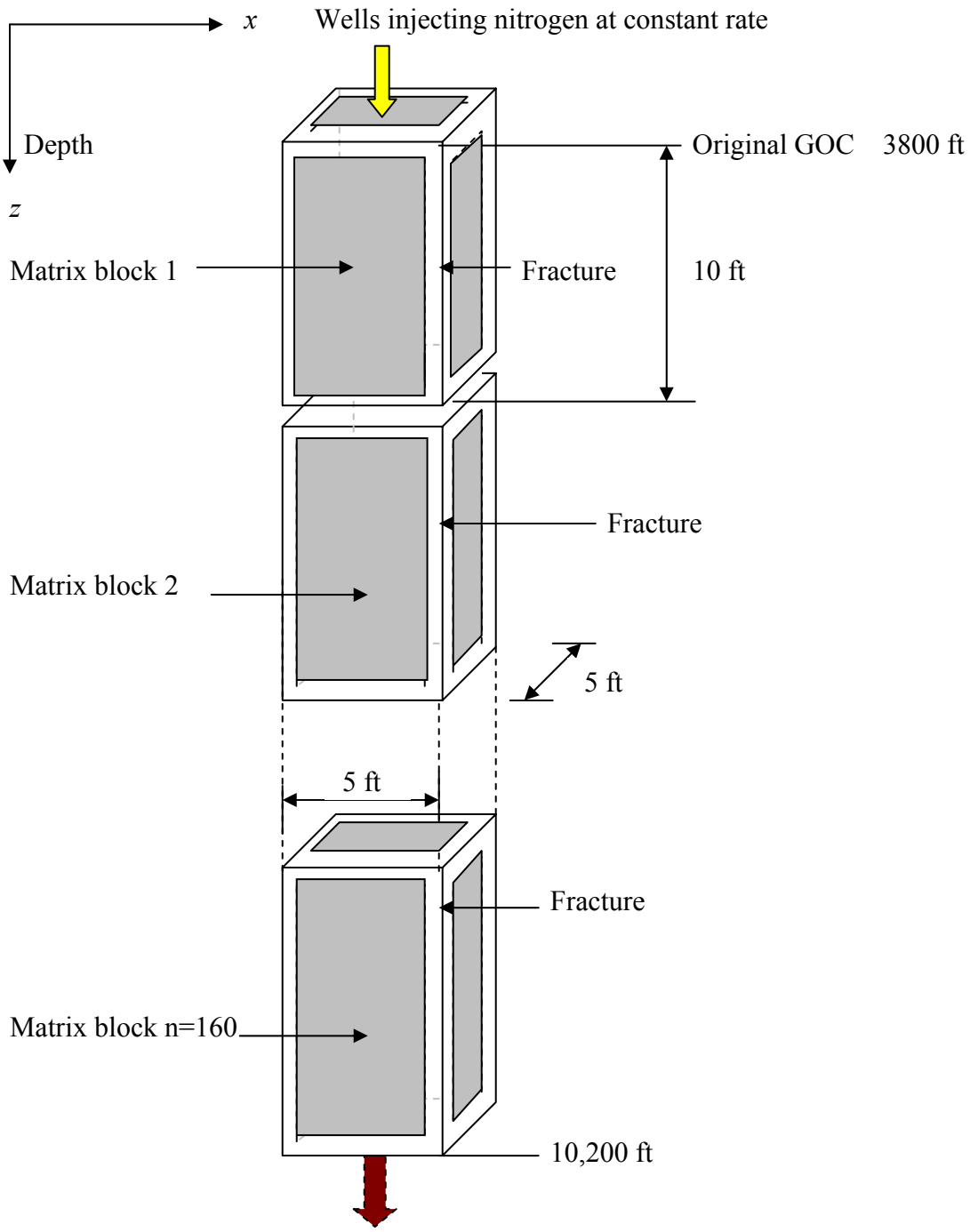

Figure 7.1 Stacked simulation model used to validate analytical model.

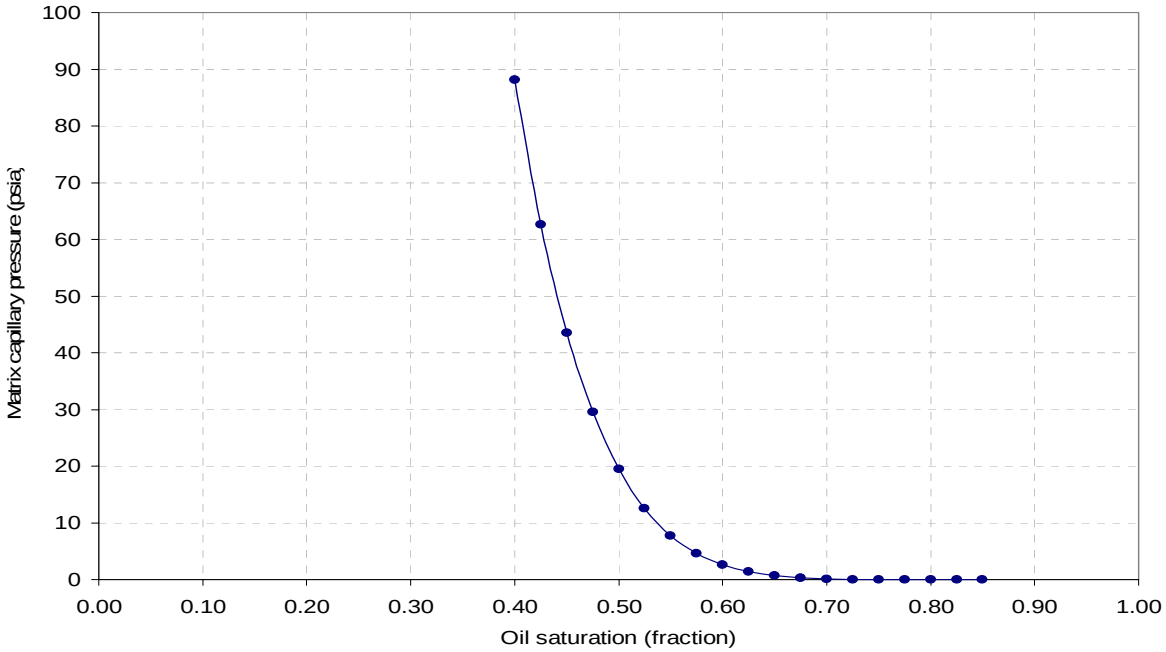

Figure 7.2 Matrix capillary pressure for the oil-gas system.

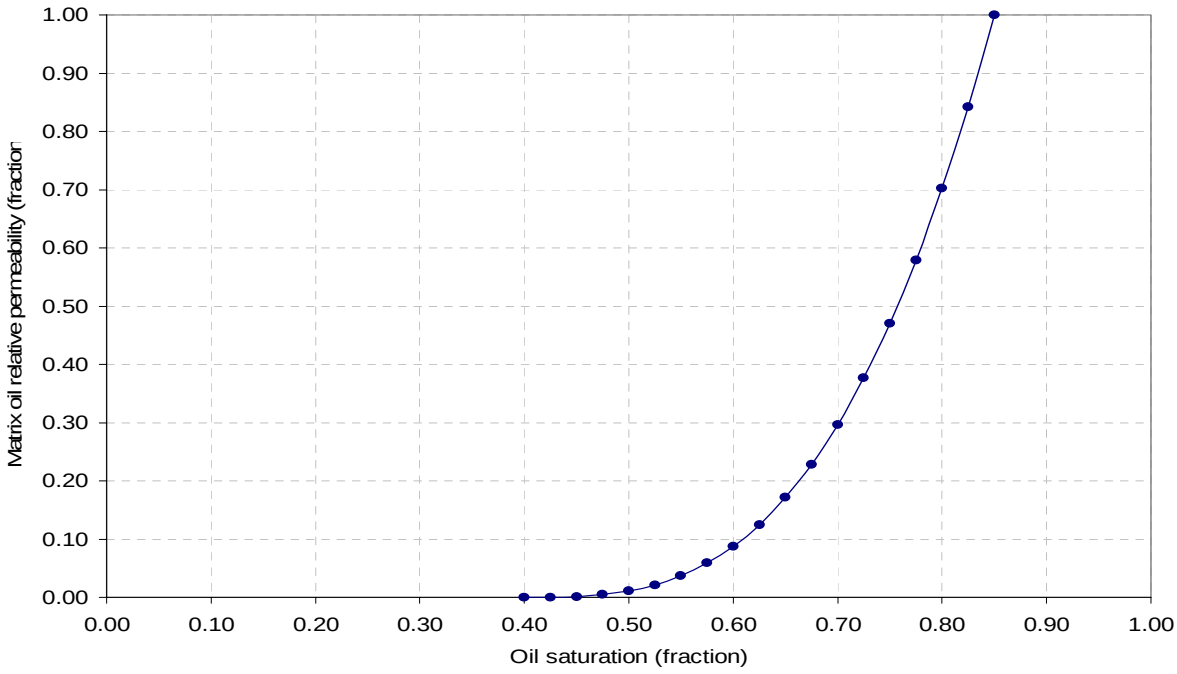

Figure 7.3 Oil relative permeability for the matrix system.

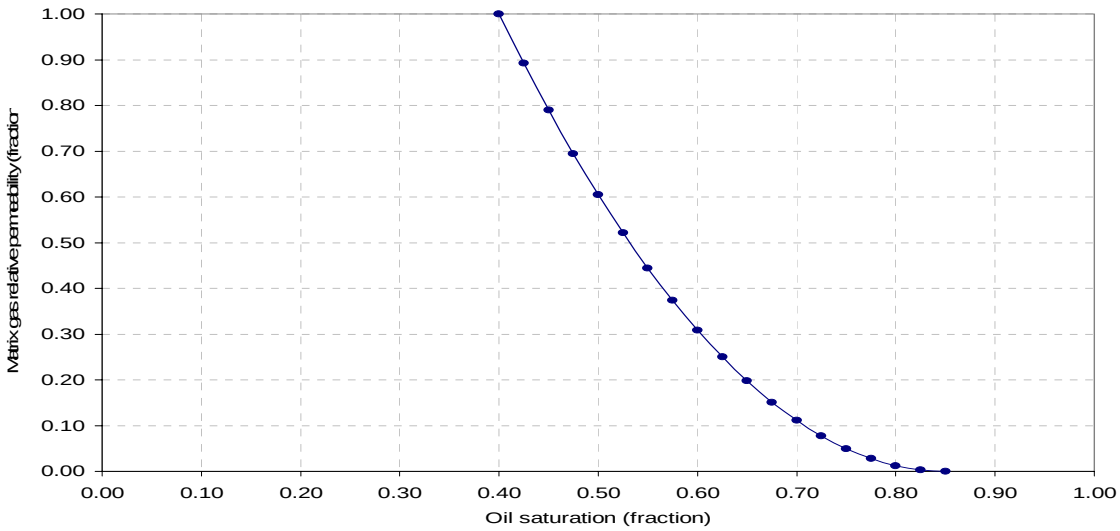

Figure 7.4 Gas relative permeability for the matrix system.

.

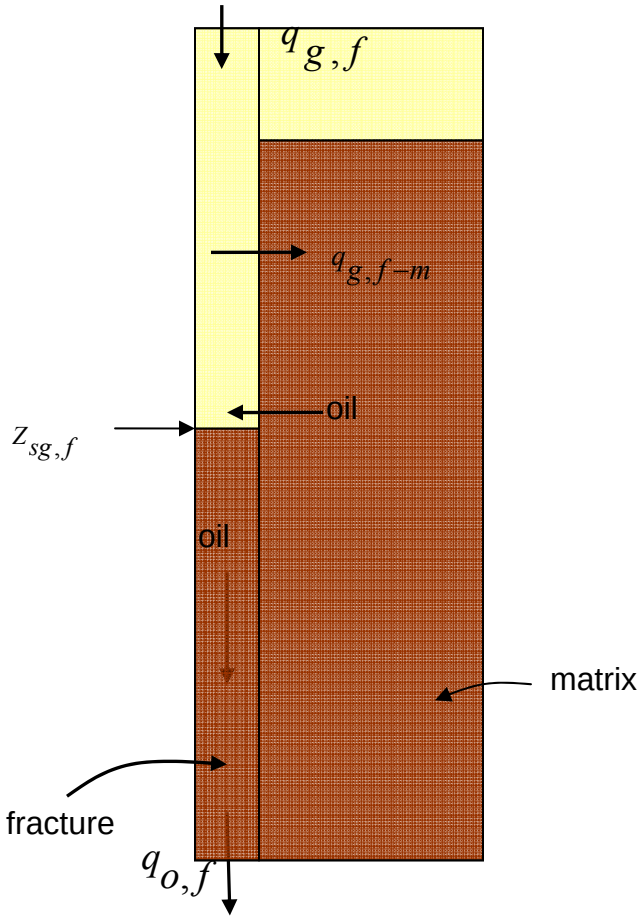

Figure 7.5 Phase flow representation in stacked model used for gas material balance.

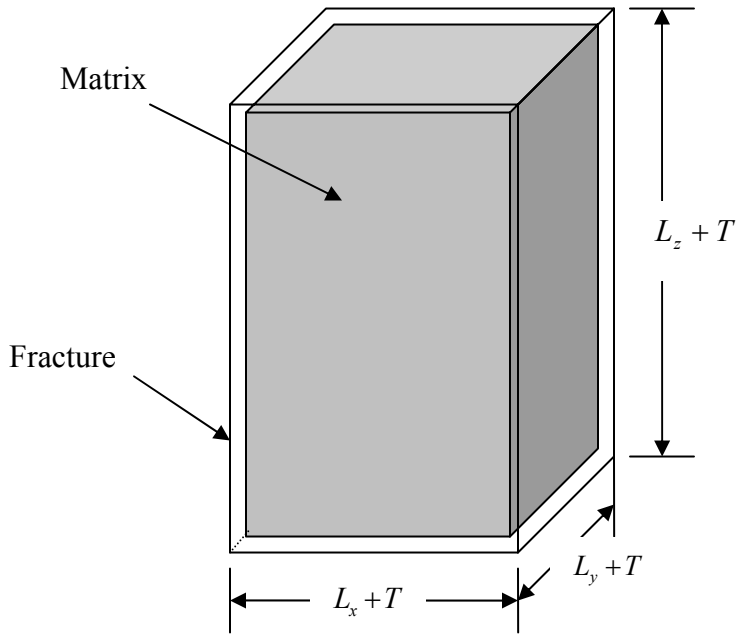

Figure 7.6 Schematic presentation of a slab surrounded by fractures.

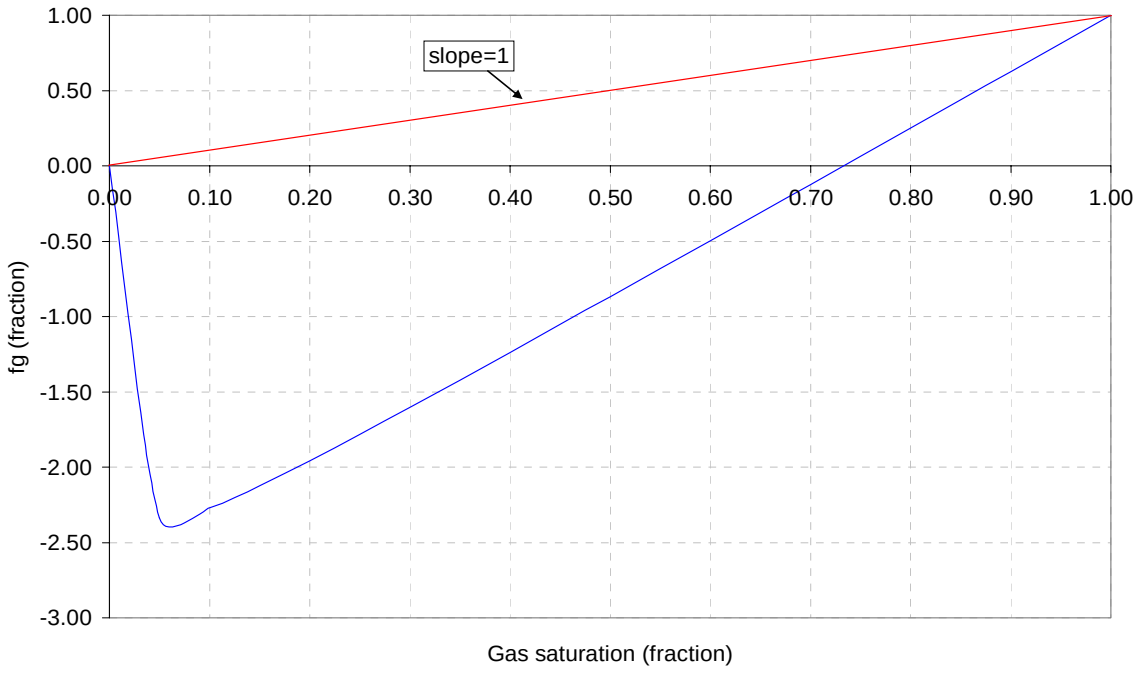

Figure 7.7 Fractional gas flow curve for the fracture system.

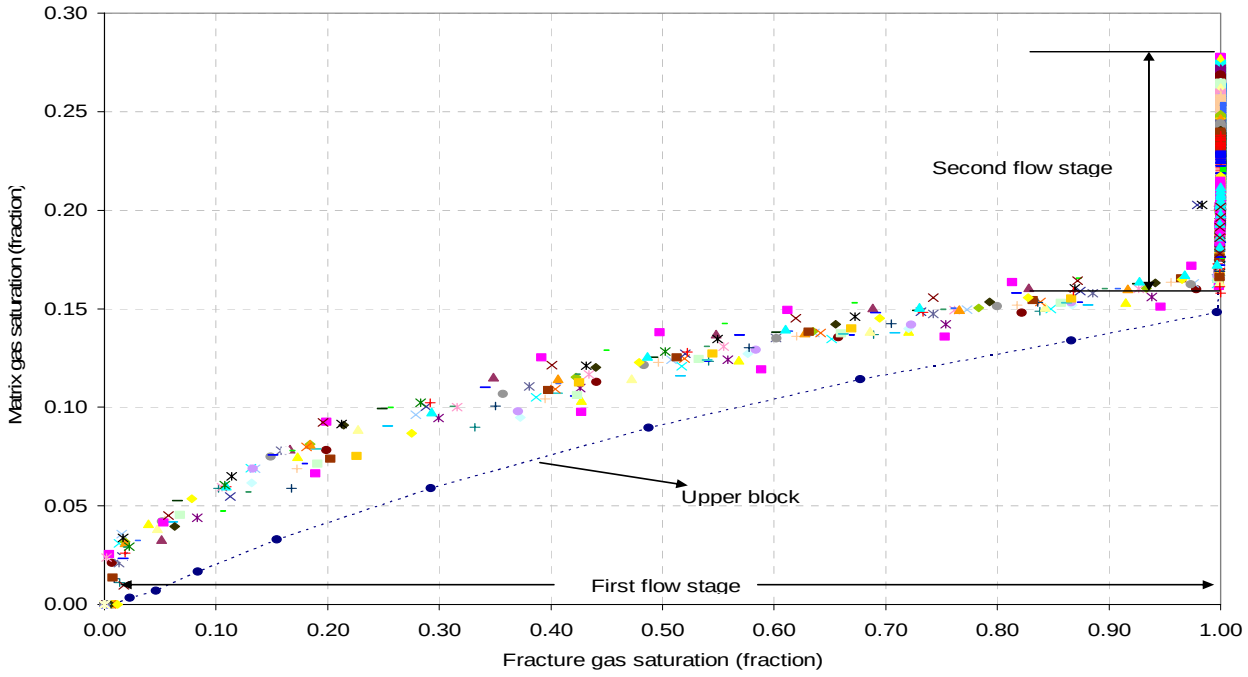

Figure 7.8 Fracture gas saturation versus matrix gas saturation for forty gridblocks up to 1000 days of nitrogen injection.

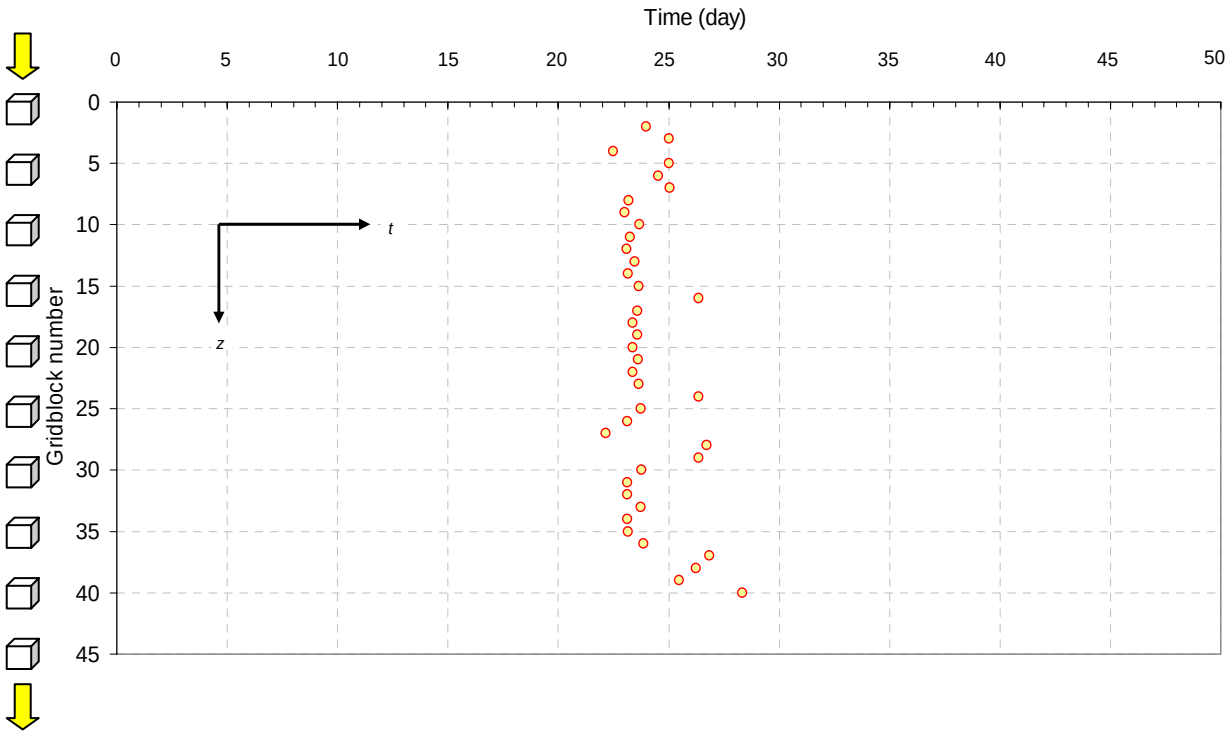

Figure 7.9 Time to reach 100% fracture gas saturation in each gridblock.

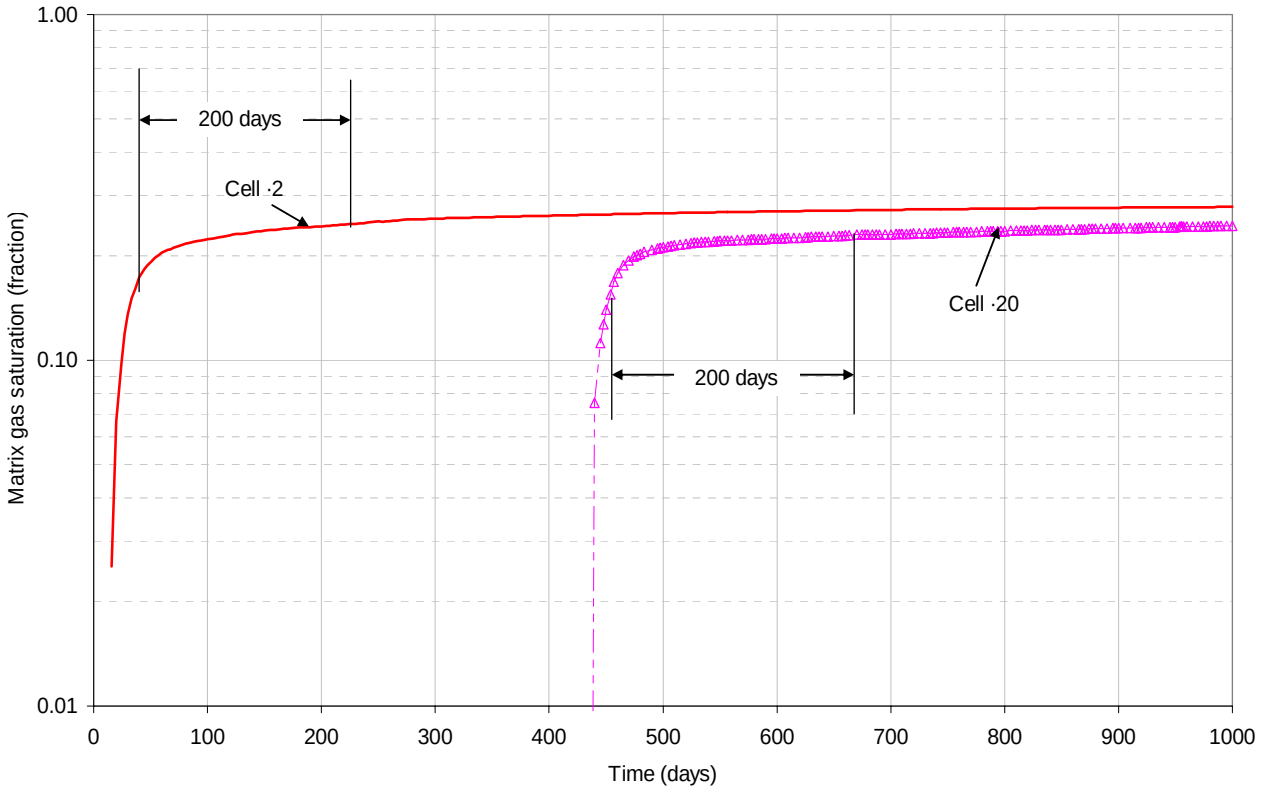

Figure 7.10 Matrix gas saturation for two gridblocks (2 and 20) versus time.

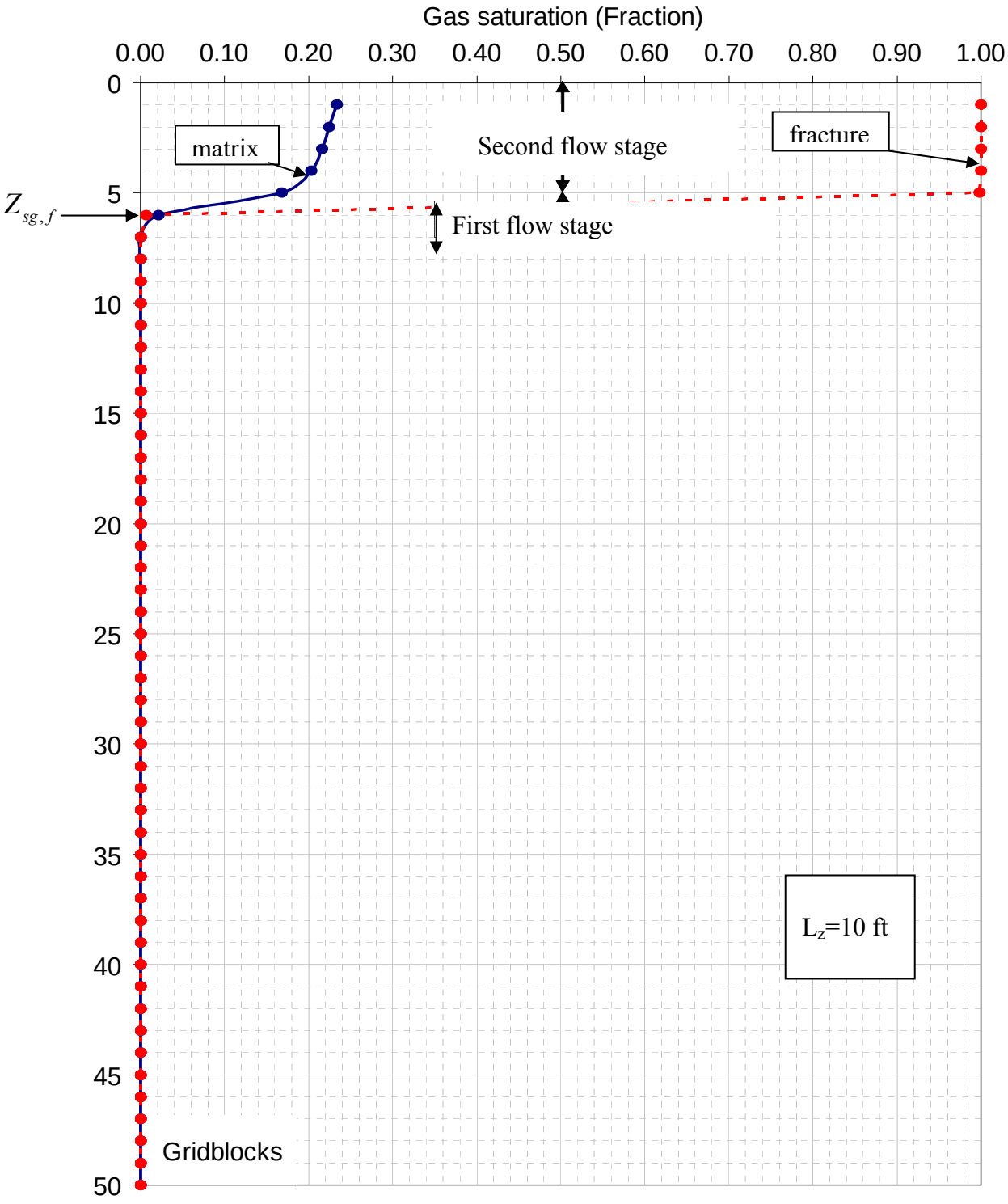

Figure 7.11 Matrix and fracture gas saturations after 100 days of nitrogen injection.

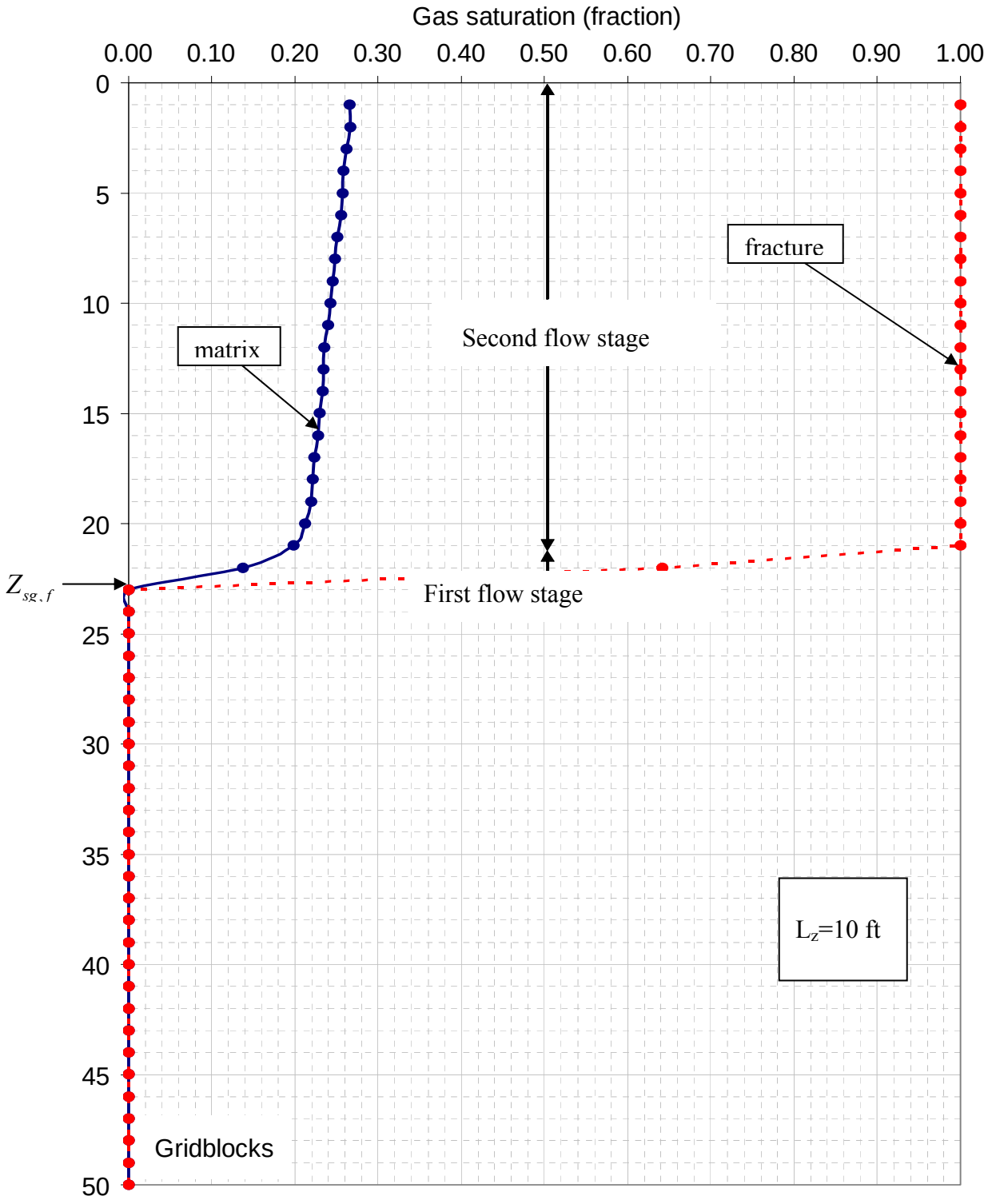

Figure 7.12 Matrix and fracture gas saturations after 500 days of nitrogen injection.

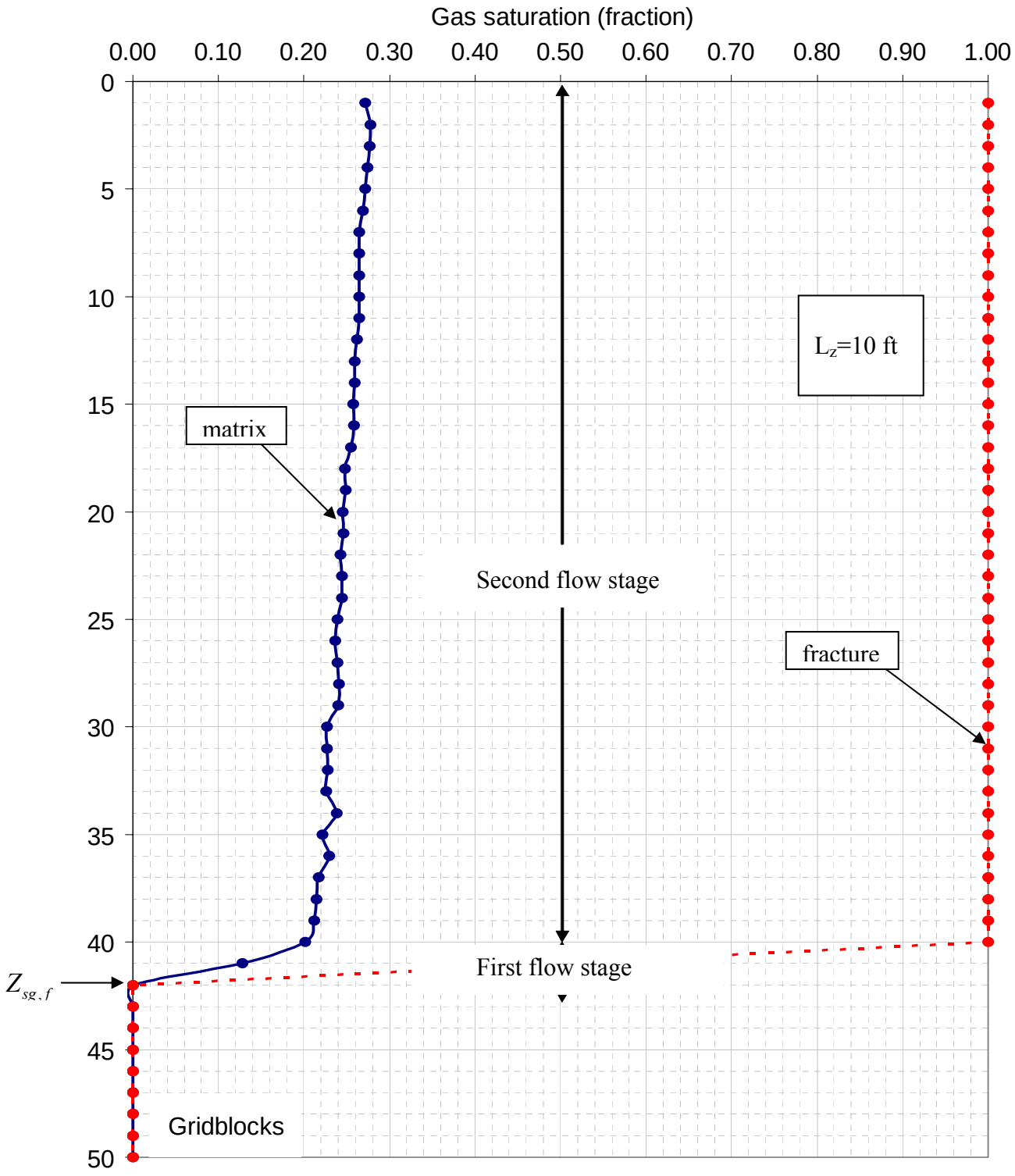

Figure 7.13 Matrix and fracture gas saturations after 1000 days of nitrogen injection.

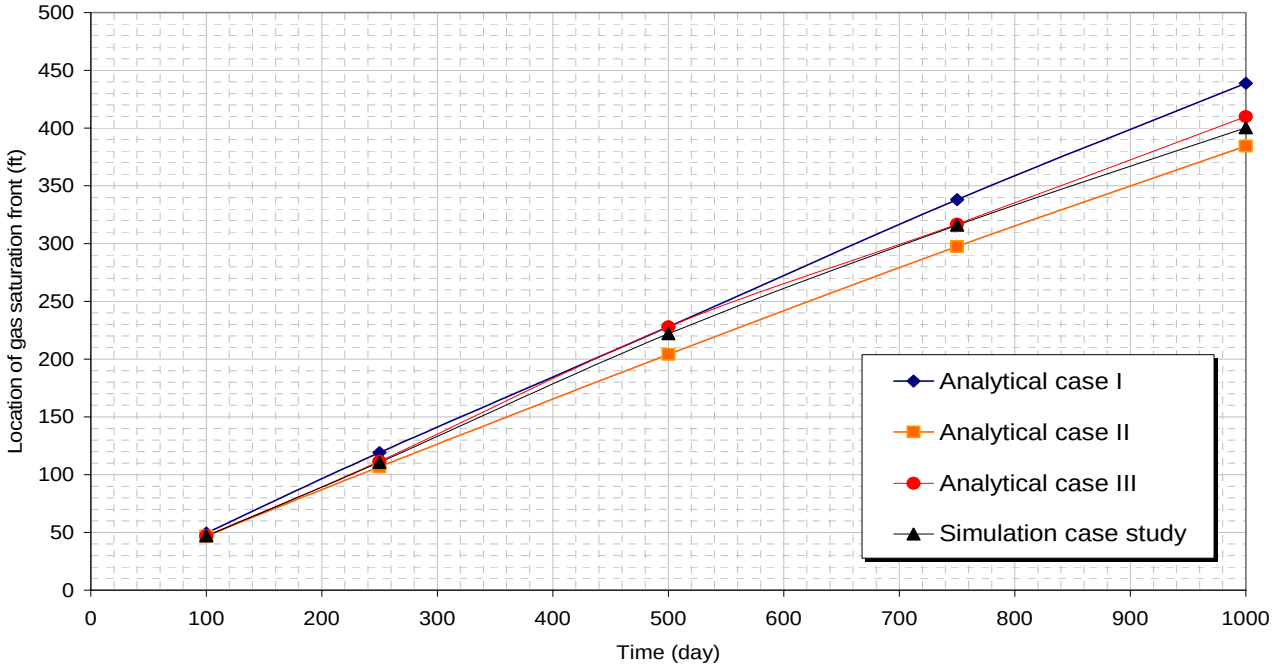

Figure 7.14 Location of gas saturation front using analytical model (cases I-III) and simulation case study.

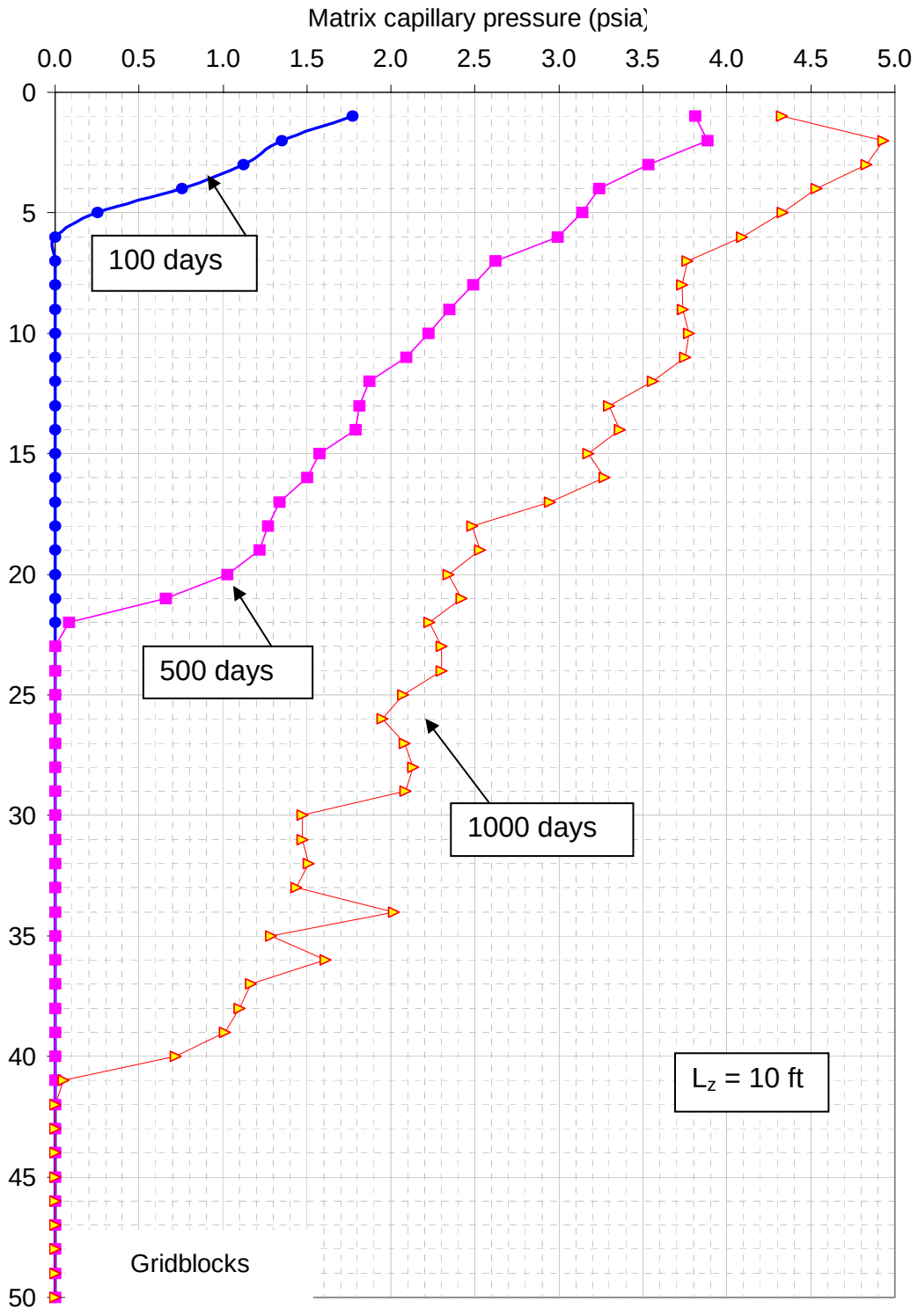

Figure 7.15 Matrix capillary pressure after nitrogen injection.

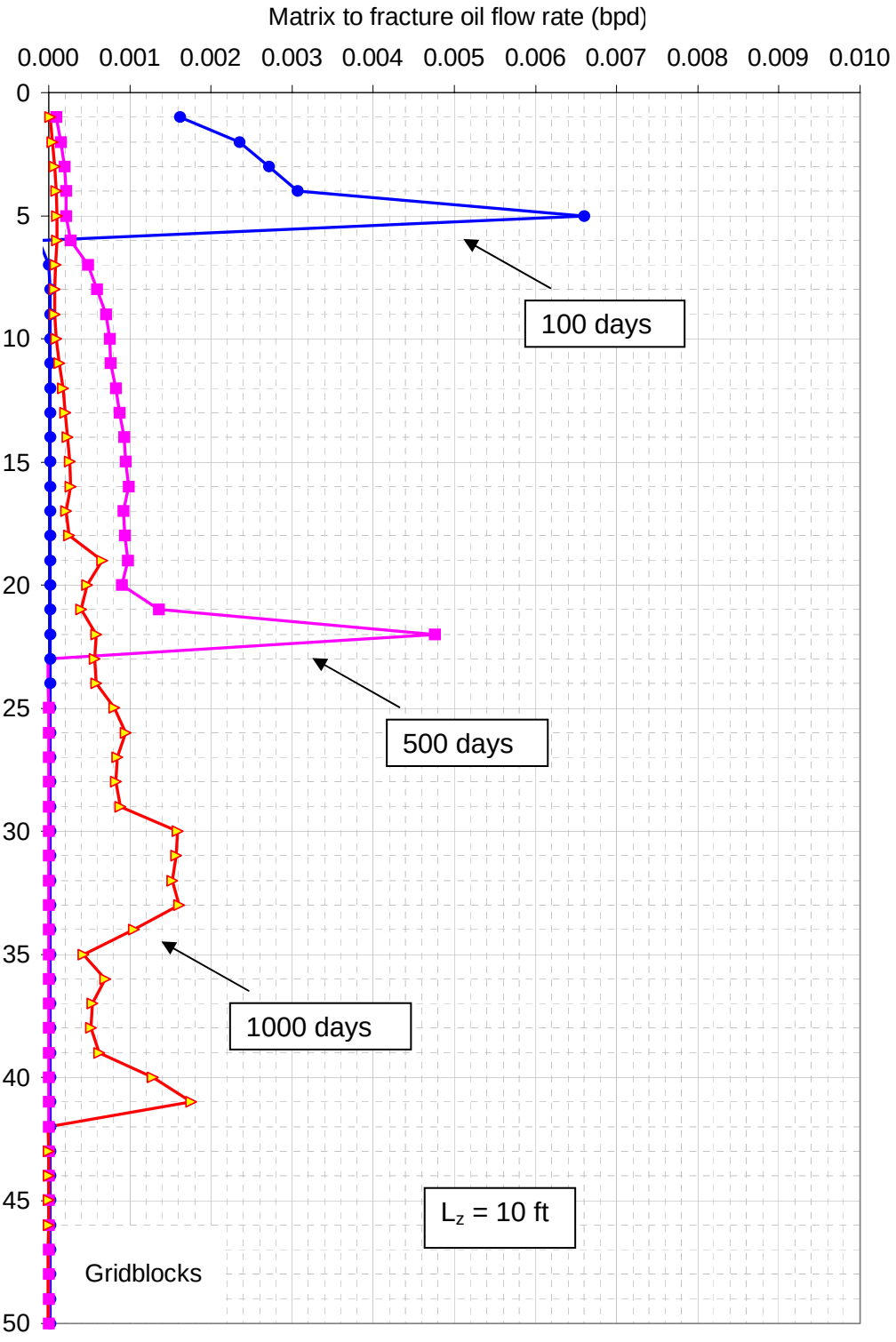

Figure 7.16 Matrix-fracture oil flow rate after nitrogen injection.

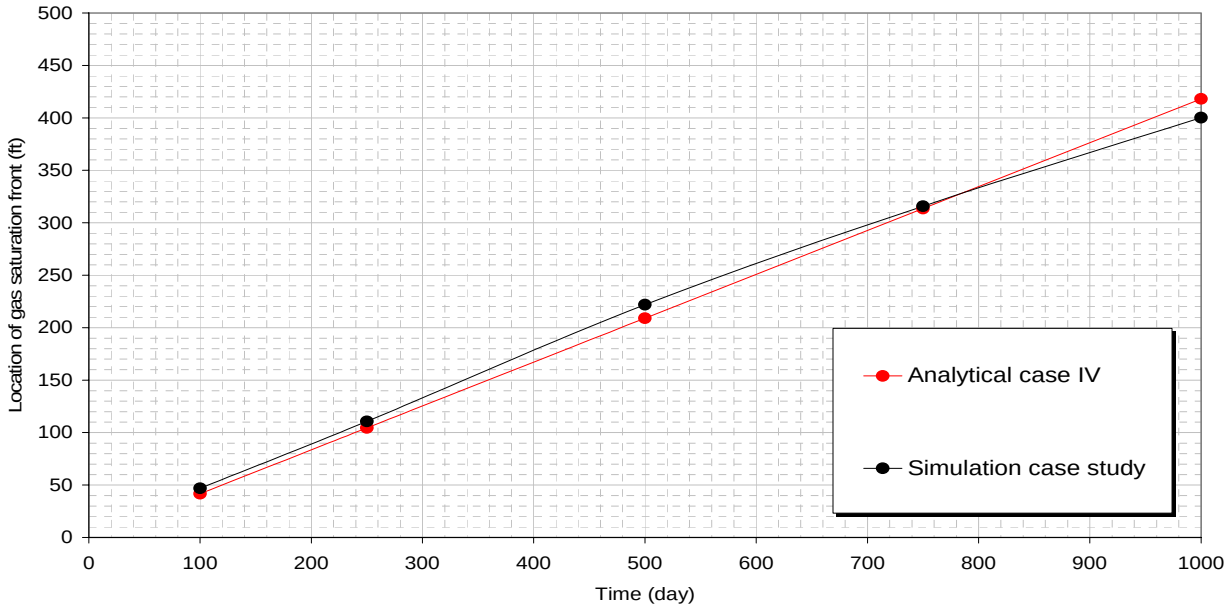

Figure 7.17 Location of gas saturation front using analytical case IV and simulation case study.

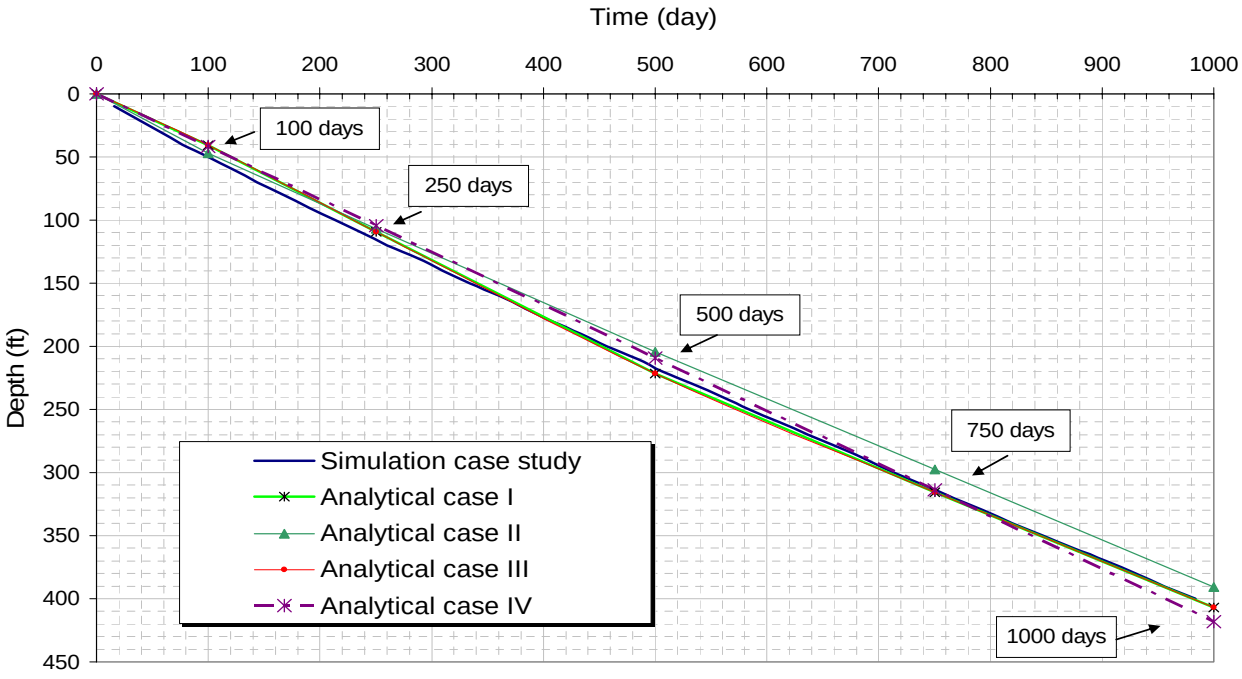

Figure 7.18 Location of gas saturation front for simulation and analytical models.

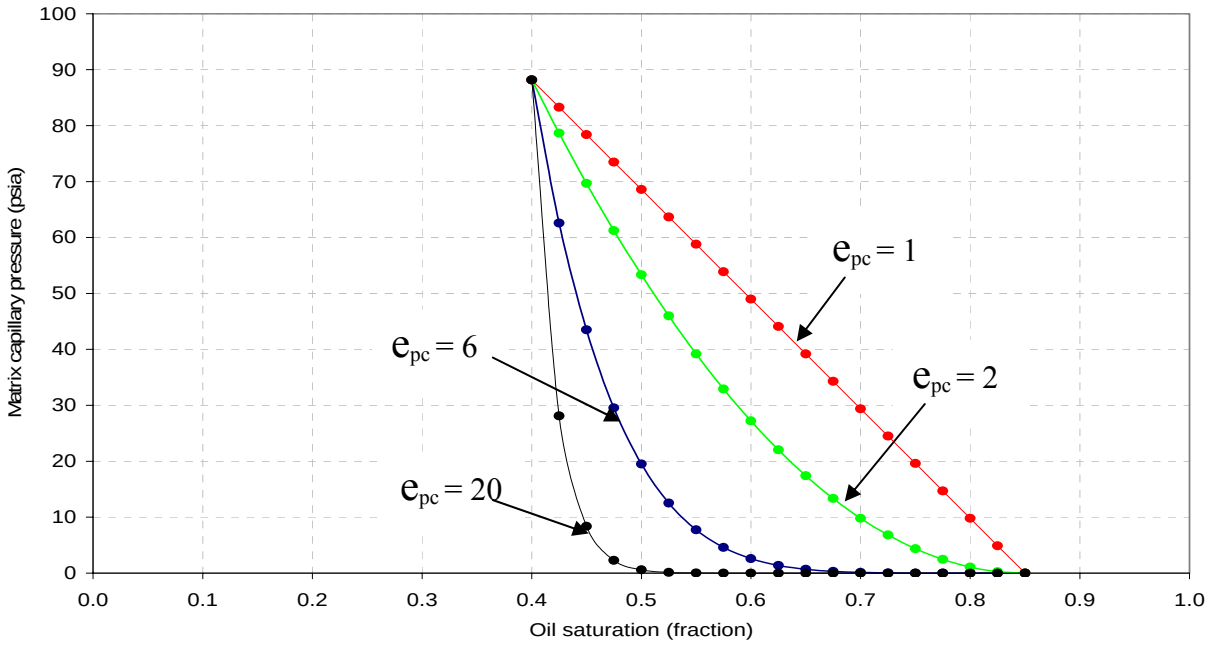

Figure 7.19 "Pseudo" matrix capillary pressure curves used for the sensitivity study.

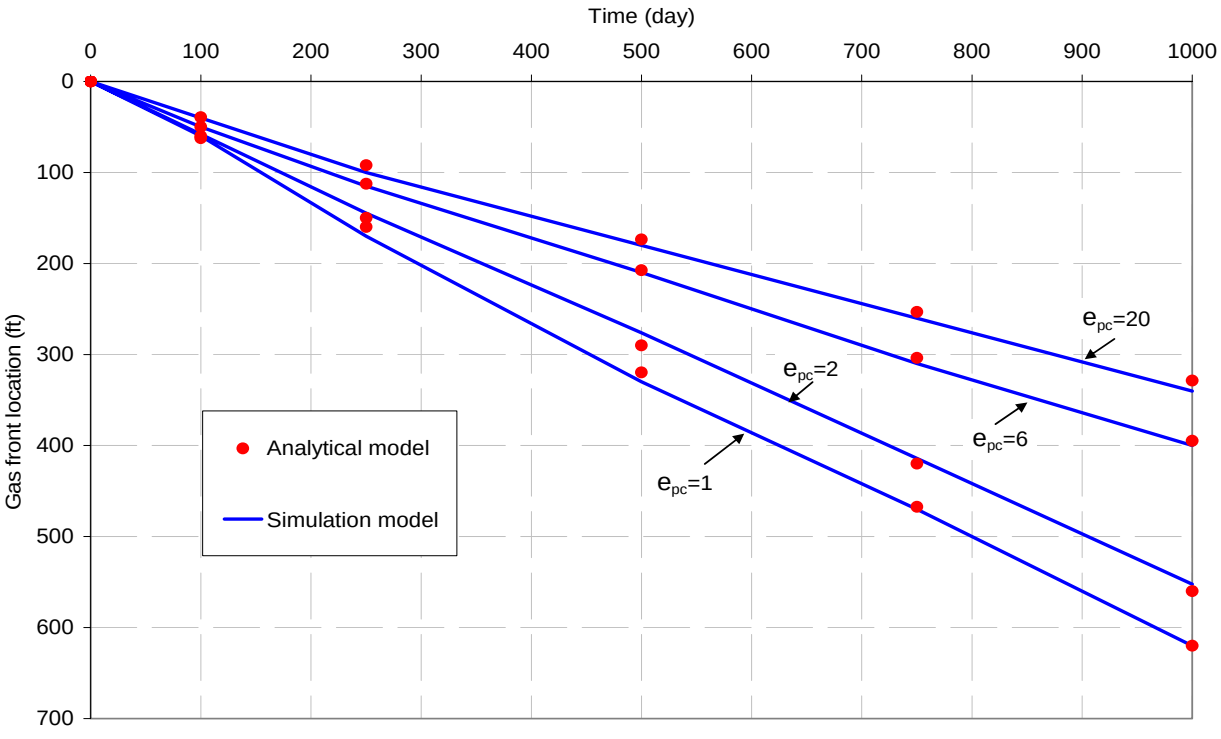

Figure 7.20 Gas front locations for the "pseudo" matrix capillary sensitivity study.

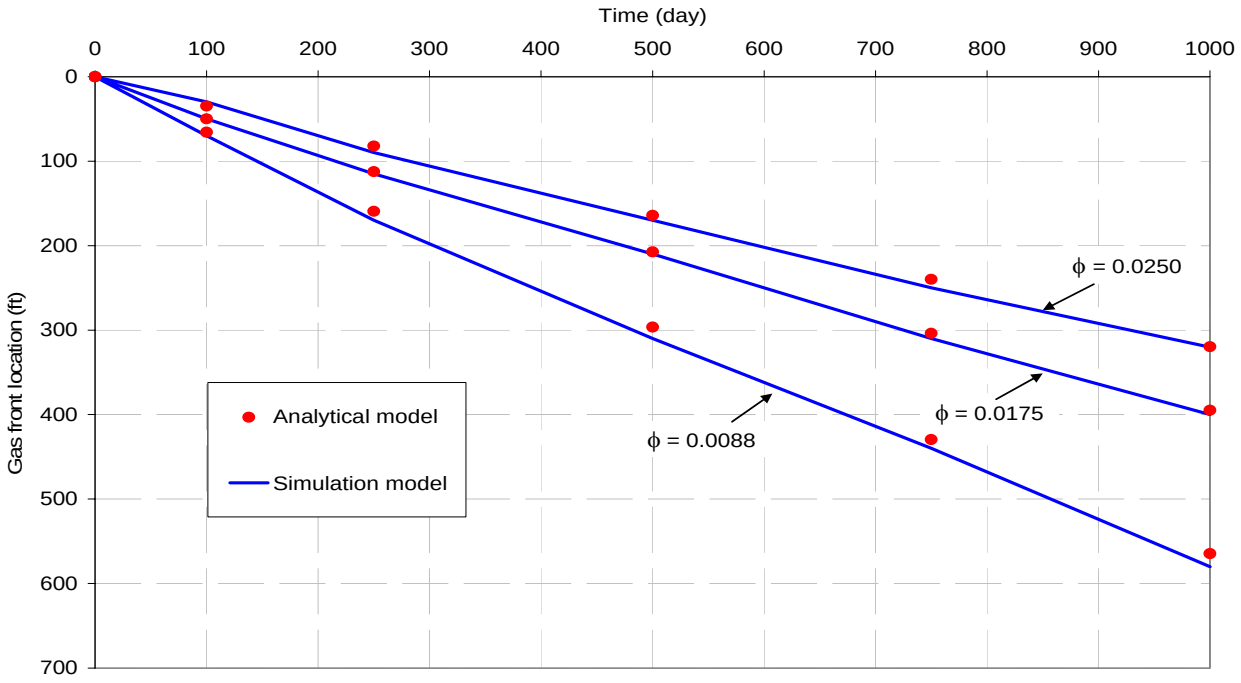

Figure 7.21 Gas front locations for fracture porosity sensitivity study.

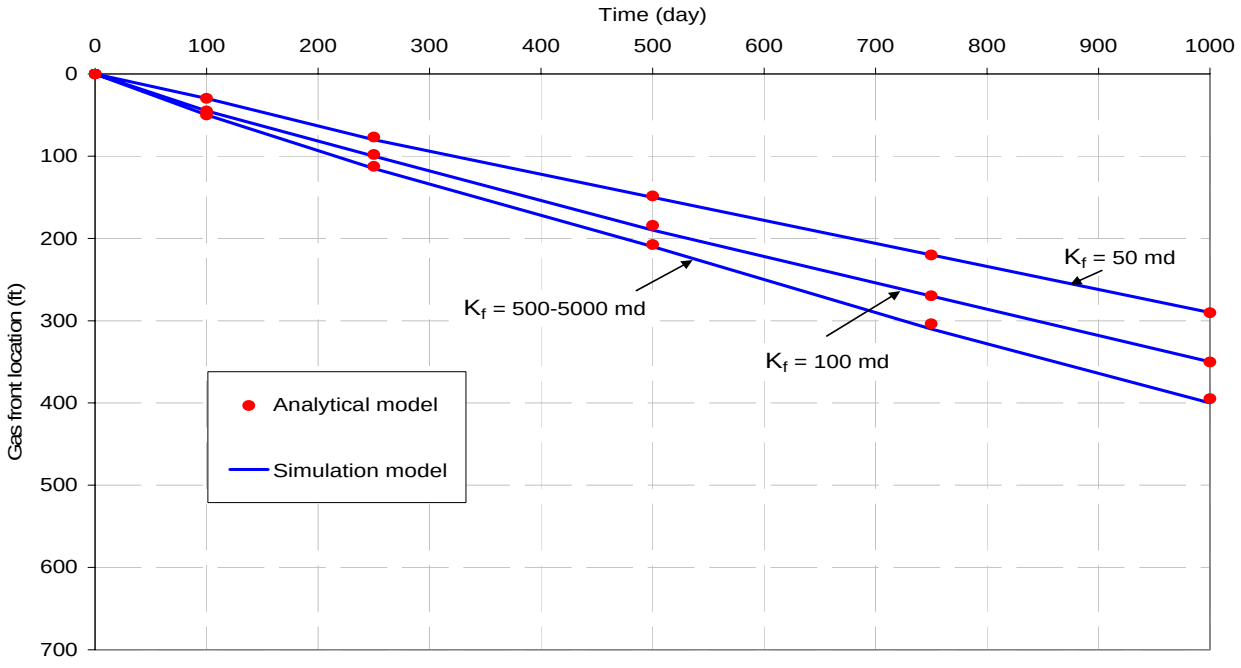

Figure 7.22 Gas front locations for fracture permeability sensitivity study.

CHAPTER 8

CONCLUSIONS AND RECOMMENDATIONS FOR FUTURE WORK

8.1 Conclusions

The following conclusions are drawn from this study:

1. When nitrogen is injected into a naturally fractured reservoir with a gas cap, we encounter two main mechanisms: gravity force in the gas cap and gravity drainage in the oil zone. The distribution of nitrogen in the gas cap (under the gravity force mechanism) depends mainly on the density difference between the nitrogen-injected and the reservoir gas. If the injected gas is less dense (i.e. methane) than the reservoir gas, then the injected gas will stay at the top of the reservoir. But in the case of nitrogen injection, since nitrogen is denser than the reservoir gas, it tends to move straight to the gas-oil contact and then spread horizontally. In this case, gravity drainage occurs with high nitrogen molar concentrations in the fracture system.

2. For the reservoir in this study, under nitrogen injection, the oil matrix drainage occurs faster than other gases (methane and reservoir gas) due to the strong impact of the gravity-force mechanism during the nitrogen injection. Higher oil production rates were also obtained for nitrogen injection due to the fact that nitrogen has more contact area, with the oil in the field, and this increases the sweep efficiency.

3. The temperature variations in the reservoir caused by injection of nitrogen at standard temperatures occur mainly in the gas cap particularly close to the injection well, while negligible temperature changes occur in the oil zone.

4. The injection of nitrogen at higher temperatures (900 ^{o}F) decreases the reservoir gas density. But since a practical point of view, the shape flow pattern at 900 ^{o}F (using a thermal compositional model) behaves similarly to the shape flow pattern at 220 ^{o}F (using an isothermal compositional model). This is mainly because variations of gas densities occur in a small zone of the reservoir.

5. Due to small variations in the reservoir properties, the simulation results for nitrogen injection into an isotropic and heterogeneous naturally fractured reservoir displayed similar behavior to the simulation of a fractured reservoir by averaging the reservoir properties.

6. Based on the sensitivity studies of different matrix block sizes and capillary continuity degrees, oil recovery is affected by a factor that ranges from 1 to 2.2 by considering fracture apertures between 10 to 300 microns, respectively. The highest oil recovery was obtained for slabs with the biggest matrix block height, and since the fracture aperture for the reservoir under study averaged 250 microns, capillarity discontinuity was a good assumption to be used for the reservoir under study.

7. Based on sensitivity studies defining a proper grid resolution for the matrix system, we concluded that, the vertical grid refinement case study using 3x3x68

gridblocks had 1.124 times higher oil recovery than the base case using 3x3x5 gridblocks. It gave us a better understanding of the necessity of using higher resolution matrix gridblocks, specifically when gravity drainage is the dominant mechanism of oil production. The matrix subgridding study indicated that gravity drainage has more impact in a vertical direction than in a horizontal direction. Therefore, matrix subgridding is especially important when we have gravity drainage as the main oil recovery mechanism.

8. We developed a simple analytical model that describes the movement of a nitrogen-injected front through a fractured system by using basic equations for fluid-flow in permeable media, such as the Buckley Leveret theory. This basic equation was applied successfully when nitrogen displaced oil during an immiscible process, under a strong gravity drainage mechanism, and when there is no water flow. Due to the importance of matrix capillary pressure, fracture porosity, and fracture permeability on the advancement of the gas front through the fractured system, we performed sensitivity studies to validate the developed analytical model.

9. The use of a conceptual model for naturally fractured reservoirs is needed to make intelligent reservoir management decisions, especially if critical performance data are unavailable. This is because a conceptual model relies on simple process evaluations, and uses average properties, either measured or estimated, to achieve an idealized representation of the reservoir. It also helps to compare the results with published analytical models in literature, which become more effective as the system decreases in complexity.

8.2 Recommendations for future work

The following are recommendations for future study:

1. Fracture characterization considering different scales for a reservoir model should be coupled with a geomechanics module to adequately reproduce the gravity drainage mechanism and movement of nitrogen through the fractured system.

2. A comparison between a discrete fracture network model and the constructed dual porosity model is strongly desirable to investigate the accuracy of the models. A comparison of results using a discrete fracture network model and the developed analytical model is also strongly recommended.

3. For more realistic simulations using the entire field and considering grid refinement takes a large amount of CPU time and memory, we may have to use a simulator that has parallel processing capability. Therefore, using a parallel reservoir simulator with compositional and dual porosity options that considers vertical matrix grid refinement under a dynamic subgridding scheme is strongly recommended, in order to automatically adjust the number of subgriddings during simulation, and also to increase the accuracy and minimize the computational time.

4. It is necessary to perform scale-up studies using the developed analytical model to adequately represent the characterization of flow models from a detailed geologic model.

5. The use of a simulator that allows changes in rock wettability during the field exploitation, the consideration of a fluid film surrounding the fractured system, and the use of a triple porosity system where vuggy porous media are separated from the fractured system should be considered.

Nomenclature

A_c	=	Acentric value (dimensionless)
A_f	=	Flow area of the fracture system, L^2
A_m	=	Matrix flow surface in contact with the fracture system, L^2
b_o	=	Mean fracture half-width, L
B_o	=	Oil volume factor (dimensionless)
d_{fm}	=	Difference in depth between fracture and matrix, L
DZ_{mat}	=	Matrix block height, L
D_x	=	*x* dimension of the gridblock, L
D_y	=	*y* dimension of the gridblock, L
e_o	=	Exponent for oil relative permeability model (dimensionless)
e_g	=	Exponent for gas relative permeability model (dimensionless)
e_{pc}	=	Exponent for oil-gas capillary pressure model (dimensionless)
$f_{g,f}$	=	Gas fractional flow in the fracture system (dimensionless)
F_g	=	Flow of gas, L^3/t
g	=	Gravitational acceleration, L/t^2
GMOB	=	Gas mobility, $(M/Lt)^{-1}$
GOC	=	Gas oil contact, (L)
h	=	Net thickness (L)
H_{wj}	=	Wellbore pressure head between the connection and well, M/Lt^2
K	=	Absolute permeability, L^2
K_f	=	Absolute fracture permeability, L^2
k_o	=	Effective oil permeability, L^2

K^o_{r1} = End point relative permeability of displacing fluid (dimensionless)

K^o_{r2} = End point relative permeability of displaced fluid (dimensionless)

k_{rg} = Gas relative permeability (dimensionless)

k^o_{rg} = End-point gas relative permeability (dimensionless)

k_{ro} = Oil relative permeability (dimensionless)

$k_{ro,f}$ = Fracture oil relative permeability (dimensionless)

k^o_{ro} = End-point oil relative permeability, (dimensionless)

K_x = x directional absolute permeability, L^2

K_y = y directional absolute permeability, L^2

L_x = Matrix block size in x direction, (L)

L_y = Matrix block size in y direction, (L)

L_z = Matrix block size in z direction, (L)

$M_{p,j}$ = Phase mobility at the connection, $(M/Lt)^{-1}$

P_c = Capillary pressure, M/Lt^2

$P_{c,m}$ = Matrix capillary pressure, M/Lt^2

P_{cf} = Capillary pressure in the fracture system, M/Lt^2

P^o_c = End-point capillary pressure, M/Lt^2

P_{cogf} = Oil-gas capillary pressure in fracture, M/Lt^2

P_{cogm} = Oil-gas capillary pressure in matrix, M/Lt^2

P_j = Nodal pressure in the grid block containing the connection, M/Lt^2

P_{of} = Oil phase pressure in fracture, M/Lt^2

P_{om} = Oil phase pressure in matrix, M/Lt^2

P_w = Bottomhole pressure of the well, M/Lt^2

$q_{g,f}$ = Volumetric gas rate through fracture system at r.c., L^3/t

$q_{g,f-m}$ = Volumetric gas rate through fracture to matrix at r.c., L^3/t

$q_{o,f}$ = Volumetric oil production rate at s.c., L^3/t

$q_{p,j}$ = Volumetric phase production rate at s.c. for j cell, L^3/t

r_i = Pore radius, L

r_{mt} = Rate of mass transfer between matrix and fracture systems, L^3/tL^2L

r_o = Pressure equivalent radius, L

r_w = Wellbore radius, L

r_1 = Radio of curvature, L

s = Skin factor (dimensionless)

$S_{g,f}$ = Fracture gas saturation (dimensionless)

$S_{g,m}$ = Matrix gas saturation (dimensionless)

$\overline{S_{g,m}}$ = Average matrix gas saturation (dimensionless)

S_{nw} = Saturation of no wetting phase (dimensionless)

S_o = Oil saturation (dimensionless)

S_{or} = Residual oil saturation (dimensionless)

S_{wi} = Initial water saturation (dimensionless)

t = Time (t)

T = Temperature (T)

TR = Transmissibility (L^3)

T_{wj} = Connection transmissibility factor (L^3)

u_f = Volumetric gas flux (L^3/tL^2)

$V_{g,m}$ = Cumulative gas volume flowed from fracture into matrix, L^3

w = Fracture aperture, L

x_i = Liquid composition (dimensionless)

X_g = Partial of mobile gas in matrix (dimensionless)

X_G = Partial of mobile gas in fracture (dimensionless)

y_i	=	Gas composition (dimensionless)
z	=	Gas deviation factor (dimensionless)
$Z_{sg,f}$	=	Location of gas saturation front in the fracture system, L

Greek Symbols

α	=	Inclination angle (degrees)
$\alpha(r_i)$	=	Pore size probability density function, L^{-1}
β	=	Thermal expansion coefficient, T^{-1}
ϕ_f	=	Fracture porosity (dimensionless)
ϕ_m	=	Matrix porosity (dimensionless)
γ	=	Specific gravity (dimensionless)
μ	=	Viscosity (M/tL)
μ_1	=	Displaced fluid viscosity (M/tL)
μ_2	=	Displacing fluid viscosity (M/tL)
μ_g	=	Gas viscosity (M/tL)
θ	=	Angle of the segment connecting with the well (xxx)
ρ	=	Density, M/L^3
ρ_1	=	Displacing fluid density, M/L^3
ρ_2	=	Displaced fluid density, M/L^3
σ_{go}	=	Sigma, L^{-2}
σ_{go}	=	Interfacial tension, M/t^2

APPENDIX A

ANALYTICAL MODEL FOR NITROGEN INJECTION FRONT USING AN OVERALL (WEAK FORM) MATERIAL BALANCE

The overall (weak form) material balance, considering that only gas is injected in a stack simulation model illustrated in Figure 7.5, can be expressed as

(Gas rate IN at the top of reservoir) – (Gas rate OUT down to the gas-oil contact) = Accumulation term

$$(q_{g,f}+q_{g,m})_{\xi=0}-(q_{g,f}+q_{g,m})_{\xi=Z_{sg,f}}=\frac{d}{dt}\left[\int_{\xi=0}^{\xi=Z_{sg,f}}(\phi_f S_{g,f}A_f+\phi_m S_{g,m}A_m)d\xi\right]$$

This equation presumes that densities are constant because it is applied in a pressure maintenance project. Since only the gas is injected in the fracture system and there is no gas below the gas front, this becomes

$$q_{g,f}=\frac{d}{dt}\left[\int_{\xi=0}^{\xi=Z_{sg,f}}(\phi_f S_{g,f}A_f+\phi_m S_{g,m}A_m)d\xi\right]$$

By performing algebra

$$q_{g,f}=\frac{d}{dt}\left[Z_{sg,f}\frac{1}{Z_{sg,f}}\int_{\xi=0}^{\xi=Z_{sg,f}}(\phi_f S_{g,f}A_f+\phi_m S_{g,m}A_m)d\xi\right]$$

$q_{g,f}=\frac{d}{dt}\left[Z_{sg,f}(\phi_f\overline{S_{g,f}}A_f+\phi_m\overline{S_{g,m}}A_m)\right]$, where $\left[\overline{S_{g,f}}\right]$ and $\left[\overline{S_{g,m}}\right]$ are the averaged saturations behind the front.

Since $q_{g,f}$ is constant at reservoir conditions and is equivalent to q_oB_o, this becomes

$$q_oB_o=\frac{d}{dt}\left[Z_{sg,f}(\phi_f\overline{S_{g,f}}A_f+\phi_m\overline{S_{g,m}}A_m)\right]$$

Rearranging terms and performing integration, it becomes

$$q_o B_o \int_0^t dt = \left[Z_{sg,f} (\phi_f \overline{S_{g,f}} A_f + \phi_m \overline{S_{g,m}} A_m) \right]$$

where

$$Z_{sg,f} = \frac{q_o B_o t}{(\phi_f \overline{S_{g,f}} A_f + \phi_m \overline{S_{g,m}} A_m)}$$

Since averaged gas saturation in the fracture system behind the front, $\overline{S_{g,f}} \approx 1$, this final expression is the same as equation 7.21.

References

Aguilera, R.: "Recovery Factors and Reserves in Naturally Fractured Reservoirs," *Journal of Canadian Petroleum Technology* (Jul. 1999) **38**, No.7, 15-18.

Aguilera, R.: "Relative Permeability Concepts for Predicting the Performance of Naturally Fractured Reservoirs," *Journal of Canadian Petroleum Technology* (Sept. 1982) 36, 41-48.

Al-Qahtani, M. and Z. Rahim: "A Mathematical Algorithm for Modeling Geomechanical Rock Properties of the Khuff and Pre-Khuff Reservoirs in Ghawar Field," paper SPE 68194 presented at the 2001 SPE Middle East Oil Show held in Bahrain (Mar. 17-20, 2001).

Araktingi, U. G. and W. M. Bashore: "Effects of Properties in Seismic Data on Reservoir Characterization and Consequent Fluid-Flow Predictions when Integrated with Well Logs," paper SPE 24752 presented at the 67th Annual Technical Conference and Exhibition of the SPE held in Washington, DC (Oct. 4-7, 1992).

Arango, S., E. A. Idrobo and H. H. Perez: "A New Methodology to Estimate Fracture Intensity Index for Naturally Fractured Reservoirs," paper SPE 86935 presented at the SPE International Thermal Operations and Heavy Oil Symposium and Western Regional Meeting held in Bakersfield, CA (Mar. 16-18, 2004).

Arevalo, J. A., F. Samaniego, F. Lopez and E. Urquieta: "On the Exploitation Conditions of the Akal Reservoir Considering Gas Cap Nitrogen Injection," paper SPE 35319 presented at the International Petroleum Conference and Exhibition of Mexico held in Villahermosa, Mexico (Mar. 5-7, 1996).

Barkve, T. and A. Firoozabadi: "Analysis of Reinfiltration in Fractured Porous Media," paper SPE 24900 presented at the 67th SPE Annual Technical Conference and Exhibition held in Washington, DC (Oct. 4-7, 1992).

Beckner, B. L., H. M. Chan, A. McDonald and T. Jones: "Simulating Naturally Fractured Reservoirs Using a Subdomain Method," paper SPE 21241 presented at the SPE symposium on Reservoir Simulation held in Anaheim, CA (Feb. 17-20, 1991).

Bratton, T., D. Canh, N. Duc, P. Gillespie, D. Hunt, B. Li, R. Marcinew, B. Montaron, R. Nelson, D. Schoderbek and L. Sonneland: "The Nature of Naturally Fractured Reservoirs," *Oilfield Review* (Summer 2006) 4-23.

Carlyle, J.: "Latent heat of vaporization of Nitrogen," Physics Class 210, Lab Section B. University of Illinois (1998).

Christian, L. D., J. A. Shirer, E. L. Kimbel and R. J. Blackwell: "Planning a Tertiary Oil-Recovery Project for Jay/LEC Fields Unit," paper SPE 9805 presented at the SPE/DOE Symposium on Improved Oil Recovery held in Tulsa OK (Apr. 5-8, 1981).

Clancy, J. P., R. E. Gilchrist, L. H. K. Cheng and D. R. Bywater: "Analysis of Nitrogen-Injection Projects to Develop Screening Guides and Offshore Design Criteria," paper SPE 11902 presented at the SPE 1982 Offshore European Conference held in Aberdeen, UK (Sep. 6-9, 1982).

Clauser, C. and E. Huenges: *Thermal conductivity of rocks and minerals*. Copyright by American Geophysical Union (1995).

Coats, K. H.: "An Equation of State Compositional Model," *Soc. Pet. Eng. J.* (Oct. 1980) 8284, 363-376.

Daltaban, T. S., A. Noyola, G. Trejo and R. Toledo: "An Investigation Into the Technical Feasibility of Gas Injection Into Fractured CHUC Reservoir in the Gulf of Mexico," paper SPE 74357 presented at the International Petroleum Conference and Exhibition in Mexico held in Villahermosa, Mexico (Feb. 10-12, 2002).

Daly, C. and D. Mueller: "Characterization and Modeling of Fractured Reservoirs: Static Model," proceedings of the. 9th European Conference on the Mathematics of Oil Recovery in Cannes, France (Aug. 30 - Sep. 2, 2004).

Dean, R. H. and L. L. Lo: "Simulation of Naturally Fractured Reservoirs," paper SPE 14110 presented at the 1986 SPE International Meeting on Petroleum Engineering held in Beijing, China (Mar. 17-20, 1986).

De la Porte, J. J., C. A. Kossack and R. W. Zimmerman: "The Effect of Fracture Relative Permeabilities and Capillary Pressures on the Numerical Simulation of Naturally Fractured Reservoirs," paper SPE 95241 presented at the 2005 SPE Annual Technical Conference and Exhibition held in Dallas, TX (Oct. 9-12, 2005).

Firoozabadi, A. and K. Aziz: "Analysis and Correlation of Nitrogen and Lean-Gas Miscibility Pressure," *SPE Reser. Eng.* (Nov. 1986) 575.

Firoozabadi, A. and J. Hauge: "Capillary Pressure in Fractured Porous Media," paper SPE 18747 presented at the 1989 SPE Regional Meeting held in Bakersfield, CA (Apr. 5-7, 1989).

Firoozabadi, A. and L. K. Thomas: "Sixth SPE Comparative Solution Project: Dual-Porosity Simulators," *J. Pet. Tech*. (June, 1990) 18741, Vol. 42, 710-715.

Firoozabadi, A.: "Some Recovery Issues of Immiscible and Miscible Gas-Oil Flow in Fractured Reservoirs: Laboratory Data and Theoretical Analysis," special publication of the Technology Research Center presented at the JNOC-TRC International Symposium on Carbonate Rocks-Hydrocarbon Exploration and Reservoir Characterization, Chiba, Japan (Mar. 1-5, 1993).

Galarraga, M. and B. Hansen: "Detailed 3D Seismic Interpretation Using HFI Seismic Data, Fault Throw, and Stress Analysis for Fault Reactivation in the Cogollo Group, Lower Cretaceous, Urdaneta West Field, Maracaibo Basin," paper SPE 95060 presented at the 2005 SPE Latin American and Caribbean Petroleum Engineering Conference held in Rio de Janeiro, Brazil (Jun. 20-23, 2005).

Gilman, J. R., J. L. Bowzer and B. W. Rothkopf: "Application of Short-Radius Horizontal Boreholes in the Naturally Fractured Yates Field," paper SPE 28568 presented at the 69th SPE Annual Technical Conference and Exhibition, New Orleans, LA (Sept. 25-28, 1994).

Gilman, J. R. and H. Kazemi: "Improvements in Simulation of Naturally Fractured Reservoirs," paper SPE 10511 presented at the 1982 SPE Reservoir Simulation Symposium held in New Orleans, LA (Jan. 31–Feb. 3, 1982).

Greenwalt, W. A., S. Vela, L. D. Chistian and J. A. Shirer: "A Field Test of Nitrogen WAG Injectivity," *J. Pet Tech.* (1982) 266-272.

Gurpinar, O., J. Kalbus and D. F. List: "Numerical Modeling of a Large Naturally Fractured Oil Complex," paper SPE 59061 presented at the 2000 SPE International Petroleum Conference and Exhibition in Mexico held in Villahermosa, Mexico (Feb. 1-3, 2000).

Han, C., M. Delshad, K. Sepehrnoori and G. A. Pope: "A Fully Implicit, Parallel, Compositional Chemical Flooding Simulator," paper SPE 97217 presented at the 2005 SPE Annual Technical Conference and Exhibition held in Dallas, TX (Oct. 9-12, 2005).

Horie, T., A. Firoozabadi, and K. Ishimoto: "Laboratory Studies of Capillary Interaction in Fracture/Matrix Systems," paper SPE 18282 presented at the 63rd SPE Annual Technical Conference and Exhibition held in Houston, TX (Oct. 2-5, 1990).

Jensen, J.: *Statistics for Petroleum Engineers and Geoscientists*, Prentice Hall Petroleum Engineering Series, Upper Saddle River, NJ (1997).

Kazemi, H., J. R. Merrill and K. L. Porterfield: "Numerical Simulation of Water-Oil in Naturally Fractured Reservoirs," paper SPE 6890 presented at the SPE-AIME 52nd Annual Fall Technical Conference and Exhibition held in Denver, CO (Oct. 9-12, 1977).

Labastie, A. and E. Aquitaine: "Capillary Continuity between Blocks of a Fractured Reservoir," paper SPE 20515 presented at the 65th SPE Annual Technical Conference and Exhibition held in New Orleans, LA (Sept. 23-26, 1990).

Lake, L. W.: *Enhanced Oil Recovery*, Prentice Hall, Englewood Cliffs, NJ (1989).

Lake, L. W.: "Using Simulation Models to Predict Uncertainty," Presentation gave on a SPE Distinguished Lecture at The Michigan Basin Geological Society held in Lansing, MI (Jan. 8th, 2003).

Lawrence, J. J., N. K. Maer, D. Stern, L. W. Corwin and W. K. Idol: "Jay Nitrogen Tertiary Recovery Study: Managing a Mature Field," paper SPE 78527 presented at the 10th Abu Dhabi International Petroleum Exhibition and Conference held in Abu Dhabi, United Arab Emirates (Oct. 13-16, 2002).

Limon-Hernandez, T., G. De-la-Fuente, G. Garza-Ponce and M. Monroy-Hernandez: "Overview of the Cantarell Field Development Program," paper OTC 10860 presented at the 1999 Offshore Technology Conference held in Houston, TX (May 3-6, 1999).

Limon-Hernandez, T. and G. Garza-Ponce: "Status of the Cantarell Field Development Program: An Overview," paper OTC 13175 presented at the 2001 Offshore Technology Conference held in Houston, TX (Apr. 30-May 3, 2001).

Lisle, R. J.: "Detection of Zones of Abnormal Strain in Structures Using Gaussian Curvature," *AAPG* (Dec. 1994) 78, 12, 1811-1819.

Litvak, B. L., A. Satter and S. Etebar: "An Analysis of Naturally Fractured Reservoir Performance Using a Novel Fractured Reservoir Simulation," paper SPE 17615 presented at the SPE International Meeting on Petroleum Engineering, held in Tianjin, China (Nov. 1-4, 1988).

Manceau, E., E. Delamaide, J. C. Sabathier, S. Jullian, F. Kalaydjian, J. E. Ladron de Guevara, J. M. Sanchez Bujanos and F. D. Rodriguez: "Implementing Convection in a Reservoir Simulator: A Key Feature in Adequately Modeling the Exploitation of the Cantarell Complex," paper SPE 59044 presented at the 2000 SPE International Conference and Exhibition in Mexico, Villahermosa, Mexico (Feb. 1-3, 2000).

Manrique, E. J., V. E. Muci and M. E. Gurfinkel: "EOR Field Experiences in Carbonate Reservoirs in the United States," paper SPE 100069 presented at the SPE/DOE Symposium on Improved Oil Recovery held in Tulsa OK (Apr. 22-26, 2006).

Marcondes, F., C. Han, and K. Sepehrnoori: "Implementation of Corner Point Mesh Into a Parallel, Fully Implicit, Equation of State Compositional Reservoir Simulator,"

paper presented at the 18th International Congress of Mechanical Engineering, Ouro Preto, MG (Nov. 6-11, 2005).

McCain, W. D. Jr.: *The Properties of Petroleum Fluids* Second Edition. PennWell Publishing Company (1998).

Miguel, N., M. A. Miller and K. Sepehrnoori: "Scaling Parameters for Characterizing Gravity Drainage in Naturally Fractured Reservoirs," paper SPE 89990 presented at the 2004 SPE International Petroleum Conference held in Puebla, Mexico (Nov. 8-9, 2004).

Naimi-Tajdar, R., C. Han, K. Sepehrnoori, T. J. Arbogast, and M. A. Miller: "A Fully Implicit, Compositional, Parallel Simulator for IOR Processes in Fractured Reservoirs," paper SPE 100079 presented at the SPE/DOE Symposium on Improved Oil Recovery held in Tulsa OK (Apr. 22-26, 2006).

Naimi-Tajdar, R.: "Development and Implementation of a Naturally Fractured Reservoir Model into a Fully Implicit, Equation-of-State Compositional, Parallel Simulator," PhD. dissertation, University of Texas, Austin (Aug. 2005).

National Institute of Standards and Technology, NIST: *Nitrogen 1-4*. Copyright by the U.S. Secretary of Commerce on behalf of the U.S.A. Chemistry Web Book. (Mar. 2003).

Nelson, R. A.: *Geologic Analysis of Naturally Fractured Reservoirs*, Second Edition, Gulf Publishing Company, Houston, TX (2001).

Parsons, R. W.: "Permeability of Idealized Fractured Rock," *Soc. Pet. Eng. J.* (1966) 1289, 126-136.

PEMEX, personal communication. PEMEX Exploracion y Produccion. Proyecto Cantarell. (2004).

Peters, E.: "Advanced Petrophysics," PGE 381L Course Supplement, University of Texas at Austin (2004).

Ponting, D.: "Characterization and Modeling of Fractured Reservoirs: Flow Simulation," Proceedings of the 9th European Conference on the Mathematics of Oil Recovery held in Cannes, France (Aug. 30-Sept. 2, 2004).

Prats, M.: *Thermal Recovery*, Monograph Series, Society of Petroleum Engineers, Vol. 7. New York, NY (1986).

Pruess, K. and T. N. Narasimhan: "A Practical Method for Modeling Fluid and Heat Flow in Fractured Porous Media," paper SPE 10509 presented at the 1982 SPE Reservoir Simulation Symposium held in New Orleans, LO (Jan. 31-Feb 3, 2002).

Qasem, F. H. and I. Ershaghi: "Optimizing Gas Injection into Naturally Fractured Reservoirs," paper SPE 26979 presented at the III Latin American/Caribbean Petroleum Engineering Conference held in Buenos Aires, Argentina (Apr. 27-29, 1994).

Rangel-German, E., S. Akin and L. Castanier: "Experimental and Theoretical Investigation of Multiphase Flow in Fractured Media," Internal Report at the Petroleum Engineering Department, Stanford University (1998).

Rivas-Gomez, S., J. Cruz-Hernandez, J. A. Gonzalez-Guevara and A. Pineda-Muñoz: "Block Size and Fracture Permeability in Naturally Fractured Reservoirs," paper SPE 78502 presented at the 10th Abu Dhabi International Petroleum Exhibition and Conference held in Abu Dhabi, United Arab Emirates (Oct. 13-16, 2002).

Rodriguez, F., G. Ortega and J. L. Sanchez: "Reservoir Management Issues in Cantarell Nitrogen Injection Project," paper OTC 13178 presented at the 2001 Offshore Technology Conference held in Houston, TX (Apr 30-May 3, 2001).

Rodriguez, F., J. L. Sanchez and A. Galindo-Nava: "Mechanisms and Main Parameters Affecting Nitrogen Distribution in the Gas Cap of the Supergiant Akal Reservoir in the Cantarell Complex," paper SPE 90288 presented at the SPE Annual Technical Conference and Exhibition held in Houston, TX (Sept. 26-29, 2004).

Rossen, R. H. and E. I. C. Shen: "Simulation of Gas/Oil Drainage and Water/Oil Imbibition in Naturally Fractured Reservoirs," paper SPE 16982 presented at the 1987 SPE Annual Technical Conference and Exhibition held in Dallas, TX (Sept. 27-30, 1987).

Rossen, W. R., Y. Gu and L. W. Lake: "Connectivity and Permeability in Fracture Networks Obeying Power-Law Statistics," paper SPE 59720 presented at the SPE Permian Basin Oil and Gas Recovery Conference held in Midland, TX (Mar. 21-23, 2000).

Rossen, W. R., A. and T. A. Kumar: "Single and Two-Phase Flow in Natural Fractures," paper SPE 24915 presented at the 67th Annual Technical Conference and Exhibition of the SPE held in Washington, DC (Oct. 4-7, 1992).

Saidi, A. M. and S. Sakthikumar: "Gas Gravity Drainage under Secondary and Tertiary Conditions in Fractured Reservoirs," paper SPE 25614 presented for presentation at the SPE Program Committee. (1993).

Saidi, A. M.: *Reservoir Engineering Of Fractured Reservoir*, Total Edition Press, Paris (1987).

Saidi, A. M.: "Simulation of Naturally Fractured Reservoirs," paper SPE 12270 presented at the Reservoir Simulation Symposium held in San Francisco, CA (Nov. 15-18, 1983).

Sanchez-Bujanos, J. L., M. A. Miller and K. Sepehrnoori.: "Scaling Parameters for Characterizing Waterflood Recovery from Anisotropic Matrix Blocks in Naturally Fractured Reservoirs," paper SPE 39826 presented at the 1996 SPE International Petroleum Conference and Exhibition of Mexico held in Villahermosa, Mexico (Mar. 3-5, 1996).

Schlumberger Simulation Software Manuals 2005A. ECLIPSE Technical Description (2005).

Sharp, I., P. Guillespie, A. Lonoy, S. Horn and D. Morsalnezhad: "Outcrop Characterization of Fractured Cretaceous Carbonate Reservoirs, Zagros Mountains, Iran," paper SPE 104001 presented at the First International Oil Conference and Exhibition held in Cancun, Mexico (Aug. 31-Sept. 2, 2006).

Shen, F. and S. Li: "Streamline-Based Production-Data Integration in Fractured-Reservoir Characterization and Its Application," paper SPE 95779 presented at the 2005 SPE Annual Technical Conference and Exhibition held in Dallas, TX (Oct. 9-12, 2005).

Sonier, F., P. Souillard and F. T. Blaskovich: "Numerical Simulation of Naturally Fractured Reservoirs," paper SPE 15627 presented at the 1986 SPE Annual Technical Conference and Exhibition held in New Orleans, LA (Oct. 5-8, 1986).

Sychev, V. V., A. A. Vassrman, A. D. Kozlov, G. A. Spiridonov and V. A. Tsymarny: *Thermodynamic Properties of NITROGEN*. National Standard Reference Data Service of the USSR, A Series of Property Tables (2000).

Talukdar, M. S., H. A. Banu, O. Torsaeter and J. Kleppe: "Applicability and Rate Sensitivity of Several Up Scaling Techniques in Fractured Reservoir Simulation," paper SPE 59048 presented at the 2000 SPE International Petroleum Conference and Exhibition in Mexico held in Villahermosa, Mexico (Feb. 1-3, 2000).

Thomas, L. K., T. N. Dixon, R. G. Pierson and H. Hermansen: "Ekofisk Nitrogen Injection," *SPE Formation Evaluation* (June 1991) 151-160.

Thomas, L. K., T. N. Dixon and R. G. Pierson: "Fractured Reservoir Simulation," paper SPE 9305 presented at the 1980 SPE Annual Technical Conference and Exhibition held in Dallas, TX (Sept. 21-24, 1980).

Van Golf-Racht, T. D.: *Fundamentals of Fractured Reservoir Engineering*, Development in Petroleum Science No. 12, Elsevier Scientific Pub. Co., Amsterdam (1982).

Vargaftik, N. B., Y. K. Vinagrado and V. S. Yargin: *Handbook of Physical properties of Liquids and Gases*. Pure Substances and Mixtures Third augmented and revised edition Chapter 5 Nitrogen Properties. Hemisphere Pub. Corp. Washington, D.C. (1996).

Vicencio, O. A., T. D. Bui, S. Sinha, R. Kalita and Y. Jalali: "In-Situ Diagnosis of Inflow Behavior in Horizontal Wells," paper SPE 84873 presented at the SPE International Improved Oil Recovery Conference in Asia Pacific held in Kuala, Lumpur Malaysia (Oct. 20-21, 2003).

Vicencio, O. A., K. Sepehrnoori, and M. A. Miller: "Simulation of Nitrogen Injection into Naturally Fractured Reservoirs," paper SPE 92110 presented at the 2004 SPE International Petroleum Conference held in Puebla, Mexico (Nov. 8-9, 2004).

Vicencio, O. A. and K. Sepehrnoori: "Simulation of Nitrogen Injection into Naturally Fractured Reservoirs Based on Uncertain Properties and Proper Matrix Grid Resolution," paper SPE 104038 presented at the First International Oil Conference and Exhibition in Mexico held in Cancun, Mexico (Aug. 31-Sept. 2, 2006).

Young, D. A.: *Phase Diagrams of the Elements*, University of California Press. Oxford. (1991).

Wang, P., S. Balay, K. Sepehrnoori, J. Wheeler, J. Abate, B. Smith and G. A. Pope: "A fully implicit Parallel EOS Compositional Simulator for Large Scale Reservoir Simulation," paper SPE 51885 presented at the 1999 SPE 15th Reservoir Simulation Symposium held in Houston, TX (Feb. 14-17, 1999).

Winokur, M. J.: "H-3 Latent heat of vaporization of Liquid-N2," Polymer Structure's Web Site. Department of Physics U.W. Madison. Polymer Structure Group. (2004).

Wolff, M.: "Geologically-Based Simulator of Naturally Fractured Reservoirs," PhD dissertation, University. of Texas, Austin (1987).

Zeno, G. P., J. W. Jennings Jr., J. E. Olson, S. E. Laubach and J. Holder: "Modeling Coupled Fracture-Matrix Fluid Flow in Geomechanically Simulated Fracture Networks," paper SPE 77340 presented at the 2002 SPE Annual Technical Conference and Exhibition held in San Antonio, TX (Sept. 29-Oct. 2, 2002).

Vita

Omar Alan Vicencio was born in Cerro Azul Veracruz, Mexico on September 10th, 1966; he is son of Raul Vicencio Gomez and Carolina Fuentes Lopez. He has two brothers, Nelson and Eliseo, one sister, Evelyn, and a nephew Alan David. He received his B.Sc. and M. Sc. Degrees from The Petroleum Engineering School of The Universidad Nacional Autonoma de Mexico (UNAM). He has worked for PEMEX since June 1990 in the Reservoir Department. In fall of 1999, he started his Ph.D program in petroleum engineering at The University of Texas at Austin (USA). He performed summer jobs for Chevron Petroleum Technology (CPTC) in San Ramon California, where he studied and analyzed the production response of different geological models of Meren Field, applying the entire process that Chevron Simulation Consulting Team uses for studying fields. He also worked for Schlumberger Reservoir Completions Center in Rosharon, TX, he performed a modeling study for temperature behavior in horizontal wells using compositional simulator ECLIPSE 300 with thermal and multi-segment options. In fall 2005, he returned to PEMEX to work in reservoir studies and continued his dissertation research on part-time basis.

Permanent address: Obregón No.44. Col. La Puerta. Cerro Azul Veracruz. México C.P. 92560.

This dissertation was typed by the author.